Development and Control of Energy Exchange Processes between Electric Vehicle and Utility Network

MAREK MÄGI

TALLINN UNIVERSITY OF TECHNOLOGY
Faculty of Power Engineering
Department of Electrical Engineering

This dissertation was accepted for the defence of the degree of Doctor of Philosophy in Engineering on May 27, 2013.

Supervisor: Ph.D. Elmo Pettai, Department of Electrical Engineering,
                    Tallinn University of Technology, Estonia

Advisor: Ph.D. Hardi Hõimoja, Industrial Electronics Laboratory,
                    Swiss Federal Institute of Technology Lausanne, Switzerland

Opponents: Professor Dr. Hab. Ing. Grzegorz Benysek, University of Zielona
                    Gora, Poland

                    Professor Ph.D. Andres Annuk, Department of Energy
                    Engineering, Institute of Technology, Estonian University of Life
                    Sciences, Estonia

Defence of the thesis: June 27, 2013

Declaration:
Hereby I declare that this doctoral thesis, my original investigation and achievement, submitted for the doctoral degree at Tallinn University of Technology has not been submitted for any academic degree.

Marek Mägi ....

Elektriauto energiasalvesti ja elektrijaotusvõrgu energiavahetusprotsesside uurimine ja juhtimine

MAREK MÄGI

Contents

INTRODUCTION

In recent years *Smart Grids* and *Microgrids* have attracted much attention due to the increasing awareness of energy conservation and environmental problems. In parallel the race for manufacturing *electric vehicles* (EV) has picked up considerably. The main reasons are firstly reducing the dependency of fossil fuels as oil has limited resources and oil prices are growing higher, secondly climate change issues with CO_2 reductions and greener thinking. With new battery solutions (e.g. high-density lithium-ion batteries) the cruising range of EVs has extended, making EVs more practical in everyday use, thus making EVs more competitive with fuel engines. Electric vehicles can improve air quality in cities, implement new and innovative technical solutions and technologies in the economy, increase public awareness of the importance and benefits of electric transportation and energy use.

Studies have shown that EVs sit unused, on average, for more than 90% of the day [1]. Electric vehicles are mobile energy storing systems, which can participate in energy trading. It is the focus of electric engineers to develop and implement new technologies how EVs could be used in microgrids. In particular, EV and *vehicle-to-grid* (V2G) concept could be interesting for utility networks. Vehicle-to-grid (V2G) describes a system, in which EVs communicate with the utility network to sell demand response services by either delivering electricity into the grid or by throttling their charging rate. Aggregated number of EVs can participate in the future in microgrid solutions, where EVs are connected to charging stations with bidirectional energy flow capability. V2G must provide a source of revenue for the vehicle owner. If this revenue helped offset the initial cost of the EV, it could increase the incentive for consumers to purchase EV [1].

The major concern with charging EV batteries is time. Charging procedure has to fulfil two main criteria regarding where it takes place: in public places the charging must be fast (people cannot wait for hours), in private homes and semi-public places (e.g. factories, offices) charging can be slower or scheduled. Charging at homes will take the whole night and does not enable to travel several hundred kilometres with EV during day time. In the urban environment many citizens do not own personal garages and there is not much space to develop single charging station areas for 8 hour charging periods. Charging can be done more efficiently at EV filling stations similarly to petrol stations nowadays. In the near future new EV filling stations will all be built on a concept of fast charging. Preferably a discharged 16 kWh EV battery should be recharged to 80 % level in 30 minutes [2]. EV filling stations are a burden for low voltage (LV) networks and should be connected to medium voltage (MV) grids. Thus, the use of modern EVs and their effective integration into power grids depends on the technologies applied around distribution substations.

Transformer substations are a part of the electric power system, concentrated in a given place to transmit electric energy, distribute power and step up or down the voltage. Substations for medium voltage grids (typically 6-24 kV) transform 3-phase MV to 3-phase low voltage (typically 400 V AC). EVs with V2G

capability could be charged or discharged through distribution substations. As distribution substations are directly related with energy distribution for a local area, active and reactive power management related issues can be efficiently solved inside distribution substations. Distribution substations equipped with energy storing and V2G capability (Fig. 1) enable peak load shaving and demand response, which will reduce/postpone the need to make new investments into building new power sources or power grids to meet peak demand. In addition, enhance renewable energy resources efficiency, compensate reactive power peaks in the grid to reduce losses and enhance active power let through in the utility network.
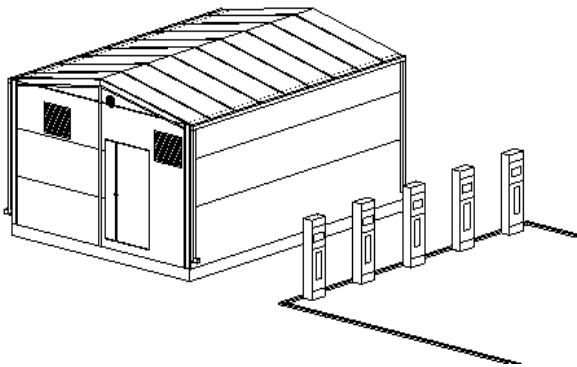
Fig. 1 Distribution substation with EV supply equipments (EVSEs)

The background for this doctoral thesis is the development of EV infrastructure in Estonia [2] – the world's first nationwide fast-charging network for EVs. The proposal of this doctoral thesis was made directly from the industry to solve the problem of integrating EVs with distribution substations for microgrid applications. The research work was done in cooperation with the Estonian company AS Harju Elekter Elektrotehnika [3]. Given company produces distribution substations, medium voltage and low voltage switchgears. The weak point of the conventional distribution substations are that these are either unidirectional in energy transfer or for energy storing purposes [4]. These types of substations are not suitable for automated bidirectional energy exchange between EVs and utility networks. In this doctoral project a novel distribution substation topology with novel control architecture is presented. The topology allows bidirectional energy exchange between several electric vehicles, battery pack energy storage devices and utility networks. EVs can be charged with fast charging. EVs can be utilized for peak shaving of utility network loads both in the low voltage and in the medium voltage side. The distribution substation can act as a service provider in a microgrid.

The results of the project will be discussed in three doctoral theses. The first is oriented for microgrid specific functions in distribution substations (author Kristjan Peterson, Ph.D. student of Tallinn University of Technology). The second is oriented for energy auction control through distribution substations (author Tarmo Korõtko, Ph.D. student of Tallinn University of Technology). The current thesis is

mainly concentrating on the distribution substation's topology and control system research, design and development.

In order to specify and define the exact field of interest of the current doctoral thesis, several published scientific papers and current V2G pilot projects were analysed.

Papers can be found in literature, which describe the benefits of V2G applications, but do not present any technical analysis (e.g. [5]).

Papers can be found in literature, which describe charging of aggregated number of EVs, but only consider unidirectional power converters (e.g. [6]).

Several papers describe smart scheduling algorithms for charging aggregated number of EVs for reducing the load for the utility networks [7] - [14]. In the same context the idea is proposed that V2G applications could be utilized during some periods of day. These papers do not present any system topologies or simulations with power converters. These papers do not indicate how the charging or discharging of batteries could be physically controlled through power converters.

Papers can be found in literature, which indicate that EVs are connected to charging stations to perform V2G capability for EV coordinator (e.g. [15]). These papers do not indicate the interconnection of EVs with utility networks and where the potential of EVs could be utilized. The discharging is limited to LV applications.

Papers can be found in literature, which present topologies of discharging EVs to common AC bus (e.g. [16]). These topologies do not allow discharging of EVs to the MV voltage level. These topologies do not allow fast charging of EVs with parallel of AC consumers as fast charging of several EVs is a burden for LV networks.

Several papers propose an idea for V2G application to utilize three-phase inverters on a common AC bus with a step-up transformer [17] - [19]. These types of topologies have potential hazards, which the utility networks try to avoid. Integrating several three phase inverters side-by-side start to influence the current and voltage of neighbour EVSEs thus making potentially the system unstable in real applications. This requires an additional control mechanism to coordinate several inverters in real time. The most crucial setback of these topologies is the fact that in such topologies the transformer can only be a star-star type transformer (for star-delta e.g. Dyn11 transformer type all inverters would have to have current transformers and voltage transformers in the MV side to overcome the phase shift of the transformer). Star-star type transformers do not nullify uneven harmonics (especially 3rd harmonic content) during charging of EVs, thus the system is a potential hazard for the utility networks due to additional losses generated in the grid. There has not been indicated in these papers how the MV output is compared to the target value and how inverters would be controlled. These types of topologies do not utilize EVs as a source for peak shaving of LV consumer loads. The simulations have been made in a simplified manner (inverters are simulated as ideal three-phase sources), which rises a question whether these systems would even work in real applications.

Several papers have presented EVs as a source inside a microgrid along other renewable energy sources such as photovoltaic system and wind turbine on a common AC bus [20] - [22]. Some papers present topologies where EVs are connected to a common DC bus [20]. These topologies only allow utilizing EVs as energy sources inside the microgrid (problem presented in [20]). These topologies do not allow discharging of EVs to the MV voltage level. These papers have presented some simulations with power converters, but the control principles for controlling aggregated number of EV charging or discharging for Smart Grid applications have not been presented.

Several papers present topologies with one transformer, bidirectional AC-DC converter and several DC-DC converters. Paper [23] implements topology without battery energy storage unit (BESU) and paper [24] with BESU. These topologies are not utilized for peak shaving of LV consumer loads. The topology without BESU requires larger transformer. The paper [23] implements topology only with ideal switches as power converters. The topology does not implement isolating transformers in DC-DC converters to galvanically isolate the battery from the utility network (mandatory according to IEC 60364-7-722). Both papers do not indicate control principles for participating in Smart Grid applications and control of individual bays.

Practical field tests of V2G applications have been mainly done with one phase V2G power injection (Industry-University Research Partnership, USA, 2008 [25]). In ECOtality North America bi-directional charging project V2G capability was demonstrated to support/offset peak building loads [26]. In 2011, an American company Nuvve designed a server that connected EVs to grid operator. In 2010 Italy began its pilot project E-moving to test the technology and distribution of charging resources, commercial processes and offerings. In 2009 a project MeRegio Mobil in Germany was started to investigate how EVs can be connected to a house electromagnetic system by way of an intelligent charging station while testing bi-directional energy management. In 2007 Google.org began RechareIt program where vehicles are shared between employees during work hours to encourage the use of EVs. In 2008 SmartGridCity project was initiated in USA to study effectiveness of technologies in their delivery of power, the incorporation of Smart Grid technology in the business world and replicating the results on a wider scale. In 2006 Austin Energy and V2Green project was initiated to examine the potential of EVs through maximizing the use of renewable energy. EVs were fitted with module to control timing of charging. In 2006 Mid-Atlantic Grid Interactive Cars Consortium conducted a V2G test to control charging of EVs with manually discharging power into the local grid. In 2002 AC Propulsion V2G Demonstration project an aggregator function was developed to act as a commercial middleman between a grid operator and the vehicle [26].

In the United States current environmental issues are playing a vital role in the demand for V2G technology [26]. The University of Delaware has signed its first licence for V2G testing with Autosport, Inc 2011. Japan is currently leader in the EV industry. This may allow the country to pioneer new V2G technology for the

mainstream. Nissan offers a kit compatible with the LEAF that will be able to provide power back into a Japanese home. Denmark currently is a world leader in wind power generation. The EDISON project plans to use EVs for storing additional wind energy that the grid can not handle and in peak hours power stored in EVs will be fed back into the grid. United Kingdom started programs in 2011 to assist adoptation of EVs. South Korea has set goal that by 2030 100 % of electric customers will be using Smart Grid technology [26]. The German E-Mobility Berlin [27] project was initiated by Daimler AG (Mercedes-Benz) and the utility RWE. The project introduces a fleet of 100 EVs supplied by Daimler and 500 EVSE's which are delivered and powered by RWE in the streets of Berlin for a large field test. The project is aimed at developing and testing standardized solutions for electric vehicles.

Integration of V2G fast charging stations with the electricity grid is in the objective of e-DASH [28]. The problem stated is that the sustainable integration of EVs requires an intelligent charging system for the real-time exchange of charge related data between EVs and the grid in order to allow the management of: high-current fast-charging for large numbers of EVs brand-independently, price-adaptive charging/reverse-charging at optimum price, the real-time grid balancing according to spatial and temporal needs and capacities, influenced by the demand and the supply side, remote load charging process control.

The differences in the architectures of different projects are an indication of a fundamental question in V2G integration [27]: which entity is responsible for influencing or controlling the EVs utilization behaviour (aggregator, the EVSE or the EV itself). Standards in the field of V2G are EV-centric (IEC 15118). In EV-centric approach an embedded computer in the vehicle will take certain decisions. The approach creates challenges and problems to the Aggregator, as the Aggregator hast to communicate with each EVSE individually. It would much more convenient for the Aggregator or distribution system operator (DSO), if there would be an intermediate buffer which would collect data of EVSEs and present the data in a compact way. This would speed up the decision making for the Aggregator or DSO. This doctoral thesis proposes the distribution substation as the intermediate buffer or virtual power plant (VPP).

The results of the analysis of different scientific papers and V2G projects indicate that utilization of several EVs as energy resources for peak shaving of utility networks loads is scarce. None of the papers or current V2G projects do not consider fast charging, discharging of EVs to the medium voltage and to the low voltage side through distribution substations in the same context. Standards in the field of Smart Grid [29] are oriented in the standardization of communication protocols and describe general functionalities, but do not indicate for electrical engineers how the energy exchange between different entities should be physically controlled. This doctoral thesis proposes control system architecture for electrical engineers how to handle several EVs connected to the bays of the distribution substation. The doctoral thesis is orientated for system integrators. The purpose of this doctoral thesis is not to develop new type of power converter topologies, but

analyzis of power converters are presented for the development of the novel topology for power distribution and control architecture with bidirectional power converters.

Current doctoral project was launched in 2011. This research work has been supported by European Social Fund (project "Doctoral School of Energy and Geotechnology II"), Estonian Ministry of Education and Research (project SF0140016s11), Estonian Science Foundation (Grant ETF9350), Estonian Archimedes Foundation (project AR10126), SmartGrids Era-Net (project GERA1) and European Regional Fund. The results of this project will be used to prepare and conduct a production development in AS Harju Elekter Elektrotehnika in the near future.

Thesis Objectives

The general objective of the doctoral work is to develop and build a state of the art substation control system that ensures efficient and reliable operation of the distribution substation for bidirectional energy exchange between electric vehicles and utility network according to requirements of international standards and specific energy transmission norms.

The main research tasks to be achieved are as follows:
1. analysis of current technologies and trends in Li-ion batteries and charging methods for EVs (chapter 1.1 and chapter 1.2);
2. analysis and classification of international standards for EV charging and V2G interconnections to formulate tasks the new control system has to fulfil (chapter 1.3);
3. analysis of current technologies and trends in the development of distribution substations (chapters 1.4 and 1.5);
4. analysis of current trends in the control of aggregated number of EVs and considerations regarding the usage of EVs as distributed energy resources (chapters 1.6 and 1.7);
5. formulation of technical requirements and methods for constructing distribution substations that interconnect EVs with the utility network (chapter 2.3.1);
6. analysis and classification of control and protection requirements for distribution substation's low voltage bays to obtain the optimal methods for reliable and efficient operation of the distribution substation (chapter 2.3.2);
7. development of distribution substation topologies for integrating aggregated number of EVs with utility networks (chapter 2.3.3);
8. research and analysis of recent technologies and development trends used in bidirectional power converters and their control systems (chapter 3.2 and chapter 3.3) for design and development of a new control system for managing of distribution substation's low voltage bays (chapter 4.1);

9. development of computer models to simulate, test and analyze different control and protection algorithms for distribution substation's low voltage feeders (chapters 3.1, 3.2, 3.3, 4.2);
10. design and development of the control system for fast charging electric vehicles and discharging of electric vehicles through distribution substation with V2G capability (chapter 4.3.2 and 4.3.3);
11. design and development of the control system for energy storing inside the distribution substation with V2G capability (chapter 4.3.4 and 4.3.5);
12. analysis of impact to utility network from bidirectional energy exchanging (chapters 4.3.2 – 4.3.6);
13. practical verification of the simulation and analysis results on the test prototype (chapter 5);
14. elaboration of design guidelines and recommendations for constructing distribution substation with V2G capability (chapter 6);
15. elaboration of proposals for postdoctoral studies (chapter 7).

Scientific novelty

The scientific novelty of the current work involves following:
1. development of distribution substation topology with integrated AC and DC bus to solve the problem of integrating aggregated number of EVs for both to the low voltage and the medium voltage side of the utility network (Chapter 2.3.3);
2. new method for solving the problem of selection of power converter topologies for the distribution substation topology with integrated AC and DC bus (Chapters 3.2.10 and 3.3.5);
3. development of a new control algorithm to solve the control problem related to charging and discharging of aggregated number of EVs and energy storage units through the distribution substation's bays (Chapter 4.1);
4. development of automatic transfer switching algorithm to solve the energy routing problem in the distribution substation topology with integrated AC and DC bus (Chapter 4.7);
5. elaboration of methology to design distribution substations with V2G capability for the EV infrastructure (Chapter 6).

Practical novelty

The practical novelties of the thesis are as follows:
1. design and development of the state of the art control system for the distribution substation's low voltage bays for bidirectional energy exchange applications between EVs and utility network (Chapter 4.1);
2. development of computer models for the distribution substation with V2G capability that enables testing of different control algorithms and prediction of the behaviour of the system in various failure situations (Chapter 4.2);

3. development and implementation of the concept of scattering different protection and control functions between different substation control layers to reduce the control system load (Chapter 4.3);
4. development of prototype of modular 460 V DC Li-ion battery pack energy storage device in cooperation with Estonian company AS Harju Elekter Elektrotehnika (Chapter 5);
5. investigation and usage of IEC 61850 protocol to speed up the data flow and error identification to increase the overall reliability of the control system (Chapter 5);
6. recommendations and guidelines for design of distribution substations with V2G capability for the EV infrastructure (Chapter 6).

Direct practical output of the thesis

Tallinn University of Technology sold a manufacturing licence "Li-ion Energy storage" with appropriate technical documentation to Estonian company AS Harju Elekter Elektrotehnika. Design guidelines that were elaborated and algorithms for the control system of the distribution substation were used for construction of the Li-ion Energy storage unit in AS Harju Elekter Elektrotehnika. As a result of usage of the scientific results in this doctoral project, prototype control system for the distribution substation with V2G capability was designed, assembled and partially tested in Tallinn University of Technology.

Significance for worldwide science and technology development

In this doctoral project first distribution substation modules for bidirectional energy exchange applications between electric vehicles and utility network were implemented on a real microgrid prototype. A detailed report with problems and general improvement suggestions was sent to the manufacturer company AS Harju Elekter Elektrotehnika. The feedback has been taken into consideration in the R & D development of improved edition of distribution substations.

A valuable feedback was also provided about functionality of ABB new AC-DC power converter series and Orion BMS used in the real microgrid prototype.

The new and existing problems for integrating EVs for Smart Grid applications were summarized in the proposal of international collaborative project (author as the team member participates in the consortium) FP7-ICT-2013-11 under the 7th framework programme [30].

Dissemination of results and publications

The author has over 8 international scientific publications, 6 of those are directly connected to the topic of the doctoral research. 1 paper connected to this thesis has been published in the Institute of Electrical and Electronics Engineers database (IEEE *Xplore*) and 1 paper will be published in the IEEE *Xplore* in June 2013. Latest paper has been published in the Scientific Journal of Riga Technical University – Electrical, Control and Communication Engineering. The scientific results have been presented and discussed in different international conferences.

Acknowledgements

First of all, I would like to thank my wife and family for the constant support during my studies.

I would like to express special gratitude to my supervisor Ph.D. Elmo Pettai, who has encouraged me in my PhD studies and who has given me valuable advice and guidance.

Next, I would like to express my gratitude to my advisor Ph.D. Hardi Hõimoja for his advices.

Special thanks to the team members of Tallinn University of Technology microgrid research team M.Sc Kristjan Peterson and M.Sc Tarmo Korõtko for their support and valuable help in the development of the experimental microgrid.

I am grateful to the staff of the company AS Harju Elekter Elektrotehnika, especially to Alar Ollerma and Ülo Merisalu for their help and support in my studies.

I also thank the staff of the Department of Electrical Engineering of Tallinn University of Technology. My sincere thanks to Mare-Anne Laane for her revising and corrections advise to my English writing during my PhD study.

Tallinn   Marek Mägi
May, 2013

ABBREVIATIONS

AC	alternating current
ACSI	abstract communication service interface
APS	area electric power system
ATS	automatic transfer switching
BESU	battery energy storage unit
BMS	battery management system
C	rated current of batteries
CANbus	controller area network bus
CC	constant current
CCCV	constant current constant voltage
CML	computing layer
CMLDS	computing layer for extension substations
COML	communication layer
CP	connection point
CPL	component layer
CT	current transformer
CTL	control layer
CV	constant voltage
CHAdeMO	charging protocol for rapid DC charging
DC	direct current
DER	distributed energy resources
DI	digital input
DO	digital output
DL	data layer
DS	distribution substation
D-STATCOM	distribution static compensator
DSO	distribution system operator
DOD	depth of discharge
DR	distributed sources
ECU	electronic control unit
EMC	electromagnetic compability
EMI	electromagnetic interface
EPS	electric power systems
ERL	energy routing layer
ESU	energy storage unit
EV	electric vehicle
EVCC	electric vehicle communication controller
EVSE	electric vehicle supply equipment
ESM	energy storage module
GFI	ground fault interrupter
GOOSE	generic object oriented substation event
GW	gateway

HMI	human machine interface
HV	high voltage
IED	intelligent electronic device
IGBT	isolated gate bipolar transistor
LV	low voltage
MMI	multi measurement input
MPL	monitor and protection layer
MRL	market layer
MV	medium voltage
MW	middleware
N	neutral
NCC	network control centre
NPC	neutral point clamped
OCV	open circuit voltage
OEM	original equipment manufacturer
OWL	owner layer
PCC	point of common coupling
PEN	protective earth and neutral
PFTM	priority filter and task manager
PI	proportional-integral
PFC	power factor corrector
PLL	phase lock loop
PQ	power quality
PWM	pulse width modulation
RMS	root-mean-square value
RTU	remote terminal unit
SA	substation automation
SAS	substation automation system
SCADA	supervisory control and data acquisition
SCS	self consumption of substation
SECC	supply equipment communication controller
SGAM	Smart Grid architecture model
SM	storage medium
SMV	sampled measured value multicast
SOC	state of charge
SOH	state of health
SSN	secondary substation node
TDD	total current demand distortion
THD	total harmonic distortion
V2G	vehicle to grid
VOC	voltage oriented control
VSC	voltage source converter
VT	voltage transformer
VPP	virtual power plant

SYMBOLS

A	voltage drop in exponential zone
B	exponential capacity at the end of the exponential zone
C	capacitance
C_b	base capacitance
C_f	capacitor of LCL filter
C_{DC}	DC side capacitor
C_p	capacitance of capacitor
D	duty cycle
E_0	battery constant voltage
E_{avl}	actual energy stored inside battery
E_{Batt}	nonlinear no-load voltage of battery
E_{cap}	energy capacity
$\Delta E_C(t)$	energy loss of capacitor
E_{ESU}	energy of ESU
E_{Exp}	voltage at the end of the exponential zone
E_{Full}	fully charged voltage
E_{Nom}	voltage at the end of the nominal zone
E_{rated}	full energy capacitance of battery
f	frequency
f_{res}	resonance frequency
f_s	switching frequency
i	current
I_1	fundamental current
I_{BVS}	load current before voltage sag
$I_C(t)$	instantaneous converter current
i_d	direct current component
I_{DVS}	load current during voltage sag
I_n	rated current
i_q	quadrature current component
I_h	harmonic current
I_L	full load current
ΔI_L	inductor ripple current
Δi_{Imax}	maximum allowable peak ripple current
I_{SC}	peak value of charge current
k	factor
K	polarization voltage
L	inductor
L_b	base inductance
L_C	line inductor
L_g	inductance of grid side reactor of LCL filter
L_i	inductance of converter side reactor of LCL filter
m	modulation index

m_E	gravimetric specific energy
m_P	gravimetric specific power
N	number of turns of the transformer winding
n_{sw}	frequency multiple of the fundamental frequency
P	active power
ΔP	active power reduction gradient
P_{AV}	maximum average load
P_{bay}	active power of bay
$P_{ch}(t_{ch})$	active power for charging
$P_{com}(t_{ch})$	active power available on common DC bus
P_{ESU}	power of ESU
$P_{grid}(t_{ch})$	available grid active power
P_M	power generated
P_{pwr}	required power
Q	reactive power, battery capacity
Q_0	initial batter capacity
Q_C	required capacitor output
Q_{Exp}	capacity at the end of the exponential zone
Q_i	i^{th} capacitance measurement in time
Q_n	rated capacity of battery
Q_{max}	maximum capacity
Q_{Nom}	capacity at the end of the nominal zone
r	inductor ratio
R	resistance
R_i	resistance of converter side reactor of LCL filter
R_d	damping resistor in LCL filter
R_g	resistance of grid side reactor of LCL filter
S	apparent power
t	time
Δt	time step
T	period of one cycle
ΔT	period
t_{bat}	battery temperature
t_{ch}	charging time
TDD_i	total current demand distortion
THD_i	total harmonic distortion for current
THD_U	total harmonic distortion for voltage
T_s	switching period
U_1	fundamental voltage
U_c	declared voltage
ΔU_C	voltage ripple in common DC bus
u_d	direct voltage component
U_h	harmonic voltage
U_L	sinusoidal AC voltage

U_n	nominal voltage
U_{ph}	phase voltage
u_q	quadrature voltage component
U_V	fundamental line to line voltage
V	voltage
V_{Batt}	battery voltage
V_{CMAX}	pre-set upper limit of voltage
V_0	DC load voltage
V_d	voltage on d axis, supply DC voltage
V_{DC}	DC side voltage
V_E	volumetric specific energy
V_I	inverter voltage
V_{L-L}	line to line voltage
V_P	volumetric specific power
V_{sag}	voltage sag
V_{SC}	peak phase voltage
V_q	voltage on q axis
$v_C(t)$	instantaneous bridge converter voltage
V_s	system voltage
$v_S(t)$	instantaneous line voltage
X	reactance
X_L	line reactance
Z	impedance
Z_b	base impedance
γ_{UL}	angle of voltage vector
δ	phase angle
η	efficiency
θ	phase synchronous angle
ω_b	angular frequency
ω_{res}	angular resonant frequency
ω_{sw}	angular switching frequency
ϑ ,	phase grid angle

1. STATE OF THE ART

1.1 Li-ion batteries

1.1.1 Structure of Li-ion batteries and trends in the world

Li-ion rechargeable batteries are best suited for energy storage applications and for electric vehicles where small-size, light weight and high performance energy sources are required. Lithium is the lightest of all metals, has the greatest electrochemical potential and provides the largest density for weight. These properties give lithium the potential to achieve very high energy and power densities in high power battery applications such as automotive and standby power [31].

Li-ion batteries have many attractive performance advantages compared to other battery chemistry types. Shortcomings of Li-ion batteries are far outweighed by the advantages. Main benefits of Li-ion batteries are [31], [32]:
- high cell voltage (3.6 V DC), which is approximately three times the voltage of Ni-MH or Ni-Cd batteries, thus fewer cells and associated connections and electronics are required for high cell voltage batteries;
- high energy density, approximately 70-200 Wh/kg, as Li-ion batteries are high cell voltage/light weight batteries (about 4 times better than lead acid);
- very high power density (high energy cells 200-400 W/kg and high power cells 2000-4000 W/kg);
- flat discharge voltage, allowing the production of stable power throughout the discharge period of the battery;
- high open circuit voltage (max. voltage in charged state at zero current), which increases the amount of power that can be transferred at a lower current;
- high discharge cycle efficiency (approx. 90-99 %);
- lower self-discharge rate (approx. 5-10% per month), which is less than half of nickel-based batteries;
- no memory effect compared to Ni-Cd batteries, where the apparent discharge capacity of a battery is reduced, when it is repetitively discharged incompletely and then recharged;
- wide variety of shapes and sizes efficiently fitting the devices they power (cylindrical, pouch, prismatic);
- low maintenance battery;
- does not need prolonged priming when new (one regular charge is all that is required);
- no liquid electrolyte means they are immune from leaking;
- high cycle life 1000-10000 cycles (service life 5-15 years).

Main drawbacks of Li-ion batteries that must be taken into account are [33], [34]:
- more expensive per watt-hour than Ni-Cd batteries, but operate over a wider temperature range with higher energy densities, while being smaller and lighter;
- higher internal resistance compared to Ni-MH or Ni-Cd batteries (resistance increases with both cycling and age reducing the maximum draw current and the battery can no longer operate for an adequate period);
- high charge levels and elevated temperatures (whether from charging/discharging or ambient air) hasten capacity loss;
- diminishing of cell's capacity over time, where older batteries do not charge as much as new ones (especially in high-current applications);
- fragile and requires a protective circuit to limit peak voltages and current;
- deep discharge may short-circuit the cell, in which case recharging would be unsafe.

The three primary functional components of a lithium-ion rechargeable battery are the negative electrode, positive electrode and the electrolyte, which are put together in a whirl pattern and stored in the case [32]. An example structure of Li-ion battery is shown in Fig. 1.1 [32]. The battery consists of a spiral structure with 4 layers (cathode plate, separator, anode plate and separator). The negative electrode of a conventional lithium-ion cell is made from highly-crystallized carbon (commercially popular material is graphite). The positive electrode is generally either lithium cobalt oxide $LiCoO_2$ (LCO), lithium iron phosphate $LiFePO_4$ (LFP) or lithium manganese oxide $LiMn_2O_4$ (LMO), which have superior cycling properties at high cell voltages. Electrolytic fluid is a lithium salt in an organic solvent, optimized for the specialty carbon. The principle behind the chemical reaction in the lithium ion battery is one where the lithium in the positive electrode material is ionized during charge, and moves from layer to layer in the negative electrode. During discharge, the ions move to the positive electrode and return to the original compound. In EVs are also used lithium titanate $Li_4Ti_5O_{12}$ (LTO) batteries, which use lithium-titanate nanocrystals on the surface of its anode instead of carbon, which allow electrons to enter and leave the anode quickly making fast recharging possible with high currents [32].
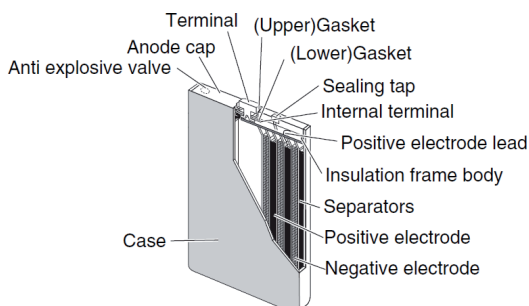

Fig. 1.1 Structure of a lithium ion battery (prismatic type) [32]

Batteries also incorporate a variety of safety protection systems such as a gas discharge valve, which helps prevent the battery from exploding by releasing internal gas pressure, if it exceeds the design limit [32].

Trends for lithium-ion batteries in the following years [35]:
- higher current densities (e.g. electric vehicles);
- higher energy densities (e.g. consumer market, electric vehicles);
- reducing of manufacturing costs;
- alternative active materials, which require less supervising hardware (e.g. less sophisticated voltage control);
- low cost active materials for applications with reduced demands (e.g. less capacity, power).

1.1.2 Li-ion batteries in electric vehicles

The concept of battery electric vehicles is to use charged batteries on board vehicles for propulsion. Battery electric cars are becoming more and more attractive with the advancement of Li-ion battery technology. Many car manufacturers have developed their own versions of electric vehicles with Li-ion battery technology (or with other type of Lithium based chemistries, e.g. lithium cobalt): BMW Mini E, Ford Focus EV, Mitsubishi i-MiEV, Nissan Leaf, Tesla Roadster, Toyota Plug-in Prius, Volvo Electric C30 etc. Battery packs of different car manufacturers vary in battery total capacity (15-90 kWh), nominal voltage and charging power. As an example, battery packs of Mitsubishi i-MiEV and Nissan Leaf are described in more detail.

The Mitsubishi i-MiEV is a five door hatchback electric car produced by Mitsubishi Motors. The i-MiEV is also sold in Europe rebadged by PSA Peugeot Citroën as the Peugeot iOn and Citroën C-Zero [36]. Mitsubishi i-MiEV has a 16 kWh (58 MJ) Li-ion battery pack that consists of 88 cells and is placed under the base floor (single cell nominal voltage 3.7 V, rated capacity 50 Ah and max. output current 300 A at 25 °C) [37] [38]. Maximum output power of the battery is 60 kW [39]. The pack has 22 cell modules connected in series at the nominal voltage of 330 V. The following parameters in future modelling are taken from Citroën C-Zero: each cell is designed for voltages 2.5-4.5 V (total for battery pack 220-396 V) and resistance for single cell is 1.5 mΩ (total for battery pack 132 mΩ) [40]. The production version of the 2009 i-MiEV has a single permanent magnet synchronous motor mounted on the rear axle with a power output of 47 kW and torque output 180 Nm. With the on-board charger, the vehicle battery can be charged in European markets with a 230 V 1-phase (16 A) current typical for household applications (charging time approximately 6 h). With quick-charger systems, the vehicle battery can be charged with 3-phase 200 V AC (max. DC 50 kW) power supply (charging up to 80 % level of nominal capacity in approximately 30 minutes). Quick charging with 120 A, the battery pack will retain 84 % of its nominal capacity after 1000 charging cycles [38].

The Nissan Leaf is a five door hatchback electric car manufactured by Nissan. Nissan Leaf has a 24 kWh (86 MJ) Li-ion battery pack that consists of 192 cells (single cell average voltage 3.8 V and rated capacity 33.1 Ah) [41], [42]. The pack has 48 cell modules (module consists of 4 cells – 2 cells in series pairs in parallel) connected in series at the nominal voltage of 360 V. The battery pack can deliver up to 90 kW power. Nissan Leaf has a synchronous electric motor mounted on the front with a power output of 80 kW and torque output 280 Nm. For charging Nissan Leaf has an on-board charger 3.3 kW for 230 V 1-phase household applications and 480 V DC fast charging option with CHAdeMO protocol (charging up to 80 % level of nominal capacity in approximately 30 minutes with charging power 50 kW DC).

In network analyzis it is recommended that average EV energy consumption of 150 Wh/km and storage capacity of 25 kWh/EV is used for planning with a short horizon (10 years) and 40 kWh/EV with longer horizons. The EV battery storage capacity will be affected by battery prices, mobility needs (request for range) and deployment of charging infrastructure [43].

An example description of an electric vehicle's propulsion system is shown in Fig. 1.2 [36], which is based on Mitsubishi i-MiEV. The electric motor is driven by an alternating current. The inverter converts high-voltage direct current from the battery unit to alternating current and supplies electric motor with the power required to drive the vehicle. The vehicle uses single-speed reduction gear transmission, exploiting the high low-end torque inherent to the electric motor and eliminating the need for complex gear shifting mechanism as found in internal combustion engine powered vehicles.
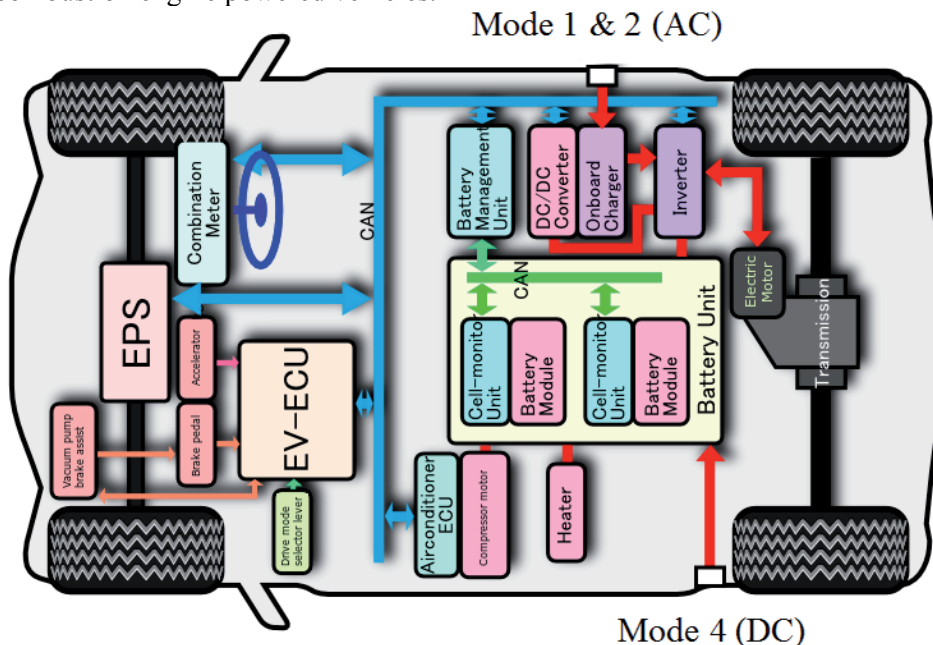

Fig. 1.2 System diagram of Mitsubishi i-MiEV electric vehicle [36]

On-board charger allows the traction battery to be charged using domestic AC line (voltage depend on the country). With the on-board charger is integrated DC-DC converter, which is used to charge 12 V auxiliary battery and power electrical equipment. The on-board EV electronic control unit (EV-ECU) gathers data and information via CAN bus from all the major EV components to provide integrated management of the car's performance. This management system constantly monitors battery status and the energy recovered from the regenerative brakes, while regulating output to ensure smooth and powerful acceleration from a full stop. Combination meter displays power consumption, energy recovery status and indicates remaining power in the traction battery [36]. Electric power steering (EPS) improves car handling and increases fuel efficiency [44].

1.1.3 Charging methods for Li-ion battery packs

Batteries are charged with rectifiers, which voltage has to be greater than the voltage on battery bank's terminals. The differences between voltages determine the charging current and recharging time.

The main criteria in choosing a charging curve are the considerations about battery's health and avoidance of overvoltage. Excess charging causes temperature rise in cells, which leads to failures.

Batteries charging and discharging curve graphics show a variety of "C" figures (e.g. from C/5 to C/100). This C/XX number is a rate of charge or discharge in Amperes proportioned to the capacity of the battery. 1 C stands for the rated charge current of the battery cell that will fully charge the battery in one hour. For example, if a battery with 500 Ampere-hours, is charged or discharged in 10 hours, then the process current is 50 Amperes and it is described with figure C/10. Same "C" figure for different battery capacities give different current values, but the effect on the battery's voltage is the same. For very fast charging, the charging time is described in minutes (e.g. 30 minutes equals to 1/2 hours) and "C" figure is above "1" (e.g. for 30 minutes the figure is 2 C).

Trickle charging is charging of battery under no-load at a rate equal to its self-discharge rate, thus enabling the battery to remain at its charged level. Li-ion batteries cannot accept overcharge. Li-ion can only take as much as it can absorb, anything extra causes stress. For this reason it is not recommended to use "floating voltage" (constant voltage that is applied continuously to a battery) method to charge Li-ion batteries. When Li-ion battery is fully charged, the charging voltage must be stopped and should not be applied any longer. Trickle charging can be though applied to restore deeply depleted cells. During this stage the cells are charged with a constant current of 0.1 C maximum [45]. After the cell voltage has risen above the trickle charge threshold, the charge current is raised to perform constant current charging. This prevents the cell of the battery from being damaged from high fast charge currents when it is in a deeply discharged state. If voltage does not rise over threshold value in predefined time range (e.g. 1/8 of charge time), then the battery is possibly shorted or damaged.

Constant Current Constant Voltage (CCCV or UI) charging is the most used and safest method to charge Li-ion batteries (Fig. 1.3 [46]). The battery is charged at first with a constant current (CC) until a certain voltage is reached. Then, the charging is switched to constant voltage (CV) charging, where the battery voltage is kept constant and the current decreases. When the constant voltage is reached, it takes a long time until the battery is completely charged. The charging will be stopped, when the current reaches a certain threshold (typically C/20). This method is perfect, if the charging time is not important. The battery cells and electronics do not get much stress as the current values are quite low to avoid over-heating. Therefore, a current control loop by the battery monitoring system is not necessary. The duration time for CC phase and CV phase depends of battery's chemical structure. For some battery types the CV phase is longer than CC phase, for other types this is vice versa.
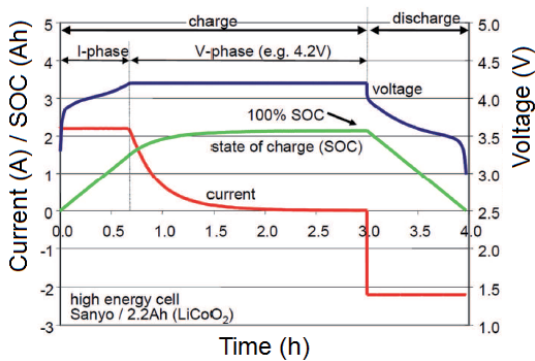
Fig. 1.3 Charging/discharging curve of Li-ion batteries with CCCV charging [46]

In Fig. 1.4 [32] is presented typical charge flowchart for single-cell Li-ion battery pack, where T_1 is the charge total timer count, t_{bat} is the battery temperature, t_{min} is the low temperature threshold setting value, t_{max} is the high temperature threshold setting value, OCV is the battery pack load open voltage, it is the rated current, CV is the constant voltage, $ichg$ is the charge current, $iset1$ and $iset2$ are electrical current set values, T_2 is the charge complete timer count, and T_3 is the recharge timer count.

Fast charging [47] is used to charge the battery form 20 % to 80 % in a short period of time (e.g. 30 minutes) with a high rate of constant current. The fast charging has to be controlled from the battery management system (BMS). Charging currents depend on the capacity of battery packs. Not all batteries can be charged with fast charging as high current values generate more heat. The BMS must be able to manage the balancing and temperature of the cells or otherwise this can cause decrease of the battery's lifetime. Most likely a cooling system for the battery is necessary.

Boost charging [47], also known as "5 Minute Charging", is used to charge the battery to 33 % in a very short period of time (e.g. 5 minutes), after what the

charging is switched to fast charging to charge the battery to 80 %. The BMS must be able to control the charging current. No degradation of the battery is expected.

Temperature throttling [47] is used to charge the battery with monitoring the battery temperature that the maximum allowed cell temperature would not be exceeded. This protects the battery against degradation during charging. The BMS controls the charging current. In systems, where maximum temperature is likely to be achieved during charging, cooling systems are added and controlled by BMS.

Constant power charging – the battery is charged with constant power until the required energy has been charged or the charging power is limited by battery constraints. Forced power charging – the charging power is gradually reduced until the required energy has been charged or the charging power is limited by battery constraints. Pulsed power charging – the battery is charged with constant power in pulses until the required energy has been charged or the charging power is limited by battery constraints [48].
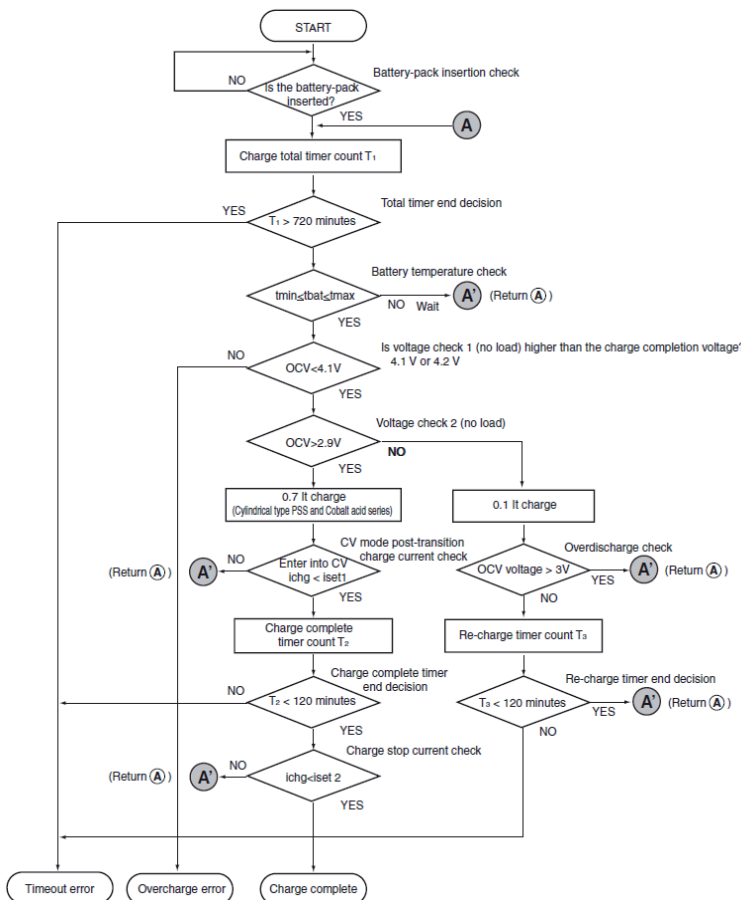

Fig. 1.4 Flowchart for charging Li-ion battery pack (single-cell) [32]

1.1.4 Battery management system (BMS)

Battery degradation is mainly caused by over voltage and high temperature [49]. The Battery Management System (BMS) is required for keeping the charging process under control and protecting the battery pack. The BMS mainly protects the single battery, thus extend the cycle life of the battery pack. The BMS relies on many inputs such as cell voltage tap sensors, a total pack voltage sensor, current sensor, thermistors for temperature measurements, and data provided by the end user to calculate safe limits for the battery pack. The BMS monitors the charging voltage in real time (e.g. for no over-currents and over charging), battery cell voltage (for balancing) and the state of battery. The BMS calculates the State of Charge (SOC) for controlling charging (especially in high current mode) and State of Health (SOH) for indicating the lifetime of the battery. State of charge can be calculated using coulomb counting and dynamically corrected using SOC drift points. Coulomb counting is a method that keeps track of current going into and out of the battery pack. Coulomb counting generally works quite well as long as the capacity of the battery is known and the current sensor is accurate enough. Because no Coulomb counting system can be perfectly accurate, error will eventually build up. To correct those errors, dynamic SOC drift is used to compensate. SOC drift points are specific points on the discharge plot of a cell, where the SOC can be roughly calculated based on the open cell voltage (typically these points would be around the 10 %, 20 %, 80 % and 90 % of SOC [49], where the voltage change is most significant). State oh Health of the battery pack can be determined by examining both internal resistances of the battery pack as well as the observed capacity (measured in Ah). As the observed capacity decreases from the nominal (starting) capacity and the internal resistance increases from the nominal capacity, SOH will go down. However, defective cells or premature aging due to abuse and/or improper wiring can cause the increase of battery pack aging [49].

The BMS provides information to external components (e.g. battery chargers) to protect, manage, and monitor the battery. The BMS relies on the external components to respect the limits set by the BMS. It cannot directly cut charge or discharge currents to protect the battery and relies on the end user to provide appropriate controls. The SOC and SOH values can be transmitted (e.g. to the charging station interface panel) to indicate the duration of charging.

The BMS for battery pack consists of a single battery detection module, CAN communication, controller, charger, equalizing charge equipment and other components [50]. Structure diagram of the BMS is shown in Fig. 1.5 [50]. The voltage and temperature of each battery, as well as the total voltage and total current of the battery pack are detected. BMS controller communicates with the charger, equalizing charge equipment and between external controller (e.g. EV motor controller, substation controller) by CAN communication. The controller monitors and controls charge and discharge process of the battery pack, which is the core of the BMS.

In EV applications DC voltage connector connects battery to the DC voltage bus of the car [47]. Current sensor contains resistive or inductive current

measurement. Battery modules monitor voltage, temperature and perform cell balancing. Central battery management controller does SOC, SOH calculations, balance control, thermal management, internal and external data exchange, isolation test.
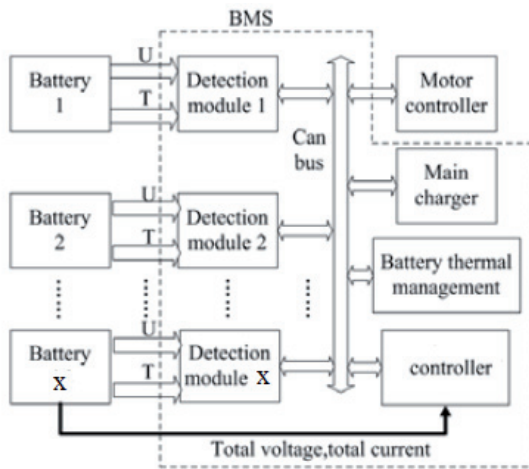
Fig. 1.5 Structure diagram of BMS [50]

BMS are essential to protect the batteries from overcharging [51]. Overcharge is defined as charging the cell above maximum voltage given by the manufacturer (Fig. 1.6 [51]). The result of the overcharge is damage to the cells. Additionally, overcharge can be a result of keeping the charging voltage at the full charge voltage for a prolonged period of time (Fig. 1.6).
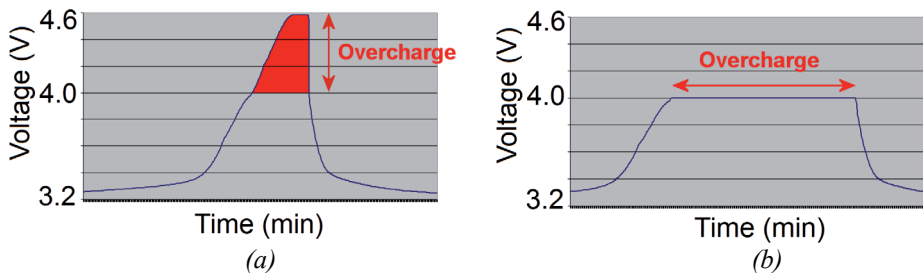
Fig. 1.6 Damaging of Li-ion batteries with overcharge by exceeding the maximum voltage (a) or keeping full charge voltage for long period of time (b) [51]

When charging multiple cells, it is necessary to have all of them to reach the full voltage, to make sure all of the cells in the battery pack have been charged to full. This way the battery pack will be fully charged. It is the task of the BMS with balancing function to keep the voltage of the cells within the proper voltage limits. Majority of the BMS systems with balancing, will simply "shunt" the fully charged cell(s), thus allowing the charging current to bypass the fully charged cell(s).

1.1.5 Prolonging options for batteries

The Li-ion battery works on ion movement between the positive and negative electrodes. In theory, such a mechanism should work forever, but cycling, elevated temperature and aging decrease the performance over time. The decrease of Li-ion battery pack cycle life is mainly due to the decrease of individual batteries capacity. The decrease of individual batteries capacity is mainly due to over-charge, over-discharge, applying high charging currents, high current discharge and over-temperature. High energy Li-ion cells have cycle lifetime up to 5000 full cycles. High power Li-ion cells may have cycle lifetime up to 1 million cycles (3.3 % depth of discharge (DOD)) [46].

Similar to a mechanical device that wears out faster with heavy use, so does DOD determine the cycle count. The shorter the DOD, the longer the battery will last. Partial discharge reduces stress and prolongs battery life as shown in Table 1.1 [52].

Table 1.1. Discharge cycles in relation to DOD [52]

Depth of discharge	Discharge cycles
100% DOD	300-500
50% DOD	1200-1500
25% DOD	2000-2500
10% DOD	3750-4700

Most Li-ion batteries are charged to 4.2 V/cell and every reduction of 0.1 V/cell is said to double cycle life as shown in Table 1.2 [52]. Over-charging stresses the battery and compromises safety.

Table 1.2. Discharge cycles in relation to charging voltage [52]

Charge level (V/cell)	Discharge cycles	Capacity at full charge
[4.3]	[150-250]	[110%]
4.2	300-500	100%
4.1	600-1000	90%
4.0	1200-2000	70%
3.92	2400-4000	50%

For prolonging batteries charging rate should not be faster than 1 C. Moderate charge rate of 0.7 C is preferred. This increases charging time and is controversy for the demand to charge faster in public places. Harsh discharges should be avoided as it adds stress to batteries [53].

1.1.6 Li-ion batteries for energy storing applications

Future distribution substations for microgrid applications require energy storing capability. For choosing a suitable energy storage technology, two main parameters must be kept in mind:
- specific energy – energy stored either in mass (gravimetric m_E) or in volume unit (volumetric V_E);
- specific power – available power per mass (gravimetric m_P) or volume unit (volumetric V_P).

A comparison between available storage technologies can be made based on a radar diagram as presented in Fig. 1.7 [54], which helps to sort out three main candidates for energy buffering in a distribution substation, namely Li-ion batteries (energy density 100-150 Wh/kg), flywheels (energy density 50-100 Wh/kg) and ultracapacitors (energy density 5 Wh/kg) [55].
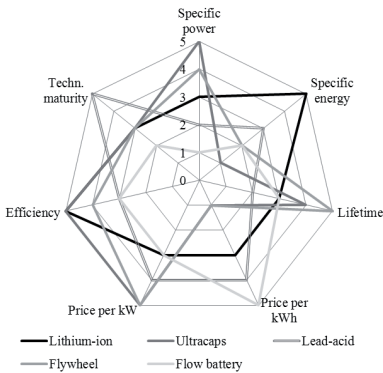
Fig. 1.7 Energy storage qualitative comparison [54]

Energy storage unit (ESU) in a distribution substation comprises of storage medium (SM) and interfacing power converter. The SM inside the distribution substation is charged from the grid and can be e.g. discharged through a distribution substation output bay to support fast charging of EV batteries. For e.g. if required ESU power $P_{ESU}(10\ min) \approx 41$ kW and required ESU energy $E_{ESU}(10\ min) \approx 6.8$ kWh. The necessary storage media required is compared in Table 1.3.

Table 1.3. Storage media for an i-MiEV 30 min fast charger

Storage medium	Necessary mass (kg)
Flywheel	68-137
Ultracapacitors	1367
Li-ion battery pack (high-energy)	46-68

With the present storage media state of art, the Li-ion ion batteries have obvious advantage before other options for the given energy storage application.

1.2 Charging methods for electric vehicles

1.2.1 On-board and off-board chargers for electric vehicles

Inevitably, batteries do discharge and need to be recharged with battery chargers. A battery charger is a device, where AC electric energy is converted into DC with an appropriate voltage level for charging the battery. Battery chargers control the charging process and therefore have a great impact to the condition and health of the battery.

Battery charging systems can be integrated either into the vehicle (on-board charger) or specially constructed charging station (off-board charger). On-board systems allow batteries to be recharged anywhere, where there is an electric outlet in present (e.g. home charging or charging at work with ground protection). The drawback with on-board charging systems is the limitation in their power output as their size and weight is restricted with vehicle design. Due to these restrictions it takes more time to recharge an EV battery compared to off-board systems. Off-board charging systems enable fast charging, where the vehicle is charged in less time. It is possible to charge a battery in 15-30 minutes with increasing battery's state of charge (SOC) from 20 % to 70-80 %. Off-board charging systems are limited in their power output only by the ability of batteries to accept higher charging currents. The drawback with off-board systems is the restriction with flexibility to charge at different locations. As off-board charging systems are big in size, they are quite costly solutions as investments have to be made into property.

Additional charging options include contactless inductive charging or battery replacement (swapping) services.

1.2.2 IEC 61851 charging modes and applications

Standards for EV charging is a widely discussed topic nowadays. There are existing different types of charging modes, different types of connectors and protocols. Japan, e.g. has the CHAdeMO standard for ultrafast DC charging, while in Europe, IEC 61851-x standard is still under discussion for EV charging as well as the IEC 62196-x standard for the charging connectors. According to the IEC 61851-1 standard there are 4 types of charging modes (Fig. 1.8) [56]:

- Mode 1 - slow charging from a household-type socket-outlet (Fig. 1.8 a));
- Mode 2 - slow charging from a household-type socket-outlet with an in-cable protection device (Fig. 1.8 b));
- Mode 3 - slow or fast charging using a specific EV socket-outlet with control and protection function installed (Fig. 1.8 c));
- Mode 4 - fast charging using an external charger (Fig. 1.8 d)).

The IEC 61851-1 standard documents the pilot signal flagging the charging requirements by using pulse width modulation. The pilot signal is integrated into the IEC 62196 plugs of EV charging equipment for controlling higher charging currents.

Fig. 1.8 Charging modes according to IEC 61851 [56]

For Mode 1 the electric outlet is non-dedicated, conventional household plug can be used. Earthing is essential for safety and a residual current device is mandatory. The charging mostly takes place with Single-Phase 230 V AC voltage, with maximum current of 16 A per phase, where the charging power is in the range of 3-11 kW. This type of normal AC charging has a long charging time (approximately 8 hours) and is usually done overnight. This is mainly due to a fact that domestic household plugs are usually designed up to 16 A (moreover the maximum continuous current is also limited up to 10-13 A). The basic converter is located inside car. This type of charging is relatively simple and cheap.

For Mode 2 the electric outlet is non-dedicated. An additional inline control box is required, which must be located near the plug or in the plug. The supply network side of the cable does not require a control pin (it is required only on the side of the EV) and the control function is governed by the control box in the cable. Cable contains an intermediate electronic device for control pilot and residual current device. These provisions allow charging stations to be with low complexity, while extending the permissible range of charging currents compared to Mode 1 charging. The charging mostly takes place with 3-phase 400 V AC voltage, with maximum current of 32 A per phase, where the charging power is in the range of 7.4-22 kW. Mode 2 is suitable for semi-public charging (e.g. in/outdoor office garages or car parking places).

For Mode 3 the electric outlet is dedicated, socket outlet specific for EV must be used (5 or 7 pins for EV connection). The mode is commonly known as AC fast charging. Mode 3 connectors according to IEC 61851-1 require a range of control and signal pins for both sides of the cable. EV power demand is regulated through the control pilot line modulating a pulse width modulation signal. Protection is realised with control pilot function. The charging station socket is dead, if no vehicle is present - the pilot pin in the plug on the charger side controls the circuit breaker. The charging mostly takes place with 3-phase 400 V AC voltage, with maximum current of 63 A per phase, where the charging power is in the range of 14-44 kW. The communication wire between car electronics and charging station allows integration into microgrid scenarios. This type of AC fast charging (semi-fast with charging power 6-10 kW, fast over 22 kW) takes approximately 2 hours. The drawback with such charging is the necessity of an advanced converter inside the car, which has a high weight. Mode 3 is also suitable for semi-public charging.

For Mode 4 the supply network AC power is converted in the charging station to DC, thus the mode is commonly known as DC fast charging. The electric outlet is dedicated, socket outlet specific for EV must be used. The plug type ensures that

only a matching electric vehicle can be connected to the off-board charging station. Control pilot function extends to equipment permanently connected to the supply. The charging mostly takes place with 500-600 V DC voltage, with maximum current of 400 A, where the charging power is in the range of 50-150 kW. This type of DC fast charging is ideal for public charging for quick top-ups of battery power. Charging takes approximately 30 min (e.g. for 25 kW battery). Mode 4 (and also Mode 3) charges the battery only to a certain degree (typically to 80 %). Fast charging does not allow final charging. The advantages with this type of charging is that only a basic converter is required inside the car, which has low weight. High power converter is located outside the car. Charging powers can go up to much higher values compared to the on-board charging. The drawbacks include expensive costs for high power charger and investments into infrastructure as higher powers are not available in domestic environment. Infrastructure consists of a filling station, specific charging hardware (charging station, plug, cable) and software (station's panel). Software must be able to identify the user, collect data from electricity meter, manage payment and billing, roaming, remote maintenance and load management.

With public fast charging risks are considerably higher than with AC low voltage home charging. The two main risks are in personnel safety and higher short circuit levels. Also connectors used in charging must be able to handle higher power levels. Charging has to be comfortable, have an easy-to-use human-machine-interface for operation, client must be easily authentified.

The initial signalling in IEC 61851 has the purpose of indicating the state of operation between the EV and the EVSE (see Table 1.4).

Table 1.4. States of operation between EV and charging station in IEC 61851

State A	No vehicle connected
State B	Vehicle connected, not ready for energy flow
State C	Vehicle connected, ready for energy flow, ventilation not required
State D	Vehicle connected, ready for energy flow, ventilation required
State E	Vehicle connected, charge spot fault
State F	Charge spot not available for action

1.2.3 CHAdeMO standard

"CHAdeMO" is an abbreviation of "CHArge de MOve", equivalent to "charge for moving", and is a pun for "O cha demo ikaga desuka" in Japanese, meaning "Let's have a tea while charging" in English [57]. CHAdeMO is a charging protocol for rapid DC charging issued from TEPCO (Tokyo Electric Power Company). Common type of charging is with 50 kW DC voltage. Max figures include DC output 62.5 kW, DC voltage 500 V, DC current 125 A. CHAdeMO does not work for current battery chemistries to much over 90 % SOC. Charging curves are typically 1.2 C – 4 C (up to 10 C).

High (ultra) voltage power grid can supply electricity to quick charger easily. If there are enough quick chargers in public areas, drivers will satisfy with small size

on-board chargers. Fig. 1.9 [58] represents a basic off-board charger, which consists of: main supply income (power grid), ground fault interrupter (GFI) between grid and charger, AC input filter, input rectifier (e.g. diode bridge), DC link, full or half bridge inverter, isolation transformer, output diode rectifier, output LC filter, ground fault interrupter (GFI) between charger and EV. Filter in AC part removes higher harmonics distortion to protect the power grid. Power factor corrector improves conversion efficiency and performance. Isolation transformer is necessary for separating battery circuit from the grid for operator protection against electric shock. Output LC filter reduces ripple noise from output current to protect battery system. Ground fault interrupters/earth leakage breakers (GFI/ELB) are for rapid response for earth leakage to protect operator from electric shock. One GFI/ELB is for monitoring charger's primary side of transformer and other for monitoring secondary side of transformer and vehicle.

Advanced off-board charger has in addition to basic configuration also bidirectional energy flow capability and additional energy storage device.

Fig. 1.10 [59] illustrates connector interface and Fig. 1.11 [59] illustrates charging sequence flowchart according to CHAdeMO standard. EV computer decides optimal charging current based on its battery condition (BMS observation). Charging current signal is sent to charger using CANbus and the quick charger sets supply DC current to meet the EVs command value (following order from EV computer). Additional analogue communication allows fail safe design. CHAdeMO quick charger can change charging speed to meet each batteries characteristics and condition. When charging speed is well controlled there is no negative influence to the lifetime of battery (battery must support fast charging). The more higher current the battery can absorb the more higher power it can receive.
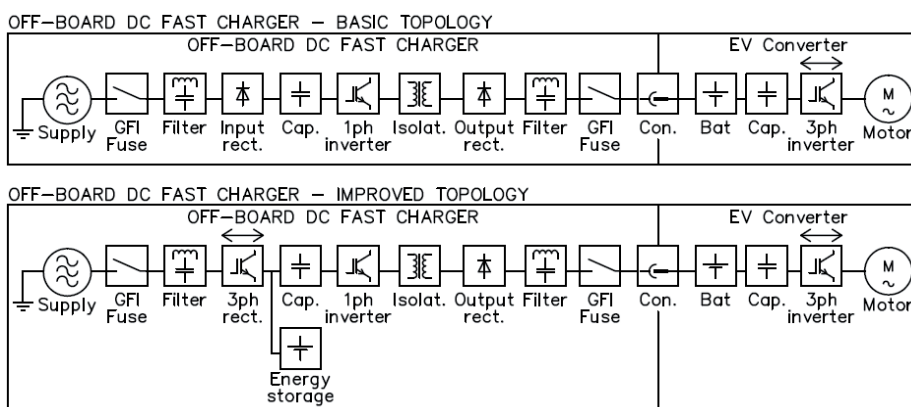
Fig. 1.9 Topologies of DC fast chargers according to CHAdeMO standard [58]

Initially the EV-ECU sends constant charging current command, which is set below the upper limit according to the temperature, to the quick charger. Then after the maximum cell voltage reaches the upper limit, the EV-ECU lowers the

charging current so that the maximum cell voltage can be kept at the limit. That is, CC-CV (constant current and constant voltage) charging method is applied [39].

The charger's power cabinet can be separate from the charging station or integrated with the charging station. When separated, there is less visual impact for customers. With multi-output topology there can be one common input section for all the charging converters. Incoming power can be reduced, if a simultaneity index is considered. Should there be only one charging station the one cabinet solution is cheaper.
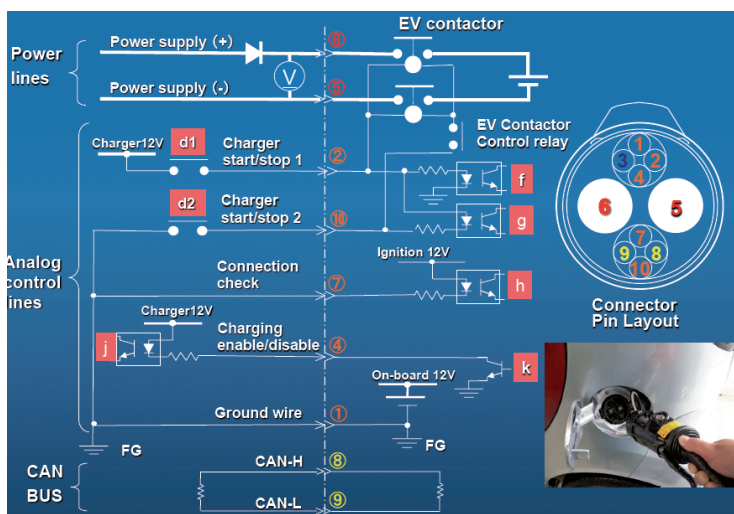
Fig. 1.10 Connector interface according to CHAdeMO standard [59]
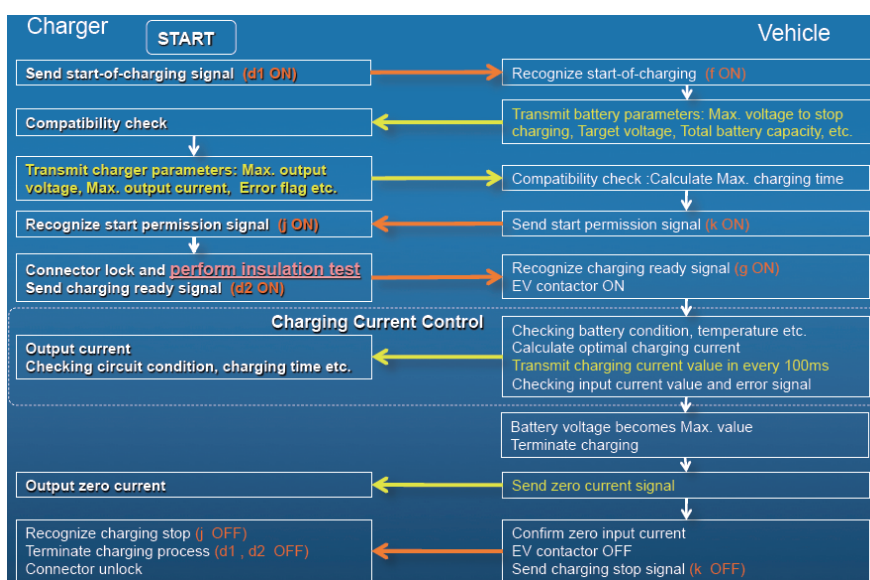
Fig. 1.11 Charging sequence flowchart according to CHAdeMO standard [59]

State of art charging of electric vehicles is made through unidirectional single DC fast charging stations. Charging stations are CHAdeMO standard compliant. Single charging stations are ideal choice when only a single vehicle needs to be charged at any given time. Typical charging times are between 15 and 30 minutes, making the stations suitable for business and commercial fleet owners, as well as light commercial vehicle fleet owners and utility infrastructure suppliers. Table 1.5 [60] and Fig. 1.12 present an example DC fast charging station of ABB type Terra 51.

Table 1.5. Technical specifications of ABB Terra 51 charge station [60]

Input	
AC power connection	3PH+N+PE
Input voltage range	400 V AC +/- 10 %
Nominal input voltage	400 V AC
Input frequency	50 Hz
Nominal input current	80 A
Nominal input power	55 kVA
Power factor (full load)	> 0,98
Efficiency	> 92 % at nominal output power
Output AC	
Maximum output power	22 kW
Maximum output current	32 A
Output voltage range	400 V AC
Output DC	
Maximum output power	50 kW
Maximum output current	120 A
Output voltage range	50-500 V DC
General	
DC connection standard	CHAdeMO compliant
DC plug type, cable length	JEVS G105, 2,5 m
Standby power consumption	100 VA (nominal, idle)
	1000 VA (max, climate control)
Operation noise level	< 45 dBA
Operating temperature	-30 $^{\circ}$C to +40 $^{\circ}$C

Fig. 1.12 State of art – unidirectional ABB Terra 51 charge stations near a distribution substation

1.2.4 Ultrafast charging stations

Ultrafast charging stations are capable of charging EVs in the timeframe of ~5 minutes [61]. Reported nano lithium-titanate batteries battery cells support 300 A fast charging [62]. To mitigate variances and peaks caused by high energy transfer rate and pulse-like load, an ultrafast charging station must be partially decoupled from the utility grid by the usage of intermediate energy buffers. A buffered EV charging station can be described as a three port entity with connection ports for the utility grid, electric vehicle and energy storage buffer (Fig. 1.13 [61]). This general conception is based upon the DC architecture with a common DC bus and each port characterised by power P_{gr}, P_{EV}, P_{st} (Fig. 1.13) as well as energy conversion and transmission efficiency η_{gr}, η_{EV}, η_{st}, (Fig. 1.13) respectively. The connection to utility grid is done in the MV level.
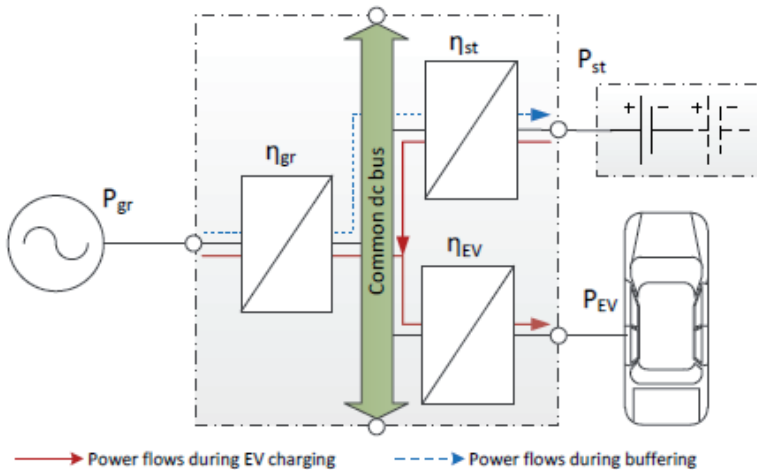
Fig. 1.13 Power flows in a buffered EV ultrafast charging station [61]

1.3 Standards and norms related distribution substations with V2G capability

1.3.1 Standard EN 50160 – voltage characteristics of electricity supplied by public electricity networks

Electrical energy is a product and, like any other product, should satisfy the proper quality requirements [63]. If electrical equipment is to operate correctly, it requires electrical energy to be supplied at a voltage that is within a specified range around the rated value. A significant part of the equipment in use today, especially electronic and computer devices, requires good power quality (PQ). However, the same equipment often causes distortion of the voltage supply in the installation, because of its non-linear characteristics, e.g. it draws a non-sinusoidal current with a sinusoidal supply voltage. Thus, maintaining satisfactory PQ is a joint

responsibility for the supplier and the electricity user. According to standard EN 50160 [64] the supplier is the party who provides electricity via a public distribution system, and the user or customer is the purchaser of electricity from a supplier. Standard IEC 61000 series includes limits for harmonic currents.

In standard EN 50160 several voltage parameters are defined. The most important are:

- *Supply voltage* – the rms value of the voltage at a given moment at the point of common coupling, measured.
- *Nominal voltage of the system (U_n)* – the voltage by which a system is designated or identified and to which certain operating characteristics are referred.
- *Declared supply voltage (U_c)* – is normally the nominal voltage U_n of the system. If, by agreement between the supplier and the user, a voltage different from the nominal voltage is applied to the terminal, then this voltage is the declared supply voltage U_c.
- *Normal operating condition* – the condition of meeting load demand, system switching and clearing faults by automatic system protection in the absence of exceptional conditions due to external influences or major events.
- *Voltage variation* – is an increase or decrease of voltage, due to variation of the total load of the distribution system or a part of it.
- *Flicker* – impression of unsteadiness of visual sensation induced by a light stimulus, the luminance or spectral distribution of which fluctuates with time.
- *Supply voltage dip/sag* – a sudden reduction of the supply voltage to a value between 90% and 1% of the declared voltage U_c, followed by a voltage recovery after a short period of time. Conventionally the duration of a voltage dip is between 10 ms and 1 minute. The depth of a voltage dip is defined as the difference between the minimum rms voltage during the voltage dip and the declared voltage. Voltage changes which do not reduce the supply voltage to less than 90% of the declared voltage U_c are not considered to be dips. The common cause for these types of failures are short circuits, faults to ground, transformer energizing inrush currents and connection of large induction motors. The consequence of voltage dips/sags are the disconnection of power electronic devices from the grid.
- *Supply interruption* – is a condition in which the voltage at the supply terminals is lower than 1% of the declared voltage U_c.
- *Transient overvoltages* – are oscillatory or non-oscillatory, highly damped, short overvoltages with a duration of a few milliseconds or less, originating from lightning or some switching operations, for example at switch-off of an inductive current.
- *Harmonic voltage* – a sinusoidal voltage with a frequency equal to an integer multiple of the fundamental frequency of the supply voltage.

- *Voltage unbalance* – is a condition where the rms value of the phase voltages or the phase angles between consecutive phases in a three-phase system are not equal.

Harmonic voltages can be evaluated:
- *individually* by their relative amplitude U_h related to the fundamental voltage U_1, where h is the order of the harmonic;
- *globally*, usually by the total harmonic distortion factor THD_U, calculated using the following expression [65]:

$$THD_u = \sqrt{\frac{\sum\limits_{h=2}^{40}(U_h)^2}{U_1}} \; . \tag{1}$$

Similarly harmonic currents can be evaluated globally [65]:

$$THD_i = \sqrt{\frac{\sum\limits_{h=2}^{40}(I_h)^2}{I_1}} \; . \tag{2}$$

Total Current Demand Distortion (TDD_i) is calculated harmonic current distortion against the full load (demand) level I_L of the electrical system [65]:

$$TDD_i = \frac{\sqrt{\sum\limits_{h=2}^{40}(I_h)^2}}{I_L} \; . \tag{3}$$

There are limits for the individual harmonics as well as THD in EN 50160. The limits are 10 minute average values and the harmonic content in the supply voltage must be kept below the limit for 95 % of time. The limits for individual harmonic voltages can be seen in Table 1.7. The limit for THD_u is 8%. In several studies it has been concluded that THD_u over 5% is not preferable [65].

EN 50160 gives the main voltage parameters and their permissible deviation ranges at the customer's point of common coupling in public low voltage and medium voltage electricity distribution systems (Table 1.6), under normal operating conditions [66]. In this context, LV means that the phase to phase nominal rms voltage does not exceed 1000 V and MV means that the phase-to-phase nominal rms value is between 1 kV and 35 kV.

Table 1.6. Supply voltage requirements according to EN 50160 [63]

Parameter	Supply voltage characteristics according to EN 50160
Power frequency (50 Hz)	LV, MV: mean value of fundamental measured over 10 s ±1% (49.5 - 50.5 Hz) for 99.5% of week -6%/+4% (47- 52 Hz) for 100% of week
Voltage magnitude variations	LV, MV: ±10% for 95% of week, mean 10 minutes rms values
Rapid voltage changes	LV: 5% normal, 10% infrequently, $P_{lt} \leq 1$ for 95% of week. MV: 4% normal, 6% infrequently, $P_{lt} \leq 1$ for 95% of week
Supply voltage dips	Majority: duration <1s, depth <60%. Locally limited dips caused by load switching on: LV: 10-50%, MV: 10-15%
Short interruptions of supply voltage	LV, MV: (up to 3 minutes) few tens - few hundreds/year. Duration 70% of them < 1s
Long interruption of supply voltage	LV, MV: (longer than 3 minutes) < 10-50/year
Transient overvoltages	LV: generally < 6kV, occasionally higher; rise time: ms - μs. MV: not defined
Supply voltage unbalance	LV, MV: up to 2% for 95% of week, mean 10 minutes rms values, up to 3% in some locations
Harmonic voltage	see Table 1.7

Table 1.7. Values of individual harmonic voltages at the supply terminals for orders up to 25, given in percent of U_n [63]

Odd harmonics				Even harmonics	
No multiples of 3		Multiples of 3			
Order h	Relative voltage (%)	Order h	Relative voltage (%)	Order h	Relative voltage (%)
5	6	3	5	2	2
7	5	9	1.5	4	1
11	3.5	15	0.5	6...24	0.5
13	3	21	0.5		
17	2				
19	1.5				
23	1.5				
25	1.5				

EN 50160 as principally informative and accept no responsibility when the limits are exceeded [63]. On the other hand, the consumer's point of view is usually totally different – they regard the limits given in EN 50160 as requirements that must be guaranteed by the supplier. However, as mentioned before, for many consumers, even fulfilling the requirements given in EN 50160 does not assure a satisfactory level of PQ. In such cases the level of PQ required must be defined in a separate agreement between supplier and consumer [63].

1.3.2 Standards related with distribution substations

Various standards are related with distribution substations. Standards specify requirements for prefabricated substations, MV and LV switchgears inside the substation and to other power devices inside the substation (Table 1.8).

The standard EN 62271-202 specifies the service conditions, rated characteristics, general structural requirements and test methods of HV/LV or LV/HV (HV – high voltage) prefabricated substations, which are cable-connected, to be operated from inside (walk-in type) or outside (non-walk-in type) for alternating current of rated voltages above 1 kV and up to and including 52 kV on the HV side, and for one or more transformers for service frequencies up to and including 60 Hz for outdoor installation in locations with public accessibility.

EN 61936-1 provides common rules for the design and the erection of electrical power installations in systems with nominal voltages above 1 kV AC and nominal frequency up to and including 60 Hz, so as to provide safety and proper functioning for the use intended. For the purpose of interpreting this standard, one of the electrical power installations is considered a substation (including substation for railway power supply).

EN 50522 is applicable to specify the requirements for the design and erection of earthing systems of electrical installations, in systems with nominal voltage above 1 kV AC and nominal frequency up to and including 60 Hz, so as to provide safety and proper functioning for the use intended.

EN 62271 standard series specify requirements and testing procedures for high-voltage switchgear and controlgear inside the distribution substations. EN 60255 standard series specify requirements for measuring relays and protection equipment.

EN 61439 standard series specify requirements and testing procedures for LV switchgear and controlgear assemblies inside the distribution substations.

Table 1.8. The most important standards related with distribution substations and switchgears, devices inside the distribution substation

Standard	Title
Distribution substation	
EN 50522:2010	Earthing of power installations exceeding 1 kV a.c.
EN 61936-1:2010	Power installations exceeding 1 kV a.c. - Part 1: Common rules
EN 62271-202:2007	High-voltage switchgear and controlgear – Part 202: High voltage/low voltage prefabricated substation
Medium voltage switchgear	
EN 60255 *series*	Measuring relays and protection equipment
EN 62271-1:2007	High-voltage switchgear and controlgear - Part 1: Common specifications
EN 62271-100:2009	High-voltage switchgear and controlgear - Part 100: Alternating current circuit-breakers (Addition of requirements and tests for 1100 and 1200 kV)
EN 62271-102:2002	High-voltage switchgear and controlgear - Part 102: Alternating current disconnectors and earthing switches
EN 62271-103:2011	High-voltage switchgear and controlgear - Part 103: Switches for rated voltages above 1 kV up to and including 52 kV
EN 62271-105:2003	High-voltage switchgear and controlgear - Part 105: Alternating current switch-fuse combinations for rated voltages above 1kV up to and including 52 kV
EN 62271-200:2012	High-voltage switchgear and controlgear - Part 200: AC metal-enclosed switchgear and controlgear for rated voltages above 1 kV and up to and including 52 kV
Low voltage switchgear	
LVD 2006/95/EC	Low voltage directive
EMCD 2004/108/EC	Electromagnetic Compability directive
EN 61439-1:2011	Low-voltage switchgear and controlgear assemblies - Part 1: General rules
EN 61439-2:2011	Low-voltage switchgear and controlgear assemblies - Part 2: Power switchgear and controlgear assemblies
EN 61439-3:2012	Low-voltage switchgear and controlgear assemblies - Part 3: Distribution boards intended to be operated by ordinary persons (DBO)
EN 61439-6:2012	Low-voltage switchgear and controlgear assemblies - Part 6: Busbar trunking systems (busways)
EN 60947-1:2007	Low-voltage switchgear and controlgear – Part 1: General rules
EN 60947-2:2006	Low-voltage switchgear and controlgear – Part 2: Circuit-breakers

Table 1.8. The most important standards related with distribution substations and switchgears, devices inside the substation (continued)

Standard	Title
EN 60947-3:2009	Low-voltage switchgear and controlgear – Part 3: Switches, disconnectors, switch-disconnectors and fuse-combination units
Enclosures of MV and LV switchgears	
EN 60529:2001	Degrees of protection provided by enclosures (IP Code)
EN 62262:2002	Degrees of protection provided by enclosures for electrical equipment against external mechanical impacts (IK code)
Devices related standards	
EN 60076 *series*	Power transformers
EN 60044 *series*	Instrument transformers

1.3.3 Standards related with electric vehicle infrastructure

Various standards are related with electric vehicle infrastructure (Table 1.9 and Table 1.10). IEC 61851-1:2010 applies to on-board and off-board equipment for charging electric road vehicles at standard AC supply voltages (as per IEC 60038) up to 1000 V and at DC voltages up to 1500 V, and for providing electrical power for any additional services on the vehicle if required when connected to the supply network. It includes characteristics and operating conditions of the supply device and the connection to the vehicle; operators and third party electrical safety, and the characteristics to be complied with by the vehicle with respect to the AC-DC. General Electrical vehicles charging modes 3 and 4, as defined in EN 61851, require dedicated supply and charging equipment incorporating control and communication circuits. Modes 1 and 2, as defined in EN 61851, can be achieved by connection of an electric vehicle to mains socket outlets.

The particular requirements contained in standard EN 60364-7-722 apply to:
- circuits intended to supply electric vehicles for charging purposes;
- protection for safety when feeding back electricity from the electric vehicles into the public supply network;
- inductive charging is not covered.

Requirements on the charging station assemblies are defined in the standard EN 61439-7:2011.

IEEE 1547 standard establishes criteria and requirements for interconnection of distributed resources (DR) with electric power systems (EPS).

V2G technology can be viewed as a system in which there is capability of controllable, bidirectional electric energy flow between a vehicle and the electric grid [26]. It should be noted that V2G would work if a vehicle had such capability, but most car manufacturers are still developing their own versions. E.g. there were no original equipment manufacturer (OEM) vehicles available to the general public

in the United States in September 2012 [26]. For utilities V2G would be attractive for two main reasons: as a storage medium and load-levelling sink for intermittent renewable energy and as means for fulfilling their grid support/ancillary services obligations. For vehicle owners motivation are reduced electric rates in the exchange with V2G or direct compensation. There are differing opinions about the importance of workplace charging at an employer's facility. It is difficult to predict what role the workplace charging will have in long term, but it will most certainly enable more commuters to venture longer distances on electric power if this recharge option is available. Fleet charging is similar to employer facility parking that it occurs at the work environment. Vehicle manufacturers face extremely difficult economic challenges in a highly competitive world market for automobiles. Sufficient scope or duration of testing has not yet been performed by industry or academia to provide supporting data that would minimize risks and remove or mitigate the barriers to adoption of V2G. This leaves the subject of V2G net benefits largely in the theoretical domain. Current V2G evaluations mostly are limited to the simpler "smart charging" control schemes that extend basic charging applications. Recommended test programs to fully evaluate V2G encompass three board areas of investigation: battery impact, network operation and system response [26].

IEC 15118 specifies the communication between EV and the EVSE. The purpose of IEC 15118 standard is to make a standard for scenarios that require advanced communication between the EV and charging stations. The communication parts of this generic equipment are the electric vehicle communication controller (EVCC) and the supply equipment communication controller (SECC). IEC 15118-1 provides a general overview and a common understanding of aspects influencing the charge process, payment and load levelling. In the first part (IEC 15118-1) which describes the use cases and terms and definitions following use case elements have been identified (Figure 1.14).

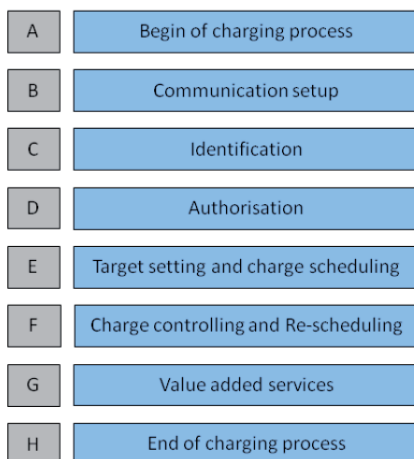| A	Begin of charging process
B	Communication setup
C	Identification
D	Authorisation
E	Target setting and charge scheduling
F	Charge controlling and Re-scheduling
G	Value added services
H	End of charging process

Fig. 1.14 IEC 15118-1 use case function groups

IEC 62196-1:2011 is applicable to plugs, socket-outlets, connectors, inlets and cable assemblies for electric vehicles (EV) intended for use in conductive charging systems which incorporate control means, with a rated operating voltage not exceeding: 690 V AC 50-60 Hz at a rated current not exceeding 250 A, 1500 V DC at a rated current not exceeding 400 A.

IEC 61851-23 sets requirements for DC electric vehicle charging station and IEC 61851-24 to control communication protocol between off-board DC charger and electric vehicle.

Table 1.9. Standards related with electric vehicle infrastructure

Standard	Title
IEC 61851-1:2010	Electric vehicle conductive charging system - Part 1: General requirements
EN 60364-7-722: 2012	Low voltage electrical installations - Part 7-722: Requirements for special installations or locations - Supply of electric vehicle
EN 61439-7:2011	Low-voltage switchgear and controlgear assemblies - Part 7: Assemblies for specific installations at public sites such as marinas, camping sites, market squares and similar applications and for charging stations for electrical vehicles
IEEE 1547	Standard for Interconnecting Distributed Resources with Electric Power Systems
IEC 15118-1:2013	Road vehicles - Vehicle to grid communication interface - Part 1: General information and use-case definition
IEC 62196-1: 2011	Plugs, socket-outlets, vehicle connectors and vehicle inlets - Conductive charging of electric vehicles

Table 1.10. Standards under development

Standard	Title
IEC 61851-23	Electric vehicle conductive charging system - Part 23: DC electric vehicle charging station (1000 V DC, 400 A)
IEC 61851-24	Electric vehicle conductive charging system - Part 24: control communication protocol between off-board DC charger and electric vehicle

Following standards addressing plug in electric vehicles: SAE J1772-3 (Electric Vehicle and Plug in Hybrid Electric Vehicle Conductive Charge Coupler), SAE J2836-1 (Use Cases for Communication Between Plug-in Vehicles and the Utility Grid), SAE J2847-1 (Communication between Plug-in Vehicles and the Utility Grid), SAE J2293 (Communications between plug-in electric vehicles and electric vehicle supply equipment for direct current energy).

1.3.4 Standards related with Smart Grids

The Smart Grid will ultimately require hundreds of standards. In the development of Smart Grids there are six key functionalities required plus cybersecurity and network communications. These functionalities are especially critical to ongoing and near-term deployments of Smart Grid technologies and services. The six key functionalities are [29]:

- Demand response and consumer energy efficiency (e.g. cut energy use during times of peak demand);
- Wide-area situational awareness (e.g. monitoring and display of power-system components and performance across interconnections in near real time);
- Energy storage (e.g. distributed storage to benefit the entire grid);
- Electric transportation (e.g. enable large-scale integration of EVs);
- Advanced metering infrastructure (e.g. create a two-way network between advanced meters and utility business systems);
- Distribution grid management (e.g. maximizing performance of feeders, transformers and other components of network distribution systems and integrating them with transmission systems and customer operations).

Anticipated Smar Grid benefits for a modernized national electric grid [29]:

- Improves power reliability and quality;
- Optimizes facility utilization and averts construction of backup (peak load) power plants;
- Enhances capacity and efficiency of existing electric power networks;
- Improves resilience to disruption;
- Enables predictive maintenance and "self-healing" responses to system disturbances;
- Facilitates expanded deployment of renewable energy sources;
- Accommodates distributed power sources;
- Automates maintenance and operation;
- Reduces greenhouse gas emissions by enabling EVs and new power sources;
- Reduces oil consumption by reducing the need for inefficient generation during peak usage periods;
- Presents opportunities to improve grid security;
- Enables transition to EVs and new energy storage options;
- Increases consumer choice;
- Enables new products, services, markets and consumers access to them.

Among the potential benefits of the Smart Grid, consumers see three as being "best benefits" [29]:

- Detect power outages;
- Reduce voltage sags;
- Integrate renewable energy sources.

Large, integrated, complex systems require different layers of interoperability, from a plug or wireless connection to compatible processes and procedures for participating in distributed business transactions [29]. Referred to as the "GWAC stack," the eight layers shown in Fig. 1.15 [29] comprise a vertical cross-section of the degrees of interoperation necessary to enable various interactions and transactions on the Smart Grid. Very simple functionality - such as the physical equipment layer and software for encoding and transmitting data - might be confined to the lowest layers. Communication protocols and applications reside on higher levels with the top levels reserved for business functionality. As functions and capabilities increase in complexity and sophistication, more layers of the GWAC stack are required to interoperate to achieve the desired results. Each layer typically depends upon—and is enabled by—the layers below it.
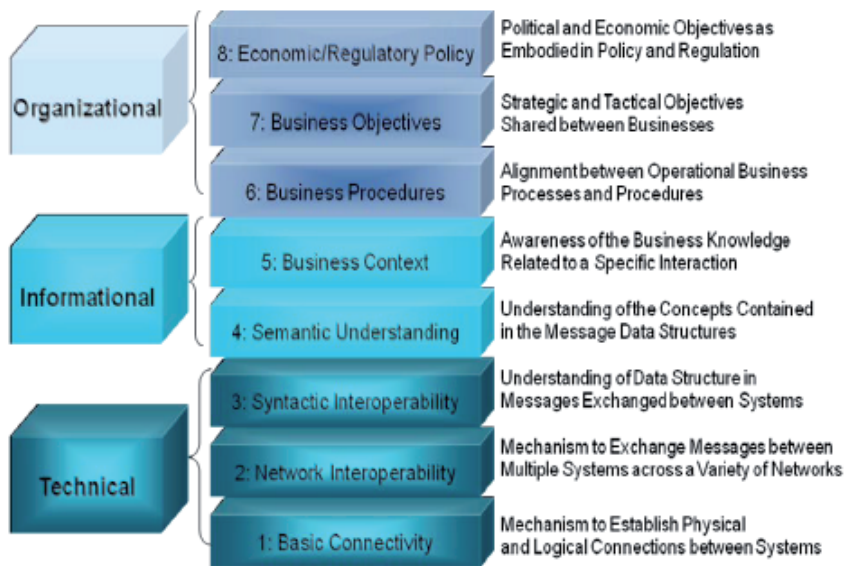

Fig. 1.15 The GridWise Architecture Concil's (GWAC) eight-layer stack provides a context for determing Smart Grid interoperability requirements and defining exchanges of information [29]

The conceptual model for describing Smart Grids provide a high-level, overarching perspective of a few major relationships that are developing across the Smart Grid domains. It is not only a tool for identifying actors and possible communications paths in the Smart Grid, but also a useful way for identifying potential intra- and inter-domain interactions, as well as the potential applications and capabilities enabled by these interactions. Architecture documentation goes much deeper than illustrated in Fig. 1.16 [29], but stops short of specific design and implementation detail. In other words, the conceptual model is descriptive and not prescriptive. It is meant to foster understanding of Smart Grid operational intricacies but not meant to prescribe how a particular stakeholder will implement the Smart Grid.
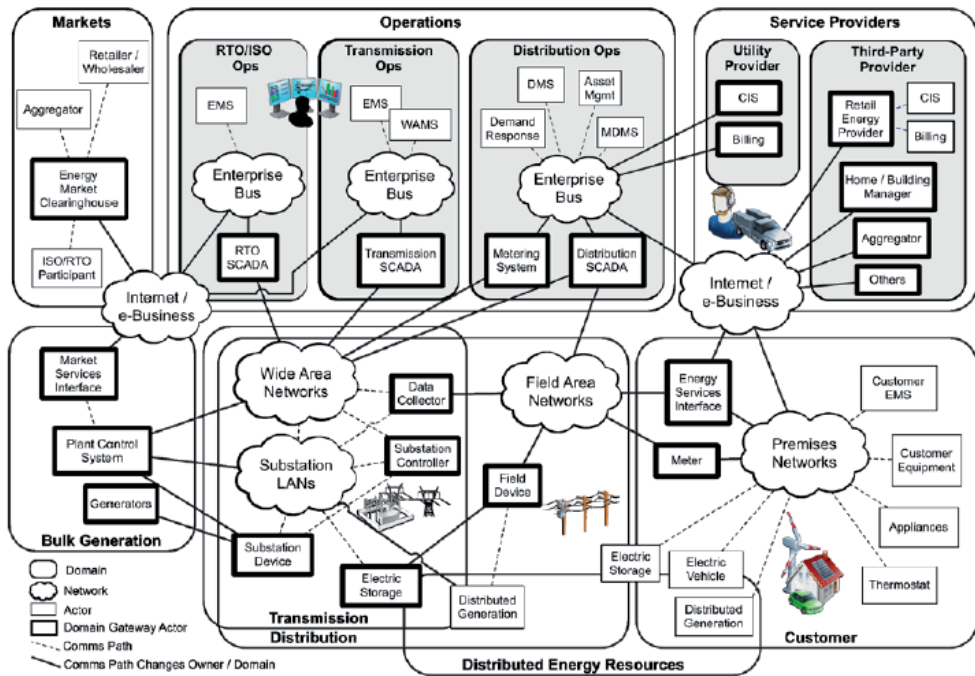
Fig. 1.16 Conceptual Reference Diagram for Smart Grid Information Networks [29]

On March 1st 2011, The European Commission issued a Mandate (M/490 EN) for Smart Grids standards to the European Standardization Organizations [67]. Through this mandate, the EC requested CEN, CENELEC, and ETSI to develop or update a set of consistent standards within a common European framework of communication and electrical architectures and associated processes, that will enable or facilitate the implementation in Europe of the different high level Smart Grid services and functionalities as defined by the Smart Grid Task Force that will be flexible enough to accommodate future developments. Building, Industry, Appliances and Home automation are out of the scope of this mandate; however, their interfaces with the Smart Grid and related services have to be treated under this mandate. The report intends to build a first list of standards, enabling or supporting the deployment of Smart Grid systems in Europe. The Smart Grid Architecture Model (SGAM) framework and its methodology are intended to present the design of Smart Grid use cases in an architectural but solution and technology-neutral manner. The SGAM framework Fig. 1.17 [67] is established by merging the concept of the interoperability layers Fig. 1.18 [67] with the introduced Smart Grid plane. This merge results in a model, which spans three dimensions (X: Domain, Y: Abstract Interoperability (Layer); Z: Zone).
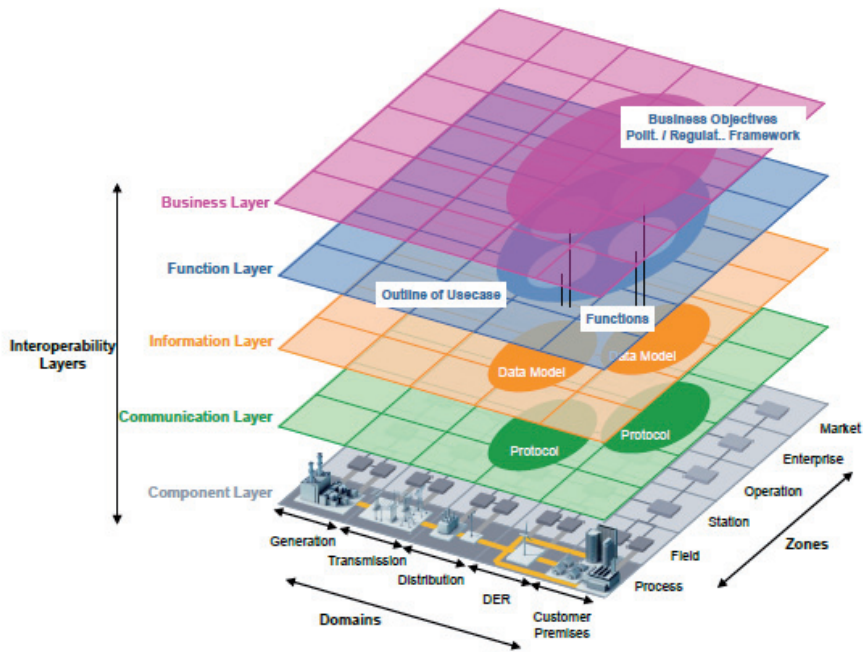
Fig. 1.17 The SGAM Framework [67]
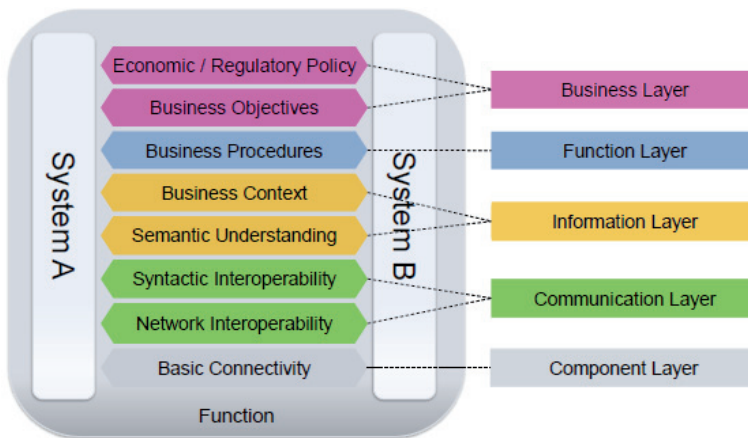
Fig. 1.18 Grouping into interoperability layers [67]

The Substation Automation System (SAS) refers to the system and all the elements needed to perform automated operation of a substation, and of connected assets (grid lines, loads etc) [67]. The typical considered operations are protection functionalities, automatic equipment control for network reconfiguration, including possibly feeder reconfiguration, automatic power quality regulation etc. Substation automation system may also act as a remote terminal for upper levels of grid monitoring and control for operation (monitoring & control) and/or maintenance.

Some of the capabilities are fully automatic, i.e. are providing a spontaneous response of the system triggered by external events. Some others are in support of remote and/or manual operation [67]. Use case clusters specified for SAS are [67]:

- Protecting grid assets (e.g. bay, transformer);
- Monitoring the grid flows (e.g. electric flow, power quality);
- Maintaining grid assets (e.g. support periodic maintenance);
- Controlling the grid (locally, remotely, manually, automatically);
- Managing power quality (e.g. VAR regulation);
- Reconfiguring the network in case of fault (e.g. support reclosing sequence);
- Provide and collect contractual measurements (e.g. revenue purpose);
- Connect an active actor to the grid;
- Blackout management (e.g. restore power after black-out);
- System and security management (e.g. discover a new component in the system).

The substation automation component architecture (Fig. 1.19 [67]) is mostly made of 3 zones of components, which may be interconnected through wires or communication. The Process zone includes the primary equipment of the substation mainly switching (i.e. circuit-breakers, switches and disconnectors), power transformer regulator and measuring elements (i.e. current and voltage sensors/transformers). The Field zone includes equipment to protect, control and monitor the process of the substation, mainly through IEDs, and controllers. The Station zone supports the aggregation level which interface with other elements and systems of the electrical network. It is mostly supporting 4 main technical functions, which can be grouped or separated in different components, which are: RTU (remote terminal unit), HMI (human machine interface), Controller, Communication (router). Communication protocols (Fig. 1.20 [67]) can be used either (within the substation or outside the substation). The information layer of substation automation (Fig. 1.21 [67]) is mostly based on the IEC/EN 61850 information model (e.g. EN 61850-7-420).
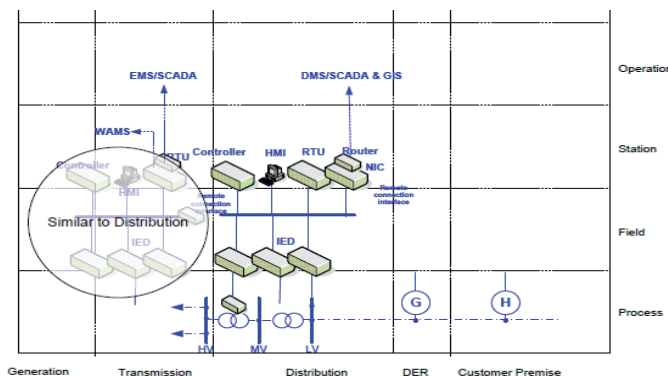
Fig. 1.19 Substation automation system – component layer [67]
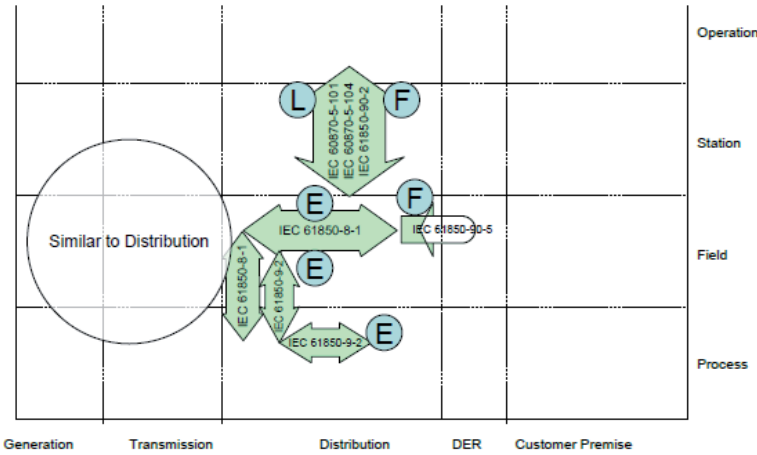
Fig. 1.20 Substation automation system – communication layer [67]
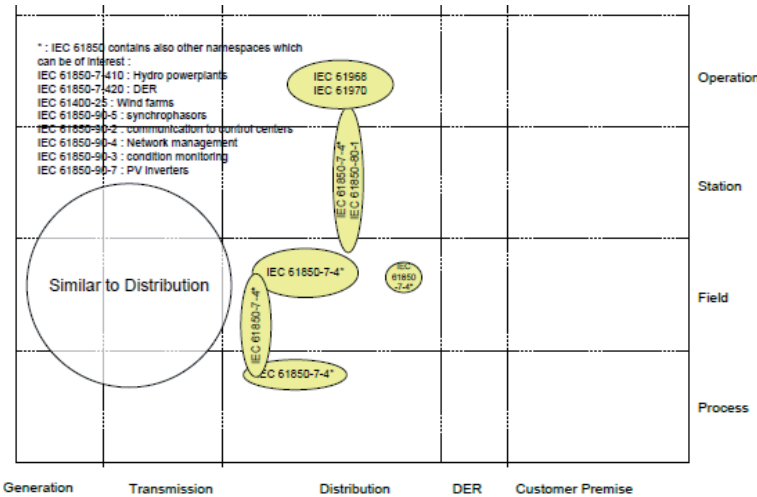
Fig. 1.21 Substation automation system – information layer [67]

A Feeder automation system [67] refers to the system and all the elements needed to perform automated operation of components placed along the MV network itself (bays). Systems standard mapping for E-mobility comprises all elements and interfaces which are needed to efficiently operate Electric Vehicles as a flexibility resource in a future Smart Grid system. The Standardization work within the E-mobility domain is currently on-going under the leadership of the E-Mobility co-ordination group (EM-CG), and a working group for Smart Charging was specifically built-up to define role model, associated use cases and to identify standards for E-mobility. In order to avoid duplication or even divergence, this section of the current FSS report will consequently remain empty [67].

OpenNode project [68] focuses on the electrical distribution grid operation and explores answers on the challenges introduced:
- how can be improved the distribution grid monitoring to cope with unstable states in the grid;
- how can be integrated the "smart" substation automation devices to increase the efficiency of the distribution grid;
- how can be inter-operated with the different roles e.g. smart meters maintenance, grid operation, etc.

OpenNode's R&D efforts converge in the creation of an open *Secondary Substation Node* (SSN in Fig. 1.22 [68]) as an essential control component of the smart distribution grid, a *Middleware* (MW) to couple the SSN operation with the Utility systems for grid operation and a modular standard-based *Communication Architecture* to grant the flexibility required by the stakeholder diversification and to cope with massively distributed embedded systems in the distribution grid. OpenNode brings together the two main aspects of future smart distribution grids: the communication with customer meters supported by the use of standardized protocols such as DLMS/COSEM; the metering infrastructure goes hand in hand with automation of the distribution network, using legacy (IEC 60870-5-104) and future-oriented protocols (IEC 61850). SSN is a link between the Metering Devices and the control system / the Middleware. The typical use case is where utility asks MW smart meter data, MW request reading order of one smart meter from SSN, SSN reads metering data, smart meter answers to SSN, SSN transmits data to MW and MW transmits data to utility operator.
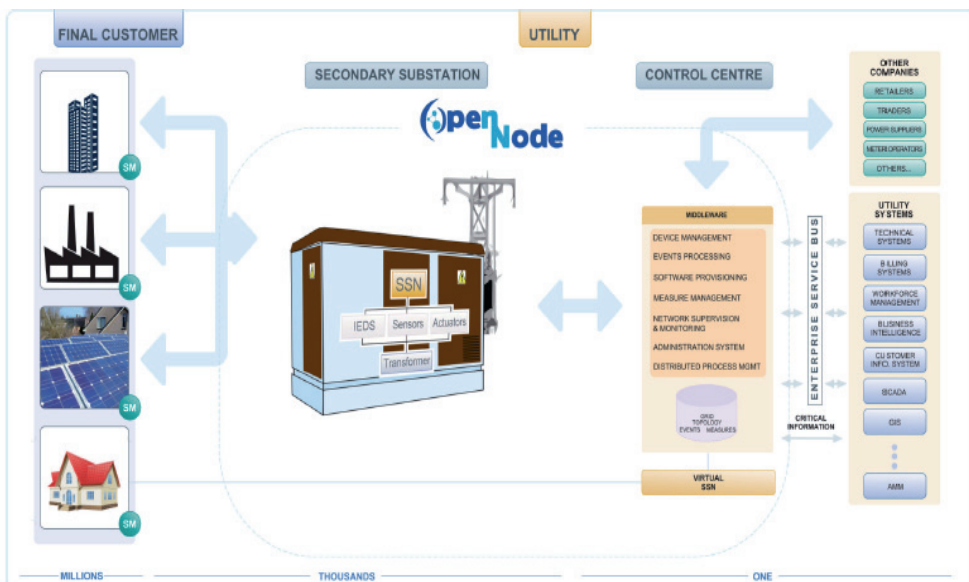

Fig. 1.22 Overall framework of OpenNode [68]

The problems for integrating EVs for Smart Grid applications can be summarized in the proposal of international collaborative project (Tallinn University of Technology also participates in the new consortium) FP7-ICT-2013-11 under the 7th framework programme [30]:

-   Exploration of different architectures for the Smart Grids, in particular the alternatives presented by different levels of microgrids and virtual power plants by the active distribution grids/networks;
-   Analyze the trade-off possibilities offered by scalable microgrids in the various architectural alternatives explored;
-   Study, develop control and optimisation schemes for the microgrid central controller at the MV/LV substation automation system;
-   Develop novel schemes for the interactions between the distribution grid and the Microgrids or VPPs based on emerging or anticipated standards;
-   Evaluate the performance of these schemes for selected architectures in laboratory environments.

A key underlying objective in the abovementioned objectives is the elaboration of an appropriate control architecture (or layered services architecture) supporting the bottom-up system organization, and allowing the (autonomous) prosumers (union of words producer and consumer [140]) to create clusters at various aggregation layers, thereby allowing dynamic reconfiguration, which will allow for scalability.

1.4 Communication protocol IEC 61850

Communication between intelligent electronic devices (IEDs) of the next generation should be realized in the next generation substations with the IEC 61850 protocol as much as applicable. The standard IEC 61850 "Communication Networks and Systems in Substations" is the first and only global standard that considers all the communication needs within a substation [69]. The IEC 61850 standard defines the complete communications architecture for a station and a process bus. The IEC 61850 standard offers high-level interoperability, free configuration, overall cost saving, and simple architecture. The IEC 61850 uses Ethernet as the basic communication technology, currently with a speed of 100 MBit/s at the intelligent electronic devices (IEDs). Support of message priorities (QoS protocol) by managed switches allows time critical requirements, such as the 3 ms application to the application transfer time, to be met.

A typical high voltage substation architecture is shown in Fig. 1.23 [70]. The substation network is connected to the outside wide area network via a secure gateway. Outside remote operators and control centres can use the abstract communication service interface (ACSI) defined in IEC 61850 Part 7-2 to query and control devices in the substation. There are one or more substation buses connecting all the IEDs inside a substation. A substation bus is realized as a medium bandwidth Ethernet network, which carries all ACSI requests/responses and generic substation events messages (GSE, including GOOSE and GSSE). There is another kind of bus called process bus for communication inside each bay.

A process bus connects the IEDs to the traditional dumb devices (e.g. merge units) and is realized as a high bandwidth Ethernet network. A substation usually has only one global substation bus but multiple process buses, one for each bay [70].
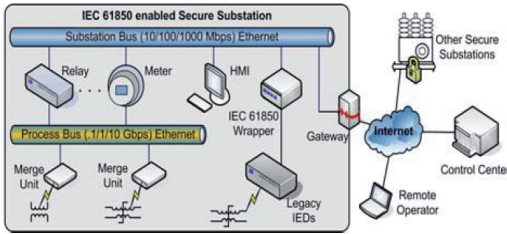
Fig. 1.23 An example substation architecture [70]

ACSI requests/responses, GSE messages and sampled analogue values are the three major kinds of data active in the substation network [70]. Interactions inside a substation automation system mainly fall into three categories: data gathering/setting, data monitoring/reporting and event logging [70]. The former two kinds of interactions are the most important – in the IEC 61850 standard all inquiries and control activities towards physical devices are modelled as getting or setting the values of the corresponding data attributes, while data monitoring/ reporting provides an efficient way to track the system status, so that control commands can be issued in a timely manner. To realize the above kinds of interaction, the IEC 61850 standard defines a relatively complicated communication structure, as is shown in Fig. 1.24 [71]. Five kinds of communication profiles are defined in the standard: the abstract communication service interface profile (ACSI), the generic object oriented substation event profile (GOOSE), the generic substation status event profile (GSSE), the sampled measured value multicast profile (SMV), and the time synchronization profile. ACSI services enable client-server style interaction between applications and servers. GOOSE provides a fast way of data exchange on the substation bus and GSSE provides an express way of substation level status exchange. Sample measured value multicast provides an effective way to exchange data on a process bus [70].

Fig. 1.24 IEC 61850 protocol mapping [71]

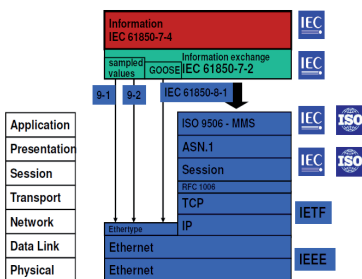The hierarchical data model defined in the IEC 61850 is depicted in Fig 1.25 [71]. Server is the topmost component in this hierarchy [70]. It serves as the joint point of physical devices and logical objects. Theoretically one IED may host one or more server instances, but in practice usually only one server instance runs in an IED. A server instance is basically a program running in an IED, which shares the same meaning with other servers like FTP server etc. Each server has one or more access points. When a client is to access data or service of the server, it should connect to an access point of this server and establish a valid association. Each server hosts several files or logical devices. Clients can manipulate files in the server like talking to a FTP server, which is usually used as a means to upload/update the configuration file of an IED [70].

A logical device is the logical correspondence of a physical device [70]. It is basically a group of logical nodes performing similar functions. Functions supported by an IED are conceptually represented by a collection of primitive, atomic functional building blocks called logical nodes. The IEC 61850 standard predefines a collection of template logical nodes as presented in Fig. 1.26 [71].

Data exchanged between logical nodes are modelled as data objects [70]. A logical node usually contains several data objects. Each data object is an instance of the DATA class and has a common data class type (Fig. 1.27 [71]). Similar to the concept of objects in most object-oriented programming languages, a data object consists of many data attributes, which are instances of data attributes of the corresponding common data class [70].
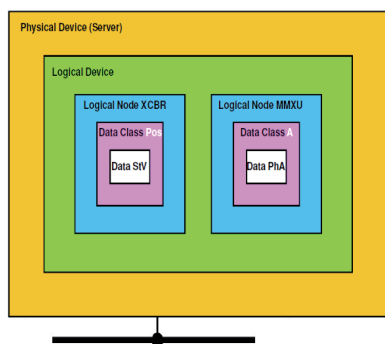
Fig. 1.25 Logical groupings – devices, nodes, classes and data [71]

Substation automation (SA) is used for controlling, protecting and monitoring substations [72]. At least from a logical point of view, SA systems comprise three levels, the station level (with the substation host, the substation HMI and the Gateway (GW) to the remote Network Control Centre (NCC)), the bay level (with all the control and protection units) and the process level (with more or less intelligent process interfaces to the switchgear (Fig. 1.28 [72]). Extended implementations show all three levels equipped with IEDs, where for example a conventional RTU comprises all three levels in one unit. All implemented levels are interconnected by serial communication links. There is not only vertical

communication between the levels (e.g. between bay and station level), but also horizontal communication within the level (e.g. in the bay level between bay units for functions like interlocking).

Logical node groups		Number of logical nodes
System logical nodes	L	3
Protection functions	P	28
Protection related functions	R	10
Supervisory control	C	5
Generic references	G	3
Interfacing and archiving	I	4
Automatic control	A	4
Metering and measurement	M	8
Sensors and monitoring	S	4
Switchgear	X	2
Instrument transformer	T	2
Power transformer	Y	4
Further power system equipment	Z	15
Total number of logical nodes		92

PDIR — Directional element
PHAR — Harmonic restraint
PSCH — Protection Scheme
PTEF — Transient Earth Fault
PZSU — Zero speed or underspeed
PDIS — Distance protection
PVPH — Volts per Hz relay
PTUV — Undervoltage
PDOP — Directional over power
...more

MMXU — Measuring (Measurand unit)
MMTR — Metering
MSQI — Sequence and Imbalance
MHAI — Harmonics and Inter-harmonics
MDIF — Differential Measurements
...more

XCBR — Circuit Breaker
XSWI — Circuit Switch

Fig. 1.26 Logical nodes – 92 logical node classes [71]
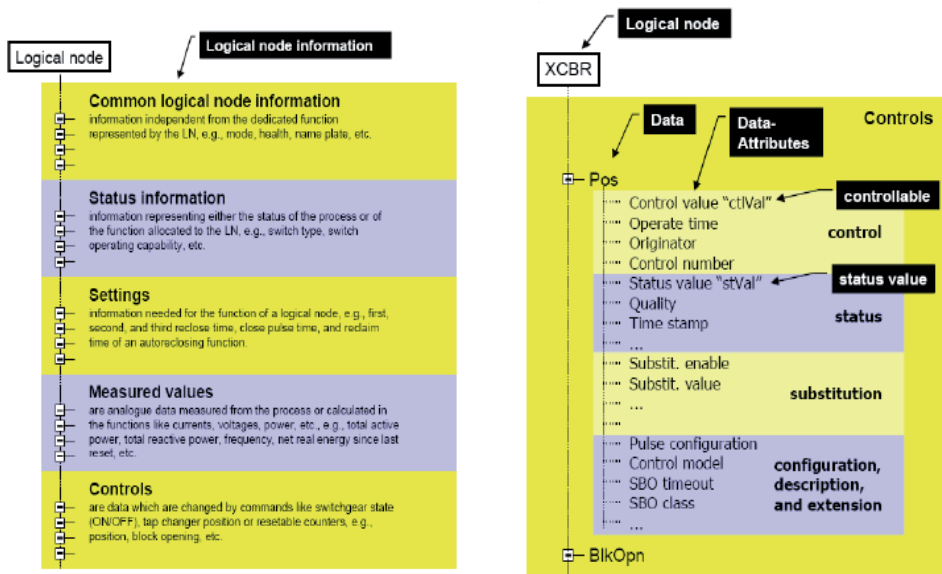
Fig. 1.27 Data classes and example [71]
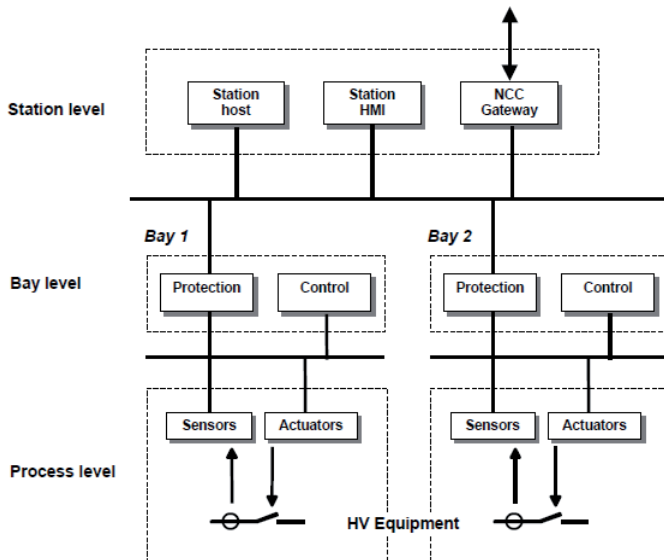
Fig. 1.28 Logical scheme of the three levels of a substation automation system [72]

Tree and ring communication topologies are possible with the switches [72]. Examples of substation systems with the same functionality but with different performance requirements are given in Fig. 1.29 [72]. For some level of communication availability, response time and cost, the star type solution may be acceptable, for an higher level in communication availability, the ring with its given ring-redundancy (in case of loosing one switch only one bay is affected) is the proper solution. The substation functionality of both architectures is exactly the same.
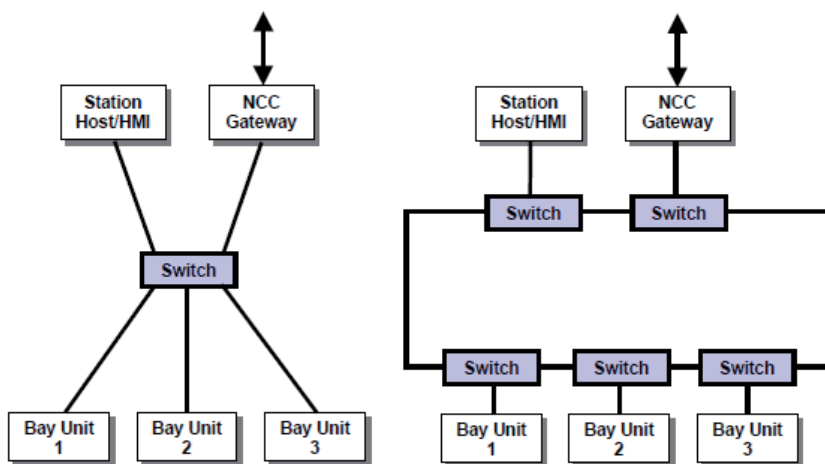
Fig. 1.29 Substation communication architecture with star type (left) and ring type (right) [72]

1.5 Distribution substations

1.5.1 Distribution substations for energy distribution

Substations are used to transmit electrical energy, distribute power and step up or down the voltage. Transformer substations for MV grids (typically 6-24 kV) transform 3-phase medium voltage to 3-phase AC low voltage (typically 400 V).

The simplest substation [73] for an MV grid consists of an MV load switch, a transformer and fused switches connected directly to the secondary side of the transformer distribution busbar to protect consumers (Fig. 1.30 [73]). The substation is optionally equipped with current transformers, an energy measurement device, surge arresters and devices for self-consumption of the substation (SCS, e.g. lighting, socket connections).

Fig. 1.30 Example layout of 1000 kVA non walk-in prefabricated metal enclosure substation (with MV section – 1; transformer section – 2; LV section – 3) [73]

Distribution substations [73] consist of an MV distribution switchgear (SF6 or vacuum air breaking technology), a transformer, a low voltage (LV) distribution switchgear (with a main supply circuit breaker and fused switches for outgoing feeders), self-consumption (SCS) and as an option a remote terminal unit (RTU). Energy meters are placed to the MV and LV side according to substation specifications. Depending on the construction, the substations are equipped with one or two transformers (Fig. 1.31).

In the case of two transformers, the substation is equipped with either manual bus coupler or for ensuring higher reliability with an automatic transfer switch system (ATS) for uninterruptible power supply (Fig. 1.31). In normal operation, both transformers ("TR1" and "TR2") distribute energy to AC consumers. Transformers are separated from each other through bus coupling switch "LVBC". In case of supply interruption, bus coupling switch will connected all consumers to one of the operating transformers and disconnects the interrupted circuit's low voltage side main circuit breaker ("LVCB1" or "LVCB2"). The switching is controlled through ATS. The ATS system can be designed on relay connections or smaller logical controller. The ATS status signals can be connected with RTU.
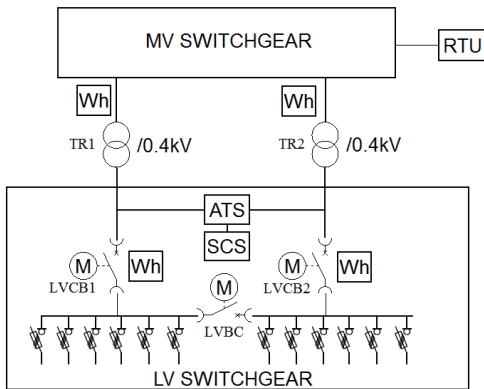
Fig. 1.31 Example of simplified topology of modern distribution substations with two incoming transformers

The modern distribution substations for the MV grid deliver energy in one direction (from the grid to the consumers). Outgoing feeders are not equipped with smart energy meters. Energy meters in the MV and LV side are for commercial purposes and do not include control functions. Communication in substations is made either by the conventional parallel copper wiring or by a private serial communication system through the RTU interface to the remote network control or to an operator's work place of HMI at station level. Remote terminal units are for remote supervision or with limited remote control. RTU transfers typically control signals (e.g. MV circuit breakers in or out), position signals (e.g. position of breakers and earthing switches, security and fire alarms), measuring values (e.g. current, voltage, active and reactive power, short circuit fault location). The structure of these substations does not allow connecting prosumers or several charging stations for electric vehicles with them.

1.5.2 Substations for energy storage

At its heart, energy storage is an economic decision [74]. Without storage, an industry must develop and maintain an entire delivery network capable of meeting the highest peak of the year at any given moment. Without storage, the industry must operate within a "just in-time" framework that is dependent not only on variable end-use demands, but is also completely at the mercy of one of the most uncontrollable variables known: weather. With storage, the owners only must build out what is necessary to carry a heavy, but normal load – resulting in a much higher utilization of the existing equipment, and hence a higher return on their investments (ROI). Energy storage can help reduce the costs associated with building new electric infrastructure, whether in the form of generating facilities (power sources), transmission lines (power grids), or substation improvements [75] to meet peak demand. Costs for such improvements can be delayed in many cases, reduced in others, and sometimes completely eliminated. Storage can also provide enough power to maintain operations until systems can be shut down in an orderly

fashion or provide enough power until other on-site generation sources come on-line. With the incorporation of energy storage into the grid, the utility sector and customers can expect reduced financial losses due to outages and poor power quality. Although electricity cannot be directly stored (cheaply), it can be easily stored in other forms and converted back to electricity when necessary (Fig. 1.32 [76]).
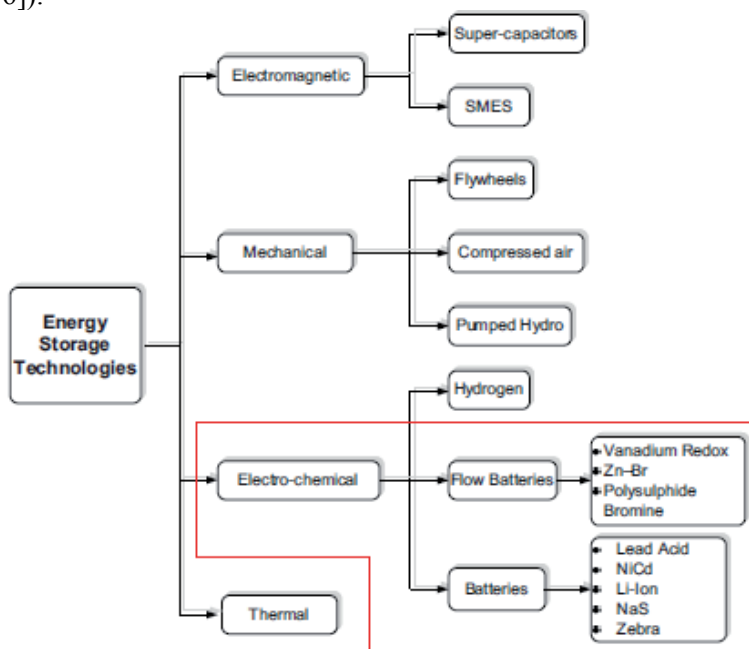
Fig. 1.32 Classification of energy storage technologies [76]

Substation for energy storage is called Energy Storage Module (ESM), which is a packaged solution that stores energy for use at a later time [4]. The energy is usually stored in batteries for specific energy demands or to effectively optimize cost. ESM can store electrical energy and supply it to designated loads as a primary or supplementary source. It provides a stable and continuous power supply regardless of the supply source status. Voltage and frequency regulation can also be improved by using ESM modules. ESM contains inverters that rectify the AC energy into DC to store in the batteries and then invert the DC energy into AC energy [4].

ESM is an integrated system of power equipment such as transformers, low and medium voltage switchgear together with automation equipment such as inverters in a galvanized steel enclosure. An example ESM from ABB is illustrated in Fig. 1.33 [4]. The energy inverted into AC power can be connected to the electrical network at LV (<1000 V) or MV (<40.5 kV). ESM are typically available in several capacities with individual modules up to 4 MW and an output voltage range from 120 V to 40.5 kV at 50 or 60 Hz, single or three phase system [4].
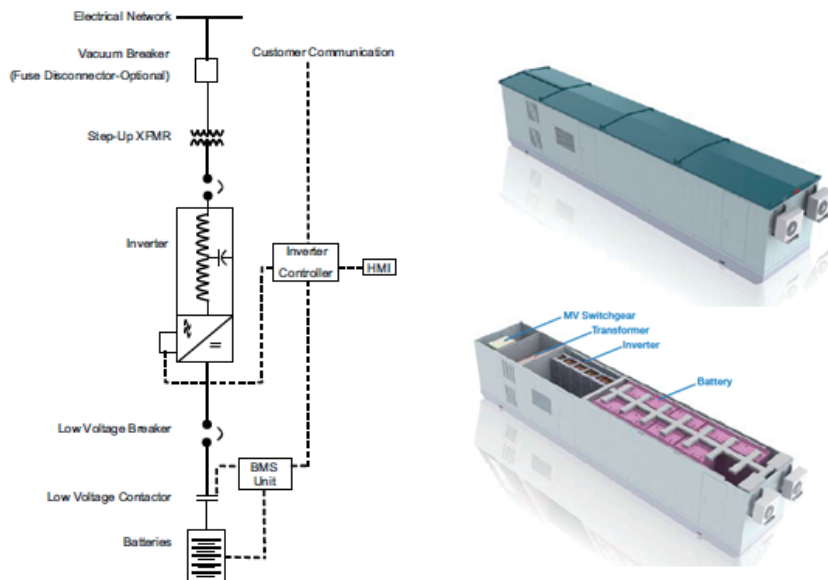
Fig. 1.33 Example single line diagram (left) and layout (right) of a three-phase ESM of ABB ESM 1000 kW/250 kWh [4]

ESM has different applications within the distribution network aiming to improve the quality and continuity of the power at optimal cost. The main applications of the ESM are [4]:

- *Load shifting / time of use management* – the practice of altering the pattern of energy use so that on-peak energy use is shifted to off-peak periods. Reduces the cost of energy by charging the system with low priced energy and discharging later when the energy prices are high. Shifts renewable generation to peak times, allowing for participation in capacity markets as a dispatchable resource, smoothing the renewable output.
- *Peak shaving* – peak shaving is related to load shifting. Both are part of the demand management in which the ultimate goal is to increase the load factor. Commercial and industrial customers reduce their energy charges by improving their load factor. Utilities reduce the operational cost of generating power during peak periods (reducing the need for peaking units). Investment in infrastructure is delayed because they have latter loads with smaller peaks.
- *Balance of power by renewable energy smoothing or ramp control* – reduces the impact of quick changes in renewable generation levels. It can be used to ensure that wind-farm ramp-rates (MW/min) are kept within design limits and to eliminate rapid voltage and power swings on the electrical grid.
- *Renewable capacity firming* – helps maintain the power output at a committed (firm) level for a period of time.

- *Frequency regulation* – In this application, the ESM charges and discharges in response to analogue signals received every 1 to 4 seconds. ESM implies active power supply to the grid to reduce sudden unbalance and keep the frequency between specific limits, while keeping a state-of-charge of approximately 50%. ESM is an attractive option for this application due to its rapid response time.
- *Spinning reserves* – In this application, the ESM remains charged and responds in case of a generation or transmission outages. Depending on the application need, the system can respond within milliseconds or minutes. The ESM supplies power until the back-up generator is started and running. This application allows the generators to work at optimum power, without the need to keep idle capacity for spinning reserves. The system can also eliminate the need of having back-up generators running idle.
- *Outage management* – ESM can provide power for short periods of time to a network reducing or eliminating the effect of a temporary outage.
- *Delay in line upgrades* – An ESM can be placed electrically downstream in a congested transmission system, helping to reduce the overloads in the lines and delay investments in line upgrades.
- *Power quality* – mitigation of problems (harmonics, power factor, flicker etc.) that affect the magnitude and shape of voltage/current. An ESM helps protect the loads further downstream against short-duration events that affect the quality of power delivered to the load.
- *Voltage and VAR support* –An ESM can help to maintain the grid voltage by injecting or absorbing reactive power (VAR).
- *Railroad applications* –Accelerating a heavy train can expose the grid to a peak load that traditionally necessitated extensive investment in capacity expansion. An ESM unit can supply the required acceleration power that is taken from the most recent deceleration.

The peak shaving application is particularly attractive for utility networks. Often industrial customers run apparatuses and devices that require significant amounts of power over relatively short time intervals during a day. EVs or BESUs can be used to reduce peak demand by discharging stored energy during load peaks (Fig. 1.34 [141]). For describing a load peak a reference value [77] is required (P_{Limit}). The load peaks on the load curves are defined as the area above the reference value (peaking generation in Fig. 1.34). The required energy capacity E_{cap} of EVs or BESUs for peak shaving can be visualized as the area of the peak demand graph $y = P_{pwr}(t)$, where P_{pwr} is the required power at time t and ΔT is the required period for discharging. The area of peak generation in Fig. 1.34 is [141]:

$$E_{cap}(\Delta T) = \int_{t_1}^{t_2} P_{pwr}(t)dt - P_{Limit} \cdot \Delta T . \qquad (4)$$

The storage technology with the highest demand over the next five years will be Li-ion battery systems [78]. Li-ion batteries have been used in several grid support applications. One of the largest ESM systems e.g. is a 32 MW energy storage at Laurel Mountain Wind Farm in West Virginia USA [76]. Li-ion batteries represent promising candidates for medium-scale stationary energy storage applications due to their characteristics such as high energy density, low self-discharge rate, long lifetime etc. The Public Service Company of New Mexico demonstration project installed an energy storage system with a single 0.75MW Power Conditioning System, are co-located with a separately installed 500kW solar PV plant, at a utility-owned site, to create a firm, dispatchable, renewable generation resource [79].
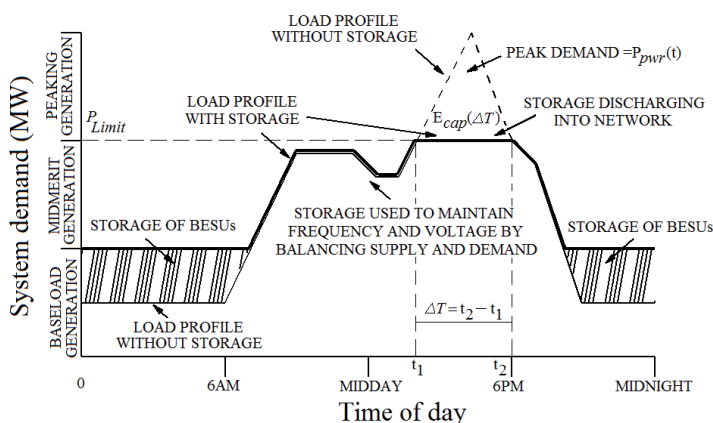
Fig. 1.34 Load profile of an utility network [141]

1.6 Virtual Power Plants with electric vehicles

The EDISSON project [80] proposes the concept of virtual power plants (VPP) for integrating EVs with the electric grid. The purpose of the EDISON project is to use Aggregators of electrical vehicles (EV) including plug-in hybrid electric vehicles to provide the required balancing power for increasing the usage of wind power in the Danish electricity grid (Fig. 1.35 [80]). In the architecture of the project EV status data is sent to EVSE, EVSE communicates with the fleet operator (VPP) for scheduling, fleet operator communicates with Retailer, Retailer communicates with DSO. Electricity retailer is a body to conclude the energy supply contract with the customer (IEC 15118-3). DSO is an operator responsible for the voltage stability in the distribution grid (MV and LV power grid) (IEC 15118-3).

The EDISON VPP is a server-side software system that coordinates the behaviour of a fleet of EVs while communicating with external power system stakeholders. To illustrate the internal workings of the VPP it is useful to group its functions into three groups: data, analytics and logic [80]. This is done in Fig. 1.36 [80], which also differentiates between the aggregated and the individual level of EV management.
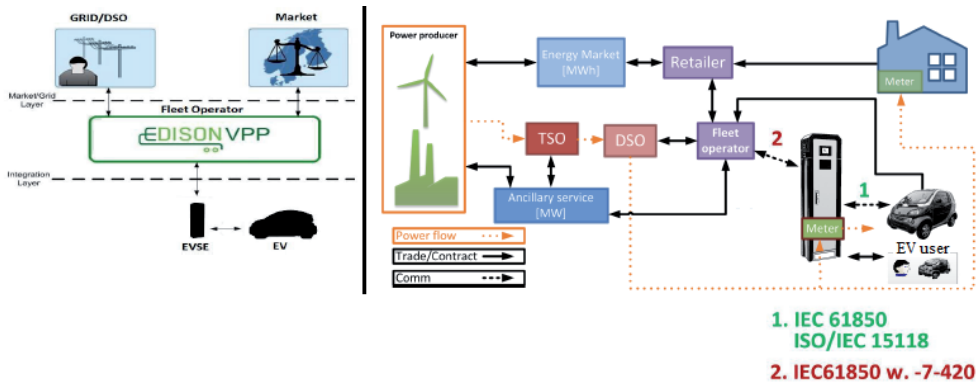
Fig. 1.35 EDISON conceptual architecture [80]

The VPP handles the EV fleet as an aggregated group when acting and optimizing towards market players (upper interfaces), but will have to take individual considerations into account when handling the behaviour of a single car (lower interfaces).

Data functional group [80] stores previous market prices and fleet behaviour on an aggregated level, enabling better forecasting and optimization for acting on the power market. On an individual level, data is stored that describes the service level agreement between the VPP and an EV owner e.g. to which degree the VPP should control the charging process. EV hardware specifications, like battery size and supported charging powers, are also stored. Finally the VPP stores the EV user's plug-in habits e.g. where, when and for how long the EV is typically connected to the grid for charging. These parameters are all vital for individually optimizing the charging of an electric vehicle.

Analytics functional group [80] makes the mathematical computations necessary to support the logic of the VPP. Forecasting relies on historical data to predict market prices on an aggregated level which supports better bids and strategies. Forecasting also determines future individual EV usage patterns. The latter helps the VPP predict when the EV user will need the EV for the next trip and can thus better estimate the time period available for smart charging. Such a prediction can be based on the statistical methods of Exponential Smoothing or using the Markov Chain approach. Optimization is used to minimize charging costs of the EVs on both the aggregated and individual level. The individual optimization is limited by the constraints introduced by the distribution grid, EV specifications and EV user energy requirements. On the aggregated level, profit maximization can be done when acting on the regulating and reserve markets. Such optimization can be achieved through stochastic or linear programming.

The logic functional group [80] defines the main operational goals of the VPP, namely to act on the power market to generate savings or revenue for itself and its clients, and to intelligently manage the charging behaviour of EVs through individually tailored charging schedules.
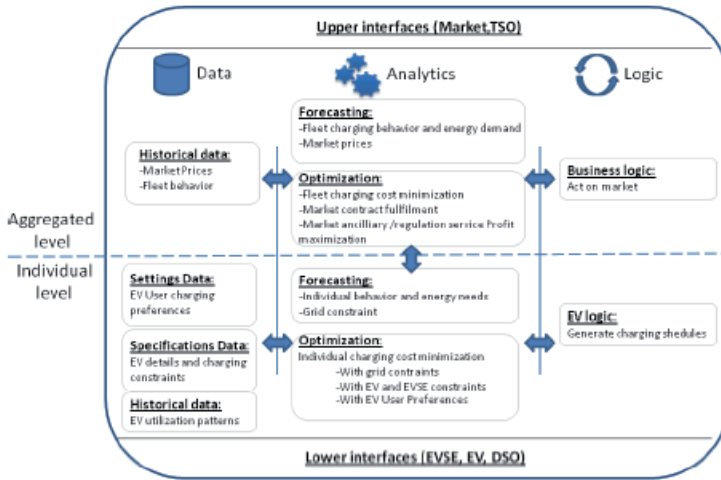
Fig. 1.36 Functionality of distribution substation as VPP [80]

The concept of VPP allows four basic charging strategies for the EV user to choose from [80]:

- Smart charging – charge according to the load on the grid and availability of green energies. This strategy is most beneficial to the power system. This also allows price responsive control of EV charging (Fig. 1.37).
- Immediate smart charging – charge up to certain minimal threshold as fast as possible. After passing the threshold continue with smart charging. There is no benefit for the grid in the first charging phase but beneficial to the power system in the second phase.
- Immediate charging (and drive away) – charge the battery full in the shortest possible time. There is no benefit for the power system from this strategy. Possible scenarios would indicate that immediate charge would require an extra payment as the service provider can not plan its charging plans ahead [81].
- Vacation Battery Care – this specifies a special charging mode for long term parking of EVs. The VPP keeps the EV battery at a specified charging state and charges it full for the end of the vacation battery care period. This strategy is very beneficial for the power system as the battery is connected for a long period, with the only constraint being the end time.
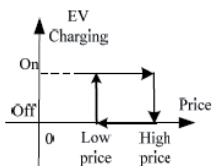
Fig. 1.37 An example of price responsive control logic for EV charging (presented in EDISON report D2.1.2)

1.7 Concerns with the integration of distributed energy resources with utility networks

The increased number of grid connected EVs and bidirectional AC-DC power converters in the LV network (common AC bus) can increase problems concerning the stability and safety of the utility grid, as well as power quality issues. The main problems are [82]:

- Voltage rise problem – the integration of large amounts of EV systems in LV networks increases the generation of active power leading to voltage rise for AC consumers;
- High penetration of EVSEs leads to increase in harmonic content at the connection point (CP). Each AC-DC converter connected to the grid injects harmonics, therefore the more EV systems are connected the more harmonic content will increase. Furthermore, if one or more non-linear loads are present, the THD can increase above the allowed limits. The increase can be noticed in both current and voltage;
- Anti-islanding – islanding occurs when the EVs are disconnected from the grid, but continue to supply power locally (e.g. inside a microgrid);
- Problem which arises due to massive EV penetration is the voltage variation caused by the injection of active power and reverse power flow (Fig. 1.38, modified from [82]). Usually, over voltages affect the network in case of light load.
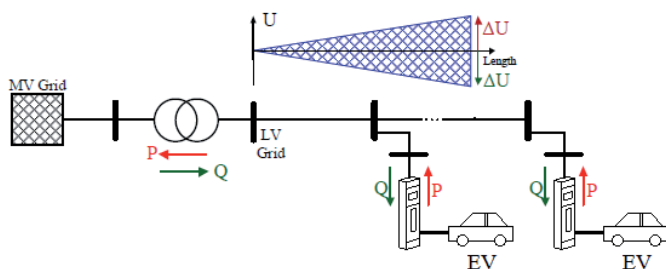
Fig. 1.38 Reverse power flow and voltage variations in LV networks with EVs

Photovoltaic, wind power, cogeneration systems as well as V2G EVSEs have all one thing in common: they generate electricity decentraly. VDE-AR-N 4105 German standard [83] points out the way ahead for the improved network integration of decentralized power generation (in particular inverter-based generators). VDE-AR-N 4105 specifies the maximum voltage increase level caused by the generating plants [82]. During normal operation, the magnitude of the voltage change caused by the generating plants must not exceed in any connection point a value of 3 % compared with the voltage, when the generating plants were not connected. Voltage change of 3 % with connection or disconnection of VPP should not occur more frequently than once every 10 minutes.

VDE-AR-N 4105 specifies the disconnection of inverters connected to LV network due to grid side disturbances [82]:

- When the voltage changes (undervoltage, overvoltage) exceed the limits $80\%U_n<U_{pcc}<110\%U_n$, disconnection is necessary within 100 ms. In case the upper limit is exceeded, according to EN 50160, inverter must shut down.
- Frequency limits are 47.5Hz<f<51.5Hz. If these values are exceeded, the inverter must disconnect in 100 ms.
- If the DC current exceeds the limit of 1 A due to abnormal operation, inverter must shut down in 200 ms (VDE 0126-1-1).

The inverter is allowed reconnection after fault as soon as the following conditions are satisfied: $85\%U_n<U_{pcc}<110\%U_n$, 47.5Hz<f<50.05Hz, minimum delay of 5 s. The purpose of the allowed time delay is to ride-through short-term disturbances [82]. The specific behaviour of the inverters under grid faults is very important, since it is desired that the system avoids as much as possible disconnection. The services delivered by the inverters are based on grid monitoring and have to follow the demands from the DSO. Main requirements from the DSO side [82]:

- Admissible voltage changes by generating units do not exceed limits;
- Possibility for frequency regulation by adjusting active power generation;
- Reactive power control;
- Reconnection after trip.

Frequency variations are a common problem that affects the power systems being caused by the unbalanced power ratio between energy production and consumption. To avoid unbalanced conditions, VPP must be capable to adjust power production by means of frequency regulation (Fig. 1.39 [82]). The requirements regarding active power control aim to ensure a stable frequency in the power system [84]. Generating plants with the capacity over 100 kW have to reduce their real power in steps of at most 10 % of the max. active power [83].
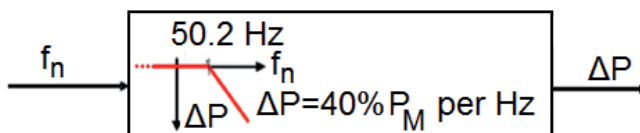
Fig. 1.39 Active power reduction in case of over frequency [82]

The gradient for active power reduction can be calculated using the following formula [82]:

$$\begin{cases} \Delta P = 20 \cdot P_M \dfrac{50.2 - f}{50} \\ 50.2 < f < 51.5 \end{cases} . \tag{5}$$

where $\mathit{\Delta}P$ is the active power reduction gradient (W), P_M is the power generated after exceeding the 50.2 Hz limit (W), and f is the network frequency (Hz).

Generating units have to reduce with a gradient of 40 % Hz their power output, when a 50.2 Hz frequency limit is surpassed [82]. The output power is allowed to increase again, when the frequency is below 50.05 Hz. Outside the frequency limits, the plant has to disconnect from the grid.

Controllable power plants have to reduce the power output to the target value within a maximum period of time of 1 minute [82]. If the set point is not reached in the mentioned period of time, the generating plant must be shutdown.

In any electricity system, active and reactive power generated has to be in constant equilibrium with the power consumed by the loads including the losses in the lines [85]. Whenever the power generated is not equal to the power demanded, the unbalance between both is offset by the kinetic energy of the rotating generators and motors connected to the system, causing a deviation of the system frequency from its set-point value (e.g. 50 Hz in Europe). The purpose of voltage and frequency control is to ensure that both voltage and frequency remain within predefined bands around the set-point values by adjusting active and reactive power generated or consumed. As the penetration of distributed generators further increases, small distributed generators, such as V2G systems connected to the low-voltage distribution grid, will need to cooperate in voltage and frequency control (Fig 1.40 [85], [86]):

$$f - f_0 = -k_p \cdot (P - P_0),$$

(6)

$$V - V_0 = -k_q \cdot (Q - Q_0),$$

(7)

where f_0 and V_0 are the rated frequency and voltage respectively, P_0 and Q_0 are the temporary set points for the active and reactive inverter power. On the other hand, low voltage cable grids generally have a mainly resistive nature, and the resistance R cannot longer be neglected. On the contrary, often X may be neglected instead of R. In the general case, both X and R have to be considered. Hence, the optimal frequency and voltage droop regulation can be deduced [85]:

$$f - f_0 = -k_p \cdot (P' - P_0') = -k_p \cdot \frac{X}{Z} \cdot (P - P_0) + k_p \cdot \frac{R}{Z} \cdot (Q - Q_0),$$

(8)

$$V_1 - V_0 = -k_q \cdot (Q' - Q_0') = -k_q \cdot \frac{R}{Z} \cdot (P - P_0) - k_q \cdot \frac{X}{Z} \cdot (Q - Q_0),$$

(9)

where V_1 is the inverter voltage (V).
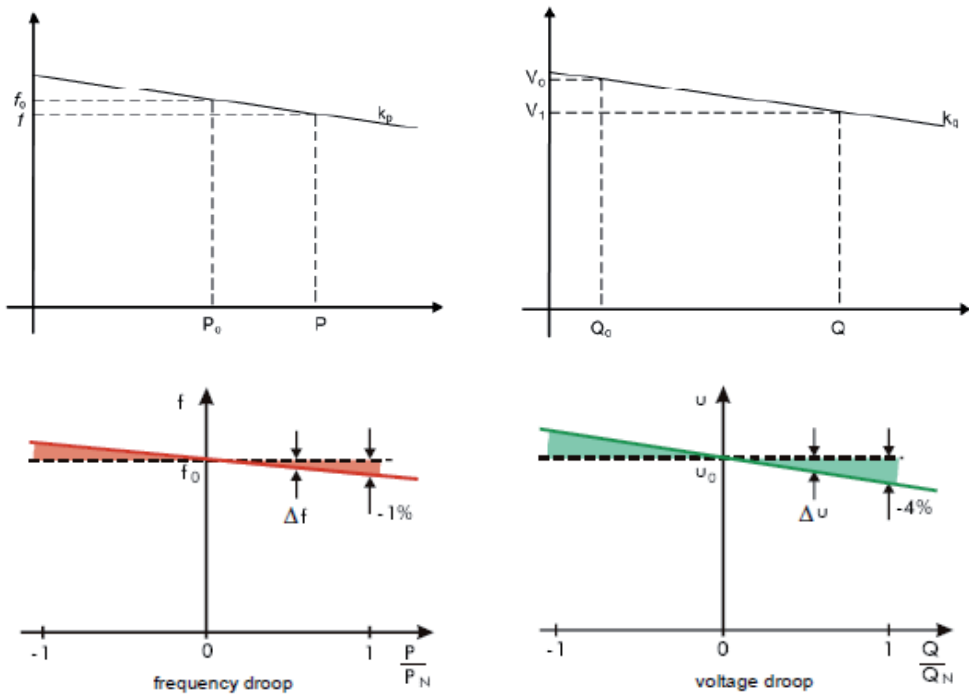
Fig. 1.40 Frequency and voltage droop characteristics [85], [86]

Components connected in parallel to the grid are distinguished by their contribution to the formation of the grid voltage and frequency and are accordingly classified in three classes: grid-forming, grid-supporting and grid-feeding components [85]:

-   Grid-forming components fixedly control the grid voltage and frequency by balancing the power generators and loads. These components are designed for stand-alone operation. Generally, such systems contain at most only one grid-forming component as they act as an ideal source with fixed frequency and zero output impedance. Thus, grid-forming components cannot be placed in parallel.
-   Grid-feeding components comprise conventional grid-connected generators and by extension also loads. These components are designed to draw or feed a certain amount of power, determined by their own needs or wishes, irrespective of grid conditions. These components do not contribute to power balancing.
-   Grid-supporting components contribute to the control of the grid voltage and frequency by adjusting their active an reactive output power according to voltage and frequency droops, allowing power sharing and expandability. These components contribute to power balancing, making a trade-off between their power rating and the local voltage and frequency quality.

Figure 1.41 [85] shows the basic control scheme of a grid-supporting inverter. The voltage amplitude and frequency are no longer fixed but obtained as a result of the droop equations as a function of active and reactive power components. Active and reactive power P and Q are calculated by multiplying direct and quadrature current components i_d and i_q by the direct voltage component u_d, as the quadrature voltage component $u_q = 0$.
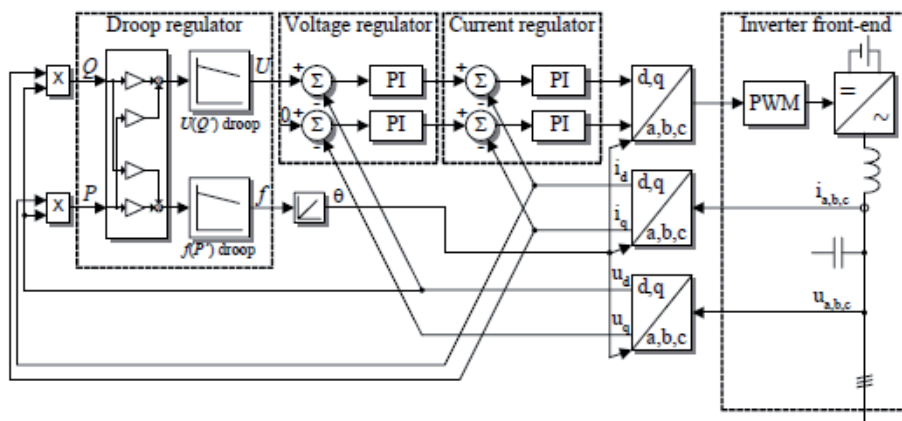
Fig. 1.41 Basic control scheme of a grid-supporting inverter (by modification of grid-forming inverter) [85]

Islanding condition occur when a part of the grid is disconnected and inverter continues to operate with local load. For safety reasons, islanding is a major concern, especially for personnel who attempt to work on lines, which they believe to be disconnected. If the reconnection is established, the voltage at the point where island occurred is not synchronized with the grid voltage causing disturbances in the system. In order to avoid these consequences, anti-islanding measures were issued in standards [87].

Detecting anti-islanding can be divided into passive methods (grid monitoring) and active methods (disturbances are injected into the supply to detect from their behaviour if the grid is still present, e.g. impedance measurement) [82].

Grid connected EV inverters are required to involve using any passive or active method to detect islanding condition [82]. If significant parameter changes are detected which could lead to transition from normal operation to islanding, the inverter will be shut down and shall not reconnect before voltage and frequency have been maintained within specified limits for at least 5 minutes. Afterwards, the inverter will automatically reconnect to the utility grid.

According to IEEE 1547, when unintentional islanding occurs, the DR interconnection system must detect the island and stop energizing the area Electric Power System within 2s [87].

Inverter islanding and resynchronization related issues are analyzed in separate Thesis [88].

1.8 Generalizations

In the following years the charging of EVs will most likely be with either home charging (IEC 61851 mode 1), with DC fast charging (IEC 61851 mode 4 or CHAdeMO standard) or through ultrafast charging stations (chapter 1.2.4). Home charging is suitable for charging over night, but not suitable for semi-public and public places during day time. State of the art charging stations are focusing only for charging of EVs (section 1.2). Existing charging stations (e.g. Terra 51 installed in the Estonian EV infrastructure) are not suitable for adapting V2G concept. Existing charging stations apply for charging of a single EV. There are no technical obstacles of replacing or upgrade existing charging stations with bidirectional power converters. The difficulties lay in controlling of such charging stations for V2G applications. It would require that every charging station is equipped with remote communication devices, separate control centres are required to control aggregated number of charging stations, e.g. virtual power plants in EDISON project (chapter 1.6). This would require complex control algorithms and thus increase the total cost of building and maintaining such systems.

Utilizing Li-ion batteries for energy storing is the most promising of energy storage technologies in the following years (specific energy, specific power and advantages of Li-ion batteries, chapter 1.1.1, compared to other storage technologies, chapter 1.1.6). This has been proven in several practical applications world wide (chapter 1.5.2). Battery management systems (chapter 1.1.4) enable effective design and control of energy storage. One the otherhand, this enables control only over the physical charging and discharging of batteries. Separate control algorithms are required for utilizing batteries in practical applications (e.g. peak shaving, reactive power compensation). In addition prolonging options for BESU Li-ion batteries must be considered (chapter 1.1.5).

Existing ESM control systems enable utilizing batteries for providing ancillary services for the utility network (chapter 1.5.2). However the concept of such control systems is only applicable over stationary batteries. EVs are mobile energy storage systems. To utilize energy stored in EVs would require different control algorithms as the aggregated number of EVs that are connected to utility network varies in time.

Existing standards and norms (chapter 1.3.1) dictate the voltage characteristics of electricity supplied by public electricity networks and interruptions of supply over period of one year. However, this seldom satisfies the final customers (e.g. manufacturing facilities) as their devices are influenced by voltage variations and during power outages manufacturing stops. This requires making investments either into stand-by generators or reactive power compensation devices. An alternative option could be utilizing energy stored in BESUs and EVs.

As EV filling stations require connection to MV level, which is supplied through distribution substations, it is clear that linking new concepts and technologies around distribution substations will give cost effective solutions. Especially control of EVs for microgrid and Smart Grid applications can be done effectively through distribution substations. Current distribution substations

(chapter 1.5.1) do not allow bidirectional energy transfer and thus require adapting of new technologies.

Next generation substations should utilize the full possibilities of IEC 61850 communication protocol (chapter 1.4) for cost effective solutions.

Development of standards (chapter 1.3.3) in the following years in the EV infrastructure are focused more on charging of EVs (e.g. IEC 61851-23 and IEC 61851-24). In the V2G concept the IEC 15118-1 standard is focused more on the communication set-up, identification and authorization of EV and EV owner. The IEC 15118-1 does not specify the control of physical connection of EVs to utility networks nor specify limits of utilizing EVs for ancillary services for the utility network. IEC 15118-1 is oriented for single EV vehicle integration for V2G. Filling stations include several EVSEs, which data has to be analyzed collectively for managing scheduling for Smart Grid applications.

Smart Grid related standards are focused on standardizing communication protocols and do not consider physical control architectures of charging or discharging EVs (chapter 1.3.4). Standards IEEE 1547 and IEC 61850-7-420 are related with distributed energy resources (DER), but the standards do not include descriptions of EVs or BESUs at all. It can be concluded that standards for utilizing EVs for ancillary services are still under the development phase. Therefore the concept of interconnecting EVs with the utility network is still open for proposals and development. One of the purposes of this PhD thesis is to make a contribution in this field, specifically introducing the concept of distribution substations as the interconnecting environment and as virtual power plants.

The EDISON project could operate in small scale but requires large servers to control several thousands or millions of EVs connected to VPP system (VPP has to communicate with each EV). The concept of V2G is proposed, but how the physical discharging would be controlled has not been clearly indicated. The considerations on major concerns regarding V2G implementation as distributed energy resources (chapter 1.7) have not been indicated.

2. BIDIRECTIONAL ENERGY EXCHANGE BETWEEN ELECTRIC VEHICLES AND UTILITY NETWORK

2.1 Introduction

This chapter describes the distribution substation topology for integrating EVs with utility networks.

There are four main different applications, where distribution substations for EV infrastructure could be used. The four main applications are:

- Public charging (e.g. highways);
- Public transportation charging (e.g. buss and taxi companies);
- Semi-public charging (e.g. industry);
- Domestic charging (e.g. charging at homes).

The strategy for public charging is to charge as fast as possible (people can not wait for hours near highways). This excludes the V2G application in such distribution substations, as there is not any open timeperiods, where V2G could be utilized. The additional benefit for constructing a distribution substation type solution instead of using standard CHAdeMO type EVSEs would be to utilize BESUs or nearby renewable energy resources to reduce peak loads for the utility networks.

For the public transportation, EVSEs are mostly unoccupied during daytime or similar strategy is required as for public charging during daytime. The charging takes place mostly during nights. The V2G application during the night is not very appealing as utility networks are in baseload generation. Though e.g. special events, which may take place during nights near the public transportation garages could utilize the energy stored in public transportation to avoid peak loads (e.g. instead of using additional generators for special events). Before departure in the morning, public transportation EVs are recharged. BESUs could be utilized similarly to public charging.

The semi-public charging refers to applications, where EVs are connected with EVSEs for a longer period of time (e.g. employees of a factory arrive to work in the morning and departure in the evening). The EVs are mostly unutilized during the daytime. Therefore, EVs with V2G capability could be utilized for peak shaving of industrial loads or loads of the utility network. Before departure, EVs are charged to the agreed limit that was inserted to the EVSE or sent to the Retailer.

Utilization of distribution substation type solution for domestic charging or residential charging is limited. Domestic charging may prefer slow charging as the primary option. The secondary option is to utilize EVSEs installed at homes for V2H (vehicle-to-home) applications. The V2G application could be then performed by EVSEs at homes not through distribution substations.

This thesis is focused to distribution substations for semi-public charging. The charging of EVs and V2G option in semi-public charging consists of several challenges and variety of applications. Distribution substations for public charging and public transportation charging can be based upon distribution substations for semi-public charging with some modifications in the hardware and in the software (control strategy). The thesis focuses only to topologies where bidirectional power converters are removed from the EVSEs and installed to the distribution substation. This enables much more efficient transfer of energy between EVs and utility networks.

Fig. 2.1 presents the general data flow diagram of the semi-public charging with the distribution substation. EVs are connected with EVSEs. EV transmits its BMS data to EVSE and EV can control the maximum charging current. EV owner inserts its preferences to EVSE or sends to the Retailer. EV/EVSE data is transmitted to the distribution substation. The distribution substation processes the data of several EVSEs that are connected with its bays. Processed data can be exchanged between the DSO, the Retailer and LV side consumers (e.g. main controller in an industrial building). Retailer or the DSO do not have to communicate with every individual EVSE as processed data can be extracted from the distribution substation. EV owners can monitor their scheduled charging times (calculated by the distribution substation) through EVSE or through the Retailer (e.g. web application).
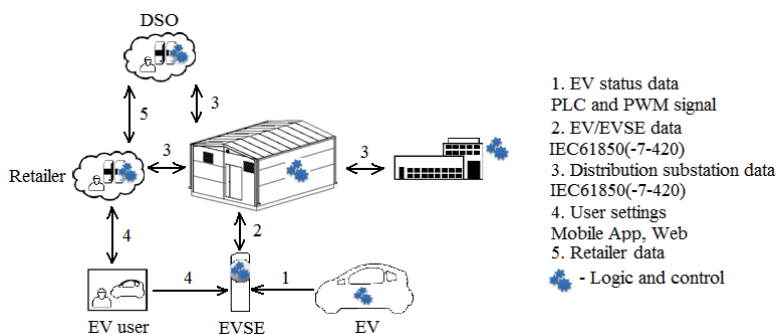
Fig. 2.1 Data flow diagram of semi-public charging with V2G capable distribution substation

2.2 Microgrids and Smart Grids

Maintaining, expanding and upgrading the electric grids to meet the growing demand for electricity is a huge cost for utility networks [75]. This assumes that electricity is produced and delivered the same way as it has been for over one hundred years, e.g. large centralized generation in remote areas, connected to distant population centres through hundreds of miles of transmission and distribution infrastructure. The new technology allows creation and implementation of small-scale automated electric networks called microgrids and virtual power plants. Automatic control systems of such microgrids and virtual power plants are configured by people. People that typically are characterized as prosumers,

consumers or even service providers play a main role in a small-scale energetic community. Computers, automatic equipment and power lines of a microgrid only provide interface to the people who own or use the local parts of an electric network.

Microgrids function in a manner similar to the large electric grid but on a much smaller and localized scale. Given their emerging nature, and the fact that microgrids are often custom designed for specific end-user requirements, several varying definitions and implementations exist. There is, however, growing agreement that microgrids must minimally incorporate distributed generation and energy storage solutions that are proximal to the point-of-use [75].

A microgrid as a distributed system is interconnected with the Area Electric Power System (APS, Utility) through a power grid and a communication network without interference or assistance of third-parties [140]. Both of the constitutive parts have the point of common coupling (PCC) [89]. Topology of a Smart Grid involving APS with an associated microgrid consisting of a substation and distributed resources is presented in Fig. 2.2 [140].
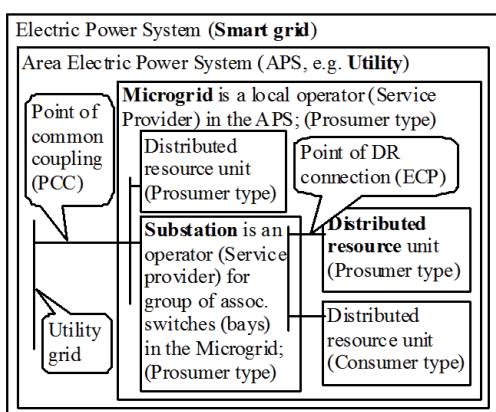
Fig. 2.2 Topology of an electric power system [140]

The battery energy storage unit (BESU) in substations serve several purposes. For e.g. EV filling stations, the BESU can be an additional buffer between the EVs and the utility network. BESUs are recharged during off-peak periods (e.g. night time). During peak periods BESUs can support fast charging of EVs, while drawing near-average power from the grid and reducing the series of charging peak loads for the utility network.

As the number of renewable energy sources is increasing in the grid (e.g. wind and solar energy), the balancing of excess generation sources and load demands can be controlled through the substation. This enables stabilization of the grid voltage and frequency. The ability of microgrids to incorporate distributed renewable energy generation and to avoid the cost and poor reliability of long distance transmission infrastructure is a significant driver of microgrid adoption. Since most microgrids leverage storage as an essential component, growth in

microgrids is also expected to drive further growth in energy storage systems, and vice versa [75].

A microgrid operates in two basic modes: online and islanding (off-line). While most microgrids are expected remain connected to the larger grid, they are also designed to be self-sufficient and thus capable of disconnecting or "islanding" [75]. In the case of a utility network power outage, the BESU will ensure backup power capability to power consumer loads in an island mode.

A microgrid is an independent partner (e.g. prosumer) or a dependent partner (e.g. consumer, client, and load) at the associated APS. Exchange of electric energy in an online (operating) microgrid is controlled (defined) by its internal prosumers and consumers and also by an external prosumer – the utility. Prosumers and consumers of the microgrid act as an associated group of agents because there is one point of common coupling between a microgrid and a utility. A substation acts in the microgrid as a service provider for the distributed resource units (that can be a prosumer or consumer type). A smart prosumer (having also the functionality of a service provider) can address the combined needs (described with a set of requirements) of neighbouring prosumers and consumers driven by the rise of smart management systems and downloadable applications that can be linked to their automatic control systems.

In the concept of Smart Grid, centralized power systems (top-down principle) [75], [90] should change to distributed power systems in the future (Fig. 2.3). Smart Grid's goal is to supply and consume energy in a reasonable way that sufficient energy can be available at all times and with high quality. Smart Grid includes data communications Network, which is integrated with the power grid. Communication Network enables power grid operators to collect and analyse data about power generation, transmission, distribution, and consumption - all in near real time. Smart Grid technology predicts energy consumption and recommends to suppliers and consumers the best way to manage power. Most of entities of Smart Grid become active. They are both users and producers of electric energy (e.g. smart buildings). Users of electric energy become prosumers. The EVs and charging stations can be a part of the interacting Smart Grid.
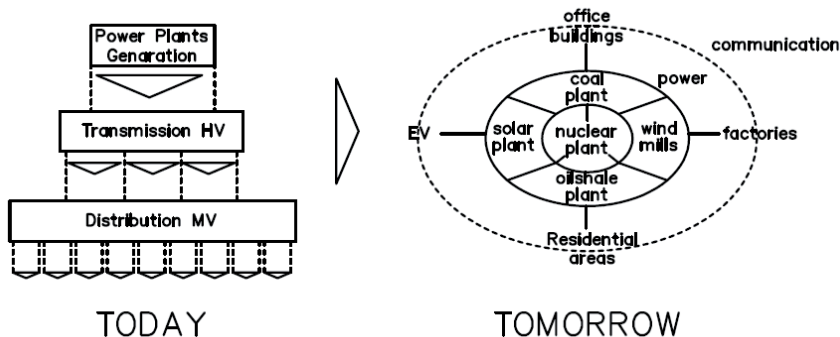

Fig. 2.3 Network topology today and in the future

2.3 Distribution substations for EV infrastructure

2.3.1 Introduction

Utility networks are typically designed for specific load carrying capability. When EVs are added to the utility network, load patterns will be changed. This may lead to overloading of the utility in some periods of the day, making electric circuits and transformers vulnerable. Before integrating a EV filling station to an existing power grid, calculations have to be made to verify that the power grid can withstand filling station loads. In the concept of smart charging, EV charging is controlled with available sources in the power grid.

Calculations have to consider that DC fast charging should not take more than 30 minutes. If we look at an EV, which requires 15 kWh of electric energy to travel 100 km (rule of thumb in most cases), this will require minimum of 30 kW charging power (15 kWh divided by 0.5 hours). If we consider that recharging the battery should take as much time as refilling a petrol car, e.g. 5 minutes, this requires 180 kW charging power. For simplification, assume that a filling station consists of 10 pcs of EVSEs. If all 10 pcs of EVSEs are occupied, the filling station requires minimum 300 kW charging power (30 minute charging time for 10 EVSE x 15 kWh) or maximum of 1800 kW charging power (5 minute charging time for 10 EVSE x 15 kWh). The difference between maximum and minimum is 6 times. In 3-phase 400 V AC power grid, this will require minimum of 433 A transfer current and maximum of 2598 A transfer current. These figures indicate clearly that a DC fast filling station is a burden for the power grid and therefore cannot be designed to a low voltage grid (e.g. residential area), but should be designed into a medium voltage (MV) grid (typically 6-10 kV in residential areas and 15-20 kV in country sides in Estonia). Without the use of BESUs the grid lines have to be overdimensioned to meet the peak demand.

The main applications of the distribution substation for EV infrastructure are:
- *Distribution and storage of electric energy* – from MV grid to EVSEs, distribute energy to other AC consumers (e.g. nearby buildings), store and produce electric energy and be a part of the power grid communication infrastructure for microgrid scenarios.
- *Control of electric energy flow* – allow active and reactive energy to flow both ways (from grid to consumer and to grid from producer). For energy measurements, all substation's outgoing bays for prosumers must be equipped with smart energy meters. For control, all substation's outgoing bays must be equipped with switching apparatuses (e.g. contactors).
- *Fast charging of EVs* – primarily with DC fast charging (charging power 50 kW, max. charging current 125 A, charging voltage 50-600 V DC, power factor 0,97-0,99) [91].
- *Protection and control functions of the MV and LV part of a substation* – described in section 2.3.2.

- *Provide ancillary services for the utility network* – described in ESM part at section 1.5.2.
- *Remote control* – to allow DSO to adjust substation settings remotely (e.g. grid constraints).
- *Modularity* – possibility to build substations in modular concept for scaling up power.
- *Islanding* – ability to go off-line in a short time (e.g. 3 ms) to protect consumers, if there are not any other options.

As several converters are required in the filling station, filters have to be included in the substation to remove higher harmonics distortion to protect the power grid. Substations equipped with supervisory control and data acquisition (SCADA) remote terminal unit systems cannot be scaled and should evolve to support next generation intelligence for microgrid scenarios. Flexible IEC 61850 compliant intelligent electronic devices (IEDs) and utility-grade rugged IP routers and Ethernet switches allow IP-based communications. IEC 61850 compliant devices have been mainly used in high voltage substations [92] for automatic relay protection and control. In the case of MV/LV distribution substations with prosumer connections, the same type of intelligent IEDs must be used.

Prosumers' equipment will have to send data (in the "producer" stage) to their substation about their power availability, which they can supply into the grid. The available power can vary in a short time and the parameters (also protection and control functions) must be updated constantly (e.g. in the electric vehicle filling station, the number of V2G connected cars can vary in time). The substation itself can be viewed as a prosumer in microgrids. In such cases the substation can provide additional power to the utility network for load peak shaving.

2.3.2 Protection and control functions of the LV part of a substation in microgrid applications

The functions of the LV part of a substation refer to continuous processes and tasks, which have to be performed in the substation. These are functions to control, monitor and protect the equipment of the substation and its bays [93]. The functions used in a substation automation system may be divided into different levels of organization of a smart power system: utility, microgrid, station (group of transformers, buses and switches), bay and distributed recourse unit. All subsystems can be prosumer type.

Prosumer type distributed resource unit functions can be divided into either functions that are performed by the prosumer internally (in a prosumer controller) or functions that are integrated (actually distributed) into the interface of the higher level prosumer, where the prosumer is connected.

A bay is a subpart of the substation [93], e.g. main circuit-breaker of the LV side of a substation, an outgoing bay for a prosumer/consumer or a bus coupler. Bay level functions are necessary to protect and control prosumer interconnections

with other prosumers (also the substation as a prosumer) and to communicate with the substation's station level.

Station level functions refer to the substation as a whole. There are two classes of station level functions: process related station level functions and interface related station level functions [93]. Process related station level functions use the data of more than one bay or the complete substation to protect or control the MV or LV part of the substation. These are functions to operate, supervise, protect and monitor the substation in the best way as possible and guarantee the reliable and economic power supply. Interface related station level functions are functions representing the interface of the substation automation system to the local station operator named HMI or to RTU serving basically local operator (the microgrid). These functions are needed for the normal operation of the substation in a microgrid every day - to present information to operators about prosumers and the substation or to allow them to control by commands. The data and commands are exchanged between the station level and RTU to the outside world. Binary values (status, events, alarms, commands, etc. for remote control) and analogue values (calculated values, e.g. energy flow) are basic values to be exchanged.

If the substation itself is a prosumer in the MV microgrid, the substation must include microgrid level functions [140], which are controlled by the microgrid automation system. In some circumstances, if there is no microgrid available on site, also utility grid level functions are needed. A substation can be in communication with another substation to exchange data. Binary values (blocking, release, etc. for distance protection and automatics) and analogue values (samples of current for current differential protection) can be exchanged depending on the functions applied.

If the substation is a prosumer in the MV or high voltage Area Electric Power Grid (Power Utility Grid), the substation must include power utility level functions, which are controlled by utility power system automation system. In some circumstances, if there is no utility available on site, also Smart Grid level functions are needed.

Fig. 2.4 [140] represents typical protection and control functions of the LV part of a substation automation system [93]. These functions are: F1 – protection data exchange between the bay and the station level; F2 – protection data exchange between the bay level and remote protection (e.g. line protection); F3 – data exchange within the bay level; F4 – analogue and binary data exchange between the prosumer and the bay level (inputs from current and voltage transformers); F5 – control data exchange between the prosumer and the bay level; F6 – control data exchange between the bay and the station level; F7 – data exchange between the substation level and remote engineer's workplace; F8 – direct data exchange between the bays (interlocking); F9 – data exchange within the station level; F10 – control-data exchange between the substation and the RTU used for microgrid or power utility levels; F11 – control-data exchange between substations (binary data for interlocking); F12 – analogue and binary data exchange between the distributed resource (prosumer) substation interface and the prosumer controller, F13 – control

data exchange between the prosumer substation interface and the prosumer controller; F14 – participation in the utility network, the microgrid or the Smart Grid market competition.
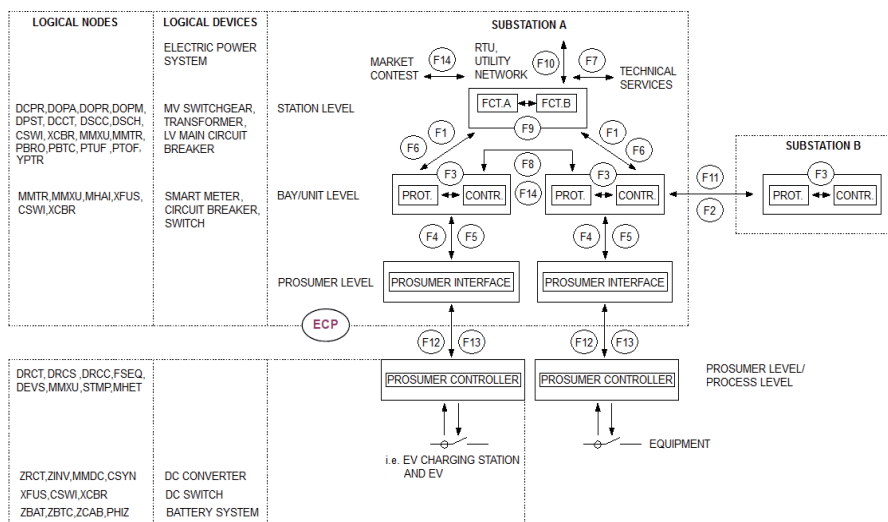
Fig. 2.4 Topology of distribution substation's low voltage function levels (with an example of logical devices and logical nodes for an EV filling station) [140]

In addition, there exist system support functions, which are needed to maintain the SAS, i.e. communication management, software management, physical device self-checking, system security management and time synchronization. These functions are performed continuously in the background of the SAS system.

2.3.3 Integrated AC and DC bus topology

An example of a distribution substation topology for microgrids is presented in Fig. 2.5 [141] (outside distribution substation or topology of an inside electric installation). The substation consists of a MV switchgear, transformers and several low voltage switchgears (with switches, smart meters, contactors and power converters). The topology consists of two independent utility network supplies for redundancy, which are connected to the examined substation's MV switchgear. The substation allows bidirectional energy exchange between EVs and consumers. Substation topology is implemented with an integrated AC and DC bus. Electric vehicles are connected with a common DC bus behind one AC-DC power converter (including LCL filters). For every EV in the common DC bus there are separate DC-DC converter subsystems, which consist of bidirectional DC-DC converters, protection, measurement and switching apparatuses. EVs are supplied from transformer T1 and consumers in the same substation are supplied from transformer T2. Bus coupler switch BC_LV separates the common AC bus for discharging EVs to the MV level. EVs can be discharged to the common AC bus if

the main breaker LVA is opened and the bus coupler switch BC_LV is closed. The topology allows the connection of DC-DC power converters with different power ratings and EVs with different current-voltage (I-V) characteristics. DC-DC power converters can adjust the output voltage to deliver maximum allowed current to the EV even when EVSEs are further away the distribution substation (compensate cable resistances). This also applies to discharging of EVs to the common DC bus.
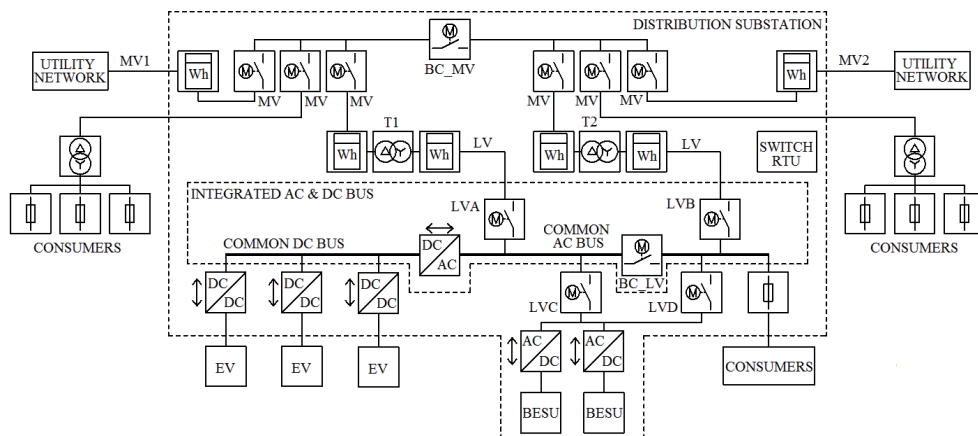
Fig. 2.5 Topology of a distribution substation with an integrated AC & DC bus for microgrid applications (IT earthing system) [141]

In Fig. 2.5 [141] BESUs are connected to the common AC bus. For every BESU in the common AC bus there are separate AC-DC-DC converter subsystems consisting of bidirectional AC-DC-DC converters, protection, measurement and switching apparatuses. BESUs can support either the LV side of EV supply or the LV side of consumers. The required number of BESUs could be connected with individual AC-DC-DC power converters (Fig. 2.5) or connected with a common DC bus behind one AC-DC power converter (Fig. 2.6) similarly to the EV side.

In Fig. 2.5 [141] it is considered that EVs are utilized for peak shaving of LV and MV side utility networks loads. In addition EV side AC-DC power converter can be utilized for voltage mitigation and reactive power compensation of LV consumer loads. BESUs are utilized for peak shaving of EV charging loads; peak shaving of LV consumer loads (e.g. reduced number of EVs are being charged at the same time), providing backup support for the consumers during power outage if energy routing can not switch through ATS to the first utility network supply; optionally for storing reverse energy flow or excess energy generation from the consumers side; supporting renewable energy storage for the utility network. Distributed energy resources (DER) could be installed to the common AC bus or to the common DC bus, but the integration of DERs with the distribution substation is not considered in this thesis. Additional elements which could be utilized in the topology are static switches (in parallel with main circuit breakers), limiting reactors for reducing inrush currents during transformer reversing.

Fig 2.6 illustrates different instrument transformers that are required for different applications in IT earthing system. For AC-DC power converter connecting EVs current transformers (CT) and voltage transformers (VT) are required in the common AC bus (A2). These can be implemented inside the AC-DC power converter itself. For discharging EVs to the MV side another set of CTs and VTs are required in the MV side (A1). For reactive power compensation of consumer loads, CTs (A3) are required in the second utility supply part to calculate reactive power consumption. For AC-DC power converter connecting BESUs CTs (B3) are required. VTs have to be placed for both sides of the LV side bus coupler (B1 and B2). Different VTs (B1, B2) provide information for the BESU side AC-DC power converter depending on the state of the energy routing. Additional set of VTs (B4) are required to perform resynchranization with the secondary utility network supply.

Fig. 2.7 illustrates different instrument transformers that are required for different applications in TN-C or TN-S earthing systems. The implementation of the topology depends on power converter topologies. In Fig. 2.7 third transformer (delta-star type) is installed for creating a bath for the returning neutral (N) or protective earth and neutral (PEN). In Fig. 2.7 CTs and VTs are required after the third transformer (B2, A4). Bus couplers BC1 and BC2 in the LV side separate the third transformer for avoiding the no load state of the transformer when energy transfer through the third transformer is not required. Additional differences with Fig. 2.6 lay in CTs and VTs of A3 and B5.
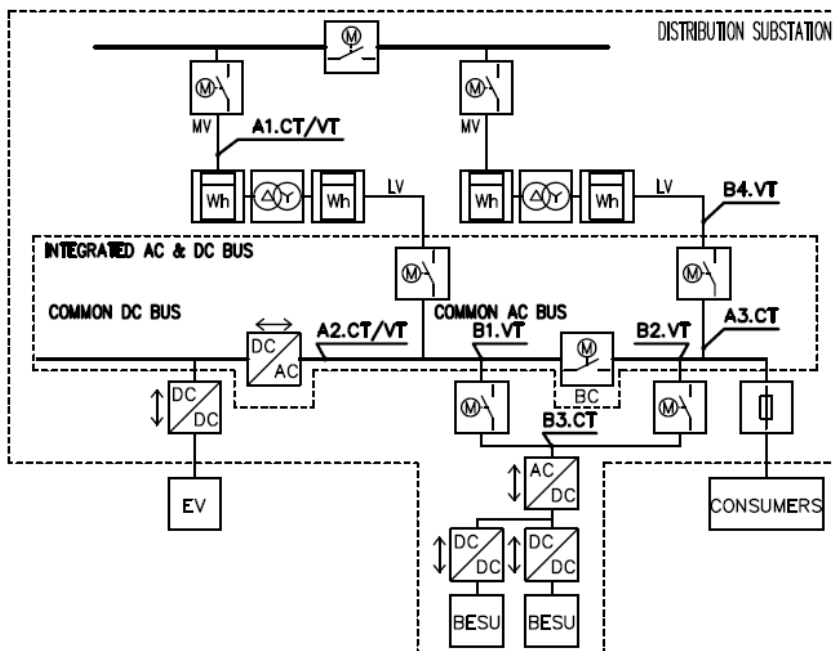
Fig. 2.6 Positions of instrument transformers in the integrated AC & DC bus for microgrid applications (IT earthing system)
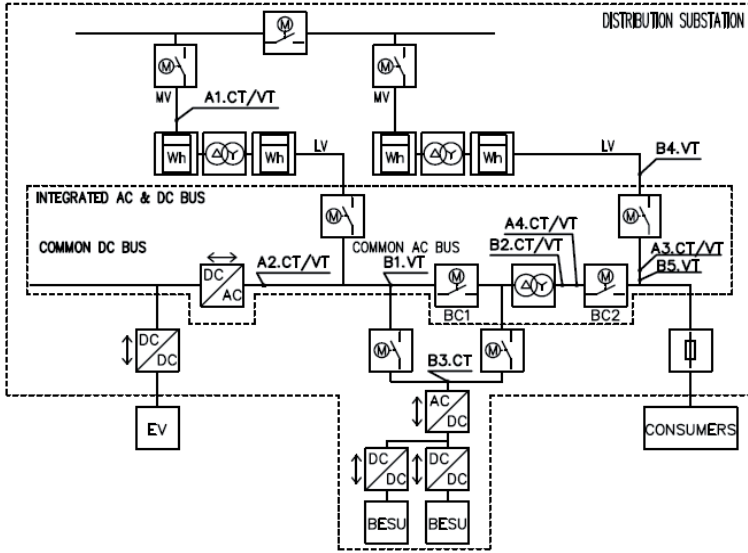
Fig. 2.7 Positions of instrument transformers in the integrated AC & DC bus for microgrid applications (TN-C or TN-S earthing system)

In large size EV parking lots (e.g. 100 pcs of EVs) it becomes unreasonable to install all the EVs behind one AC-DC power converter. It would be much more reasonable to divide EVs into groups and install extension distribution substations with interconnections to the MV side. Extension distribution substations are supplied through the main MV switchgear. The topology of the extension distribution substation can be simpler. Extension distribution substation topology is presented in Fig. 2.8. The BESU in the extension distribution substation could be utilized in the common DC bus.
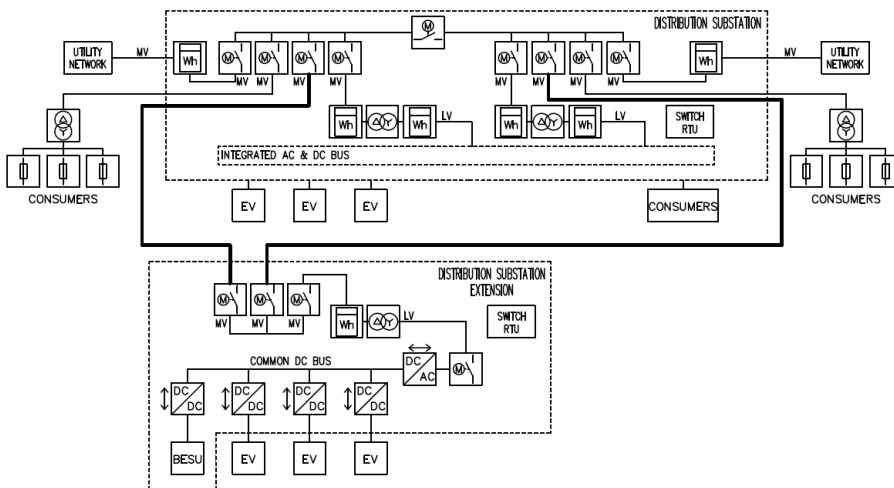
Fig. 2.8 Topology of an extension distribution substation for microgrid applications

85

2.3.4 Functions of EVSEs with bidirectional distribution substations

With bidirectional substations most of the protection and control functions will be performed by the substation automation system during bidirectional energy exchange. Some functions shall be still required from the electric vehicle supply equipments (EVSEs). EVSE facilitates the connection between an EV and the distribution substation. EVSE (charging spot acc. IEC 15118-3) is the physical unit to that EV is connected in order to transfer energy to the vehicle. With repositioning of the charger from the EVSE to the substation the EVSE shall consist of a cabinet, EV connection cable and plug, incoming terminals for power and auxiliary voltage supply, HMI. Future EVSEs consist of:

- *EV connection cable and mechanical connector interlocking* – to ensure the plug is connected with the EV;
- *Connection terminals* - for power cables (DC cables incl. earthing) and auxiliary cables (230 V 1-phase supply which can be linked between several EVSEs, emergency circuit cabling);
- *HMI, identification and payment terminals* - Operation panel for communication with EV owner, status overview (energy prices, departure times, charging packages), identification and payment (information forwarded to clearing house);
- *Communication* – Controller for communication set-up between EVSE and EV at the beginning of the charging (values predefined or transmitted from distribution substation to the EVSE, e.g. max power capability); data retrieval from EV BMS and distribution substation, data forwarding to substation, data storage of substation's parameters (kWh measurements and prices – sent from clearing house to distribution substation to EVSE for energy trading), handling of modifications made by EV owners, communication for "apps" (which EVSE is free, which is the next scheduled timezone for charging, information about EV connected with particular EVSE: SOC+modifications). 12 V DC voltage converter is required;
- *Wireless data transmission* - for authentification, identification, payment and data forwarding to distribution substation;
- *1-phase slow charge management* - circuit breaker with residual current device; contactor, energy meter, power socket, isolation control (for cases when EV battery is deeply discharged (SOC<10 %). Increase of battery pack voltage to nominal value is required for further connection of fast charging. When minimum EV battery pack voltage is restored, 1-phase connection is terminated. EVs which do not include fast charging option may be forwarded to other charging spots). Slow charging can also be utilized for final full charging (SOC=100 %);
- *Safety for slow charging* – ensure ground connection and plug present, ensure socket is dead if no vehicle present;
- *Auxiliary supplies* (e.g. converting 230 V AC to 12 V DC);
- *Inside temperature management* - heater and cooling unit (if required);

- *Emergency protection* - emergency mushroom pushbutton connected which allows physical power transmission with distribution substation through auxiliary data cabling.

The advantages of such future charging stations compared to the state of the art DC fast charging stations are:
- *Smaller size* – as there is no space required for the power converter inside the future charging stations, charging stations will have smaller dimensions and are lighter. This makes possible e.g. to install DC fast charging stations to narrow streets or for wall mounting, which increases the availability for DC fast charging and thus making purchasing of a EV more attractive.
- *Less noise* – charging stations without power converters do not require (forced) cooling facility thus do not make noise.
- *Fewer investments into infrastructure* – as larger filling stations are to be connected to the MV level through a distribution substation, the compact solution of positioning bidirectional power converters inside the substations and compact positioning of smaller size charging stations downsizes the total cost of investments into real-estate.
- *Scalability* – with the development of batteries, EV capacities and charging currents may increase in the future. This would require replacement of existing charging stations to more powerful ones. If enough reserve space is considered in the substation output bays (for at least one size higher kW rating of DC-DC converters), reserves are taken into consideration in EVSE's input cables and terminals, there is no need for replacement of EVSEs and make new investments into real-estate.
- *Competition* – as there are no power converters inside the EVSE, manufacturing of EVSE cabinets is more feasible for many enterprises without the complexity of installation and management of power converters. Telecommunication operators can compete with the development of the most user friendly HMI interface (identification and payment).

The main disadvantages of such compilation of distribution substations and future EVSEs are:
- *Investments into reconstruction* – to install new type of topology into existing substations requires investments into reconstruction, additional substation for housing new battery storages and power converters or even substituting the existing substation due to lack of necessary reserve space. This could be solved by step-by-step approach of replacing existing substations at the end of their lifetime (30-50 years) and expansion of amount of EVs in the roads.
- *Investments into energy storing* – energy storing is an additional cost at the moment of investment. This requires a long term commitment for return of investment.

- *Connection time* – to use EVs for grid support requires that EVs have to be connected to a charging station for a longer period of time (at least 2 hour – e.g. 30 min for charging, 1 h for utilizing EV battery for grid support and 30 min to charge battery to final SOC level). This means that the concept of utilizing EVs for Smart Grid applications through bidirectional substations is not suitable for public charging (EV owners want a fast charge and drive away). The solution is more applicable for semi-public places such as factories, offices, public car parks and shopping centres.

2.3.5 Generalizations

This thesis focuses on distribution substations for semi-public charging as semi-public charging allows variety of V2G applications. The selected topology with integrated AC and DC bus illustrated in Fig. 2.5 will be simulated in more detailed in Chapter 4. EV charging is supplied from MV side.

3. MODELING

In order to evaluate control and protection functions presented in Chapter 4 an adequate computer simulation model is required for dynamical simulations. From the simulation model can be followed the movement of command signals in time and measured output parameters. There are three key parts in the integrated AC & DC bus topology that needs to be simulated: Li-ion battery model (for both EV and BESU), bidirectional AC-DC power converter model and bidirectional DC-DC power converter model. Simulations are carried out in MATLAB Simulink, which has excellent simulation environment for dynamical simulations.

For dynamical simulations an adequate Li-ion battery model is required to simulate charging and discharging of EV or BESU batteries. The model should have similar characteristic curves to a real Li-ion battery. In Chapter 3.1 are described mathematical models of Li-ion batteries and simulation results of Li-ion batteries in the MATLAB Simulink.

The bidirectional AC-DC power converter rectifies AC side voltage to DC voltage (provides energy from the grid to the common DC bus as a power source) or inverts DC voltage to AC voltage (transfers energy from the common DC bus to the AC power grid). AC-DC converter controls the power factor during energy exchange, e.g. the phase angle between the AC line voltage and current. The model should have similar efficiencies reported about bidirectional AC-DC power converters in the literature and have adequate output parameters. In Chapter 3.2 are described topologies of bidirectional AC-DC power converters for transferring active and reactive power (D-STATCOM), control principles for rectification and inversion either to the LV or the MV level and LCL-filter for electromagnetic compability (EMC) reduction. Simulation results of the bidirectional AC-DC power converter in the MATLAB Simulink are presented.

The bidirectional DC-DC power converter controls charging or discharging current of a battery (by regulating output voltage). For charging batteries, the DC-DC converter lowers the common DC bus side voltage to battery specific charging voltage level. For discharging the batteries the DC-DC converter increases the battery voltage to match the common DC bus voltage level. The model should have similar efficiencies reported about bidirectional DC-DC power converters in the literature and have adequate output parameters. In Chapter 3.3 are described topologies of bidirectional DC-DC power converters. Simulation results of the bidirectional DC-DC power converter in the MATLAB Simulink are presented.

Bidirectional AC-DC-DC converters have the AC-DC and the DC-DC power converters in series.

The purpose of the computer simulation models is not to develop or simulate a particular bidirectional AC-DC or DC-DC power converter, therefore the models may include some simplifications. The simulation models should still be adequate for further evaluation of bidirectional energy exchange possibilities between the EVs and the utility network.

3.1 Li-ion batteries of electric vehicles and battery energy storage unit

3.1.1 Mathematical models of Li-ion batteries

There are basically three types of battery models reported in the literature: experimental, electrochemical and electric circuit-based [94]. Experimental and electrochemical models are not well suited to represent cell dynamics for the purpose of SOC estimations of battery packs. In this thesis a model using only SOC as a state variable is chosen. The chosen equivalent circuit of the battery is presented in Fig. 3.1 [95]. The battery is modelled using a simple controlled voltage source in series with a constant resistance.
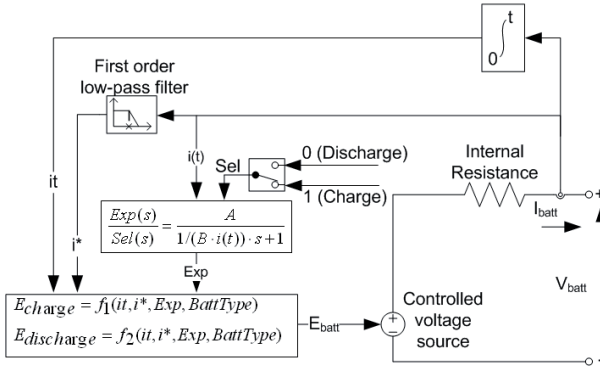
Fig. 3.1 Equivalent circuit of non-linear battery model for most popular types of rechargeable batteries (lead-acid, lithium-ion and nickel-metal-hydride) [95]

Mathematical equations for Li-ion batteries based on Fig. 3.1 are presented as follows [95]:

Discharge model (i* > 0)

$$f_1(it,i*,i) = E_0 - K \cdot \frac{Q}{Q - it} \cdot i* - K \cdot \frac{Q}{Q - it} \cdot it + A \cdot \exp(-B \cdot it), \qquad (10)$$

Charge model (i* < 0)

$$f_2(it,i*,i) = E_0 - K \cdot \frac{Q}{it + 0.1 \cdot Q} \cdot i* - K \cdot \frac{Q}{Q - it} \cdot it + A \cdot \exp(-B \cdot it), \qquad (11)$$

where E_0 is the battery constant voltage (V), K is the polarization voltage (V), $i*$ is the low frequency current dynamics (A), i is the battery current (A), it is the extracted capacity (Ah), Q is the maximum battery capacity (Ah), A is the voltage drop during the exponential zone (V), and B is the exponential capacity at the end of the exponential zone (Ah)$^{-1}$.

Model assumptions [95]:
-   the internal resistance is supposed constant during the charge and discharge cycles and doesn't vary with the amplitude of the current;
-   the parameters of the model are deduced from discharge characteristics and assumed to be the same for charging;
-   the capacity of the battery doesn't change with the amplitude of current;
-   the model doesn't take the temperature into account;
-   the self-discharge of the battery is not represented;
-   the battery has no memory effect.

With some simplifications [94] for equation (10), the battery voltage can be presented in form [94]:

$$V_{batt} = E_{batt} - i \cdot R = E_0 - K \cdot \frac{Q}{Q - \int idt} + A \cdot \exp\left(-B \cdot \int idt\right) - i \cdot R , \qquad (12)$$

where E_{Batt} is the nonlinear no-load voltage of battery (V), R is the internal resistance, and V_{Batt} is the battery voltage (V).

The parameters of the equivalent circuit can be modified to represent a particular battery characteristic, based on its discharge characteristic. A typical discharge curve is composed of three sections, as shown in Fig. 3.2 [94]. The first section represents the exponential voltage drop, when the battery is charged. Depending on the battery type, this area is more or less wide. The second section represents the charge that can be extracted from the battery until the voltage drops below the battery nominal voltage. Finally, the third section represents the total discharge of the battery, when the voltage drops rapidly. When the battery current is negative, the battery will recharge. For simplification, the charge characteristic parameters of the model are deduced from the discharge characteristics and assumed to be the same for charging.
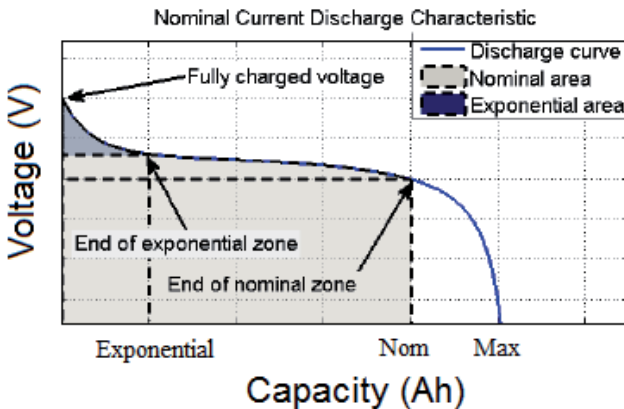
Fig. 3.2 Discharge characteristics of Li-ion batteries [94]

Internal resistance is very important in order to adequately represent the voltage drop caused by a current variation in the battery [94]. The internal impedance is generally specified in the manufacturer's datasheet. In some cases the internal impedance is not specified in the datasheets or the specified internal impedance provided by the manufacturer doesn't allow, for the purposed model, to accurately represent the potential difference caused by the variation of the current. It is therefore necessary to establish an analytical relation linking the internal resistance of the model to the nominal voltage and the rated capacity of the battery. Internal resistance affects the output voltage of the battery, thus the efficiency. Efficiency varies with the capacity and the nominal voltage of the battery [94]:

$$\eta = 1 - \frac{I_n \cdot R \cdot I_n}{U_n \cdot I_n}, \tag{13}$$

where η is the efficiency (%), I_n is the rated current (A), R is the internal resistance of the battery (ohms), and U_n is the nominal voltage (V). The rated current is the one used for the nominal discharge curve (typically 0.2 C-rate) [94]:

$$I_n = Q_n \cdot 0.2 / 1h, \tag{14}$$

where Q_n is the rated capacity of the battery (Ah), the value "0.2" represents the C-rate, and value "1h" represents time of one hour. Therefore [94]:

$$\eta = 1 - \frac{0.2 \cdot R \cdot Q_n}{U_n}, \tag{15}$$

$$R = U_n \cdot \frac{1 - \eta}{0.2 \cdot Q_n}. \tag{16}$$

The efficiency of Li-ion batteries is very high and for simplification can be taken 99% for calculations. The rest of the model parameters for equation (12) can be taken from discharge curves of battery manufacturer (Fig. 3.2). With some simplifications, the parameters can be deduced as follows [94]:

$$A = E_{Full} - E_{Exp}, \tag{17}$$

$$B = \frac{3}{Q_{Exp}}, \tag{18}$$

$$K = \frac{(E_{Full} - E_{Nom} + A(\exp(-B \cdot Q_{Nom}) - 1)) \cdot (Q - Q_{Nom})}{Q_{Nom}}, \tag{19}$$

$$E_0 = E_{Full} + K + R \cdot i - A, \tag{20}$$

where E_{Full} is the fully charged voltage (V), E_{Exp} is the voltage at the end of the exponential zone (V), Q_{Exp} is the capacity at the end of the exponential zone (Ah), E_{Nom} is the voltage at the end of the nominal zone (V), and Q_{Nom} is the capacity at the end of the nominal zone (Ah).

State of Charge (SOC) is a number from 0 % to 100 %, which indicates the level of energy left in a battery as a percentage of full battery capacity. SOC of batteries can be calculated as:

$$SOC = 100 \cdot \left(1 - \frac{1}{Q}\int_0^t i(t)dt\right) = \frac{E_{avl}}{E_{rated}} \cdot 100, \tag{21}$$

where i is the battery current (A), t is the time (s), Q is the maximum battery capacity (Ah), E_{avl} is the actual energy stored inside the battery (kWh), and E_{rated} is battery's full energy capacitance (kWh).

The battery state of health (SOH) is a measure of the battery's ability to store and deliver electrical energy. Typical SOH methods characterize either the battery power or energy. With the aging of the battery, loss of battery power will result in ineffective operation and can lead to malfunctions. The SOH can't be directly measured, it can only be estimated with different algorithms. State of health (%) can be calculated as:

$$SOH = 100 \cdot \left(\frac{Q_i}{Q_0}\right), \tag{22}$$

where Q_i is the ith capacitance (Ah) measurement in time, and Q_0 is the initial battery capacity (Ah) value. The SOH can be estimated during capacity measuring test cycles and using Ah-V characteristics [96]. Battery's SOH will decrease faster, if the battery is subject to extreme conditions like high operating temperature or excessive charging/discharging current.

Depth of discharge (%) describes the amount of energy that has been removed from a battery (DOD = 100 % - SOC) [97]. All battery manufacturers recommend keeping the depth of discharge (DOD) bellow the maximal limit of 100 %. Ideally 80 % DOD or less is recommended. The smaller the DOD the larger the number of battery cycles. DOD should be kept at the central part of the capacity range (Fig. 3.3 [97]), otherwise the cell performance may degrade faster.
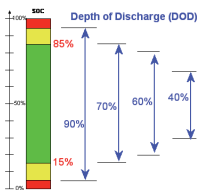
Fig. 3.3 Visualization of depth of discharge [97]

3.1.2 MATLAB Simulink models of Li-ion batteries

Mathematical equation (12) and MATLAB Simulink model should represent a real battery in an adequate way. Therefore both the mathematical equation and the MATLAB Simulink model results are compared with an example real Li-ion battery discharge curve given by the manufacturer's test results. The comparison results are taken in basis for modelling electric vehicle battery pack and BESU battery pack for further simulations.

For a practical example, discharge characteristic curves of Winston LYP90AHA and LYP100AHA batteries are presented in Fig. 3.4 [98]. The same type of batteries will be used later in laboratory test bench, but with smaller rated capacity (discharge characteristic curve will remain similar).
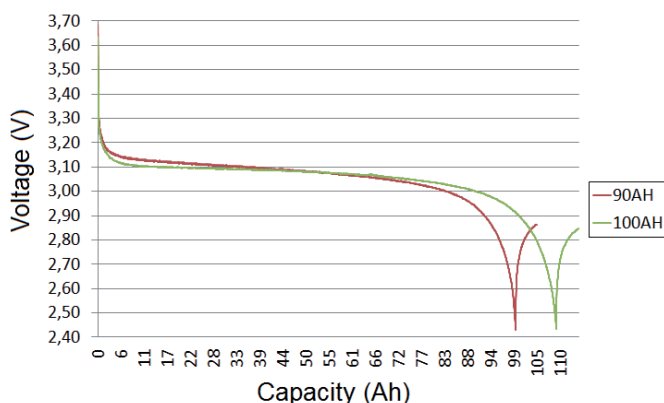
Fig. 3.4 Discharge characteristics of Winston 90 Ah and 100 Ah Li-ion batteries at 1C rate (102 A) [98]

From the Fig. 3.4 [98] can be taken the following parameter values for Winston LYP100AHA batteries: E_{Full} is 3.64 V, E_{Exp} is 3.125 V, Q_{Exp} is 1.5 Ah, E_{Nom} is 3.0 V, Q_{Nom} is 95 Ah. Maximum battery capacity Q is 109 Ah, battery current i is 102 A for the test (≈ 1 C-rate) and the internal resistance R is taken from manufacturer's datasheet, which is $<= 0.6$ mΩ. Using equations (17) (18) (19) (20), the parameters for the mathematical equation (12) are as follows: A is 0.515 V, B is 2 (Ah)$^{-1}$, K is 0.018 V, and E_0 is 3.2 V. Results of equation (12) are presented in Fig. 3.5 (a) (curve "Calculated").

The "Calculated" curve in Fig. 3.5 (a) is slightly off compared to the real 100 Ah Winston battery (+0.16 V at 0.5 Ah, +0.09 V at 50 Ah). With slight modification of changing E_0 to 3.11 V, the result of curve "Modified" in Fig. 3.5 (a) is more accurate compared to a real 100 Ah battery (+0.07 V at 0.5 Ah, -0.37 mV at 50 Ah). In practice, it is possible to get 109 % of the rated capacity out of the battery, but in future simulations the rated capacity is taken for basis.

Table 3.1 describes the parameters of MATLAB Simulink Li-ion battery model [95]. Parameters for the model are taken form the manufacturer's test results and datasheet. For getting a similar result with the manufacturer's datasheet the capacity

rating at the nominal zone is slightly modified to 88 Ah. The parameters in the Table 3.1 are presented for single cell and can be recalculated to a corresponding value of how many cells are in series or parallel in the battery pack [95]. The nominal voltage (V) represents the end of the linear zone of the discharge characteristics. The rated capacity (Ah) is the minimum effective capacity of the battery. Initial state of charge (%) indicates the SOC of the battery at the beginning of the simulation. Maximum capacity (Ah) is the maximum theoretical capacity, when a discontinuity occurs in the battery voltage. Fully charged voltage (V) shall be taken from the discharge characteristic curve. Nominal discharge current (A) is the current of the discharge curve, which is taken for basis. Internal resistance of the battery (ohms) shall be taken from technical specifications of the battery. Capacity (Ah) at nominal voltage is the capacity extracted from the battery until the voltage drops under the nominal voltage. The exponential zone parameters correspond to the end of the exponential zone [95].
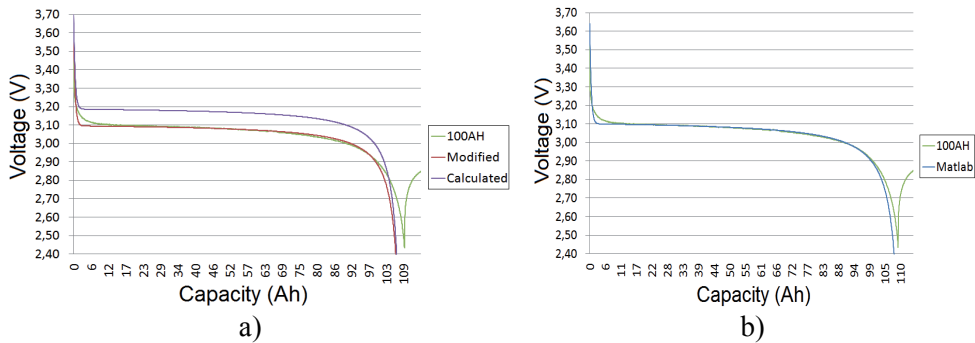
Fig. 3.5 Comparison of a real 100 Ah battery between calculated and modified discharge characteristics (a), comparison of a real 100 Ah battery between MATLAB Simulink single cell 100 Ah model (b)

Table 3.1. Data of 100 Ah single cell battery in MATLAB Simulink model

Parameter	Single cell 100 Ah
Nominal voltage	3.0 V
Rated capacity	100 Ah
Initial state-of-charge	100 %
Maximum capacity	109 Ah (109 %)
Fully charged voltage	3.64 V
Nominal discharge current	100 A (1 C)
Internal resistance	0.6 mΩ
Capacity at nominal voltage	88 Ah (88 %)
Exponential zone voltage	3.125 V
Exponential zone capacity	1.5 Ah (1.5%)

MATLAB Simulink model of Li-ion battery is presented in Fig. 3.6 [95]. The output of the battery block (m) is a vector containing three signals: state of charge of the battery (%), battery current (A) and battery voltage (V).
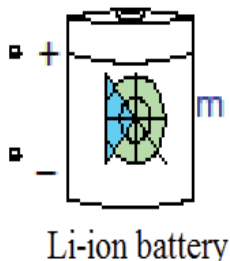
Fig. 3.6 MATLAB Simulink model of Li-ion battery block [95]

Simulation results of MATLAB Simulink model are compared with Winston LYP100AHA battery in Fig. 3.5 (b). From Fig. 3.5 (b) it can be concluded that the simulation model is quite accurate to the real battery (+0.11 V at 0.5 Ah, +1.4 mV at 50 Ah, -8.1 mV at 99.5 Ah). Therefore, adequate simulation models can be similarly deducted for the Mitsubishi i-MiEV and Battery pack 40 Ah, which will be used in the laboratory test bench. Parameters for the EV are described in the chapter 1.1.2. Parameters for the BESU are taken from the Winston LYP100AHA manufacturer's battery test results. Table 3.2 describes the technical parameters of MATLAB Simulink battery models for the EV and the BESU. Simulated discharge characteristic curve of BESU 40 Ah is presented in Fig 3.7.

Simulated charge characteristic curves of single cell 100 Ah Li-ion battery, EV and BESU 40 Ah is presented in Fig 3.8. Simulation is carried out with time step of $\Delta t = 2$ s (simulation time 3846 s $\approx$ 64 min), charge rate of 1 C (100 A for single cell, 50 A for EV, 40 A for BESU), from SOC 2 % to 100 %.

Table 3.2, Data of EV and BESU for future simulations in MATLAB Simulink

Parameter	Mitsubishi i-MiEV	Battery pack 40 Ah
Nominal voltage	3.7 V x 88 ≈ 330 V	3.0 V x 144 = 432 V
Rated capacity	50 Ah	40 Ah
Initial state-of-charge	Depending of simulation	Depending of simulation
Maximum capacity	54.5 Ah (109 %)	43.6 Ah (109 %)
Fully charged voltage	4.5 V x 88 = 396 V	3.64 V x 144 = 524.16 V
Nominal discharge current	50 A (1 C)	40 A (1 C)
Internal resistance	1.5 mΩ x 88 = 132 mΩ	0.6 mΩ x 144 = 86.4 mΩ
Capacity at nominal voltage	44 Ah (88 %)	35.2 Ah (88 %)
Exponential zone voltage	340 V	3.125 V x 144 = 450 V
Exponential zone capacity	0.75 Ah (1.5%)	0.6 Ah (1.5 %)
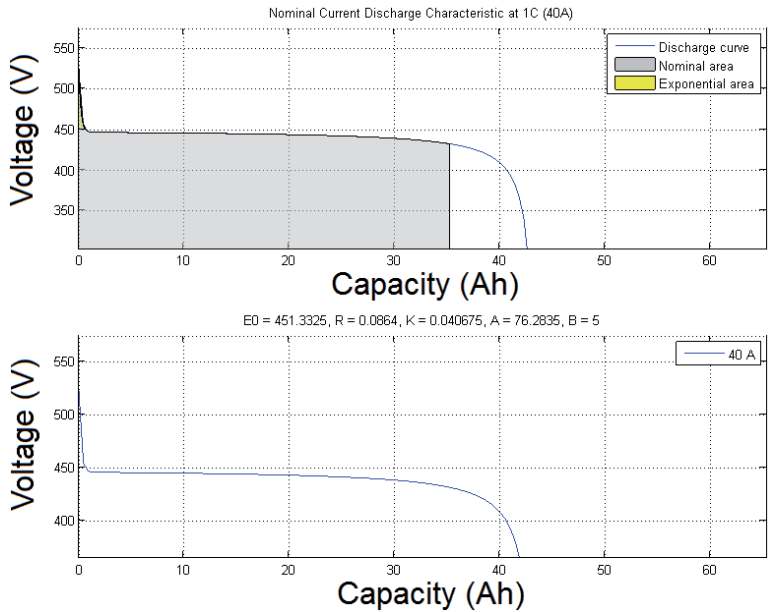
Fig. 3.7 Discharge characteristics of BESU 40 Ah in MATLAB Simulink

The initial and final battery voltages of the charging simulations in Fig. 3.8 are 2.57–3.87 V for single cell, 364.4–547.4 V for BESU and 301–417.4 V for EV.
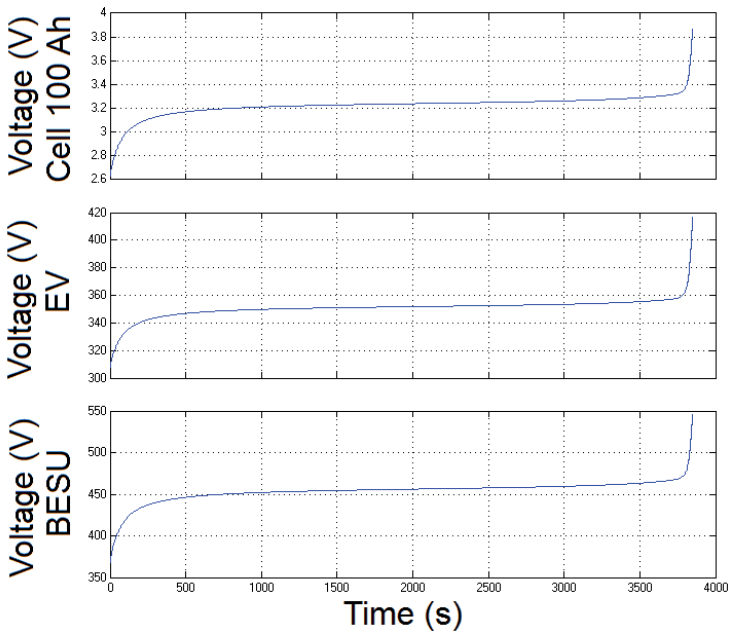
Fig. 3.8 Charge characteristics of single Li-ion battery cell 100 Ah, electric vehicle Mitsubishi i-MiEV and BESU 40 Ah in MATLAB Simulink

The MATLAB Simulink model has two limitations [95]:
- the minimum no-load battery voltage is 0 V and the maximum battery voltage is equal to $2*E_0$,
- the minimum capacity of he battery is 0 Ah and the maximum capacity is Q_{max}.

Experimental validation of the model, declared in the MATLAB Simulink, show a maximum error of 5 % (when SOC is between 10 % and 100 %) for charge (current between 0 and 2 C) and discharge (current between 0 and 5 C) dynamics [95].

3.1.3 Generalizations

The modelling of a battery is a very complex procedure and accurate models require a thorough knowledge of battery electrochemistry. The simulation of complete systems, as control functionality through distribution substations, does not require such high level of precision. It is important that general behaviour of a battery is described (e.g. voltage available depends on the SOC and current). For detailed simulations, the results of simulation models have to be compared to manufacturer's battery discharge curves given in the datasheets. The described model in this thesis is simple and requires few parameters from the manufacturer's battery discharge curve.

In practice, the internal resistance varies with the amplitude of the current and ambient temperature. The internal resistance directly influences the capacity of the battery during charging and discharging. With the aging of the battery (SOH) the efficiency of charging and discharging changes, thus 99% efficiency is only valid at the beginning of the battery's lifetime.

Considering simulation results, the MATLAB Simulink battery model can still accurately represent the discharge curves of battery manufacturers for further development of substation's control functionality.

3.2 Bidirectional AC-DC converters

Several different power electronic circuit topologies for bidirectional AC-DC converters are possible [99]. The evaluation and development of the optimized converter is still a challenge. Optimized topology depends on the power rating. Single-phase Power Factor Corrector (PFC) mains interfaces can be used for low charging power levels (P < 7 kW). For higher charging power levels 3-phase PFC interfaces have to be applied.

Voltage and current rating as well as the operating frequency are the main criteria for the selection of the power semiconductor devices. For DC fast charging of EVs the most suitable devices are isolated gate bipolar transistors (IGBTs) together with ultrafast switching diodes. In Fig. 3.9 [100] are compared MOSFET, IGBT, GTO and thyristor power semiconductors in current, voltage and switching frequency domains.
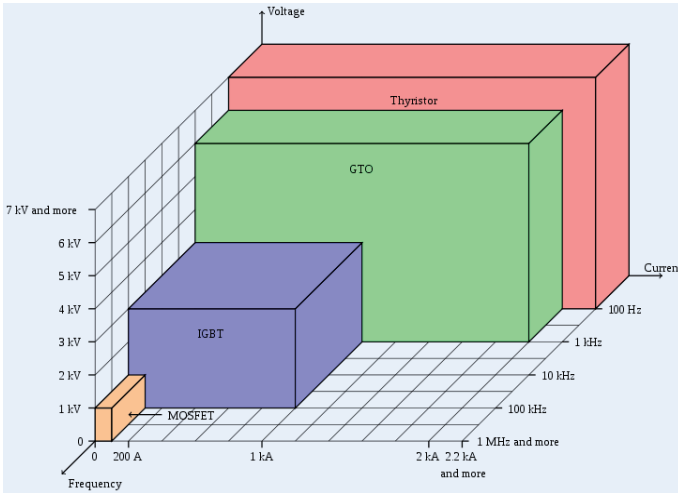
Fig. 3.9 Current/Voltage/Switching frequency domains of the main power electronic switches [100]

IGBTs have been the preferred device under the following conditions [101]:
-   low duty cycle;
-   low frequency (<20 kHz);
-   narrow or small line or load variations;
-   high-voltage applications (>1000 V);
-   operation at high junction temperature is allowed (>100 °C);
-   >5 kW output power.

3.2.1 Structure of bidirectional AC-DC converters

Pulse-width-modulation (PWM) converters with voltage source output or current source output can be used as PWM converters (Fig. 3.10) [102]. PWM converter with voltage source output works with fixed DC voltage polarity (increases the voltage at DC side). PWM converter with current source output operates with fixed DC current flow [102], [103]. A properly designed low-pass passive filter is needed in front of the PWM converter due to electromagnetic interface (EMI) concerns.
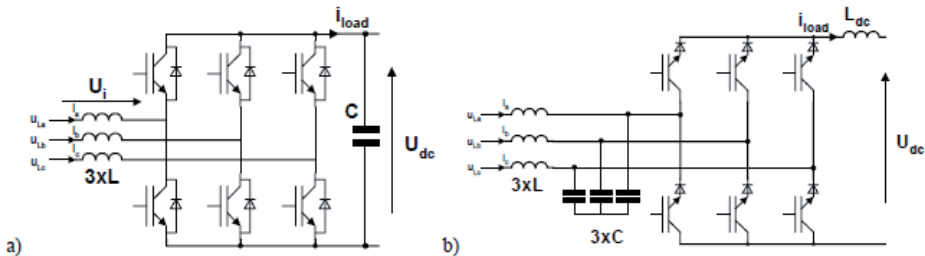
Fig. 3.10 Basic topology of PWM converter (rectifier): with voltage output (a) or current output (b) [102]

Among the main features of PWM converter are [102]:
- bidirectional power flow;
- nearly sinusoidal input current;
- regulation of input power factor to unity;
- low harmonic distortion of line current (THD below 5%);
- adjustment and stabilization of DC-link voltage (or current)
- reduced capacitor size with the continues current;
- can be properly operated under line voltage distortion and line voltage frequency variations.

Control strategies for PWM converters include e.g. virtual flux based direct power control (VF-DPC), direct power control (DPC), voltage oriented control (VOC), virtual flux oriented control (VFOC) [102].

For describing a converter working in 4 quadrants a simplified (ideal) single-phase representation of the PWM converter circuit is represented in Fig. 3.11 [104].
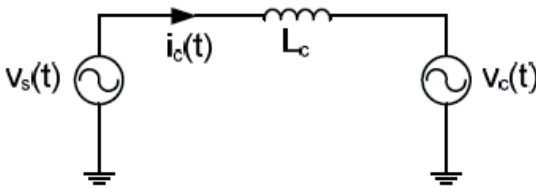
Fig. 3.11 Simplified single-phase representation of three-phase PWM converter circuit for bi-directional power flow [104]

Positive current direction from the power grid to the converter is firstly viewed [104]. The model parameters are given as follows: L_C represents the line inductor (H); $v_S(t)$ is the instantaneous line voltage (V); $v_C(t)$ is the instantaneous bridge converter voltage (V) controllable from the DC-side; $I_C(t)$ is the instantaneous converter current (A); d is the phase difference between $v_C(t)$ and $v_S(t)$; q is the phase difference between $I_C(t)$ and $v_S(t)$; f is the system frequency (50 Hz). Magnitude of $v_C(t)$ depends on the modulation index and DC voltage level.

The grid voltage is assumed to be purely sinusoidal. For simplification, high frequency components of inverter output voltage, $v_C(t)$, is neglected. Following equations can be derived [104]:

$$v_s(t) = \sqrt{2}V_s \sin(wt), \tag{23}$$

$$v_c(t) = \sqrt{2}V_c \sin(wt - d), \tag{24}$$

$$X_c = 2\pi f L_c. \tag{25}$$

For describing power transferring from the converter to the grid in the model, two voltage sources should be viewed as decoupled in Fig. 3.11 and line inductor is to

be viewed as a source. From this model simplification line current can be written as [104]:

$$i_c(t) = \sqrt{2}I_c \sin(wt - q).$$ (26)

Since the default direction for active and reactive power transfer is from grid to converter, $I_C(t)$ and $v_C(t)$ are lagging the grid voltage [104]:

$$V_s = V_c + jX_c I_c.$$ (27)

Fig. 3.12 shows phasor diagrams for converter circuit and *P-Q* plane. Fig. 3.12 [104] indicates all the different operation modes in which the converter can be working.
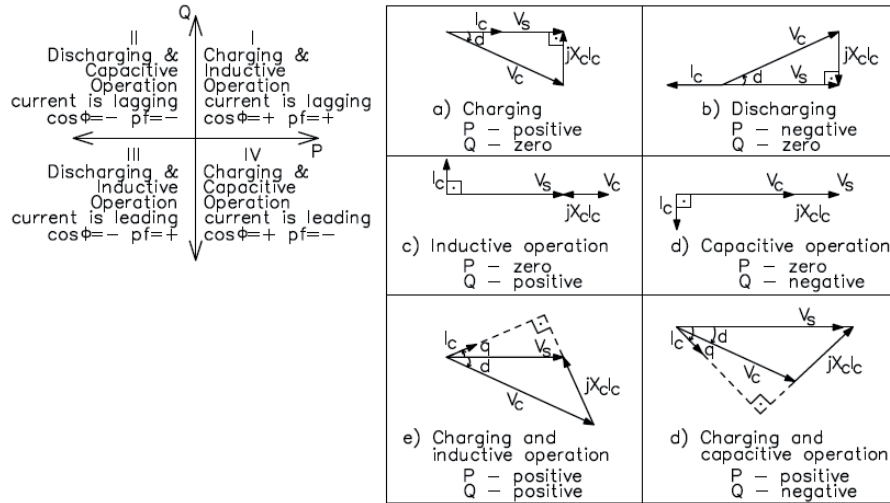
Fig. 3.12 P-Q plane showing charger operation modes and vector diagram for different operation modes [104]

Active power is provided by the grid as long as $v_C(t)$ lags $v_S(t)$, and it is sent to grid when $v_S(t)$ lags $v_C(t)$ [104]. Since $v_C(t)$ and $v_S(t)$ are sinusoidal, $I_C(t)$ is also sinusoidal as shown before. With controlling phase angle *d* and amplitude of converter voltage $v_C(t)$, it is possible to control indirectly phase and amplitude of line current. In this way average value and sign of DC current is subjected to control, what is proportional to active power conducted through converter. $I_C(t)$ phase angle, *q*, determines the direction of the reactive power flow. If *q* is positive, reactive power is sent to the grid, and if *q* is negative, reactive power is provided by the grid to the converter. The Fig. 3.12 shows that the voltage vector v_C is higher during regeneration (up to 3%) than rectifier mode, meaning that these two modes are not symmetrical [102].

3.2.2 Structure of AC-DC converters for medium voltage applications

Multi-level converters have been receiving attention in the recent years and have been proposed as the best choice in a wide variety of MV applications [105]. They enable a commutation at substantially reduced voltages and an improved harmonic spectrum without a series connection of devices, which is the main advantage of a multi-level structure. Among the high-power multi-level converters, three topologies have been successfully implemented as standard products for MV industrial drives: the three-level neutral point clamped (NPC) voltage source converter (3L-NPC VSC in Fig. 3.13 [106]), the four-level flying capacitor voltage source converters, and series connected H-bridge voltage source converters [105].
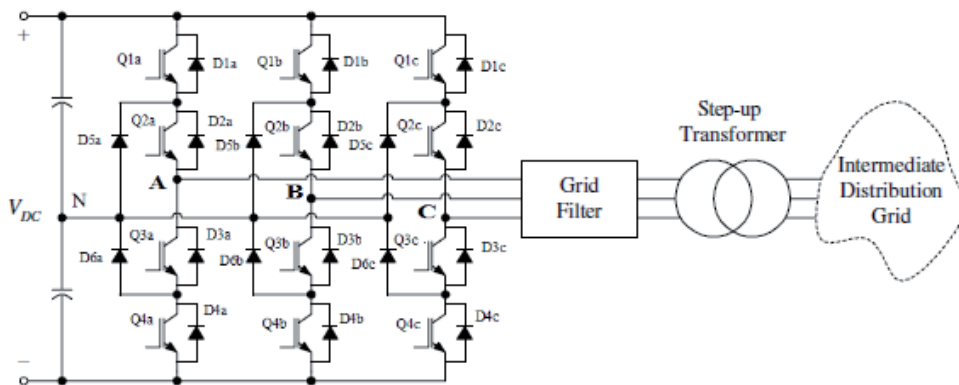
Fig. 3.13 Three-level neutral point clamped (NPC) power converter topology [106]

The 3L-NPC VSC offer technical advantages like a simple power part, a low component count, and straightforward protection and modulation schemes [105]. On the other hand, the hard-switching transients of the power semiconductors at high commutation voltage cause high switching losses and a poor harmonic spectrum, which produces additional losses in e.g. machines. The 3L-NPC VSC power converter consists of three arms of power switching devices. Each arm consists of four switching devices along with their anti-parallel diodes and two neutral clamping diodes as shown in Fig. 3.13.

For the operating principle, there are three states/voltages which can be applied for each phase. These are positive (1), negative (-1) and neutral (0). These three states can be used in the space vector modulation as shown in Fig. 3.14 with an optimal switching strategy [107]. By looking on a single phase, the switching pattern to reach each state (i, j, k) becomes quite clear. If current $i_{ph,a}$ is positive, switch $Q1_a$ and switch $Q2_a$ can be closed to reach the positive voltage level $(+V_{DC}/2)$. If switches $Q2_a$ and $Q3_a$ are turned on, the neutral point is connected to phase A and if $Q3_a$ and $Q4_a$ are conducting the negative voltage level $(-V_{DC}/2)$ is applied to phase A. The same considerations can be made if $i_{ph,a}$ is negative. With these states, space vector modulation can be used to control the power flow and power factor correction.
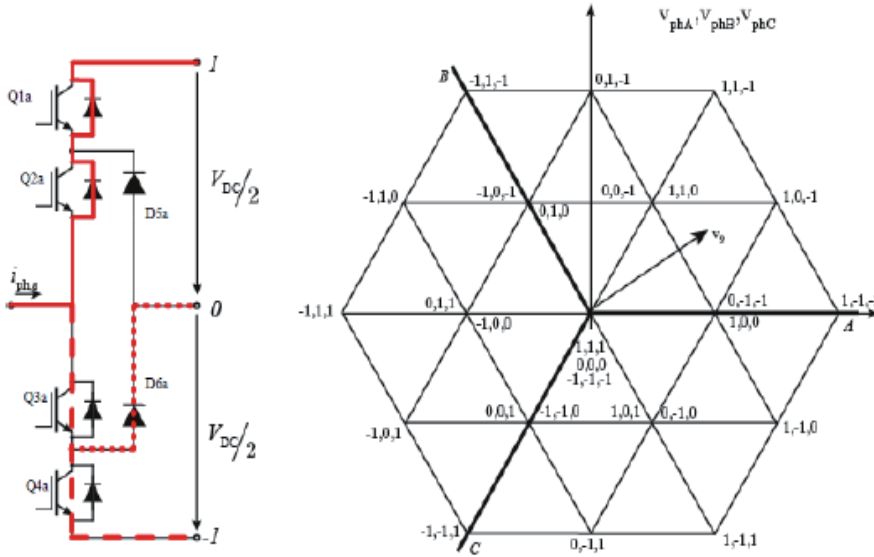
Fig. 3.14 Operating principle of one phase bridge of the NPC converter and switching pattern for the space vector modulation [107]

3.2.3 Control of rectification of AC-DC converters

An example control method for rectification can be Voltage Oriented Control. Control of PWM converter is based on coordinate transformation between stationary *α-β* and synchronous rotating *d-q* reference system [102] in Fig. 3.16. Both strategies guarantees fast transient response and high static performance via an internal current control loops. VOC scheme is shown in Fig. 3.15 [102].

Three phase measured values are converted to equivalent two-phase *α-β* system and then are transformed to rotating coordinate system in a block *α-β/d-q* [102]:

$$\begin{bmatrix} k_d \\ k_q \end{bmatrix} = \begin{bmatrix} \cos\gamma_{UL} & \sin\gamma_{UL} \\ -\sin\gamma_{UL} & \cos\gamma_{UL} \end{bmatrix} \begin{bmatrix} k_\alpha \\ k_\beta \end{bmatrix}, \tag{28}$$

where γ_{UL} is the angle of the voltage vector. With the transformation, the control values are DC signals. An inverse transformation *d-q/α-β* is achieved on the output of control system and it gives a result the rectifier signals in stationary coordinate [102]:

$$\begin{bmatrix} k_\alpha \\ k_\beta \end{bmatrix} = \begin{bmatrix} \cos\gamma_{UL} & -\sin\gamma_{UL} \\ \sin\gamma_{UL} & \cos\gamma_{UL} \end{bmatrix} \begin{bmatrix} k_d \\ k_q \end{bmatrix}. \tag{29}$$

For both coordinate transformation the angle of the γ_{UL} voltage vector is defined as [102]:

$$\sin \gamma_{UL} = u_{L\beta} \Big/ \sqrt{(u_{L\alpha})^2 + (u_{L\beta})^2} \, , \qquad (30)$$

$$\cos \gamma_{UL} = u_{L\alpha} \Big/ \sqrt{(u_{L\alpha})^2 + (u_{L\beta})^2} \, . \qquad (31)$$
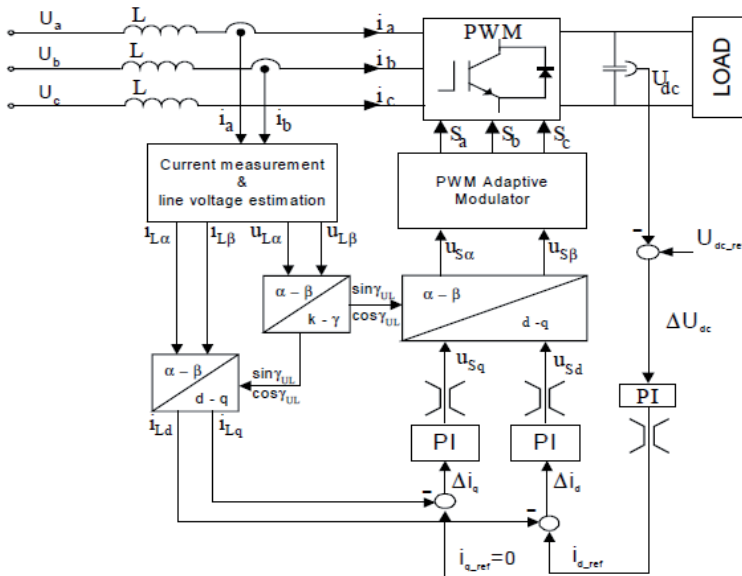
Fig. 3.15 Block scheme of AC voltage sensorless VOC [102]

In voltage oriented *d-q* coordinates, the AC line current vector $\underline{i}_L$ is split into two rectangular components $\underline{i}_L = [i_{Ld}, \ i_{Lq}]$ (Fig. 3.16) [102]. The component i_{Lq} determines reactive power, whereas i_{Ld} decides about active power flow. Thus the reactive and the active power can be controlled independently. The unity power factor condition is met when the line current vector $\underline{i}_L$ is aligned with the line voltage vector $\underline{u}_L$. By placing the *d*-axis of the rotating coordinates on the line voltage vector a simplified dynamic model can be obtained [102].
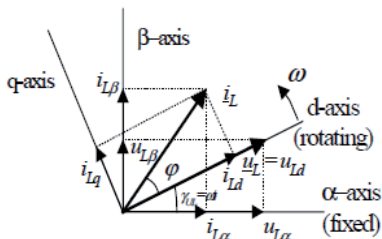
Fig. 3.16 Vector diagram of VOC. Coordinate transformation of line current, line voltage and rectifier input voltage from stationary α-β coordinates to rotating d-q coordinates [102]

Line voltage estimators perform very well even under unbalanced and pre-distorted conditions [102]. The current follows the voltage fairly well with VOC control strategies, which provides high value of total power factor.

Among the main advantages of VOC are [102]:
- low sampling frequency can be used for good performance, e.g. 5 kHz;
- fixed switching frequency (easier design of the input filter);
- cheaper analogue-to-digital converters;
- no sensitivity for inductance variation.

Among the main disadvantages of VOC are [102]:
- exist coupling between active and reactive components and some decoupling solution is required;
- complex algorithm;
- coordinate transformation and proportional-integral (PI) controllers are required;
- input power factor lower compared to DPC control techniques.

3.2.4 Control of inversion of AC-DC converters

The bidirectional AC-DC converter inverts DC side voltage to AC voltage. The bidirectional AC-DC converter transfers DC side power $P(t)$ to AC side. The bidirectional AC-DC converter in the inverter mode is represented in Fig. 3.17 [108].
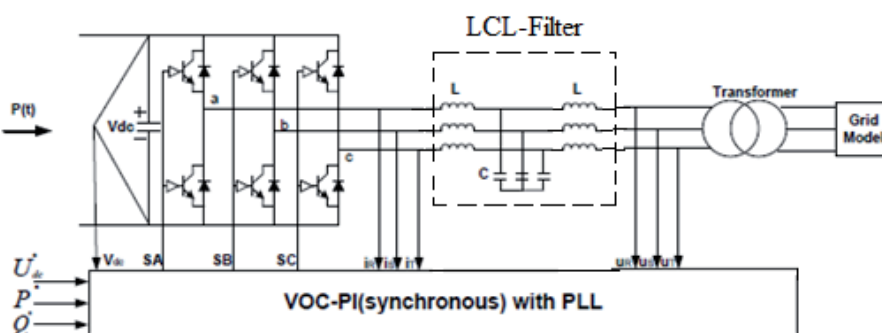
Fig. 3.17 Block diagram of AC-DC converter in inverter mode [108]

Phase angle, amplitude and frequency of the utility voltage are critical information for the operation of the grid-connected inverter systems [108]. Grid-connected operations are controlled to work close to the unity power factor in order to reach the standards. It requires the use of a synchronizing algorithm, which is able to synchronize the reference current of the inverter with the grid voltage. There are two basic synchronization methods [108]:
- Filtered Zero Cross Detection;
- Phase Locked Loop (PLL).

The first method is based on the detection of the zero crossing of the grid voltage, while the second one, PLL, is a feedback control system that automatically adjusts the phase of a logical generated signal to mach the phase of an input signal. The PLL is used to synchronize the inverter current angle, with the angle of the grid voltage, to obtain a power factor as close to unity as possible. The inverter current angle is used to calculate the reference current that is compared to the actual output current of the inverter. PLL requires two orthogonal voltages, which can be get for 3-phase systems representing the voltage vector $\underline{v}_{abc}$ in a rotating reference frame (dq). The structure of the dq PLL algorithm is represented in Fig. 3.18 [108].
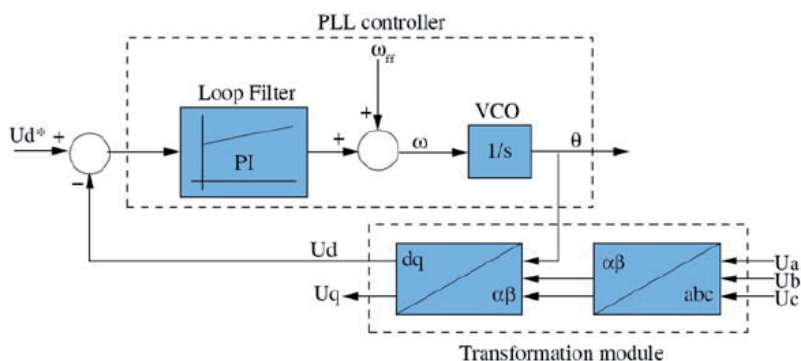
Fig. 3.18 Three-phase PLL structure [108]

The grid voltages are the input into the algorithm and they are transformed into synchronous reference frame by means of $abc{\rightarrow}dq$ transformation module [108]. The phase locking is realized by controlling the d-voltage to be zero. A regulator, usually PI, can be used to control this variable and the output of this regulator is the grid frequency. After the integration of the grid frequency, the utility voltage angle is obtained, which is fed back into the $abc{\rightarrow}dq$ transformation module in order to transform into the synchronous rotating reference frame.

A voltage oriented control method with PLL (VOC-PI with PLL) can be used to control the grid connected inverter [108]. In VOC-PI with PLL control method the current is oriented along the active voltage V_d and V_q. PLL is used to detect the phase grid angle ϑ, grid frequency and grid voltage. The frequency and voltage are needed in order to monitor the grid conditions and to comply with the control requirements, while grid angle is required for transformations to the synchronous frame (Clark and Park transformations). The currents are transformed from stationary (*abc*) to synchronous frame (*dq*) and conventional PI controllers are used. Decoupling of the cross-coupled *d* an *q* axis is performed as it is shown in Fig. 3.19 [108] to decouple the grid voltage from the output of the current controllers a voltage feed forward is used.

A standard PI controller is used also for the DC voltage and its output is feed-forwarded to the output of the PI controller to obtain the reference for the active current i_d and another PI controller is used to obtain the reference for the reactive

current i_q [108]. The biggest disadvantage for such control method is the low performance in case of unbalanced or faulty grid, where the grid angle is difficult to define.
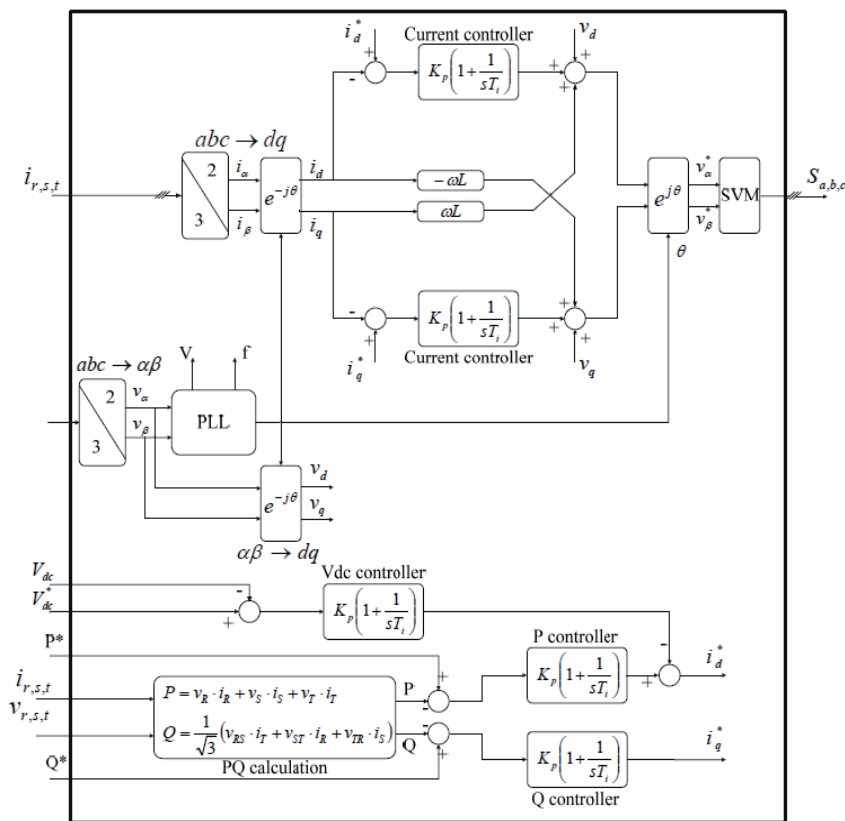
Fig. 3.19 Control structure for VOC-PI with PLL [108]

3.2.5 Control of inversion of AC-DC converters for medium voltage applications

The PLL shown in Fig. 3.20 is used to synchronise the AC-DC converter with the line voltage and also to calculate the transformation angle used in the *d-q* transformation [109]. The PLL block measures the system frequency and provides the phase synchronous angle θ for the *d-q* transformation block. In steady state, *sin(θ)* is in phase with the fundamental (positive sequence) of α component and phase A of the point of common coupling voltage (U_{abc}).

Control of converter is based on coordinate transformation between stationary *α-β* and synchronous rotating *d-q* reference system [109]. For transferring energy over the voltage transformer in the inverter mode, the Clark transformations for converting line voltages and currents from natural *abc* quantities to *α-β* reference system have to be adjusted accordingly to the transformer type.
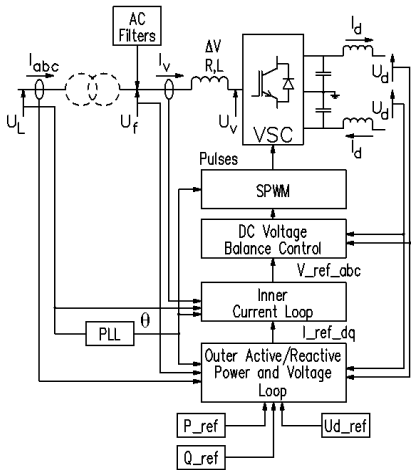
Fig. 3.20 Overview diagram of the VSC control system for 3L-NPC VSC [109]

These can be presented for star-star (Y/Y) transformer (or for transferring energy to the common AC bus without any transformer) for voltages (same principle applies for currents as well) [110]:

$$
\begin{bmatrix} v_\alpha \\ v_\beta \\ 0 \end{bmatrix} = \frac{2}{3} \begin{bmatrix} 1 & -\dfrac{1}{2} & -\dfrac{1}{2} \\ 0 & \dfrac{\sqrt{3}}{2} & -\dfrac{\sqrt{3}}{2} \\ \dfrac{1}{2} & \dfrac{1}{2} & \dfrac{1}{2} \end{bmatrix} \begin{bmatrix} v_a \\ v_b \\ v_c \end{bmatrix}.
\tag{32}
$$

Delta-star (Dyn11) transformers are the most common in utility networks as delta side nullifies 3rd harmonics. Equation (32) can be written for Dyn11 transformers (where star side voltage is leading by $\pi/6$ degrees) as [110]:

$$
\begin{bmatrix} v_\alpha \\ v_\beta \\ 0 \end{bmatrix} = \frac{2}{3} \begin{bmatrix} \dfrac{\sqrt{3}}{2} & -\dfrac{\sqrt{3}}{2} & 0 \\ \dfrac{1}{2} & \dfrac{1}{2} & -1 \\ 0 & 0 & 0 \end{bmatrix} \begin{bmatrix} v_a \\ v_b \\ v_c \end{bmatrix}.
\tag{33}
$$

The active power or the DC voltage is controlled by the control of phase shift between U_L (sinusoidal AC voltage in the AC network) and U_V (fundamental line to line voltage at valve side, Fig. 3.20). Reactive power is controlled by the control

of the modulation index (*m*). The instantaneous real and imaginary power of the inverter on the valve side can be expressed in terms of the *dq* component of the current and the voltage on the valve side (Fig. 3.20) as follows [109]:

$$p = \frac{3}{2} \cdot \mathrm{Re}(u_f^{-dq} \cdot i_v^{-*dq}) = \frac{3}{2} \cdot (u_{fd} \cdot i_{vd} + u_{fq} \cdot i_{vq}).$$ (34)

$$q = \frac{3}{2} \cdot \mathrm{Im}(u_f^{-dq} \cdot i_v^{-*dq}) = \frac{3}{2} \cdot (-u_{fd} \cdot i_{vq} + u_{fq} \cdot i_{vd}).$$ (35)

If the reference of the *dq*-frame is selected such that the quadrature component of the voltage is being very small and negligible, then the equations (34) and (35) indicate that the active (*p*) and the reactive power (*q*) are proportional to the *d* and *q* component of the current respectively [109]. Accordingly, it is possible to control the active power (or the DC voltage or the DC current) and the reactive power (or the AC bus voltage) by control of the current components i_{vd} and i_{vq} respectively. The active and reactive power and voltage loop contains the outer loop regulators that calculate the reference value of the converter current vector (I_{dq}^*) which is the input to the inner current loop.

The difference between the DC side voltages (positive and negative) are controlled to keep the DC side of the three level bridge balanced (e.g. equal pole voltages) in steady-state [109]. Small deviations between the pole voltages may occur at changes of active/reactive converter current or due to nonlinearity on lack of precision in the execution of the pulse width modulated bridge voltage. Furthermore, deviations between the pole voltages may be due to inherent unbalance in the circuit components impedance.

3.2.6 LCL filter

Power device switching frequencies between 2-15 kHz [111] may cause high-order harmonics (high frequency current ripple injected by the inverter) that will negatively affect the grid by causing non-sinusoidal voltage drop across the line impedance, disturb sensitive loads or equipments and increase losses in devices (motors, transformers, cables etc.). Extra losses increase temperature and decrease lifetime of devices. A low-pass passive LCL-filter can solve this issue, when connected between grid and AC-DC converter. LCL-filter is favoured because reduces the EMI conductive noise caused by the switching of the IGBTs.

The LCL-filter (Fig. 3.21 [108]) is composed by three reactors with resistance R_i and inductance L_i on the converter side and three capacitors C_f (damped with a resistor R_d); a further branch of the filter, represented as three reactors with resistance R_g and inductance L_g on the grid side. LCL-filters have star-connected capacitors, and the centre-star is not connected to the ground. Fig. 3.21 (a) represents equivalent circuit diagram of the filter for phase *a*. The components for very phase of the filter are supposed to be identical, so Fig. 3.21 is a suitable description also for phase *b* and *c* [108].
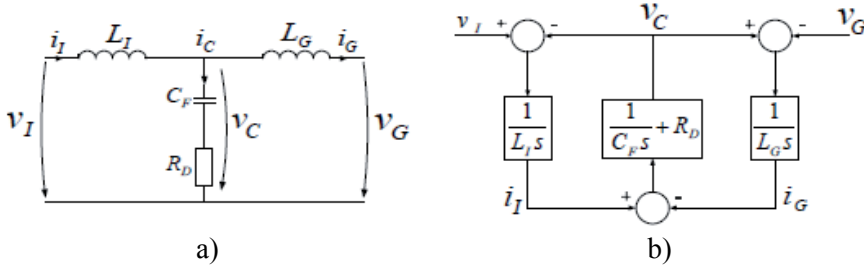
Fig. 3.21 Equivalent circuit diagram (a) and s-plane model of single phase LCL-filter (b) [108]

Grid voltage is assumed as ideal voltage source and represents short circuit for harmonic frequencies, and for filter analysis v_G is set to zero. The following transfer function of the LCL model (Fig. 3.21 (b)) can be written as [108]:

$$H(s) = \frac{i_I(s)}{v_I(s)} = \frac{L_I C_F s^2 + R_D C_F s + 1}{L_I L_G C_F s^3 + R_D C_F (L_I + L_G) s^2 + (L_I + L_G)s}.$$ (36)

Since the calculation on LCL parameters through transfer functions and simulations is complex, simplified algorithms have been presented in different literatures [106], [112], [113]. Minimum required converter side inductance L_I can be determined for neutral point clamped converter [106]:

$$L_{I_{min}} = \frac{V_{DC}}{24 \cdot \Delta i_{I_{max}} \cdot f_s},$$ (37)

where V_{DC} is the DC side voltage, Δi_{Imax} is the maximum allowable peak ripple current and f_s is the switching frequency. L_I can also be determined from [112]:

$$\frac{i_I(n_{sw})}{u_I(n_{sw})} \approx \frac{1}{\omega_{sw} L_I},$$ (38)

where ω_{sw} is the angular switching frequency, n_{sw} is the frequency multiple of the fundamental frequency at the switching frequency and u_I and i_I are the phase voltage and current on the converter side of the filter, respectively. The resonance frequency f_{res} of the LCL-filter is defined as [112]:

$$f_{res} = \frac{1}{2\pi} \sqrt{\frac{L_I + L_G}{L_I \cdot L_G \cdot C_F}} = \frac{1}{2\pi} \sqrt{\frac{1+r}{r \cdot L_I \cdot C_F}},$$ (39)

where r is the inductor ratio (r=L_G/L_I).

Ratio r can also be derived from [112]:

$$r = \frac{1}{\dfrac{i_G(n_{sw})}{i_I(n_{sw})} \cdot \left|1 - \left(\dfrac{\omega_{sw}}{\omega_{res}}\right)^2\right|} - 1 = \frac{1}{d \cdot \left|1 - k_{LCL}^2\right|} - 1,$$

(40)

where $i_G(n_{sw})$ is the line current at the switching frequency, ω_{res} is the angular resonant frequency, d is the attenuation of the switching frequency line current amplitude across the filter and $k_{LCL} = \omega_{sw}/\omega_{res}$. Capacitor value C_F can derivated from [112]:

$$C_F = \frac{1}{\omega_{res}^2 \cdot L_I \cdot (1 - d \cdot \left|1 - k_{LCL}^2\right|)},$$

(41)

The choice of capacitor value should fulfil the following criteria [113]:

$$\begin{cases} C_F = \dfrac{L_I + L_G}{L_I \cdot L_G \cdot (2 \cdot \pi \cdot f_{res})^2} \\ 10 f_n \le f_{res} \le 0.5 f_s \\ C_F \le 15\% C_b \end{cases},$$

(42)

where C_b is the base value of the system capacitance and f_n is the grid frequency. The equations (37) – (42) give the initial values for LCL filter parameters, which then have to be specified in more detail and verified through simulations [106].

3.2.7 D-STATCOM

Shunt connected reactive power compensators can be divided into static VAR compensators (SVC) and static synchronous generators (SSG) [114]. When the active energy source is replaced by a DC capacitor or DC reactor, which can not absorb or deliver active power except for short durations, SSG becomes a static synchronous compensator (STATCOM) [114]. STATCOM is a shunt connected Flexible AC Transmission System (FACTS) device, which generates a set of three phase sinusoidal voltages at fundamental frequency with controlled amplitude and phase angle [114]. When the STATCOM is applied in distribution systems or near the loads to improve power factor and voltage regulation it is called D-STATCOM (distribution static compensator) [114]. D-STATCOM provides protection for utility networks, industrial facilities or for weak distribution system against voltage sags caused by rapidly varying reactive current demand (e.g. non-linear dynamic

loads). In utility applications, a D-STATCOM provides leading or lagging reactive power to achieve system stability during transient conditions. The V-I characteristics of D-STATCOM is presented in Fig. 3.22 [114]. D-STATCOM is an active energy-exchanging device because it utilizes the passive energy storage component to realize the energy storing and exchanging and the switches to control the reactive power flow between different phases of a distribution system [114].
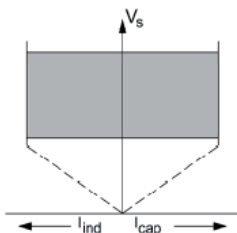
Fig. 3.22 V-I characteristics of D-STATCOM [114]

Voltage sags is one of the power quality problems for many industries as these may affect the production. Sensitive equipment (e.g. process controllers, programmable logic controllers (PLC)) in the industries may misoperate or a machine may possible shut down. Capacitor banks, parallel supply feeders or uninterruptible power supplies (UPS) are the main alternatives for D-STATCOM. AC-DC converters in distribution substations with V2G capability may provide additional compensation or support for existing distribution systems. Therefore the main control principles and opportunities are analyzed.

The main operation principles of the D-STATCOM is described in literature [115]. The D-STATCOM is a three-phase and shunt connected power electronics based device. It is connected near the load at the distribution system (Fig. 3.23) [103]. Typical D-STATCOM (Fig. 3.24) [116] consists of a DC capacitor, three-phase inverter (IGBT) module, AC filter, coupling transformer and a control system with control strategy (AC side voltage or reactive power control). The basic electronic block of the D-STATCOM is the voltage sourced inverter that converts an input DC voltage into three-phase output voltage at fundamental frequency. Passive filter are used to reduce the harmonics present in the output of the D-STATCOM. The controller of the D-STATCOM is used to operate the inverter in such a way that the phase angle between the inverter voltage and the line voltage is dynamically adjusted so that the D-STATCOM generates or absorbs the desired VAR at the point of connection. The phase of the output voltage of the inverter, V_i, is controlled in the same way as the distribution system voltage, V_S. Reactive power exchange between the D-STATCOM and the AC system is controlled by varying the amplitude of the D-STATCOM output voltage. Figure 3.25 [117] shows the three basic operation modes of the D-STATCOM output current, I, which varies depending upon V_i. If V_i is equal to V_S, the reactive power is zero and the D-STATCOM does not generate or absorb reactive power. If V_S is greater than V_i, the D-STATCOM absorbs inductive reactive power. If V_S is smaller than V_i, the

D-STATCOM generates capacitive reactive power. The injected current is kept in quadrature with the load voltage to achieve the desired voltage correction by injecting only reactive power into the system. The capacitor voltage can be decreased or increased to control reactive power output of the D-STATCOM. Therefore, voltage sag mitigation is controlled through PWM switching to switch on and off the IGBTs. Typical control circuit of D-STATCOM (Fig. 3.24) consists of PI controller is used to control the flow of reactive power to and from DC capacitor [118]. PLL components are used in the control to generate the switching signal (e.g. triangular waves) and reference signal (e.g. sinusoidal wave).
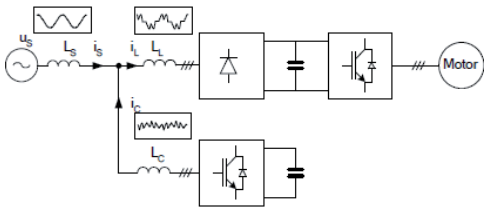
Fig. 3.23 Simplified model of the D-STATCOM [103]
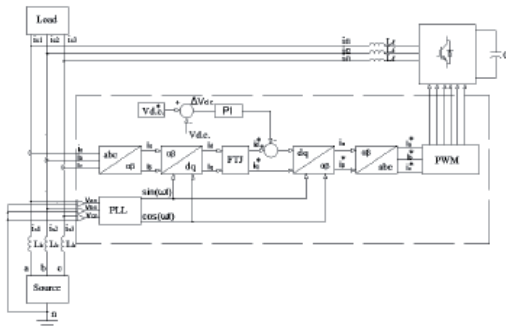
Fig. 3.24 Typical control circuit of the D-STATCOM [116]
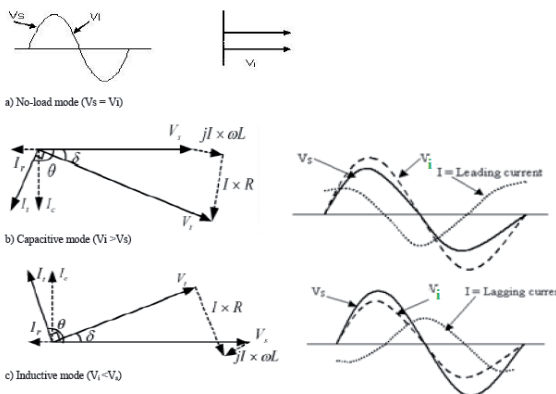
Fig. 3.25 Operation modes of D-STATCOM [117]

113

For higher voltage sags, injection of active power in addition to reactive power is essential to correct the voltage magnitude. The active power injection of the device must be provided by an external energy source [118].

The amplitude of the inverter voltage V_i is proportional to the DC voltage of the capacitor, which is proportional to the amount of energy stored in capacitor. Suitable size of DC capacitor is needed for storing energy for mitigating voltage sag. DC capacitor can be determined by considering its physical size, cost and the possibility of resonance for a given coupling reactance. Capacitor sizing [117], [118] is referred to the fault current in the system (due to voltage sag). The different load current between the current before and after the fault is considered as current faults. To determine the DC capacitor size, C_{DC}, energy loss $\Delta E_C(t)$ of the capacitor in one period must be considered [118]:

$$\Delta E_C(t) = \frac{1}{2} \cdot C_{DC} \cdot \left(V_{CMAX}^2 - V_{DC}^2\right), \tag{43}$$

where V_{CMAX} is pre-set upper limit of the voltage (V) across the capacitor, V_{DC} is the voltage across the capacitor (V). The energy loss is also supplied by the utility voltage source V_{SC} and the peak value of the charging current I_{SC} in which the energy loss can be written as [118]:

$$\Delta E_C(t) = \int_0^T V_{SC} \sin \omega t \cdot I_{SC} \sin \omega t dt = V_{SC} \cdot I_{SC} \cdot \int_0^T \sin^2 \omega t dt = \frac{1}{2} \cdot V_{SC} \cdot I_{SC} \cdot T, \tag{44}$$

where V_{SC} is the peak phase voltage (V), and T is the period of one cycle of voltage and current (20 ms for 50 Hz). While the load current is reduced during fault (voltage sag), the charging current I_{SC} will be equal to the change (step-drop) in load current ΔI_L. Therefore, an extra utility source current ΔI_L will charge the energy storage capacitor. Substituting ΔI_L for I_{SC} and with equating equations (43) and (44), the following equation can be used to calculate C_{DC} in a single phase system [118]:

$$\frac{1}{2} \cdot C_{DC} \cdot \left(V_{CMAX}^2 - V_{DC}^2\right) = \frac{1}{2} \cdot V_S \cdot \Delta I_L \cdot T. \tag{45}$$

ΔI_L can be determined as:

$$\Delta I_L = \frac{N1}{N2} \cdot (I_{BVS} - I_{DVS}). \tag{46}$$

where I_{BVS} is the load current before and I_{DVS} during the voltage sag or fault (A), $N1$ is the number of coupling transformer's turns in the primary side, and $N2$ is the

number of coupling transformer's turns in the secondary side. Using equation (46) the DC capacitance value for a three phase system can be derived as [118]:

$$C_{DC} = 3 \cdot \frac{V_{SC} \cdot \Delta I_L \cdot T}{V_{CMAX}^2 - V_{DC}^2}. \tag{47}$$

The value V_{DC} can be deducted as [118]:

$$V_{DC} = \frac{3\sqrt{3} \cdot V_{SC}}{\pi}. \tag{48}$$

The operation of the D-STATCOM, the active and reactive power flows (P_S, Q_S) between the system voltage and the D-STATCOM voltage are considered and written as [118]:

$$P_S = \frac{V_S \cdot V_i}{X_L} \cdot \sin \delta, \tag{49}$$

$$Q_S = \frac{V_S}{X_L} \cdot (V_S - V_i) \cdot \cos \delta, \tag{50}$$

where X_L is the line reactance and δ is the phase angle displacement between V_S and V_i. The percentage of voltage sag V_{sag} for the system is calculated as [117]:

$$V_{sag}(\%) = \frac{V_{pre-sag}(p.u) - V_{sag}(p.u)}{V_{pre-sag}(p.u)} \cdot 100, \tag{51}$$

where $V_{pre-sag}$ is the voltage before fault (per-unit voltage), V_{sag} is voltage during fault (per-unit voltage). The VAR rating of the D-STATCOM is calculated as [117]:

$$VAR = \frac{V_{L-L}^2}{X_C} = \omega \cdot C_{DC} \cdot V_{L-L}^2 = 314.2 \cdot C_{DC} \cdot V_{L-L}^2, \tag{52}$$

where V_{L-L} is the line-to-line voltage (V) of the system at the point of connection of the filter (50 Hz). For N number of capacitors connected in parallel the total capacitance is:

$$C_{total} = \sum_{i=1}^{N} C_i, \tag{53}$$

For reactive power compensation, the necessary VAR rating is calculated by (Fig. 3.26) [119]:

$$Q_C = P \cdot \left[\tan\left(a \cos(\varphi)\right) - \tan\left(a \cos(\varphi')\right) \right], \tag{54}$$

where Q_C is the required capacitor output (var), P is real power (W), $cos\varphi$ is the actual (initial) power factor and $cos\varphi'$ is the target (final) power factor.
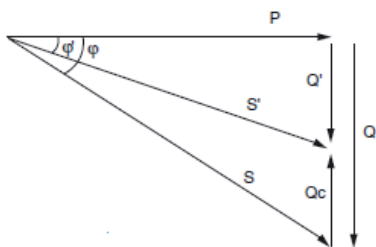
Fig. 3.26 Power diagram and reduction of declared maximum kVA by power factor improvement [119]

$$\cos\varphi = \frac{P}{S}, \tag{55}$$

$$\tan\varphi = \frac{Q}{P}, \tag{56}$$

$$S = \sqrt{P^2 + Q^2}, \tag{57}$$

Since there is no return path for the zero sequence component of the currents, the three-leg VSC with single DC capacitor cannot inject currents having a zero sequence component [120]. Hence, there will be a zero sequence component in the load current if the load is unbalanced. Full compensation will not be possible as the zero sequence component in the load current cannot be compensated. Thus, the application of this topology is limited.

Various control strategies have been exercised in the control of two-level STATCOM and Active Power Filter Converters as reported in the literature [114]:
- Modulation index is kept constant and reactive power is controlled by changing the DC link voltage. This is called "Phase Angle Control".
- DC link voltage is kept constant and reactive power is controlled by changing the modulation index of PWM waveforms. This technique is called "Constant DC Link Voltage Scheme".
- DC link voltage is kept constant and a current reference is formed according to active/reactive power set by using instantaneous *pq* theory. D-STATCOM line current is directly controlled. It is known as Direct Current Control with Instantaneous *pq* theory.

- DC link voltage is kept constant and a voltage reference is formed according to active/reactive power set by using instantaneous *pq* theory. D-STATCOM line current is indirectly controlled. It is known as Indirect Current Control with Instantaneous *pq* theory.

3.2.8 Modularity of power converters for scaling up power

For higher charging power levels, the necessary output current can by generated by connecting smaller modular chargers in parallel (Fig. 3.27). Instead of having e.g. one 250 kW power converter the same power can be achieved by connecting of 5 pcs of 50 kW power converters in parallel. Modular concept enables cost effective design solutions when power has to be scaled up. One charger will have to be the master and others slaves. Each individual modular charger has its own protection fuses, filters and IGBT bridges, which are controlled by using PWM-switching technology.

Information from the main controller is sent to the IGBTs by means of an optical link. The maximum output current depends on the power ratings of individual chargers and also on how many modular chargers can one main controller handle. Depending on the topology of chargers, preloading circuit might be necessary to charge capacitors in the DC side to ensure a smooth start-up without excessive inrush currents.
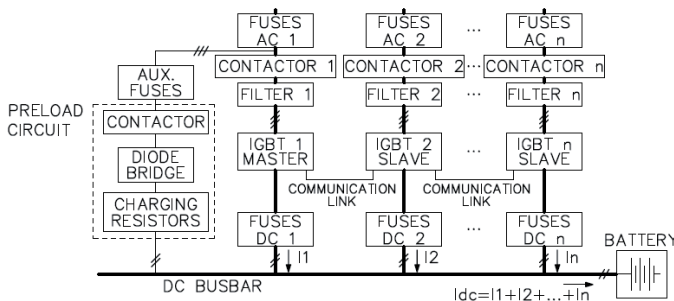
Fig. 3.27 Bidirectional power converters in parallel

3.2.9 Reported efficiencies of bidirectional AC-DC converters

Power losses of the PWM converter can be generally divided into: conduction and switching losses. Conduction losses are practically the same for different PWM techniques and they are lower than switching losses. Switching losses in power components depends on type of discontinuous modulation and power factor angle. Since the switching losses increase with the magnitude of the phase current (approximately linearly), suitable modulation can significantly improve performance of the converter.

A three-phase AC/DC buck boost PWM rectifier can reach the efficiency of 96 %. A back-to-back multilevel inverter (DC/AC) can have an efficiency of 98 %. A single multilevel inverter can achieve as high as 99 % efficiency [81].

3.2.10 MATLAB Simulink model of bidirectional AC-DC converter

In order to utilize EVs for different V2G microgrid applications, appropriate bidirectional AC-DC converter topology must be selected for integrated AC and DC bus topology. In previous chapters were described the structure of AC-DC converters (Chapter 3.2.1), topology of converters for MV application (Chapter 3.2.2), rectification for AC-DC converters (Chapter 3.2.3), inversion for AC-DC converters (Chapter 3.2.4), inversion for AC-DC converters to MV level (Chapter 3.2.5), LCL filter for reducing EMI (Chapter 3.2.6), principles for reactive power compensation and voltage mitigation (Chapter 3.2.7).

In addition, the operation of bidirectional DC-DC converters must be considered (Chapter 3.3). Bidirectional DC-DC power converters, which operate in common DC bus, turn IGBTs ON in the buck mode in the primary side of the galvanic isolation transformer, when the output voltage with the inductor in the secondary side of the transformer is lower than target output voltage. IGBTs are turned OFF, when the output voltage exceeds the target output voltage. Thus the current through the primary side of the bidirectional DC-DC converter is not continuous (duty cycle considered less than 50 %).

From these previous descriptions four operation modes are required from the bidirectional AC-DC converter:

- Rectification mode with DC side voltage output control. This mode requires a large capacitor in the DC side to maintain constant output voltage as there is no continuous output current from bidirectional DC-DC converters in the buck mode. Inductors in the DC side should be avoided as current ripple stores energy into the inductor and makes the control of the output voltage unstable.
- Inversion mode to LV side. This mode in controversy requires a small size DC side capacitor and inductors in the DC side as the inversion mode controls the injection of current and active power to the AC side. For inversion the DC side capacitors should be split into two parallel parts (one part for the inversion and the one part for rectification). For rectification the inductors in the inversion mode should be bypassed.
- Inversion mode to MV side. This mode is similar to inversion to the LV side, but with the exception that MV side current and voltage transformers are required to control the current injection to the MV side.
- Reactive power compensation and voltage mitigation mode. The mode can utilize the larger capacitor of the rectification mode. This mode requires separate control strategy and the use of additional AC side current transformers to monitor the reactive power consumption of the LV side consumers.

To control the bidirectional AC-DC converter in various modes MMI (multi-measurement input) type AC-DC converters must be utilized. Fig. 2.6 illustrates the positions of different voltage and current transformers required. A three-level neutral point clamped (3L-NPC) voltage sourced converter was chosen in this

thesis as a bidirectional AC-DC converter with IGBTs/Diodes. 3L-NPC converters have been proposed as the best choice in a wide variety of MV applications. Figure 3.20 shows a bidirectional AC-DC power converter topology that is similar to the topology simulated using MATLAB Simulink model (Fig. 3.28 [141]). Fig 3.29 shows control block of the bidirectional AC-DC converter in MATLAB Simulink for charging and discharging EVs.
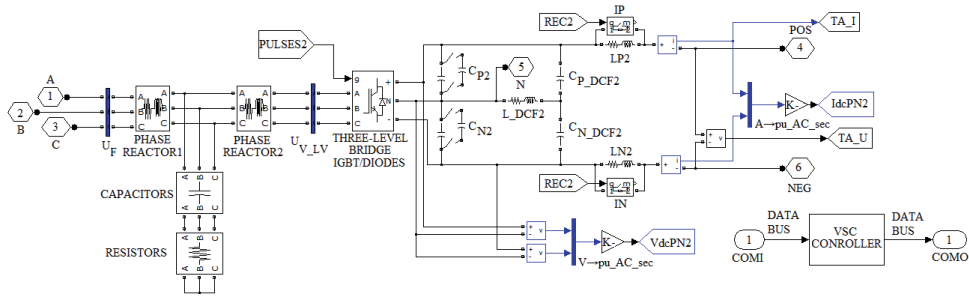
Fig. 3.28 MATLAB Simulink model of a bidirectional AC-DC power converter [141]
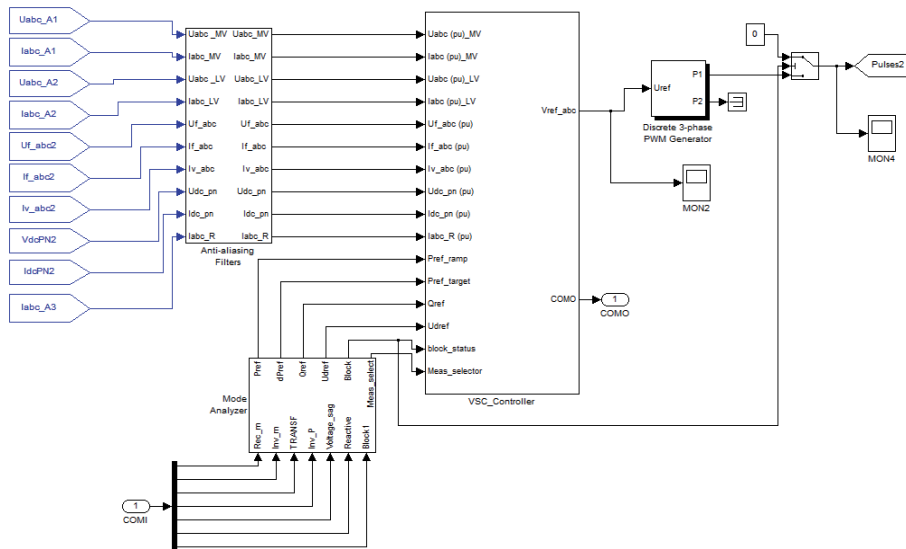
Fig. 3.29 Control block of the bidirectional AC-DC power converter for the EV side in MATLAB Simulink model

The control block consists of measurement inputs, control input and output signals, VSC controller and PWM generator for switching IGBTs. The main targets for constructing a MATLAB Simulink model for the EV side bidirectional AC-DC converters are: to have a 150 kW bidirectional AC-DC power converter, which supplies the common DC bus, efficiency of more than 92 % and the output voltage ripple less than 0.5 %.

Simulations are based on the following parameters: DC link voltage V_{DC}=800 V, nominal apparent power of the converter S_n=150 kVA, nominal AC line voltage U_n=400 V and phase voltage U_{ph}=230 V, nominal frequency f_n=50 Hz, switching frequency of the converter f_s=27*50=1350 Hz, maximum allowable peak ripple current Δi_{Imax}=7 %. Some of the later parameters can be expressed in per unit (PU). The base impedance Z_b (Ω), base inductance L_b (H) and base capacitance C_b (F) can be determined as [106]:

$$Z_b = \frac{U_n^2}{S_n},$$ (58)

$$L_b = \frac{Z_b}{\omega_b},$$ (59)

$$C_b = \frac{1}{\omega_b \cdot Z_b}.$$ (60)

From the input parameters can be deducted that the nominal three-phase current is I_n=216.5 A, angular frequency ω_b=314.16 rad/s, angular switching frequency ω_{sw}=8482 Ω, the base impedance Z_b=1.07 Ω, base inductance L_b=3.4 mH and base capacitance C_b=2984 μF. Peak ripple current Δi_{Imax} can be determined by [121]:

$$\Delta i_{Imax} = 0.07 \cdot \frac{P_n \cdot \sqrt{2}}{3 \cdot U_{ph}} = 21.5A.$$ (61)

The resonance frequency f_{res} of the LCL-filter is taken [112] f_{res}=0.5f_s=675 Hz. Therefore the angular resonant frequency is ω_{res}=4241 rad/s. Attenuation of the switching frequency line current amplitude across the filter d is taken 0.23 [112]. According to equation (37) converter side inductance ("PHASE REACTOR 2" in Fig. 3.28) L_I=1.14 mH can be determined. The L_I is chosen 15 % higher 1.32 mH (0.39 PU) to limit the current ripple [106]. Factor k_{LCL}= ω_{sw}/ ω_{res}=2 and from equation (40) the inductor ratio is r=0.45, thus grid side inductance ("PHASE REACTOR 1" in Fig. 3.28) L_G=0.6 mH (0.15 PU). According to equation (41) the capacitor value ("CAPACITORS" in Fig. 3.28) is C_F=135 μF (0.046 PU), which fulfils the criteria presented in equation (42). Damping resistors ("RESISTORS" in Fig. 3.28) R_d is taken 0.267 PU [106], which is 0.285 Ω. Resistance R_i on the converter side and resistance R_g on the grid side are neglected for simplification (taken 5 mΩ).

The primary function of the DC capacitor is to filter the common DC bus voltage and to provide a stable DC voltage link for the common DC bus. The minimum size of the DC capacitor $C_{min,NPC}$ for the NPC converter can be derived as [105]:

$$C_{\min,NPC} = \frac{P_n}{\Delta U_C \cdot \left(1 - \dfrac{\Delta U_C}{2}\right) \cdot V_{DC}^2 \cdot f_{sw}} \,, \tag{62}$$

where P_n is the converter output active power in rectifier mode (W), ΔU_C is the voltage ripple in the common DC bus (V). For simulation model $\Delta U_C = 0.03$ V is chosen, which according to equation (62) requires capacitor size (total capacitance of C_{P2} and C_{N2} in Fig. 3.28) for the common DC bus 5875 µF. The reset of the parameters in Fig. 3.28 as follows [109]: $L_{L\_DCF2} = 47$ mH, $R_{L\_DCF2} = 0.15$ Ω, $C_{P\_DCF2} = C_{N\_DCF2} = 12$ µF, $L_{LP2} = L_{LN2} = 8$ mH, $R_{LP2} = R_{LN2} = 0.025$ Ω. The parameters for the control block are taken according to [109].

Previous calculated values can be used to evaluate D-STATCOM functionality. The following parameters can be taken for basis: $V_{Cmax} = 800$ V, $V_{SC} = 326.6$ V, $T = 0.02$ s. According to equation (52) the VAR rating of the bidirectional AC-DC converter is 295 kvar. According to equation (48) voltage across DC capacitor is $V_{DC} = 540.2$ V. According to equation (47) can be calculated that the converter can support up to 104.4 A under voltage sag.

Figures 3.30-3.32 illustrate simulation results of the bidirectional AC-DC power converter in the rectifier mode in the MATLAB Simulink. Target output voltage is 800 V DC. 8 Ω resistor is connected to the load side for imitating 80 kW consumption (100 A load current).
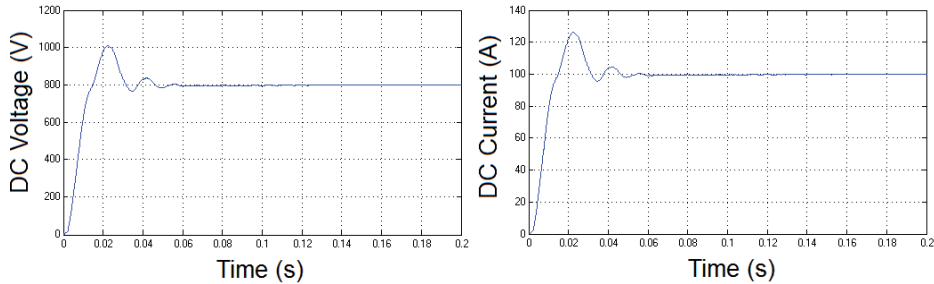
Fig. 3.30 Simulated output voltage and current of the bidirectional AC-DC power converter in the MATLAB Simulink model in the rectifier mode
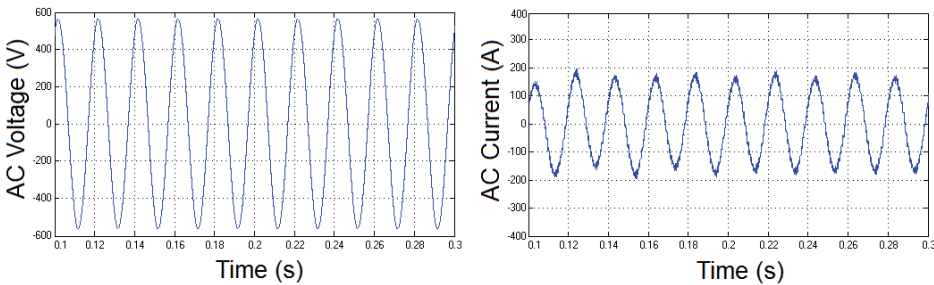
Fig. 3.31 Simulated input voltage and current of the bidirectional AC-DC power converter in the MATLAB Simulink model in the rectifier mode
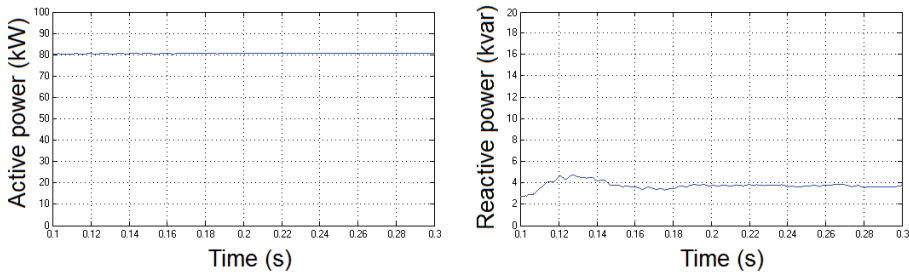
Fig. 3.32 Simulated input active and reactive power of the bidirectional AC-DC power converter in the MATLAB Simulink model in the rectifier mode

Inverter mode smoothing reactors (LP2 and LN2 in Fig. 3.28) are bypassed in the rectifier mode. Output efficiency of the bidirectional AC-DC power converter is 97.5 %. Voltage ripple ΔU_C is from -1.2 V to +0.6 V (maximum of 0.15 %). Current ripple Δi_I is 7 %. Figures 3.33-3.34 illustrate simulation results of the bidirectional AC-DC power converter in the inverter mode in the MATLAB Simulink. 800 V DC source is connected to the common DC bus side. AC side includes 400 V voltage source and consumers with active power consumption of 250 kW. Target output active power is the nominal power of the AC-DC converter 150 kW (for imitating peak shaving). Smoothing reactors (LP2 and LN2 in Fig. 3.28) are connected in the inverter mode and capacitors of the DC side (total capacitance of C_{P2} and C_{N2} in Fig. 3.28) are bypassed to a lower value of 280 µF. Output efficiency of the AC-DC power converter in the simulation is 96.1 %.
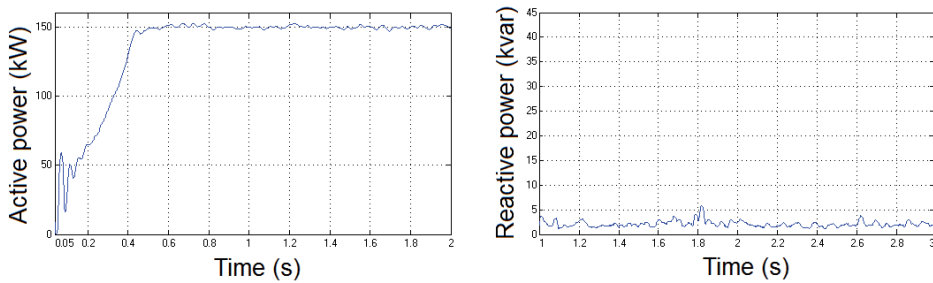
Fig. 3.33 Simulated output active power and reactive power consumption of the bidirectional AC-DC power converter in the MATLAB Simulink model in the inverter mode
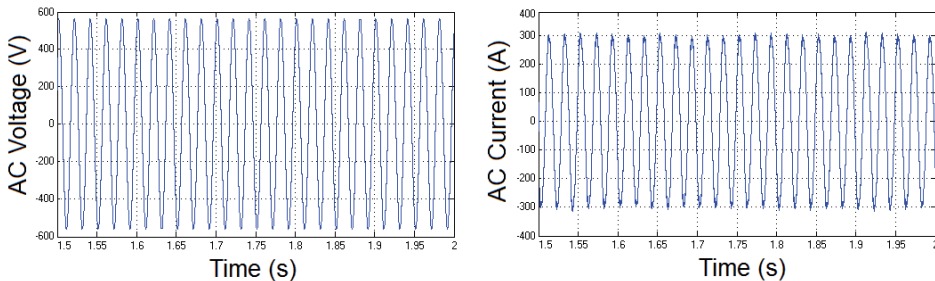
Fig. 3.34 Simulated AC side voltage and current of the bidirectional AC-DC power converter in the MATLAB Simulink model in the inverter mode

The necessary input and output parameters required for controlling the bidirectional AC-DC power converter in the MATLAB Simulink for charging and discharging of EVs or BESUs are presented in Tables 3.3 – 3.6.

Table 3.3. Main input parameters for bidirectional AC-DC converter in MATLAB Simulink model for charging and discharging of EVs

Name	Description	Data type
Rectifier mode	Setting the converter into rectifier mode	BOOLE
DC voltage	Target output voltage in rectifier mode	INTEGER
Inverter mode	Setting the converter into inverter mode	BOOLE
Transformation selection	Selection of active power supply direction in the inverter mode (for supplying active power to LV or MV side the Clark transformations have to be selected accordingly)	INTEGER
Active power rating	Target rating of active power to be supplied in the inverter mode	FLOAT
Voltage sag mode	Setting the converter into voltage sag monitoring mode for providing voltage stability at AC side	BOOLE
Reactive power compensation mode	Setting the converter into reactive power compensation mode for lowering AC voltage side reactive power consumption	BOOLE
Reactive power rating	Target rating of reactive power to be compensated in the reactive power compensation mode	FLOAT
Block mode	AC-DC converter is operational in the given mode, but outside signal does not allow switching of IGBTs.	BOOLE

Table 3.4. Main input parameters for bidirectional AC-DC converter in MATLAB Simulink model for charging and discharging of BESU

Name	Description	Data type
Rectifier mode	Setting the converter into rectifier mode	BOOLE
DC voltage	Target output voltage in rectifier mode	INTEGER
Inverter mode	Setting the converter into inverter mode (LV side)	BOOLE
Active power rating	Target rating of active power to be supplied in the inverter mode	FLOAT
Islanding mode	Setting the converter into islanding mode with virtual PLL control strategy	BOOLE
Resynchronize	Setting the converter into resynchronization with restored supply voltage	BOOLE
Block mode	AC-DC converter is operational in the given mode, but outside signal does not allow switching of IGBTs.	BOOLE

Table 3.5. Main output parameters for bidirectional AC-DC converter in MATLAB Simulink model for charging and discharging of EVs

Name	Description	Data type
Voltage AC	Measured voltage at AC side (either LV or MV side)	FLOAT
Current AC	Measured current at AC side (either LV or MV side)	FLOAT
Active power AC side	Measured active power at AC side (either LV or MV side)	FLOAT
Reactive power AC side	Measured reactive power at AC side (either LV or MV side)	FLOAT
Voltage DC	Measured voltage at DC side	FLOAT
Current DC	Measured current at DC side	FLOAT
Active power DC side	Measured active power at DC side	FLOAT
Ready	Notification of target output voltage achieved in the no-load state in the rectifier mode. Permits closing of contactors in the common DC bus.	BOOLE

Table 3.6. Main output parameters for bidirectional AC-DC converter in MATLAB Simulink model for charging and discharging of BESU

Name	Description	Data type
Voltage AC	Measured voltage at AC side (LV side)	FLOAT
Current AC	Measured current at AC side (LV side)	FLOAT
Active power AC side	Measured active power at AC side (LV side)	FLOAT
Reactive power AC side	Measured reactive power at AC side (LV side)	FLOAT
Voltage DC	Measured voltage at DC side	FLOAT
Current DC	Measured current at DC side	FLOAT
Active power DC side	Measured active power at DC side	FLOAT
Ready	Notification of target output voltage achieved in the no-load state in the rectifier mode. Permits closing of contactors in the common DC bus.	BOOLE
Resynchronized	Notification of resynchronization achieved. Permits closing of the main supply breaker	BOOLE

The additional input and output parameters required for controlling the bidirectional AC-DC power converter are: active power rating for rectifier mode (for higher efficiency, if modular topology of the power converter is implemented), general measurements, harmonic mitigation values, measured temperature values, islanding mode, faults/alarm detection, auxiliary settings, communication, events, functions, identification, general and user settings, logging, status, ramping

up/down etc. These are not implemented in MATLAB Simulink, but can be found in similar products [4], [122].

The control of inversion for the bidirectional AC-DC power converter in the MATLAB Simulink model is illustrated in Fig. 3.35 [110]. The control of rectification, reactive power compensation and voltage mitigation in MATLAB Simulink model is illustrated in Fig. 3.36 (modified from [123]). Control with virtual PLL, which could be utilized for temporary islanding purposes, is illustrated in Fig. 3.37 [124].
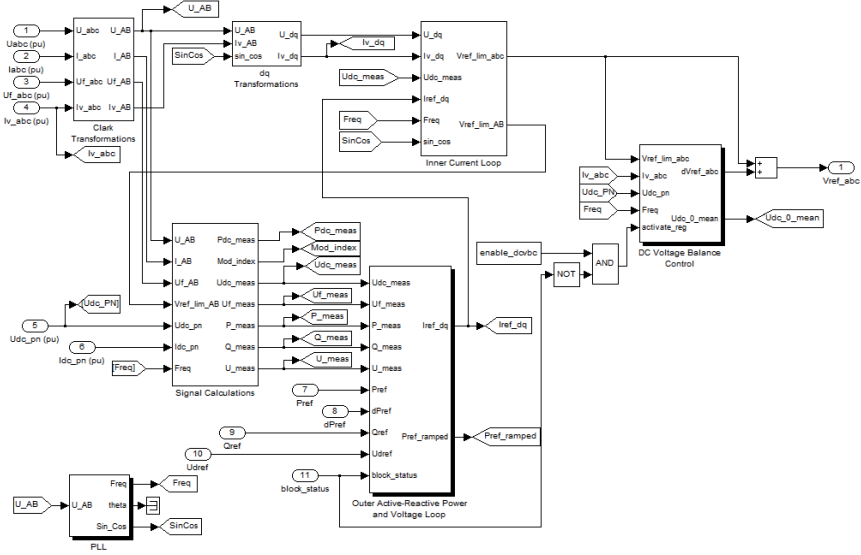
Fig. 3.35 Control of inversion for bidirectional AC-DC power converter in the MATLAB Simulink model [110]
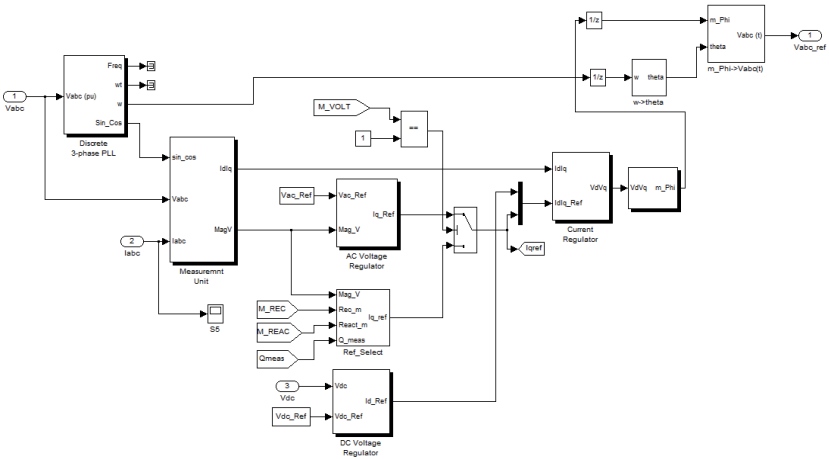
Fig. 3.36 Control of rectification, reactive power compensation and voltage mitigation for bidirectional AC-DC power converter in the MATLAB Simulink model
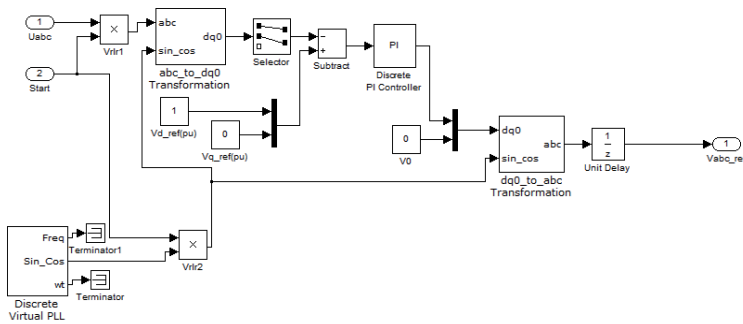
Fig. 3.37 Example of simplified control with virtual PLL for bidirectional AC-DC power converter in the MATLAB Simulink model [124]

3.2.11 Generalizations

Bidirectional AC-DC power converters are required for controlling the common DC bus voltage in the rectifier mode and forwarding active power to the grid side in the inverter mode. Although the MATLAB Simulink model has some simplifications, considering the simulation results, the MATLAB Simulink model can accurately represent the bidirectional AC-DC converter for further development of substation's control functionality. The efficiency ratings of the model are higher than the predefined more than 92 % requirement (in the range of 96-97.5 % at various operation modes). The output voltage ripples in the simulations does not exceed the 0.5 % predefined requirement. For simplifications the control of AC-DC power converter is implemented with one power converter module. For higher efficiencies parallel output power converter modules are required as described in chapter 3.28. If the efficiency of a real bidirectional AC-DC power converter is not known, 96 % efficiency can be taken for calculations.

3.3 Bidirectional DC-DC converters

3.3.1 Structure of DC-DC converters

DC-DC converters have two main operating modes: buck mode (decreasing output voltage) and boost mode (increasing output voltage). Buck-Boost DC-DC converters combine both buck and boost mode in a single converter. Fig. 3.38 [125] illustrates different type of DC-DC converters.

Buck operation [125]: The current direction is from supply V_d to load V_0 and $V_d > V_0$. During the period that *M1* is conducting, $t_{on} = DT_s$ (*D* is duty cycle and T_s is switching period), inductor *L* is charged (*M2* is reverse biased by V_d). When *M1* is off ($t_{off} = T_s - t_{on}$), inductance current will flow through *M2*. If *M2* is a diode, the topology is called non-synchronous. If *M2* is replaced with e.g. MOSFET, the topology is called synchronous. In synchronous topology two switches alternately turn on and off to regulate the output voltage in response to the input voltage variation and dynamic load transients [125].
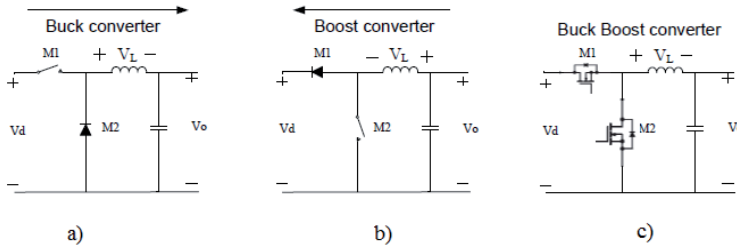
Fig. 3.38 Topologies of buck converter (a), boost converter (b) and bidirectional buck-boost converter (c) [125]

Key waveforms are presented in Fig. 3.39. The inductor ripple current ΔI_L can be obtained by [126]:

$$\Delta I_L = \frac{V_d - V_0}{L} \cdot \frac{V_0}{V_d} \cdot \frac{1}{f_s},$$

(63)

where f_s is the switching frequency (Hz). The inductor is typically chosen in such a way that the inductor ripple current is 20-30 % of the load current. Assuming all inductor ripple current flows into the output capacitor, the voltage ripple due to limited output capacitance and its equivalent series resistance can be derived [126]:

$$\Delta V_{0\_C} = \frac{(1-D) \cdot V_0}{8 \cdot f_s^2 \cdot L \cdot C},$$

(64)

where C is the capacitance of load side output capacitor (F).
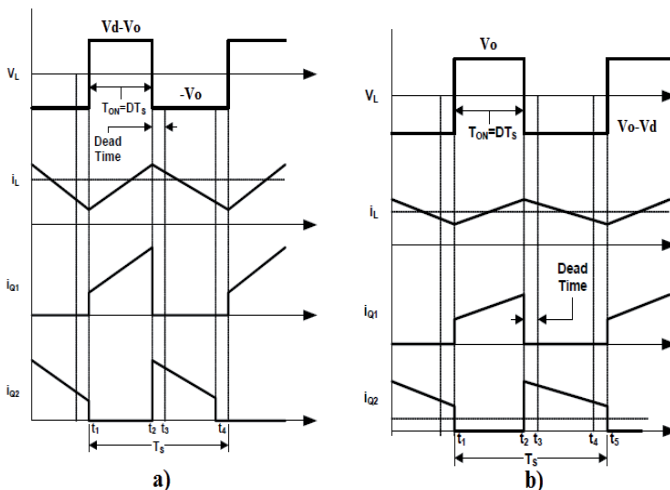
Fig. 3.39 Key waveforms of a buck converter (a) and boost converter (b) [126]

127

Boost operation [125]: The current direction is from V_0 to V_d and $V_d > V_0$. During the period that $M2$ is conducting, $t_{on} = DT_s$, inductor L is charged and when $M2$ is off $(t_{off} = T_s - t_{on})$ inductance current will be discharged through $M1$. Key waveforms are presented in Fig. 3.39.

Buck-boost operation [125]: by combining buck and boost converters a two quadrant converter is obtained that can operate bidirectionaly: from V_d to V_0 in buck mode and from V_0 to V_d in boost mode.

3.3.2 Structure of bidirectional DC-DC converter with galvanic isolation

Bidirectionality means the possibility of power flow in both directions: from the common DC main bus to the EV battery (vehicle) with the buck mode and from EV battery to the common DC main bus with the boost mode. The DC-DC converter with a galvanic isolation necessitates the use of a transformer [127]. The galvanic isolation separates battery side from the grid side for protection and EMC reduction purposes. Fig. 3.40 illustrates a bidirectional double-leg full-bridge DC-DC converter with galvanic isolation [125].
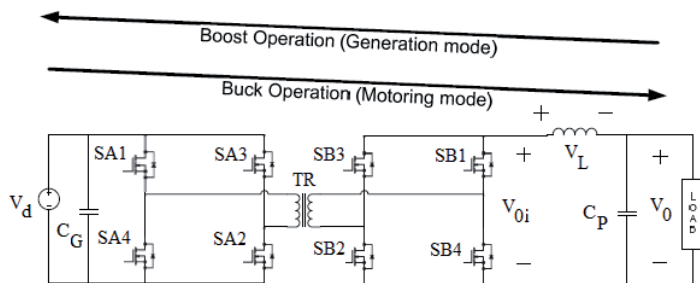
Fig. 3.40 Bidirectional Double-Leg Full-Bridge DC-DC converter topology with galvanic isolation [125]

In buck operation (motoring mode) in Fig. 3.40 [125]: switches *SA1*, *SA2* and *SA3*, *SA4* are controlled together. There is no need of any control on secondary side. All secondary switches (*SB1*, *SB2*, *SB3*, *SB4*) should be off and only anti-parallel diodes conduct. The four stages for buck operation can be summed up in the following equation [125]:

$$\begin{cases} SA1, SA2 : on \rightarrow v_L = \dfrac{N2}{N1}V_d - V_0 \\ SA1, SA2, SA3, SA4 : off \rightarrow v_L = -V_0 \\ SA3, SA4 : on \rightarrow v_L = \dfrac{N2}{N1}V_d - V_0 \\ SA1, SA2, SA3, SA4 : off \rightarrow v_L = -V_0 \end{cases}, \tag{65}$$

where v_L is the inductor voltage (V), V_d is the common DC bus side voltage (V), V_0 is the battery (load) side voltage (V), $N1$ is the number of transformer turns in primary side, and $N2$ is the number of transformer turns in secondary side. The inductor ripple current ΔI_L and output voltage ΔV_{0_C} ripple can be derived as [125]:

$$\Delta I_L = \frac{\Delta_t \cdot T_s}{L} \cdot V_0 = \frac{(0.5 - D) \cdot T_s}{L} \cdot \frac{N2}{N1} \cdot 2 \cdot D \cdot V_d = \frac{N2}{N1} \cdot \frac{(D - 2D^2)}{L \cdot f_s} \cdot V_d \text{ , (66)}$$

$$\Delta V_{0\_C} = \frac{(0.5 - D) \cdot V_0}{16 \cdot f_s^2 \cdot L \cdot C_P} \text{ , } \tag{67}$$

where Δ_t is the off time of switches (s). T_s is the switching period of switches (s), f_s is the switching frequency (Hz), D is the duty cycle of switches, L is the inductance of the inductor (H) and C_P is the capacitance of capacitor (F).

In boost operation (generation mode) in Fig. 3.40 [125]: switches $SB1$, $SB2$ and $SB3$, $SB4$ are controlled together. There is no need of any control on primary side. All primary switches ($SA1$, $SA2$, $SA3$, $SA4$) should be off and only anti-parallel diodes conduct. The switching period of switches can be divided into 4 stages. In the first stage $SB1$ and $SB2$ conduct in secondary side, the current can flow towards grid via anti-parallel diodes $D1$ and $D2$. In the second stage all switches ($SB1$, $SB2$, $SB3$, $SB4$) have to be on to make a path for inductor current, this charges the inductor and the current increases linearly. In the third stage $SB3$ and $SB4$ conduct in secondary side, the current can flow towards grid via anti-parallel diodes $D3$ and $D4$. In the final fourth stage all switches ($SB1$, $SB2$, $SB3$, $SB4$) have to be on to make path for inductor current. Based on parameters used in Fig. 3.40 the four stages can be summed up in the following equation [125]:

$$\begin{cases} SB1, SB2 : on \rightarrow v_L = V_0 - \dfrac{N1}{N2}V_d \\ SB1, SB2, SB3, SB4 : on \rightarrow v_L = V_0 \\ SB3, SB4 : on \rightarrow v_L = V_0 - \dfrac{N1}{N2}V_d \\ SB1, SB2, SB3, SB4 : on \rightarrow v_L = V_0 \end{cases} . \tag{68}$$

For continuous conditions, ripple current, as function of D can be derived [125]:

$$\Delta I_L(D) = \frac{N1}{N2} \cdot V_0 \cdot (2D - 1) \cdot (1 - D) \cdot \frac{1}{L \cdot f_s} . \tag{69}$$

3.3.3 Structure of bidirectional AC-DC-DC converter

One optional AC-DC-DC converter topology is presented in Fig. 3.41 [128]. The converter is composed of AC-DC-DC isolated converter with bidirectional power flow capability. The analysed structure consists of a 3-phase current source converter and DC-DC isolated converter. In this DC-DC converter, the primary side of the high-frequency transformer is a current source converter and the secondary side is a voltage source converter. Current of the AC-side is controlled by the voltage of the inductor in the DC-side. Current and voltage in DC-side can be regulated in a wide range from zero to the rating value. Current and voltage in AC-side have low total harmonic distortion and power factor in a wide output power range [128].

3-phase current source converter [128] consists of 6 fully controlled switches (*S11-S16*) and 6 diodes (*D11-D16*). AC-DC converter is necessary to realise the line-side sinusoidal current curve with the pulse width modulation (PWM) control strategy. Elements *S17* and *D17* provide a bypass to reduce the voltage spike of the switches, when they are turned on or off. The isolated DC-DC converter consists of high-frequency transformer with current source converter (*S21-S24* and *D21-D24*) at its primary side and the voltage source converter (*S31-S34*) at its secondary side. Converter can change the direction of the current conveniently through the voltage polarity control of the *CSC II* in the DC-DC converter. Fig. 3.42 [128] presents equivalent circuit diagrams of Fig. 3.41 for both charging and discharging.

When charging the battery [128], input current phase is the same as the input voltage phase in the 3-phase AC grid system. Converter transfers power from AC-side to the DC-side. *CSC I* works as a rectifier.
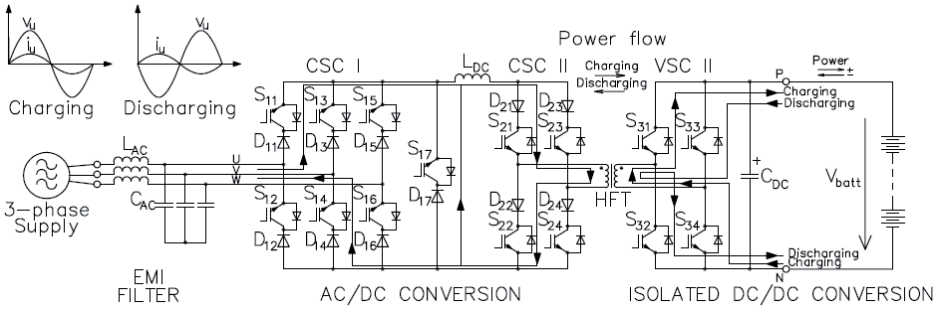
Fig. 3.41 Bidirectional AC-DC-DC converter topology with galvanic isolation [128]
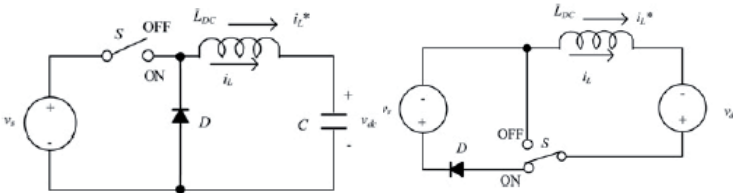
Fig. 3.42 Equivalent circuit diagram of the charging (left) and discharging (right) [128]

When discharging the battery [128], the voltage phase is reversed to the current phase in a 3-phase AC grid system. The proposed converter transfers power from the DC-side to the AC-side. *CSC I* works as an inverter. The current direction is the same when charging or discharging the battery, but the voltage phase is reversed to the current phase at the AC-side.

3.3.4 Reported efficiencies of bidirectional DC-DC converters

Power losses are in the transformer, inductor and in IGBT semiconductors (conduction (diodes) and switching losses). Most of magnetic core materials are made of iron alloys; consequently they are good electrical conductors. This means AC magnetic fields will lead to electrical eddy current. Eddy current causes losses in the resistance of the core material. Eddy currents are dominant especially at high frequency applications. In any magnetic cores two types of losses happened. One is due to the material characteristic which is generally referred to core losses and one is based on the flowing current on copper wires and is called copper losses (winding losses). Total core losses (Hysteresis and Eddy losses) in ferrite materials depend on frequency, flux density and temperature. Detailed descriptions for calculating total losses of bidirectional DC-DC converters can be found in literature [125].

The DC-DC converter efficiencies for the both directions have been reported between 94.5 % and 96.5 % [125] (depending on the battery voltage). A single buck-boost (DC-DC) inverter can have up to 98 % efficiency [81]. AC-DC-DC converters have efficiencies of 85 % [128].

3.3.5 MATLAB Simulink model of bidirectional DC-DC converter

Figure 3.40 shows a bidirectional DC-DC power converter topology that is similar to the topology simulated using MATLAB Simulink model (Fig. 3.43 [141]). The main targets for constructing a MATLAB Simulink model is to have a 50 kW bidirectional DC-DC power converter, with the efficiency of more than 92 % and the output voltage ripple less than 0.5 %.
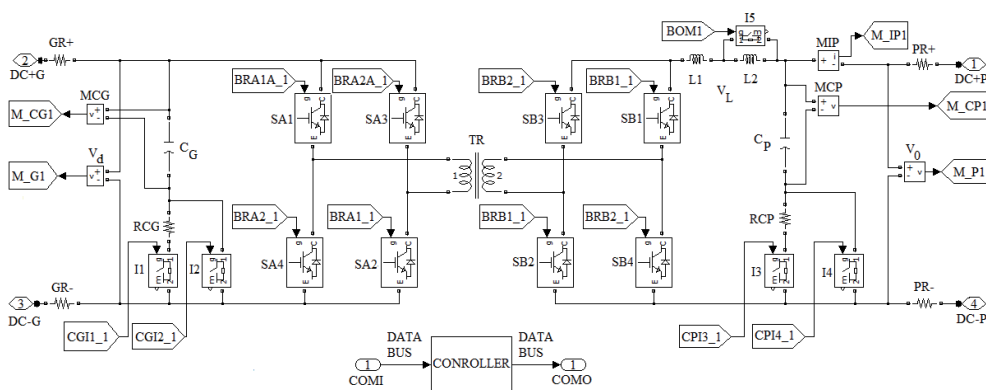
Fig. 3.43 MATLAB Simulink model of a bidirectional DC-DC power converter [141]

Simulations [141] are based on the following parameters: V_d=800 V, V_{0_min}=300 V, V_{0_max}=600 V, transformer ratio 800/600 V (4/3), D=25 %, f_s=20 kHz, ΔV_{0_C}=0.1 V and ΔI_L=0.1 A. Using equations (66) and (67), L=37.5 mH and C=C_P=3.1 µF≈5 µF can be deduced. For simplification, an isolating transformer is considered an ideal kind. PI output voltage regulator parameters for buck mode are K_P=2 and K_i=20. To adjust the output voltage in a wide range (from 300 V to 600 V) in buck mode, switches SA1 and SA3 operate as additional rectifiers.

Fig. 3.44 (a) illustrates simulation results of the bidirectional DC-DC converter in buck mode with MATLAB Simulink. 800 V DC supply is connected to the common DC bus side and different resistors are connected to the load side (3 Ω for 300 V, 4 Ω for 400 V, 5 Ω for 500 V, 100 A output current in all cases). Different output voltages are compared in Fig. 3.44 (a). For 300 V and 100 A output, the efficiency of the DC-DC converter is 98.2 %, ΔV_{0_C} is from -0.25 V to +0.45 V. For 400 V and 100 A output, the efficiency of the DC-DC converter is 98.4 %, ΔV_{0_C} is from -0.8 V to +0.5 V. For 500 V and 100 A output, the efficiency of the DC-DC converter is 98.5 %, ΔV_{0_C} is from -1.1 V to +0.4 V. The model has response time to +10 V output change in 1 ms (e.g. from 300 V to 310 V) and to +100 V output change in 3.3 ms (e.g. from 300 V to 400 V) as illustrated in Fig. 3.44 (b).
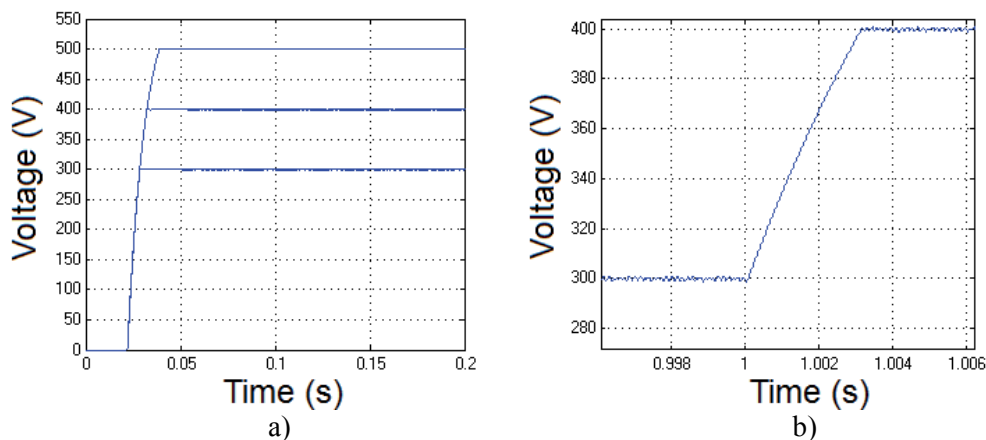
Fig. 3.44 Different simulated output voltages (a) and step respone (b) of the bidirectional DC-DC power converter in the MATLAB Simulink model in the buck mode

The relatively large inductor (37.5 mH), which is necessary for low inductor ripple current in the buck mode, causes instability in controlling of the common DC bus side voltage in the boost mode. For this reason the inductor is split into two parts L1 (3.75 mH) and L2 (33.75 mH). In the boost mode the L2 part is bypassed. A capacitor for the common DC bus side is chosen C_G=1000 µF. Precharging resistors 2 Ω (RCG, RCP) avoid sudden current peaks when connecting voltage to empty capacitors in either side. PI output voltage regulator parameters for boost mode are K_P=0.1 and K_i=20.

Fig. 3.45 illustrates simulation result of the bidirectional DC-DC converter in the boost mode with MATLAB Simulink. 300 V DC supply is connected to the battery side. Target output is 800 V in the common DC bys side. 16 Ω resistor is connected to the common DC side (50 A and 40 kW output). For 300 V input and 800 V 50 A output, the efficiency of the DC-DC converter is 97.8 %, ΔV_{0_C} is from -3.5 V to +1.5 V. For e.g. 500 V input and 800 V 50 A output, the efficiency of the DC-DC converter is 98.2 %, ΔV_{0_C} is from -3 V to +2 V.
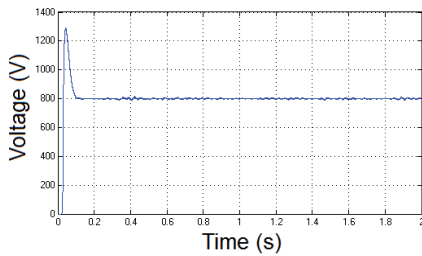
Fig. 3.45 Simulated output voltage of the bidirectional DC-DC power converter in the MATLAB Simulink model in the boost mode

The necessary input and output parameters required for controlling the bidirectional DC-DC power converter in the MATLAB Simulink is presented in Table 3.7 and Table 3.8.

Table 3.7. Main input parameters for bidirectional DC-DC converter in MATLAB Simulink model

Name	Description	Data type
Input voltage	Common DC bus voltage (for charging primary side capacitors)	INTEGER
Voltage buck	Target output voltage in buck mode	INTEGER
Voltage boost	Target output voltage in boost mode	INTEGER
Buck mode	Setting converter into buck mode	BOOLE
Boost mode	Setting converter into boost mode	BOOLE
Remote control	The DC-DC converter is activated remotely	BOOLE
No-load mode	Prevents output voltage from increasing over the target voltage incase of an output open circuit	BOOLE

Table 3.8. Main output parameters for bidirectional DC-DC converter in MATLAB Simulink model

Name	Description	Data type
Voltage primary	Measured primary side voltage (common DC bus side)	FLOAT
Voltage secondary	Measured secondary side voltage (EV side)	FLOAT
Ready	Notification of target output voltage achieved in no-load state either in buck or boost mode. Permits closing of the output contactor.	BOOLE

The additional input and output parameters required for controlling the bidirectional DC-DC power converter is presented in Table 3.9 and Table 3.10. These are not implemented in MATLAB Simulink, but can be found in similar products [129].

Table 3.9. Additional input parameters required from bidirectional DC-DC converters

Name	Description	Data type
Peak Voltage limit buck	Peak output voltage limit for battery charging	INTEGER
Bus over-voltage limit boost	Maximum output voltage limit in boost mode	INTEGER
Bus under-voltage limit boost	Minimum output voltage limit in boost mode	INTEGER
Peak Current limit buck	Battery charge current limit	INTEGER
Peak Current limit boost	Battery discharge current limit	INTEGER

Table 3.10. Additional output parameters required from bidirectional DC-DC converters

Name	Description	Data type
Temperature	Measured temperature values of converter	FLOAT
Faults/Alarms	Fault or Alarm codes (either for process limiting or shutdown)	BOOLE

3.3.6 Generalizations

Bidirectional DC-DC power converters are required for controlling the EV battery charging and discharging current. Although the MATLAB Simulink model has some simplifications, considering the simulation results, the MATLAB Simulink model can accurately represent the bidirectional DC-DC converter for further development of substation's control functionality. The efficiency ratings of the model are higher than the predefined more than 92 % requirement (in the range of 97-98.5 % at various operation modes). The output voltage ripples in the simulations does not exceed the 0.5 % predefined requirement.

The simulations do not consider pre-charging of DC side capacitors to reduce the required simulation time. The pre-charging of capacitors can be fed from separate source, which is not implemented in the simulations.

If the efficiency of a real bidirectional DC-DC power converter is not known, 95 % [125] efficiency can be taken for calculations.

3.4 Reverse feeding of transformers

In case of reverse feeding of transformers for step-up operation to increase voltage, the general remarks are [130], [131], [132]:

- If the low voltage side is wye, the neutral terminal must not be connected in any way;
- Much higher than normal inrush currents may occur with reverse feed operation and the protective devices must be selected accordingly with time-delay characteristics;
- When transformers are reverse fed, the load voltage will not match the nameplate value. Depending on kVA size the actual load voltage could be up to 15 % lower than expected.

The exact design of a control algorithm and control of inrush current limitation for transformer reverse feeding is out of the scope of this doctoral thesis. The parameters of reverse feeding depend on the transformer design. For general considerations the common DC bus (e.g 800 V) can be utilized to match the output voltage in the MV side. In the MATLAB Simulink model for 250 kVA 24/0.4 kV transformer with primary and secondary side winding parameters (resistance of 0.0025 PU (per-unit), inductance of 0.075 PU) and magnetization parameters (resistance of 500 PU, inductance of 500 PU) [110] the reverse feeding required 3.6 % higher output voltage. Duration of achieving the target kW rating compared to Fig. 3.33 was 16 % longer. The secondary side of the transformer must be constructed to withstand higher input voltages or non-standardized transformer voltage ratings must be utilized, which ratio remains uninfluenced in the step-down operation (e.g. 27.6/0.46 kV for 15 % reverse feeding voltage drop). Inrush currents can be limited with limiting reactors or with control of IGBTs of the AC-DC power converter.

4. CONTROL AND PROTECTION FUNCTIONS

This chapter presents control and protection functions of the V2G capable distribution substation. In order to physically transfer energy bidirectionaly between EVs and the utility network, system architecture is required which integrates different control and protection functions. A novel programming architecture is presented which consists of eleven layers (11L). The architecture integrates EVs, DSO, Retailer and the LV side consumers. The chapter describes the programming architecture through tables of input/output parameters and flowcharts. Different control functionalities are simulated with MATLAB Simulink using power converter topologies and battery models analyzed in Chapter 3. The architecture allows utilization of EVs for microgrid applications.

Distribution substation is in constant communication between the DSO and the Retailer. Therefore the substation automation system (SAS) receives different tasks that have to be executed in the specific timeframe considering grid constraints. SAS is required to calculate, schedule and perform control of physical processes in near real time. As SAS is most aware of its internal microgrid requirements, SAS will have to schedule and control the charging or discharging of several EVs. The concept is an improvement to the standard IEC 15118-1:2011 where EV is required to schedule charging times. V2G capable distribution substations reduce the need for electric vehicle manufacturers to develop and implement expensive solutions to their EVs in an extremely competitive automobile industry. The only requirement for the EV manufacturers is to allow EVSEs to retrieve data from EV BMS and set the EV BMS into either charging or discharging mode, which is quite simple to implement in the today's BMS technology. EV owner inserts its input data to EVSE or sends to Retailer, which is then forwarded to SAS to be considered in the scheduling.

4.1 Control algorithm based on eleven layers (11L)

The general concept of the eleven layer (11L) design is described in this chapter. For utilization of EVs through V2G capable distribution substation in microgrid applications a programming architecture has to be developed for the SAS. The 11L helps to systemize different functional requirements for the SAS. The main considerations in the 11L design are:
- Fully automatized solution, where the operator does not have to control, calculate or make measurements. The SAS can operate independently;
- Modular and fractal design, where every layer can operate independently and the number of bays could be added freely;
- Flexibility to modify SAS settings according to installation requirements.

As distribution substation with V2G capability participate in active business transactions with EV owners, the 11L layer takes into consideration that distribution substations may not necessarily belong to only DSO, but may belong

to third parties. Third parties which are interested to provide charging service for EV owners and provide (sell) services to DSO or to LV side consumers. Owner of the distribution substation may therefore be e.g. the owner of an industrial building or complex (e.g. charge EVs of employees), area developer, Retailer. The owner merges with the DSO in the MV side and develops electric infrastructure from the distribution substation and forward. Third party owners can save additional fees from DSO or Retailer with generating and consuming energy internally in the microgrid. In addition, selling services to DSO or Retailer allows earning profit. Owners are free to use their property according to their need and for business purposes. Third party owners can influence the prices of EV charging as a selling service. With over pricing EV owners will prefer home charging or other public charging services. Term "priority" summarizes the preferences of the owner of the distribution substation.

For assuring that V2G service is accessible for other participants for certainty at the required time the term "timezone" has to be implemented. The core functionality of the distribution substation which interconnects EVs with utility networks is to charge EVs to the EV owner specified departure time. In order to utilize EVs for V2G purposes at all, EVs should have enough SOC levels to provide required V2G services. In order to avoid congestions pre-set timezones have to be implemented for semi-public charging applications. EV owners know forehand when their EVs are charged before departure and other participants (DSO, LV side consumers) know forehand when V2G service can be asked for. If the owner of the distribution substation is e.g. an industrial complex interconnecting EVs of employees or company EVs the pre-set timezones for EV charging could be e.g. from 9-10 am when employees have arrived to work (to fast charge EVs for V2G application and if some owners need to drive around during the day) and from 4-5 pm. before employees leave workplace. For the timezone from 10 am – 4 pm V2G service can be provided (e.g. peak shaving of loads). Employees who drive around during the day can utilize other public charging services. Employees which stay connected for longer period of time have their EVs charged before departure and do not have to spend additional 30 minutes in a public charging station. V2G capable substations allow final charge with slow charging compared to public EVSEs (SOC=80 %). App solutions can be utilized to monitor the status of EV or to make modifications in departure times.

The main architecture of 11L is illustrated in Fig. 4.1 and sublayers are illustrated in Fig. 4.2. The first layer is the component layer (CPL), which consist of e.g. circuit breakers, contactors, power converters, EVs etc. The second layer is the communication layer (COML), which defines how data is retrieved or sent between CPL devices and internally inside the distribution substation. The third layer is the data layer (DL), where different data of devices, states or execution functions can be received or sent. The forth layer is the control layer (CTL), which physically controls the charging or discharging of EV bays. Control layer part for station level includes different control applications: charging of all EV bays, discharging of all EV bays, charging of BESU bays, discharging of BESU bays,

utilization of EV side AC-DC power converter for voltage mitigation and reactive power compensation. The fifth layer is the monitor and protection layer (MPL), which monitors that the functions of a particular CTL bay are safe to operate and gives the input data to the CTL bays how charging or discharging must be executed (e.g. maximum charging current depending on grid constraints). The sixth layer is the computing layer (CML), which schedules EV charging and calculates how much active power is required for upcoming charging session or how much active power can utilized for V2G applications. The seventh layer is the computing layer of parallel distribution substations or extension substations (CMLDS). The layer monitors states of different substations and distributes V2G application requirements between different substations. The eight layer is the energy routing layer (ERL), which purpose is to ensure that LV side consumers have constant energy supply and reconnect switches to charge EVs or discharge EVs according to applications.

```
11.MARKET LAYER (MRL)
10.DS OWNER LAYER (OWL)
9.PRIORITY FILTER/
TASK MANAGER (PFTM)
8.ENERGY ROUTING (ERL)
7.COMPUTING LAYER DSs (CMLDS)
6.COMPUTING LAYER (CML)
5.MONITOR/PROTECTION LAYER (MPL)
4.CONTROL LAYER (CTL)
3.DATA LAYER (DL)
2.COMMUNICATION LAYER (COML)
1.COMPONENT LAYER (CPL)
```
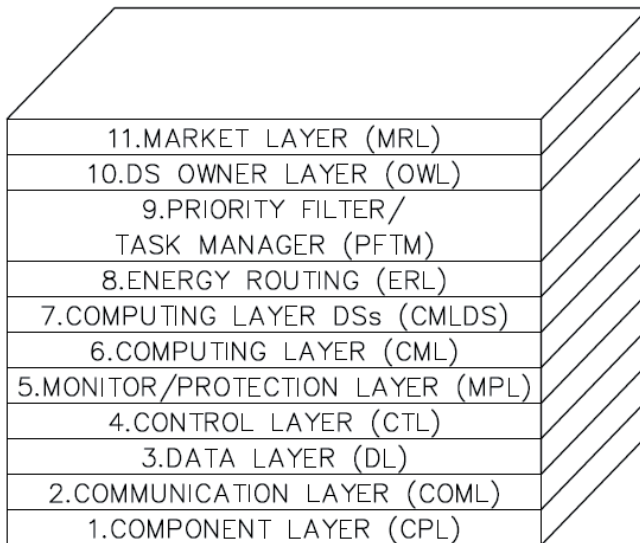
Fig. 4.1 Architecture of eleven layer (11L) design for V2G capable distribution substation

The ninth layer is the priority filter and task manager layer (PFTM), which receives data from DSO, Retailer, LV side consumers, which functions are required to be performed in the microgrid and generates task list for the next upcoming time period. In computer science, a priority queue is an abstract data type, where additionally each element has a "priority" associated with it. In a priority queue, an element with high priority is served before an element with low priority [133]. In microgrids energy generation or consumption is required in real time and can be generally predicted forehand (e.g. peak loads). The final decision of which tasks will be chosen to be executed depends on the preferences of the distribution substation owner (can be pre-programmed). These can be function/priority oriented

or business oriented (e.g. which party is willing to pay more in auction in the eleventh layer). In addition the PFTM layer sends data about energy consumption measurements and V2G support capability in a given timeperiod to DSO or Retailer.

The tenth layer is the distribution substation owner layer (OWL), where owner preferences are described and statistical reports can be extracted from CML (e.g. profit data in the given month). The eleventh layer is the market layer (MRL), which influences the preferences of the owner of the distribution substation.
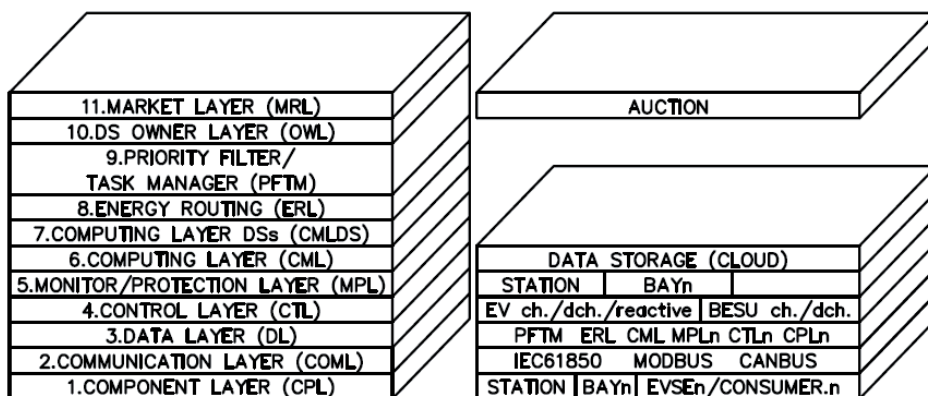
Fig. 4.2 Sublayers in the 11L architecture (right side)

Modern distribution substations consist of four main layers: CPL (components, e.g. motorized circuit breakers), COML (communication, e.g. Modbus for reading multimeter data), DL (e.g. RTU) and ERL (ATS switching). CTL layer is limited mostly to closing of a bay not for actively adjusting the output voltage of the bay. MPL layer is limited mostly to monitoring of auxiliary contact states not for influencing the maximum current in the CTL layer. CML, CMLDS, PFTM, OWL implementation is scarce. MRL layer can be considered as e.g. Nord Pool Spot (NPS). While individual layers of 11L architecture may find applications in some form in some of the practical installations, all 11L combined in one V2G capable distribution substation has not been reported.

The general requirements from the distribution substation owner to the SAS could be: charge EVs cheaply (in pre-set price limits in the energy market) and BESUs cheaply (e.g. at nights), make profit (by discharging BESUs), operate independently and maintain high energy quality level. The SAS should avoid: malfunctions in substation, contracts of EV owners should not get violated, overcharge or overdischarge BESUs. The main priorities could be return of investments or to provide solutions to particular problems inside the microgrid.

The general requirements from the EV owners to the SAS could be: charge cheaply, charge for selected departure time and SOC level. The SAS should avoid: violation of contracts, stress to EV batteries.

The general requirements from the LV consumers to the SAS could be: provide supply with backup support incase of power outage, store reverse energy flow, provide reactive power compensation or voltage mitigation, compensate certain harmonic content. The SAS should avoid: not providing support when required (e.g. peak shaving of loads) between charging timezones, providing poor energy quality.

The general requirements from the DSO to the SAS could be: lower charging currents (e.g. frequency regulation), store renewable energy, lower reactive power consumption in the LV consumers side. The SAS should avoid: overloading the grid, reducing the energy quality in the grid.

As owner of the substation prefers to prolong the usage of BESUs for higher return of investments, EVs are preferred to be used for peaking shaving of short term loads. BESUs will be utilized for peak shaving of long term loads or unplanned loads. BESUs will always be set to standby mode if ERL layer can not utilize ATS switching to connect to the EV side transformer as the primary option (e.g. EVs are being discharged to MV level). BESUs in distribution substations do not substitute UPS devices in offices (short delays in the ATS switching are inevitable – operation of motorized circuit breakers). Activation of emergency stop in EVSE must end programs running in bay level. Activation of emergency stop inside distribution substation must end programs running in the station level.

The benefit of the 11L architecture is that different parties can develop different algorithms for different layers as long as the input and output parameters are defined for each layer (maintaining the fractal design).

4.2 Simulation model of distribution substation

Figure 2.5 shows a distribution substation topology (IT earthing system) that is similar to the topology simulated using the MATLAB Simulink model (Fig. 4.3 [141]). The model is used to simulate different operations in the 11L design. The model consists of two independent 24 kV utility network supplies for redundancy, which are connected to the examined substation's MV switchgear. MV switchgear distributes MV voltage to the examined substation's low voltage sides (for EVs and consumers), and also to a nearby second distribution substation. The substation includes 250 kVA voltage transformers 24/0.4 kV (TRANSF_A, TRANSF_B); smart meters before and after voltage transformers (SMA1, SMA2, SMB1, SMB2); low voltage circuit breakers (LVA, LVB, LVC, LVD); bus coupling switches (BC_LV, BC_MV); 50 kW DC-DC power converters (DCCS1-DCCS3) at the common DC bus for EVs (with nominal voltage of 330 V DC); a 150 kW AC-DC power converter (ACDCS1) between the common DC bus and the common AC bus; 50 kW AC-DC-DC power converters (ACDCS2, ACDCS3) for BESUs (with a nominal voltage of 460 V DC).

In microgrid applications distribution substation can be viewed as an energy router and it is the function of the substation's main controller in the PFTM layer to determine when to utilize EVs or BESUs for peak shaving. The discharging of EVs or BESUs is controlled through low level control of power electronic converters in

CTL and MPL layers. Depending on the level of peak shaving, EVs and BESUs can be discharged in parallel to the LV side (only in IT earthing system).

The model was used to analyze fast charging of EVs without any peak shaving; fast charging of EVs with peak shaving by the BESUs; discharging of EVs to the common AC bus for utility load peak shaving; discharging of EVs to medium voltage side for utility load peak shaving (voltage transformers and current transformers from the MV side provide input for ACDCS1). Medium voltage transformers are simulated as ideal transformers.

The maximum active power let-through for the utility was chosen 600 kW in the simulations. The second distribution substation required 400 kW of active power for consumers in all simulations. The substation examined required 100 kW up to 250 kW of active power for consumers. Additionally, charging of EVs required 150 kW of active power. All maximum required powers added together result in 800 kW of active power. In the concept of Smart Grids generation and consumption of energy should be in balance such that sufficient energy is available at all times and with high quality.

Total harmonic distortion (THD) values registered by smart meters in simulations are also presented: THD of the current of the utility network input THD_{I_UT1} (at M_MV1); THD of the current of the common ac bus THD_{I_SMA2} (at SMA2).
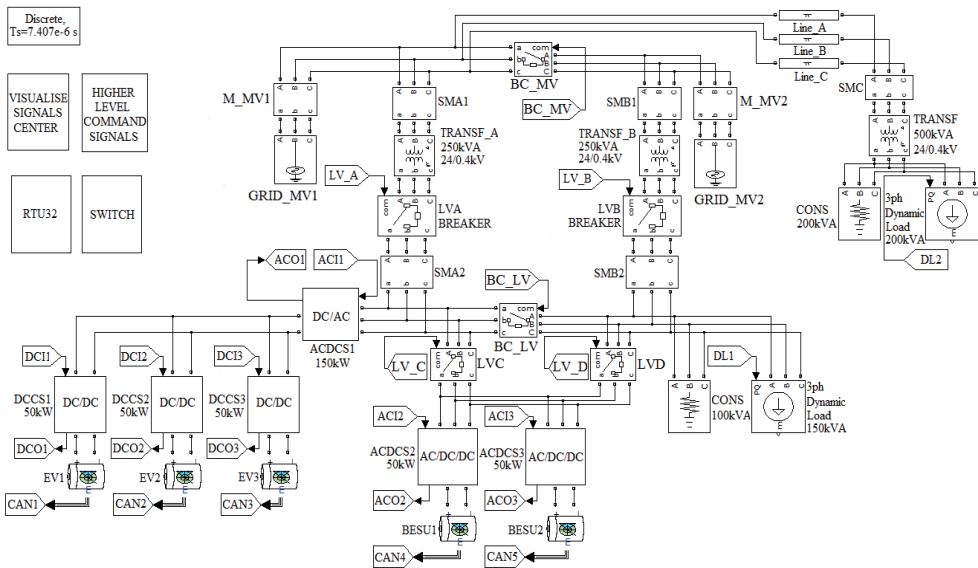
Fig. 4.3 MATLAB Simulink model of the distribution substation with an integrated AC & DC bus, EVs and BESUs [141]

Benefits of the IT earthing system are [134]:
- continuity of service incase of earth fault (current cannot loop via transformer's neutral;
- without disconnection incase of a fault there are less financial risks due to production loss and less risks to personnel (sudden loss of lighting, unavailability of safety-related equipment);
- reducing fire and explosion risks;
- optimization of corrective maintenance (clearing the fault can be postponed for a few hours depending on the probability of a second fault occurring rapidly);
- facilitating preventive maintenance as an insulation monitoring device is mandatory;
- limiting indirect costs (increasing the lifetime of the installation) as with limited fault currents equipment are subjected to less stress.

The disadvantages of IT earthing system are [134]:
- transformer required with isolation monitoring;
- the maintenance team must be capable of locating the fault;
- very low earth resistance required;
- limitations in the size and complexity of a network;
- monitoring of coupling capacitances of cables and loads with respect to earth (beyond a certain limit – several tens of kilometres – dangerous contact voltages will occur in the event of an insulation fault).

There are many applications where IT earthing system are utilized which vary from county to country: operating theatres, hospitals, cold storage, nuclear power stations, airports, official and business buildings, mines, laboratories, food-processing plants, chemical industry, industrial applications with sensitive processes, oil and gas refineries, automotive industry. All these applications may require peak shaving of loads with EVs. Often best compromise is the coexistence of various earthing systems (TN earthing system for non-critical parts and IT earthing system to critical parts) [134].

4.3 Layers of control algorithm

4.3.1 Component and data layer with EVSE and EV

One of the main components in the component layer are EVSE and EV. The functions of EVSE and communication between EVSE and EV, EVSE and EV owner, EVSE and distribution substation must be first defined (re-defined). The main principle of the operation is that EVSE and distribution substation exchange data in the data layer. EVSE communicates directly with EV owner. For the EV owner different parameters can be entered or viewed through HMI of EVSE or through application software ("apps").

In order to connect EV with EVSE for V2G application both sides have to include small modifications. This is due to fact that existing charging infrastructure is oriented only for charging EVs (Fig. 1.39 CHAdeMO fast connector). For V2G application an example modification is proposed in the Fig. 4.4. Additional output signal from EVSE side (discharge mode) and additional signal detector (m) at the EV side is required to set the EV into discharge mode. Additional relays (KA1 and KA2) close the EV contactor according to the mode selected. These modifications enable charging of EVs both through unidirectional CHAdeMO charging stations and through distribution substations with V2G capability. The standardized Yazaki DC fast connector can be utilized in both cases with taking into use the plug no 3, which is unused at the moment.

Table 4.1 includes parameters which have to be gathered from EV BMS to EVSE. Table includes names of parameters, descriptions and data type (Boole, Integer, Float, Time). These parameters are required for the distribution substation to execute control and protection functions and scheduling. The main parameters of the table are live values (state of charge (SOC), open circuit voltage of EV battery pack, current, temperature, rated capacity) and min/max ratings (of battery voltage, max currents for charging/discharging, temperature). According to CHAdeMO standard [59] EV permission signal and EV requested current signals (every 100 ms) are required. EV sends the maximum request current signal, but it is the final decision of the substation controller to determine the actual charging current (the same or lower than EV requested) based on the available power in the microgrid. EV can protect itself (if exposed to extreme conditions or due to fault at the EV side) by ending EV permission signal (socket no 4 in Fig. 4.4).

IEC 15118-1 specifies the requirements to signal that EV is V2G compatible and how much maximum power EV can deliver in V2G mode. EV must indicate the maximum voltage level where it supports fast charging and error signalling to EVSE which must terminate the connection due to fault on the EV side. State of health (SOH) is signalled for indication. It is the function of the EV BMS to adjust e.g. the maximum charging/discharging currents according to the SOH as the EV BMS has the most detailed specifications of its battery.

Table 4.2 includes parameters which have to be received from EV owner to EVSE. The main parameters are the departure time, final SOC level at the departure, connection stop requested by EV owner. According to the connection package selected the required charging timezone, discharge allowed and maximum depth of discharge level during the connection.

Table 4.3 includes parameters which have to be received from EVSE to distribution substation. In addition to the parameters presented in Tables 4.1 and 4.2, the required parameters are the signal that connection is established between EVSE and EV, whether EVSE is executing slow charging to deeply discharged battery or emergency stop has been activated. Emergency stop signal circuit requires additional control cable between EVSE and substation in order to firmly disconnect the power circuit. Auxiliary supply to the EVSE supply contactor must have physical opening contact by the emergency stop in the wiring circuit.

Table 4.4 includes parameters which are sent to EVSE by distribution substation. The main parameters are that the connection is established at the substation side, what mode is required of EV (charging/discharging) by substation, when the contract charging is executed by scheduling, kWh consumption measured by the substation with corresponding price levels (updated constantly for the EVSE throughout the connection period to avoid data loss during power outage), min/max data of connection and operation, error signals and that substation is V2G compatible.

Figure 4.5 show the flowcharts regarding the operation of EVSE and information exchange between the EV and distribution substation. When the EV present is detected (e.g. cable connected between EVSE and EV), the EVSE executes communication setup, identification and authorization according to IEC 15118-1. One of the main functionalities of the distribution substation is to transfer energy between the utility and the EV. Functionalities of e.g. communication set-up, identification and billing are the main functionalities of the EVSE. EVSE will check errors in the owner requests, initiates communication with EV BMS, checks general errors in EV data (temperature over maximum or below minimum, overcharged), determines whether slow charging is required for deeply discharged battery, makes the compability check with EV, locks the mechanical connector interlock and waits connection made signal from the distribution substation. When the substation connection is established, EVSE exchanges EV BMS data to the data layer of the substation bay, where substation can retrieve and use the data for further processing. Substation writes the kWh consumption with pricing, required EV charge or discharge mode to the data layer of bay. EVSE will forward the mode selection to the EV for closing EV contactor. Slow charging can be supplied from the LV consumers side of the distribution substation or from different source. EVSE monitors consumption of slow charging for further billing with the EV owner. When the substation side connection is ended, EVSE will receive final parameters from substation, if required continues with slow charging to higher SOC levels, ends transmission with EV BMS, executes billing with EV owner and releases the mechanical interlock.

Modifications made by the EV owner (e.g. change of departure time) are transmitted through EVSE to the distribution substation, which process the data and sends confirmation or confirmation with penalties to EVSE, which then notifies the EV owner.
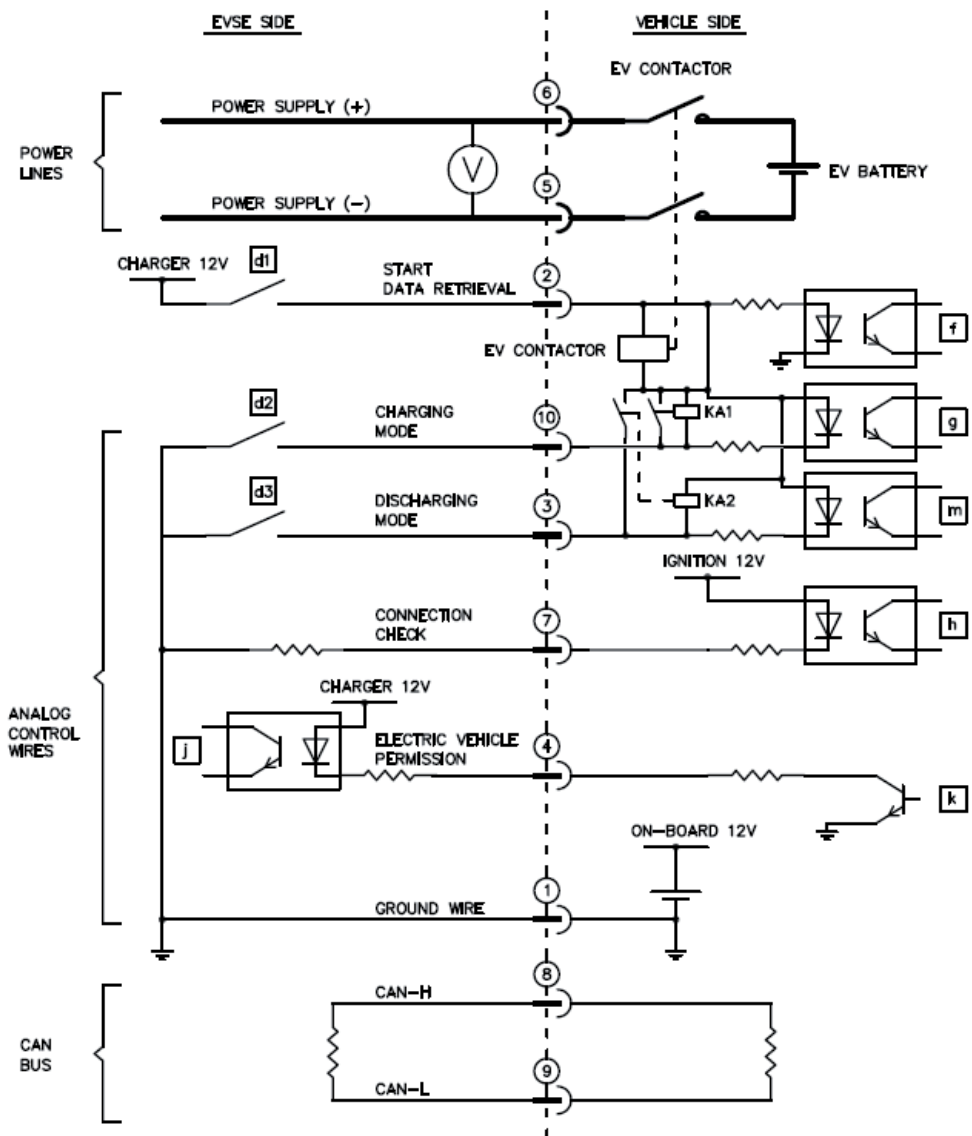
Fig. 4.4 One example for control of EVSE and EV side for V2G application with Yazaki DC fast charging connector

Table 4.1. Receive parameters for EVSE from EV BMS

Name	Description	Data type
SOC	State of charge value of EV battery pack	FLOAT
Voltage	Measured open circuit voltage value of EV battery pack	FLOAT
Current	Measured current value (charging, discharging) of EV battery pack	FLOAT
EV current request	Current requested for charging from EV BMS	INTEGER
Temperature	Temperature value of EV battery pack	FLOAT
SOH	State of health (for indication)	FLOAT
Max capacity	Max. rated capacity of EV battery pack	INTEGER
Max voltage fast charge	Max. battery voltage (SOC) where EV holds its contactor ON during fast charging. Higher voltage levels are allowed only with slow charging.	INTEGER
Min pack voltage	Min. open circuit voltage of EV battery pack, when battery is damaged	INTEGER
Max pack voltage	Max. open circuit voltage of EV battery pack, when battery is damaged	INTEGER
Max current charge	Max. charging current for EV battery pack	INTEGER
Max current discharge	Max. discharging current for EV battery pack	INTEGER
Min temperature	Min. temperature value for EV battery pack with EV side heating	INTEGER
Max temperature	Max. temperature value for EV battery pack with EV side cooling (for control of current during charging and discharging)	INTEGER
EV permission signal	EV side safety signal with EVSE. EV can permit or not permit charging if conditions with EVSE do not match. EV can stop EVSE connection if EV battery is subjected to excess stress	BOOLE
V2G compatible	EV V2G capability indication	BOOLE
Max V2G power	Information at which power V2G can be supported	INTEGER
Errors	List of Error codes	DATA

Table 4.2. Receive parameters for EVSE from EV owner

Name	Description	Data type
Departure time	Departure time	TIME
Final SOC level	Final SOC level required for departure time	INTEGER
Stop request (normal)	Request from EV owner to end connection before departure time	BOOLE
Parameters from charge package selection (influences final price)		
Timezone selection	Selection of pre-defined timezone of day when EV is charged to final SOC level (possible later changes in departure time from EV owner may not guarantee final SOC level at departure)	TIME
Discharging allowed	EV owner confirmation for participation in Smart Grid	BOOLE
DOD level	DOD level selected according to package for participation in Smart Grid	INTEGER

Table 4.3. Receive parameters for DS from EVSE

Name	Description	Data type
	EV BMS (measured values and min/max data) and EV owner data presented in Tables 4.1 and 4.2	
Connected	Connection established with mechanical interlocking	BOOLE
Slow charge	EV in slow charge mode (deeply discharged)	BOOLE
Emergency stop	Emergency stop circuit activated	Digital output

Table 4.4. Sending parameters for EVSE from DS

Name	Description	Data type
Connected	Confirmed connection from DS	BOOLE
Mode selection	Setting EV into charge or discharge mode	INTEGER
Scheduling mode	Scheduling is made by EV or by DS	BOOLE
Scheduled	Confirmed scheduled charging time for final SOC level	TIME
kWh data	Consumed/Produced kWh data of DC power circuit measurements (charging, discharging)	FLOAT
Prices	Price levels for kWh charge/discharge/penalties	FLOAT
Min/max data	Min/max data which the substation can provide for EVSE (e.g. active power, current, voltage)	FLOAT
Errors	List of Error codes	DATA
V2G compatible	DS V2G capability indication	BOOLE
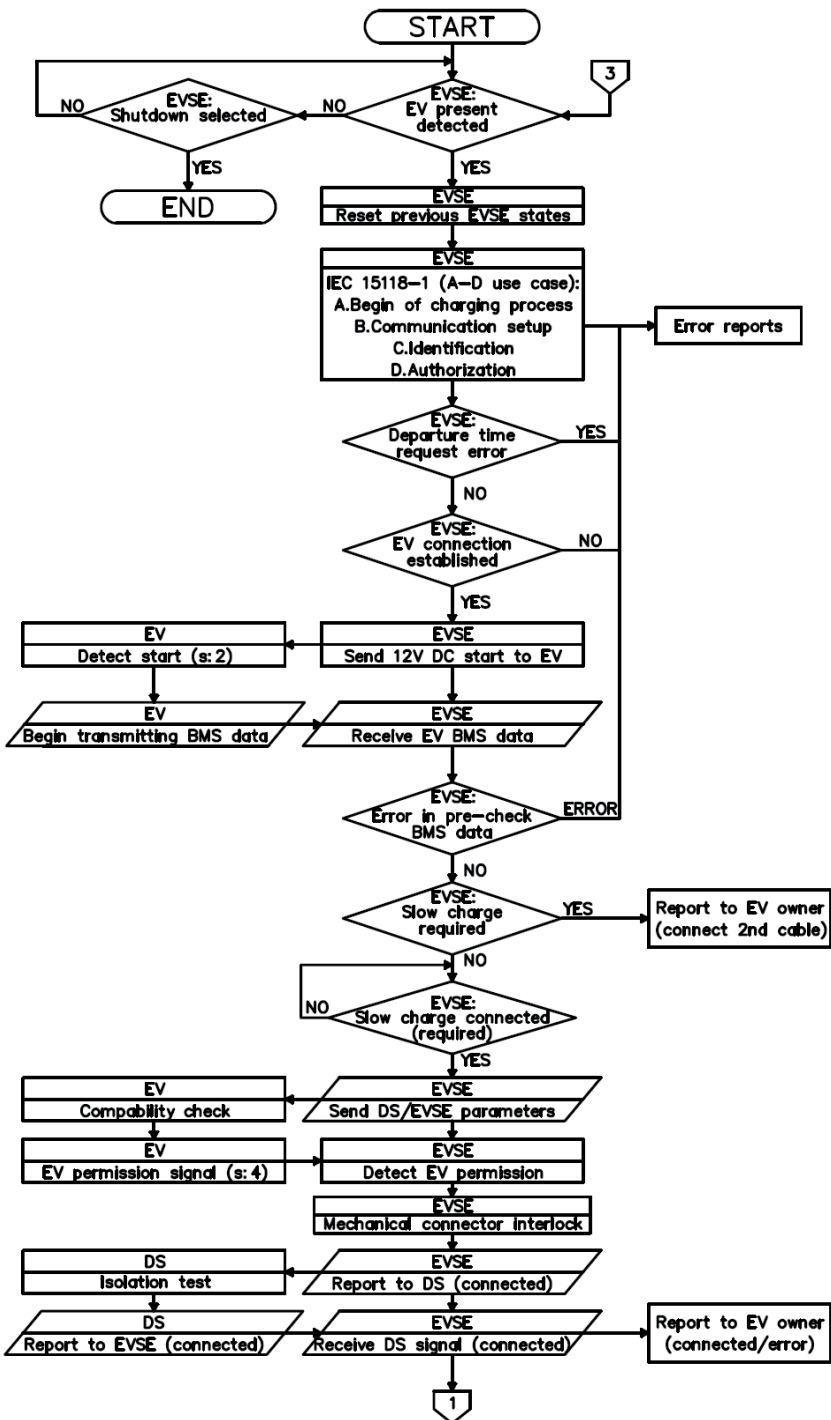
Fig. 4.5 Flowchart of EVSE operation with EV and distribution substation – Part 1/3
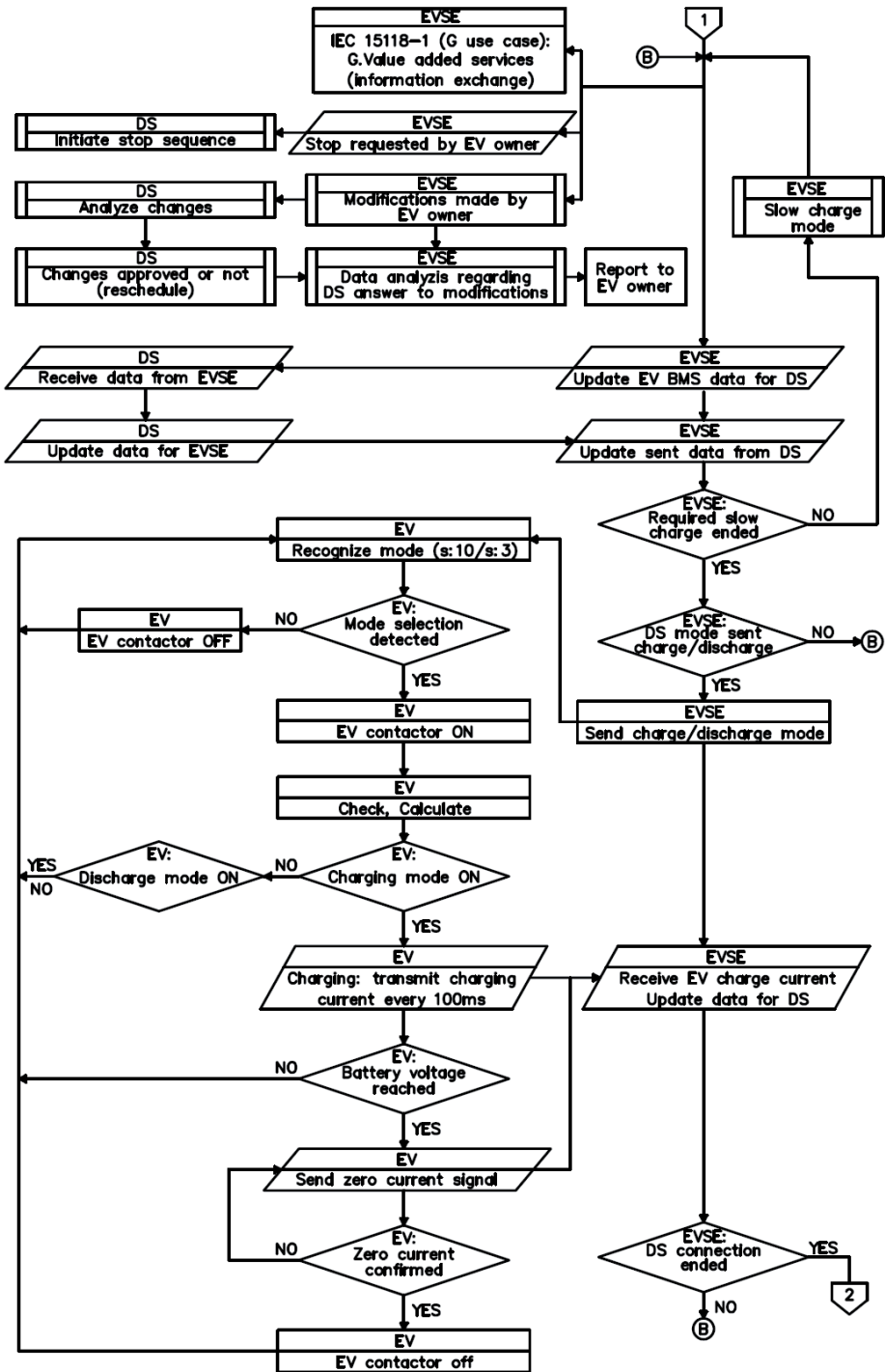
Fig. 4.5 Flowchart of EVSE operation with EV and distribution substation – Part 2/3
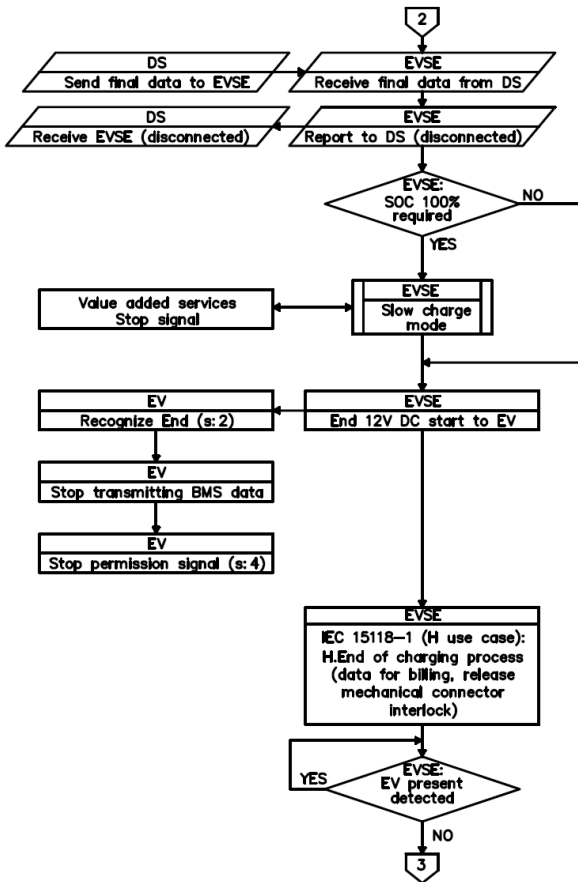
Fig. 4.5 Flowchart of EVSE operation with EV and distribution substation – Part 3/3

4.3.2 Control layer for EV charging

Control layer executes the charging of EVs. The program for bay receives input data from the data layer and controls the operation of the bidirectional DC-DC power converter. The program for the DC bus receives input data from the PFTM layer and controls the operation of all the bays. In Table 4.5 are presented the input and output parameters for the bay and in the Table 4.6 are presented the input and output parameters for the management of the DC bus. Data types are shortened in the tables as follows: B-boole, I-integer, F-float, D-data package, DI-digital input, DO-digital output. Receive and Send columns describe the layers where data is received/sent and the destination of those layers (e.g. DL-EVSE the first part DL describes the data layer and EVSE destination).

Figures 4.6 show the flowcharts regarding the operation of the bay for EV charging. When the program is executed, information is received from layers as described in the Table 4.5. Input parameters are sent to the DC-DC converter and the primary side switch of the bay (before the DC-DC converter) is closed. When

the DC-DC converter has reached the target output voltage, secondary side switch of the bay (after the DC-DC converter) is closed. Maximum charging current is received from the MPL layer. If the open circuit voltage of the EV battery pack is below the maximum voltage that is supported by the EV during fast charge, constant current mode is executed. Additional safety factor (SF) is applied to the maximum voltage to avoid damaging the battery as the voltage in the exponential zone increases rapidly (e.g. safety factor 0.95 which from e.g. 4.0 V is 3.8 V). Output voltage of the DC-DC converter is adjusted as long as the maximum charging current is achieved (measurement values from the EV side). The output voltage from the distribution substation takes into consideration the resistances of supply cables, therefore the maximum charging current is transmitted to the EV side. Measurement values are stored inside the program and forwarded to the EVSE as well. If the open circuit voltage of the EV battery pack is equal or higher than the maximum voltage that is supported by the EV during fast charge (with additional safety factor), constant voltage mode is executed. Output voltage of the DC-DC converter is hold near the maximum voltage allowed. If the charging current is below minimum current threshold, the charging is stopped. Charging is executed with softstart (ramping up the output voltage by following the measured charging current to the maximum) and normal charging is ended with softstop (ramping down the output voltage by following the measured charging current to the minimum threshold). Emergency stop immediately opens the secondary side switch of the bay (after the DC-DC converter). When the target SOC value is reached, operation of the DC-DC converter is stopped, switches of the bays are opened and final measurement values are transmitted to the data layer for forwarding to EVSE.

Figure 4.7 shows the flowcharts regarding the operation of the DC bus for EV charging. When the program is executed, information is received from layers as described in the Table 4.6. According to the maximum currents of the bays the necessary kW rating for the AC-DC converter is calculated (how many parallel modules are required for the AC-DC converter). If the target kW rating exceeds the pre-determined threshold value, immediate BESU support request is forwarded to the PFTM layer. Input parameters are forwarded to the AC-DC converter and the primary side AC switch (before AC-DC converter) is closed. When the AC-DC converter has reached the target output voltage, EV charging program of bays that are scheduled are initiated. EVs of those bays are set for charging mode. Status of the bay programs are monitored during the DC bus operation. kW rating of the AC-DC converter is adjusted if the maximum current values of bays are changed or some bays have ended their operation. When all scheduled bays have reached their targets, operation of the AC-DC converter is stopped, primary side AC switch is opened and session data (e.g. events, charging currents, kWh consumption with prices, efficiency of charging) is stored to the data storage. For safety reasons, all capacitors in the AC-DC converter and DC-DC converters are discharged with the end of the charging session.

Table 4.5. Input and output parameters for EV charging in control layer (bay)

Input	Receive	DT	Output	Send	DT
Process start/end	DL-CTL-DC BUS	B	Process status	DL-CTL-DC BUS	B
Battery OCV	DL-EVSE	F	Issue penalty	DL-EVSE	B
Final SOC (target)	DL-EVSE	I	Penalty price	DL-EVSE	F
Max. battery voltage fast charge (EV supported)	DL-EVSE	I	kWh measurement	DL-EVSE	F
Stop request	DL-EVSE	B	kWh price	DL-EVSE	F
EV connected	DL-EVSE	B	kWh cost	DL-EVSE	F
AC-DC output voltage	DL-DC BUS	F	Current measurement	DL-EVSE	F
DC-DC output parameters	CPL-DCDC	D	DC-DC input parameters	CPL-DCDC	D
Current measurement	CPL-DCDC	F	Closing of bay switches	CPL-SWP/ CPL-SWS	DO
Imax bay	DL-MPL	I	Error reports	DL	D
kWh price	DL-PFTM	F			
Penalty price	DL-PFTM	F			
kWh measurement	CPL-SM	F			
Protection status	DL-MPL	B			
Emergency stop	CPL-EVSE	DI			

Table 4.6. Input and output parameters for EV charging in control layer (DC bus)

Input	Receive	DT	Output	Send	DT
Process start/end	DL-PFTM	B	Process status	DL-PFTM	B
Process status	DL-CTL-BAY(s)	B	Process start/end	DL-CTL-BAY(s)	B
Imax of all bays	DL-MPL	I	EV mode: charge	DL-EVSE(s)	B
Bays to be connected	DL-CML	B	AC-DC input parameters	CPL-ACDC	D
AC-DC output parameters	CPL-ACDC	D	AC-DC output parameters	DL-DC BUS	D
Protection status	DL-MPL	B	BESU support immediately	DL-PFTM	B
Emergency stop	CPL-STATION	DI	BESU kW rating	DL-PFTM	F
			Closing of station switch	CPL-AC BUS	DO
			Error reports	DL	D
			Store data	DSTORAGE	D

START

Retreive initial data (DS/EVSE)

DC–DC converter remote control

Send parameters for DC–DC converter (buck)

Close primary side DC switch (protection OK)

Ready signal detected from converter — NO / YES

Close secondary side DC switch (protection OK)

Charging process activated

Start measurement count (kWh) Start timer count

5

A

Stop required by EV owner or DS — YES / NO

Softstop

Stop required by EV owner — NO / YES

Issue penalty

4

Retreive Imax value (Monitor)

Retreive kWh price level

Retreive output voltage value measured by DC–DC

U<(Umax x SF) — YES / NO

Charging in process — YES / NO

Softstart (Imax from 0 to 100%)

Emergency stop command — YES / NO

Protection fulfilled — NO / YES

Urgent error EV signal lost — YES / NO

Timer and charging mode match — NO / YES

2

Adjust U for Imax

U output value for DC–DC

kWh measurement + price level to EVSE

Specific target SOC reached — NO / YES

Softstop

A

1

3

Fig. 4.6 Flowchart of EV charging in control layer (bay) – Part 1/2

153

Fig. 4.6 Flowchart of EV charging in control layer (bay) – Part 2/2

Fig. 4.7 Flowchart of EV charging in control layer (DC bus) – Part 1/2
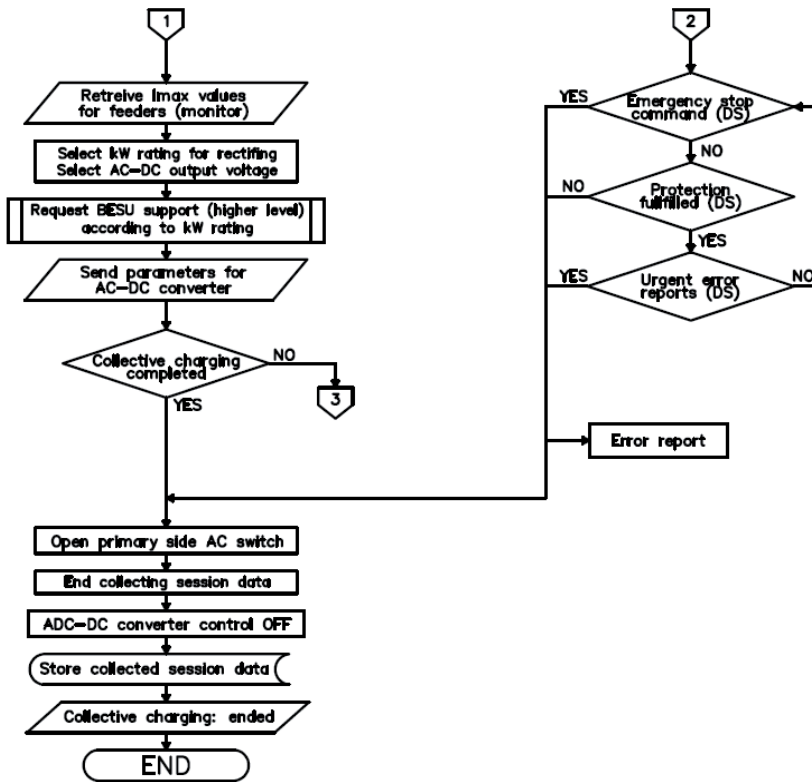
Fig. 4.7 Flowchart of EV charging in control layer (DC bus) – Part 2/2

EV fast charging without any peak shaving was simulated with MATLAB Simulink (Fig. 4.3) [141]. The second utility network supply was considered as unavailable and all the loads had fallen for the first utility network supply. Circuit breaker LVA and bus coupling breaker BC_LV were closed. Circuit breakers LVB, LVC and LVD were open. Examined substation was loaded with 100 kW of consumers (total of 500 kW for the utility network with the second substation and without EVs). All three EV charging stations were loaded simultaneously at 0.22 s (fast charging with 100 A and 36 kW). The results from the simulated model are presented in Fig. 4.8 – 4.12.

Fig. 4.8 illustrates the rms active power (e.g. 106.37 kW at 0.459 s and 113.75 kW at 0.4965 s) and rms reactive power (e.g. 5.2 kvar at 0.5 s) consumed by ACDC1 (cosφ≈0.99). Fig 4.9 illustrates voltage and current (e.g. peak current - 213.5 A at 0.4935 s) of ACDC1 at AC side. Fig. 4.10 illustrates voltage (e.g. 680 V DC at 0.5 s) and current (e.g. -100A DC at 0.4991 s and -210 A at 0.4993 s) of ACDC1 at DC side. Fig. 4.11 illustrates rms active power (e.g. 617.3 kW at 0.5 s) and rms reactive power (3.2 kvar at 0.5 s) of the utility load at MV side 1. Fig. 4.12 illustrates state of charge (SOC), current (-100A) and voltage (356.93 V) of the EV1.
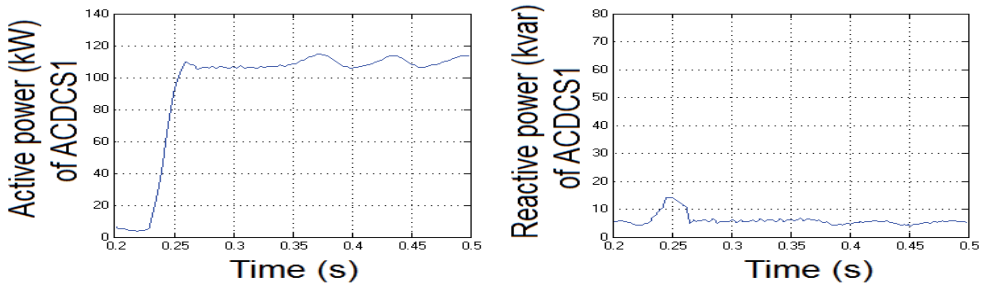
Fig. 4.8 Active and reactive power consumed by ACDCS1 in the MATLAB Simulink model during charging of EV bays
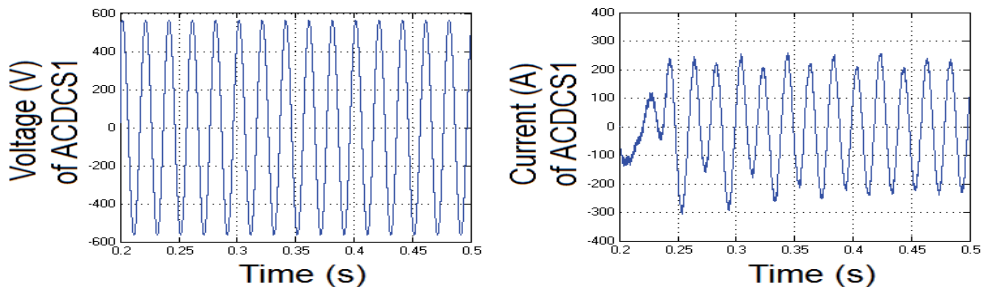
Fig. 4.9 Voltage and current of ACDCS1 at AC side in the MATLAB Simulink model during charging of EV bays
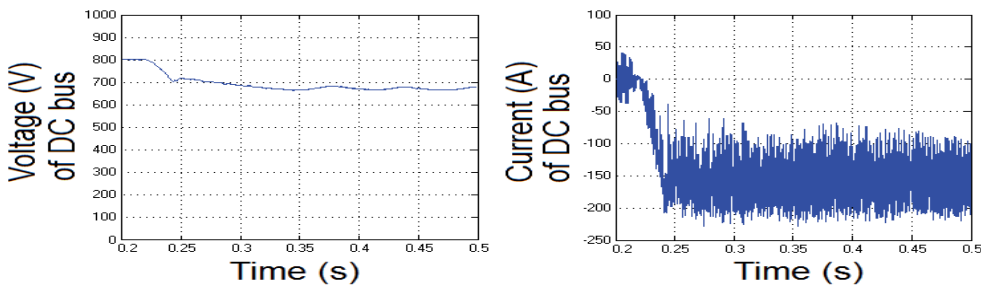
Fig. 4.10 Voltage and current of ACDCS1 at DC side in the MATLAB Simulink model during charging of EV bays
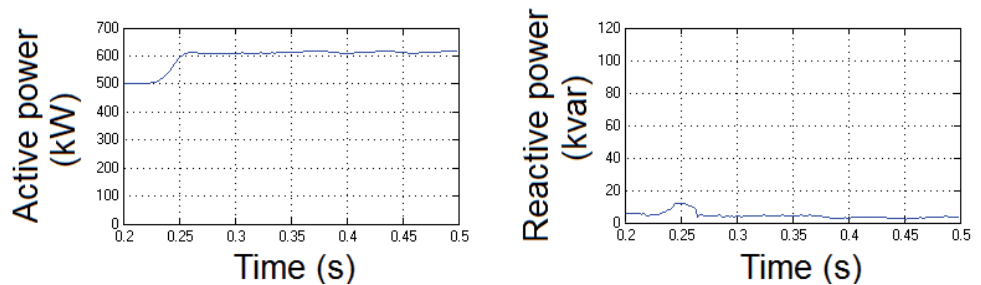
Fig. 4.11 Active and reactive power of the utility load at MV side 1 in the MATLAB Simulink model during charging of EV bays
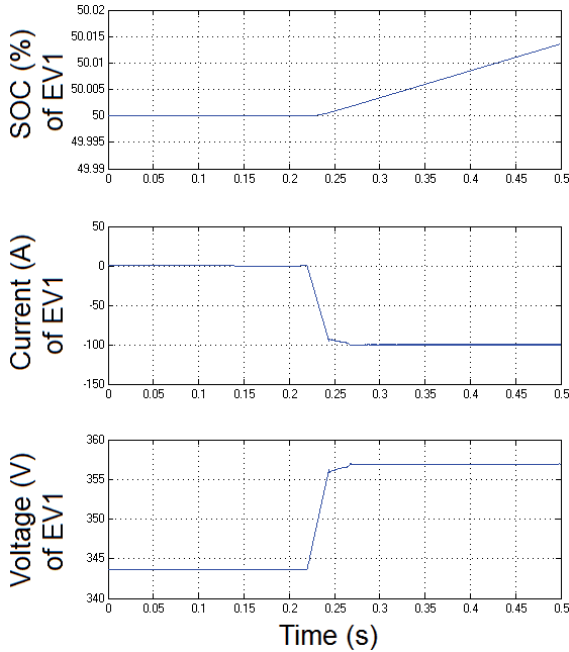
Fig. 4.12 SOC, current and voltage of the EV1 in the MATLAB Simulink model during charging of EV bays

The maximum load for the utility network was exceeded by 3 %. THD_{I_UT1}<0.1 % and THD_{I_SMA2}<0.1 % at the continuous operation of the AC-DC power converter ACDCS1. Efficiency of the AC-DC converter ACDC1 in the MATLAB Simulink model during charging of the EV bays was calculated 90.2 % over time period 0.5 s, efficiency of the DC-DC converter of the bay EV1 was calculated 98 % over time period 0.5 s. Total combined efficiency of charging was calculated 88.4 % over time period 0.5 s.

4.3.3 Control layer for EV discharging

Control layer executes the discharging of EVs. The program for bay receives input data from data layer and controls the operation of the bidirectional DC-DC power converter. The target for the bidirectional DC-DC converter is to maintain stable output voltage for the common DC bus. Current of the bay is determined by the inversion active power target of the AC-DC converter. The program for the DC bus receives input data from PFTM and controls the operation of bays and AC-DC converter. In Table 4.7 are presented the input and output parameters for the bay and in the Table 4.8 are presented the input and output parameters for the management of the DC bus. Data types are shortened in the tables as follows: B-boole, I-integer, F-float, D-data package, DI-digital input, DO-digital output. Receive and Send columns describe the layers where data is received/sent and the destination of those layers.

Figure 4.18 shows the flowcharts regarding the operation of the bay for EV discharging. When the program is executed, information is received from layers as described in the Table 4.7. Input parameters are sent to the DC-DC converter. When EVSE is set for discharge mode, measurements are being stored and secondary side switch of the bay (after the DC-DC converter) is closed. When the DC-DC converter has reached the target output voltage, primary side switch of the bay (before the DC-DC converter) is closed. The target output value is either pre-determined or calculated from the computing layer. The target output value remains constant throughout the session. Program of the bay monitors that the depth of discharge (DOD) is not exceeded according to the contract, also maximum discharging current of the EV is not exceeded. When the AC-DC is not transferring energy from the common DC bus to the common AC bus, the DC-DC converters are set to no-load mode (and vice versa in the opposite situation). Measurement values are stored inside the program and forwarded to the EVSE as well. Emergency stop immediately opens the primary and secondary side switches of the bay. When the discharging procedure is ended, switches of the bays are opened and final measurement values are transmitted to the data layer for forwarding to EVSE.

Table 4.7. Input and output parameters for EV discharging in control layer (bay)

Input	Receive	DT	Output	Send	DT
Process start/end	DL-CTL-DC BUS	B	Process status	DL-CTL-DC BUS	B
Battery voltage	DL-EVSE	F	Issue penalty	DL-EVSE	B
DOD level	DL-EVSE	I	Penalty price	DL-EVSE	F
Initial SOC level	DL-EVSE	F	kWh measurement	DL-EVSE	F
Imax discharge EV	DL-EVSE	I	kWh price	DL-EVSE	F
Stop request	DL-EVSE	B	kWh cost	DL-EVSE	F
EV connected	DL-EVSE	B	Current measurement	DL-EVSE	F
EVSE set in discharge mode	DL-EVSE	B	DC-DC input parameters	CPL-DCDC	D
AC-DC output parameters	DL-DC BUS	D	Closing of bay switches	CPL-SWP/ CPL-SWS	DO
DC-DC output parameters	CPL-DCDC	D	Error reports	DL	D
Current measurement	CPL-DCDC	F			
Imax bay	DL-MPL	I			
kWh price (discharge)	DL-PFTM	F			
Penalty price	DL-PFTM	F			
kWh measurement	CPL-SM	F			
Protection status	DL-MPL	B			
Emergency stop	CPL-EVSE	DI			

Table 4.8. Input and output parameters for EV discharging in control layer (DC bus)

Input	Receive	DT	Output	Send	DT
Process start/end	DL-PFTM	B	Process status	DL-PFTM	B
Process status	DL-CTL-BAY(s)	B	Process start/end	DL-CTL-BAY(s)	B
Imax of all bays (discharge)	DL-MPL	I	EV mode: discharge	DL-EVSE(s)	B
Current of bays	DL-EVSE	F	AC-DC input parameters	CPL-ACDC	D
Bays to be connected	DL-CML	B	AC-DC output parameters	DL-DC BUS	D
AC-DC input parameters (kW)	DL-PFTM	D	BESU support immediately	DL-PFTM	B
AC-DC output parameters	CPL-ACDC	D	BESU kW rating	DL-PFTM	F
Protection status	DL-MPL	B	Closing of station switch	CPL-AC BUS	DO
Emergency stop	CPL-STATION	DI	Error reports	DL	D
Unintentional islanding	DL-MPL	B	Recalculation	DL-CML	D
Load status	DL-AC BUS	F	Store data	DSTORAGE	D

Figure 4.19 shows the flowcharts regarding the operation of the DC bus for EV discharging. When the program is executed, information is received from layers as described in the Table 4.8. The main input parameters for the program are the bays that have to be connected, kW rating of the AC-DC converter, inversion direction (LV or MV side) and session time. Input parameters are forwarded to the AC-DC converter and the primary side AC switch (before AC-DC converter) is closed. AC-DC converter is in the no-load mode. Discharging programs of acquired bays are initiated, EVs of those bays are set for discharging mode through EVSE. Status of the bay programs are monitored during the DC bus operation. When all bays are operational, AC-DC converter is set to load mode to follow the target kW rating. If the target kW rating can not be matched due to fault in one of the bays, immediate BESU support is either requested or error report is sent to the PFTM layer. When all session has expired, operation of the AC-DC converter is stopped, primary side AC switch is opened and session data (e.g. events, charging currents, kWh consumption with prices, efficiency of discharging) is stored to the data storage. For safety reasons, all capacitors in the AC-DC converter and DC-DC converters are discharged with the end of the discharging session.

Discharging of EVs to LV and MV side for the utility load peak shaving was simulated with MATLAB Simulink (Fig. 4.3) [141]. The second utility network supply was considered as unavailable and all the loads had fallen for the first utility network supply.

For discharging EVs to the common AC bus of the LV side circuit breaker LVA and bus coupling breaker BC_LV were closed [141]. Circuit breakers LVB, LVC

and LVD were open. The substation examined required 250 kW of active power for consumers and 400 kW of active power was required by the second distribution substation. The results from the simulated model are presented in Fig. 4.13 – 4.17. The load in the examined substation was ramped up linearly, as presented in Fig. 4.20. All three EV charging stations were set to discharge mode simultaneously with the start of the simulation. The target for the AC-DC converter 1 is to utilize the full power of EVs (total of 150 kW).

Fig. 4.13 illustrates the rms active power (e.g. 171.5 kW at 0.5 s) produced and rms reactive power (e.g. 36.7 kvar at 0.5 s) consumed by ACDC1. Fig 4.14 illustrates voltage and current (e.g. peak current 369 A at 0.49 s) of ACDC1 at AC side. Fig. 4.15 illustrates voltage (e.g. 777 V DC at 0.5 s) and current (e.g. 255.5 A DC at 0.5 s) of ACDC1 at DC side. Fig. 4.16 illustrates rms active power (e.g. 482.5 kW at 0.5 s) and rms reactive power (34.6 kvar at 0.5 s) of the utility load at MV side 1. The maximum load for the utility was not exceeded. Fig. 4.17 illustrates state of charge (SOC), current (218 A at 0.5 s) and voltage (314.7 V at 0.5 s) of the EV1. THD_{I_UT1}<0.1 % and THD_{I_SMA2}<0.4 % at the continuous operation of ACDCS1. Efficiency of the AC-DC converter ACDC1 in the MATLAB Simulink model during discharging of the EV bays was calculated 89.2 % over time period 0.5 s, efficiency of the DC-DC converter of the bay EV1 was calculated 98.2 % over time period 0.5 s. Total combined efficiency of charging was calculated 87.6 % over time period 0.5 s.
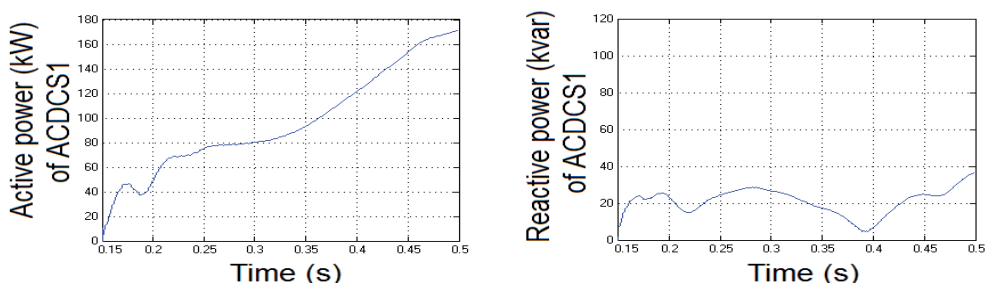
Fig. 4.13 Active and reactive power consumed by ACDCS1 in the MATLAB Simulink model during discharging of EV bays to LV side
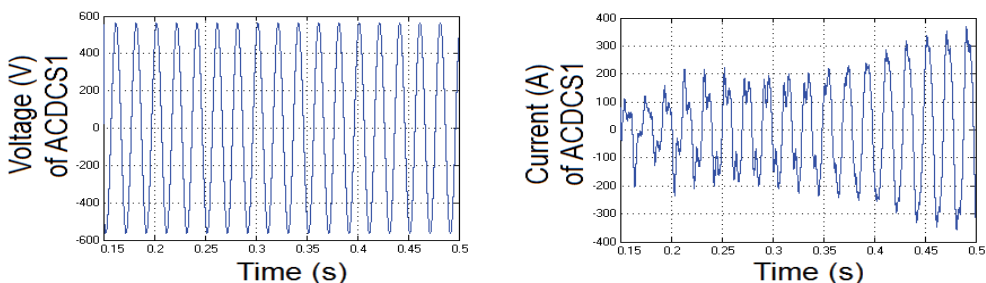
Fig. 4.14 Voltage and current of ACDCS1 at LV AC side in the MATLAB Simulink model during discharging of EV bays to LV side

161
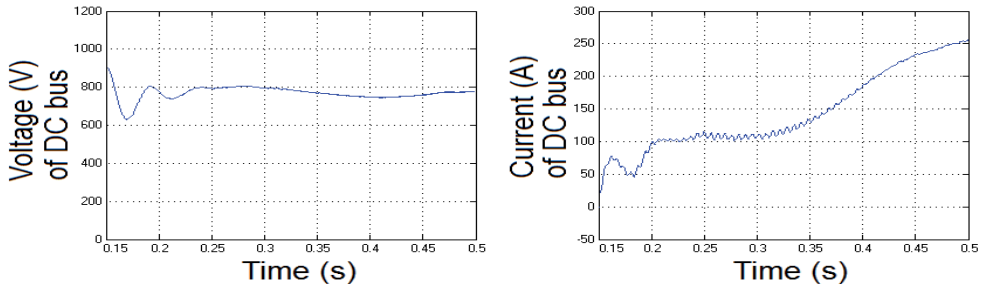
Fig. 4.15 Voltage and current of ACDCS1 at DC side in the MATLAB Simulink model during discharging of EV bays to LV side
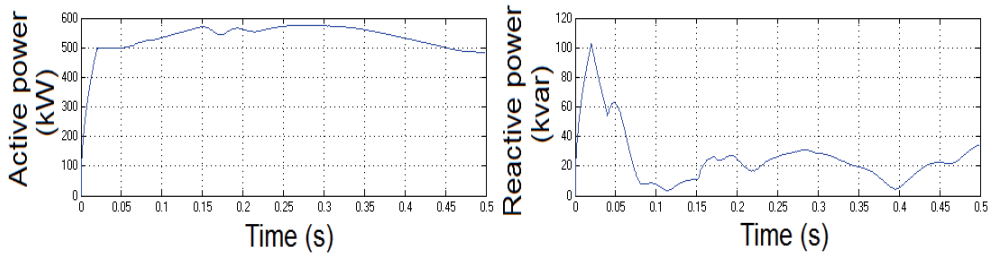
Fig. 4.16 Active and reactive power of the utility load at MV side 1 in the MATLAB Simulink model during discharging of EV bays to LV side
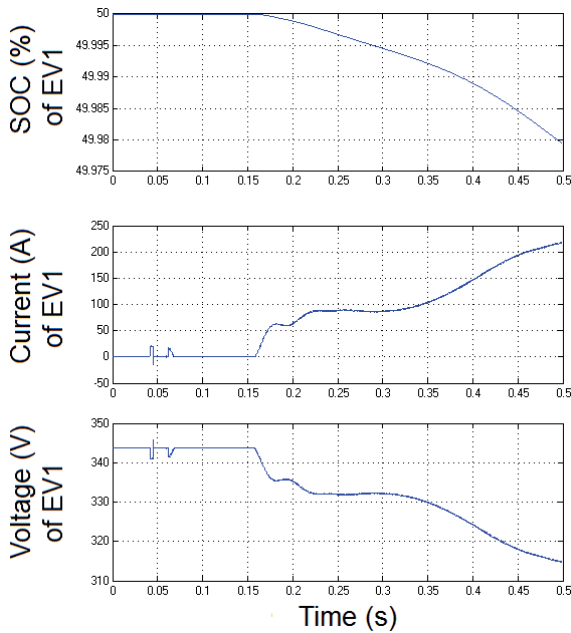
Fig. 4.17 SOC, current and voltage of the EV1 in the MATLAB Simulink model during discharging of EV bays to LV side

162
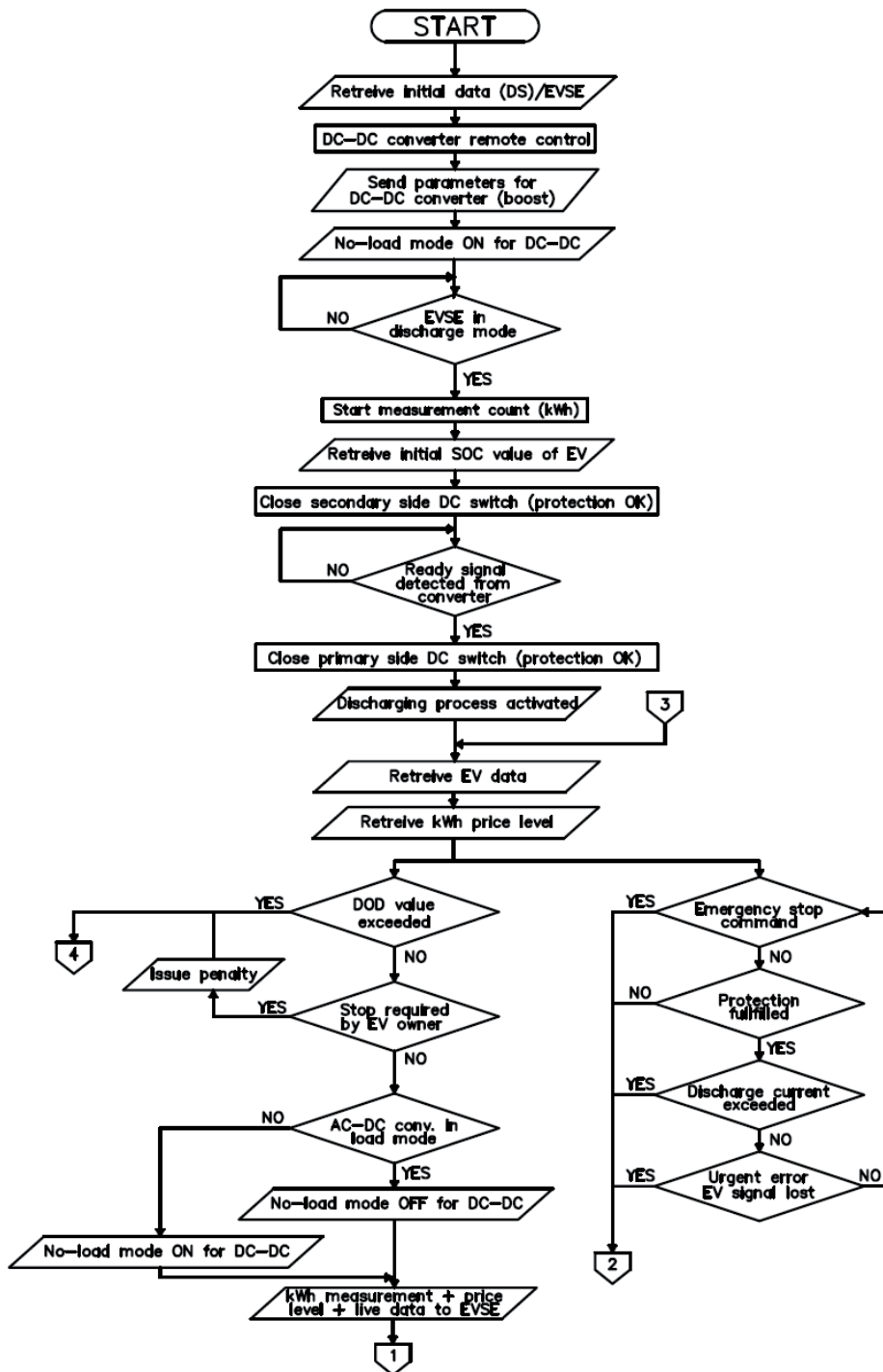
Fig. 4.18 Flowchart of EV discharging in control layer (bay) – Part 1/2
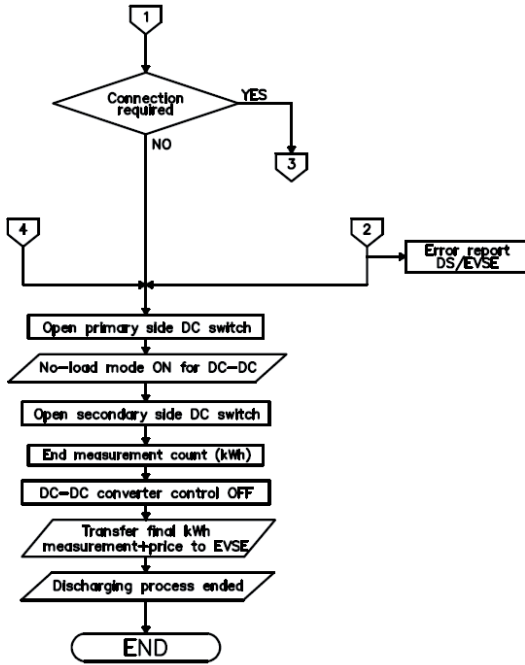
Fig. 4.18 Flowchart of EV discharging in control layer (bay) – Part 2/2

For discharging EVs to the MV side circuit breakers LVA, LVB and bus coupling breaker BC_MV were closed [141]. Circuit breakers LVC, LVD and bus coupling breaker BC_LV were open. The examined substation required 250 kW of active power for consumers and 400 kW of active power was required by the second distribution substation. The results from the simulated model are presented in Fig. 4.21 – 4.23. The load in the examined substation was also ramped up linearly, as presented in Fig. 4.20. All three EV charging stations were set to discharge mode simultaneously with the start of the simulation. The target for AC-DC converter 1 is to utilize the full power of EVs (total of 150 kW). Fig. 4.21 illustrates the rms active power (e.g. 169.1 kW at 0.5 s) produced and rms reactive power (e.g. 33.5 kvar at 0.5 s) consumed by ACDC1 measured by smart meter SMA1. Fig 4.22 illustrates voltage and current (e.g. peak current 6 A at 0.495 s) of MV side recorded by the smart meter SMA1 in the MATLAB Simulink model. Fig. 4.23 illustrates rms active power (e.g. 484 kW at 0.5 s) and rms reactive power (e.g. 31.6 kvar at 0.5 s) of the utility load at MV side 1. The maximum load for the utility was not exceeded. THD_{I_UT1}<0.1 % and THD_{I_SMA2}<0.2 % at the continuous operation of the AC-DC power converter ACDCS1. Efficiency of the AC-DC converter ACDC1 over the voltage transformer in the MATLAB Simulink model during discharging of the EV bays was calculated 88 % over time period 0.5 s, efficiency of the DC-DC converter of the bay EV1 was calculated 98.2 % over time period 0.5 s. Total combined efficiency of charging was calculated 86.4 % over time period 0.5 s.

Fig. 4.19 Flowchart of EV discharging in control layer (DC bus) – Part 1/2
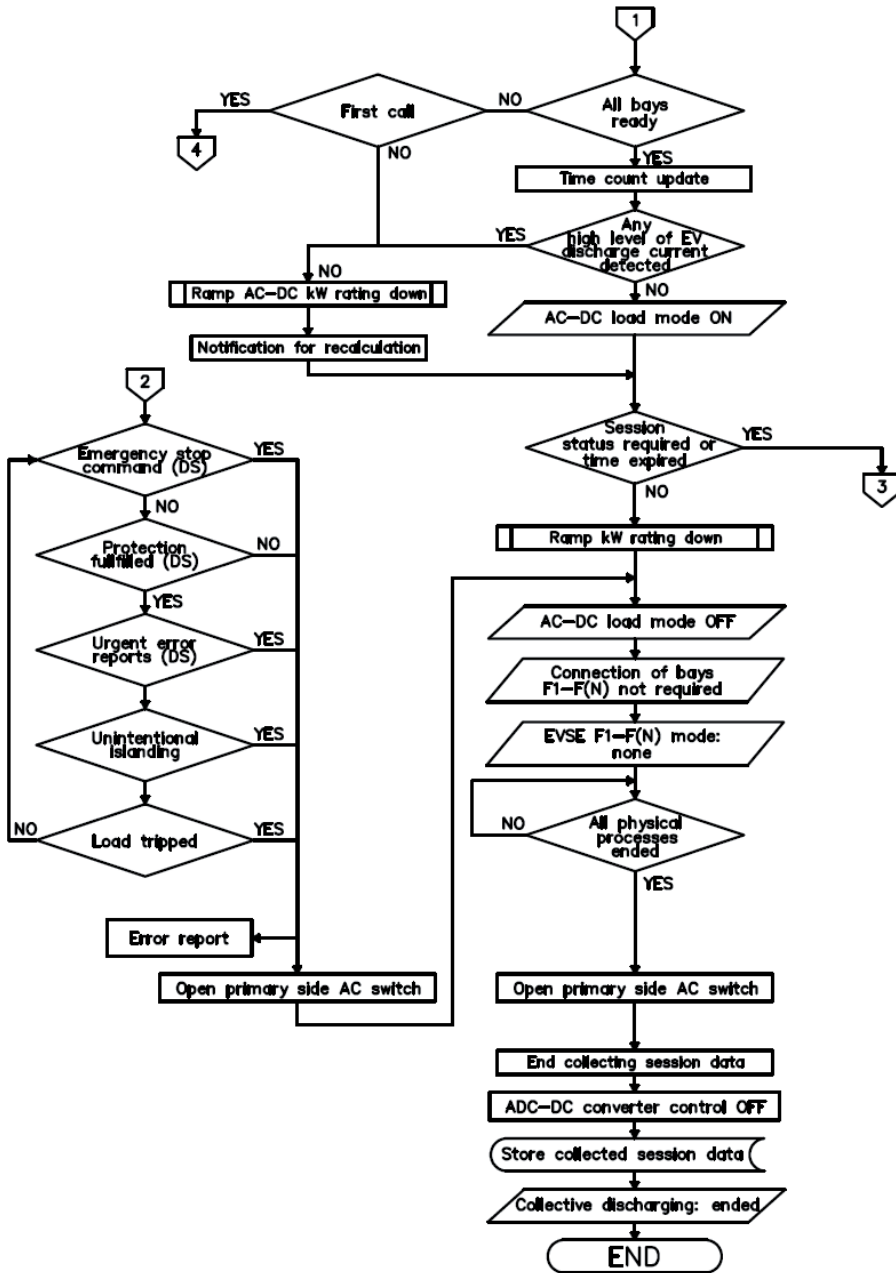
Fig. 4.19 Flowchart of EV discharging in control layer (DC bus) – Part 2/2
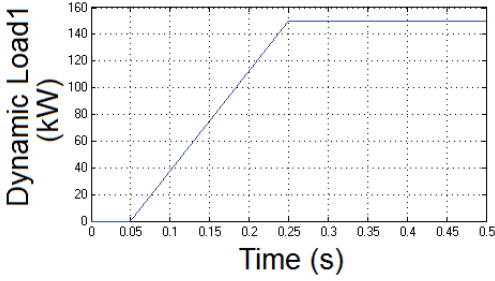
Fig. 4.20 Dynamic load 1 in the MATLAB Simulink model during discharging of EV bays to LV side
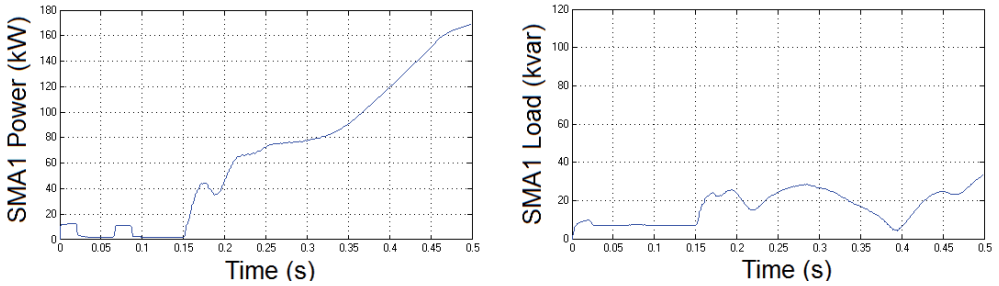
Fig. 4.21 Active and reactive power consumed by ACDCS1 recorded by the smart meter SMA1 in the MATLAB Simulink model during discharging of EV bays to MV side
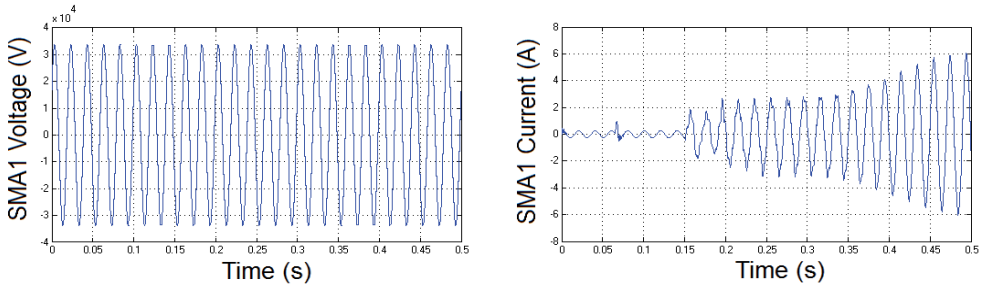
Fig. 4.22 Voltage and current of ACDCS1 at MV AC side recorded by the smart meter SMA1 in the MATLAB Simulink model during discharging of EV bays to MV side
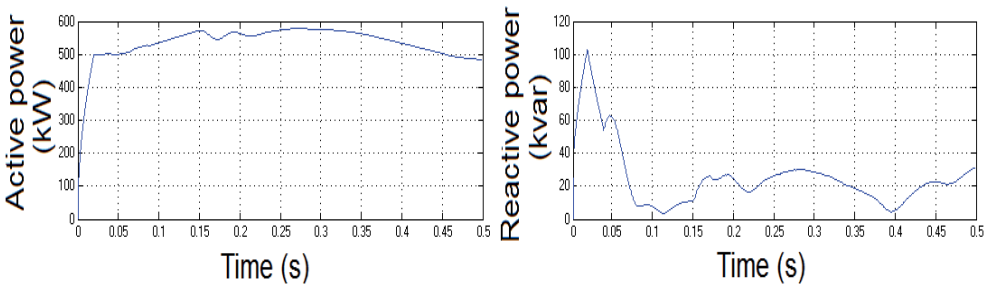
Fig. 4.23 Active and reactive power of the utility load at MV side 1 in the MATLAB Simulink model during discharging of EV bays to MV side

4.3.4 Control layer for BESU charging

Control layer executes the charging of BESU. BESU may include several parallel strings. Therefore the program for charging BESU can be viewed similar to the charging of EVs through the common DC bus. The program for bay (string) receives input data from data layer and controls the operation of the bidirectional DC-DC power converter. The program for AC-DC converter retceives input data from the PFTM and controls the operation of all bays (strings). In Table 4.9 are presented the input and output parameters for the bay and in the Table 4.10 are presented the input and output parameters for the management of AC-DC converter. Receive and Send columns describe the layers where data is received/sent and the destination of those layers.

  Differences between EV and BESU charging of Fig. 4.6 – 4.7 are described. The control of EVSE part is not required in the BESU algorithm. BESU charging requires additional algorithms for waking BMS up from sleep mode and setting the BESU into charge mode (in EV charging this was done by EVSE). The control of BESU charging can be adjusted to the control parameters received from PFTM. This includes adjusting the charging current according to the AC bus consumption level (to avoid over consumption either connected to the EV side or consumers side), reverse energy flow from consumers side (e.g. from near by factory) or with the level of renewable generation in the utility network. As BESU is utilized for the internal use no penalties are issued internally. Figures 4.24 show the flowcharts regarding the operation of the bay for BESU charging. Figures 4.25 show the flowcharts regarding the operation of the AC-DC for BESU charging.

Table 4.9. Input and output parameters for BESU charging in control layer (bay)

Input	Receive	DT	Output	Send	DT
Process start/end	DL-CTL-ACDC	B	Process status	DL-CTL-ACDC	B
Battery OCV,SOC, SOH, Capacity	DL-BESU	D	BESU mode (ready/charge)	CPL-BESU	D
Final SOC (target)	DL-PFTM	I	kWh measurement	DL-BESU	F
Max. battery voltage	DL-BESU	I	kWh price	DL-BESU	F
Stop request	DL-STATION	B	kWh cost	DL-BESU	F
AC-DC output voltage	DL-ACDC	F	Current measurement	DL-BESU	F
DC-DC output parameters	CPL-DCDC	D	DC-DC input parameters	CPL-DCDC	D
Current measurement	CPL-DCDC	F	Closing of bay switches	CPL-SWP/ CPL-SWS	DO
Imax bay	DL-MPL	I	Error reports	DL	D

Table 4.9. Input and output parameters for BESU charging in control layer (bay) (continued)

Input	Receive	DT	Output	Send	DT
Target kW rating (charge)	DL-PFTM	F	Store data	DSTORAGE	D
AC bus consumption	DL-STATION	F			
kWh price	DL-PFTM	F			
kWh measurement	CPL-SM	F			
Protection status	DL-MPL	B			
Emergency stop	CPL-STATION	DI			

Table 4.10. Input and output parameters for BESU charging in control layer (AC-DC)

Input	Receive	DT	Output	Send	DT
Process start/end	DL-PFTM	B	Process status	DL-PFTM	B
Process status	DL-CTL-BAY(s)	B	Process start/end	DL-CTL-BAY(s)	B
Imax of all bays	DL-MPL	I	BESU (sleep mode)	CPL-BESU	DO
Bays to be connected	DL-CML	B	AC-DC input parameters	CPL-ACDC	D
AC-DC output parameters	CPL-ACDC	D	AC-DC output parameters	DL-ACDC	D
Protection status	DL-MPL	B	Closing of station switch	CPL-AC BUS	DO
Battery OCV	DL-BESU	F	Error reports	DL	D
Battery Temperature	DL-BESU	F	Store data	DSTORAGE	D
Emergency stop	CPL-STATION	DI			

According to the maximum currents of the bays the necessary kW rating for the AC-DC converter is calculated (how many parallel modules are required for the AC-DC converter). When all scheduled bays have reached their targets, operation of the AC-DC converter is stopped, primary side AC switch is opened and session data (e.g. events, charging currents, kWh consumption with prices, efficiency of charging) is stored to the data storage. For safety reasons, all capacitors in the AC-DC converter and DC-DC converters are discharged with the end of the charging session.

Fig. 4.24 Flowchart of BESU charging in control layer (bay) – Part 1/2

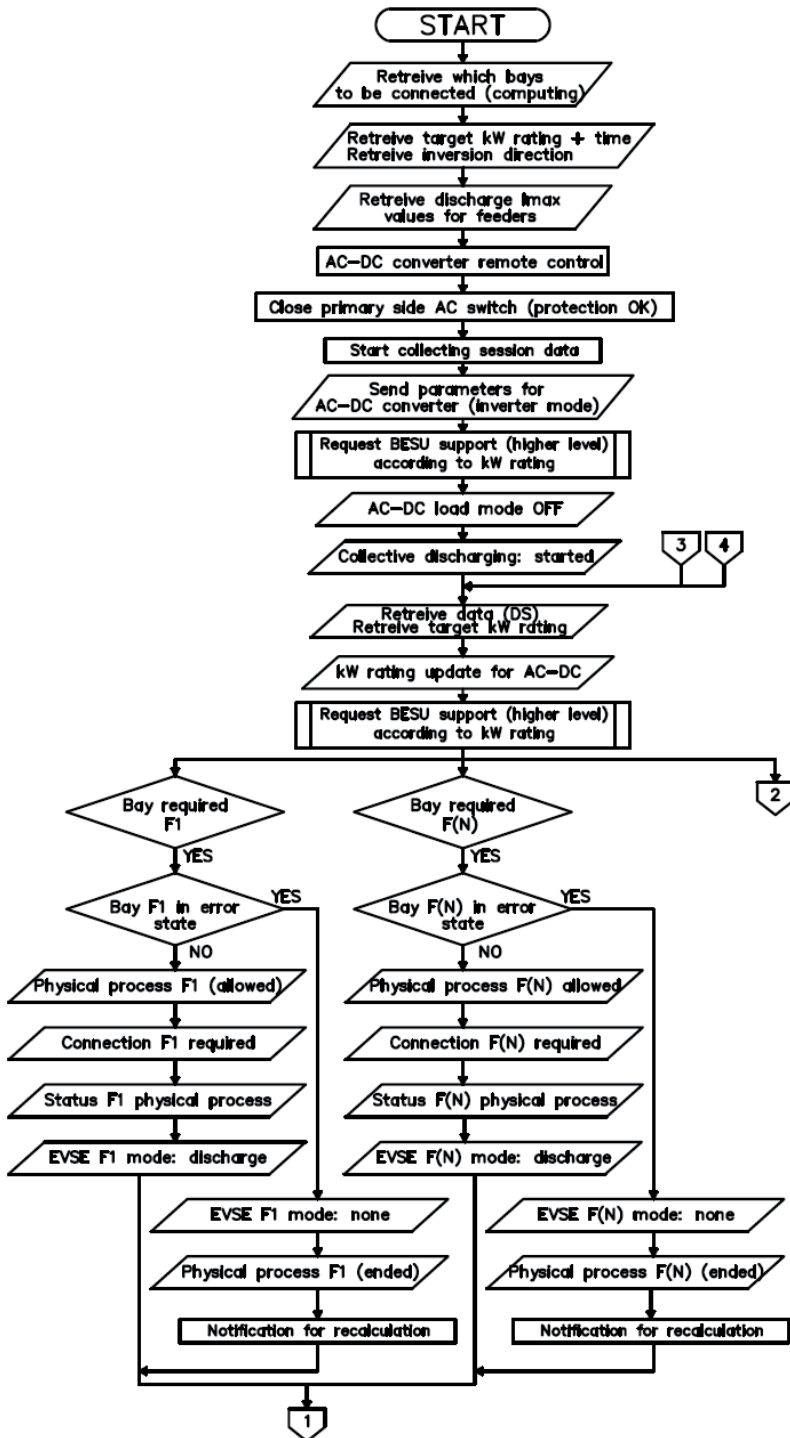*Fig. 4.24 Flowchart of BESU charging in control layer (bay) – Part 2/2*

Fig. 4.25 Flowchart of BESU charging in control layer (AC-DC) – Part 1/2

Fig. 4.25 Flowchart of BESU charging in control layer (AC-DC) – Part 2/2

4.3.5 Control layer for BESU discharging

Control layer executes the discharging of BESUs. The program for bay receives input data from data layer and controls the operation of the bidirectional DC-DC power converter of the BESU string. The target for the bidirectional DC-DC converter is to maintain stable output voltage for the internal BESU DC bus. Current of the bay is determined by the inversion active power target of the AC-DC converter. The program for the AC-DC converter receives input data from PFTM and controls the operation of bays and AC-DC converter. In Table 4.11 are presented the input and output parameters for the bay.

In the Table 4.12 are presented the input and output parameters for the management of the AC-DC converter. Receive and Send columns describe the layers where data is received/sent and the destination of those layers.

The operation principle of the bay of BESU string in BESU discharging is similar to the operation principle of the bay in the EV discharging. Differences between the EV and BESU discharging of Fig. 4.18 are described. The control of EVSE part is not required in the BESU discharge algorithm. EV data is replaced by

BESU data. DOD input does not come from EVSE but from computing layer. EV owner stop is replaced by distribution substation stop signal. BESU discharging requires additional algorithms for setting the BESU into discharge mode. As BESU is utilized for internal use no penalties are issued internally. Measurement data is not forwarded to EVSE, instead are forwarded to the data storage.

   Figure 4.26 shows the flowcharts regarding the operation of the AC-DC converter for BESU discharging. When the program is executed, BESU BMS is awaken from sleep mode and information is received from layers as described in the Table 4.12. The main input parameters for the program are the bays that have to be connected, kW rating of the AC-DC converter and inversion direction (EV or consumers side). Input parameters are forwarded to the AC-DC converter and primary side AC switch (before AC-DC converter) is closed according to the BESU support direction. AC-DC converter operation mode is initially blocked until its utilization is executed. Discharging programs of acquired bays (strings) are initiated, BESUs of those bays are set for discharging mode. Status of the bay programs are monitored during the AC-DC converter operation. When all bays (strings) are operational the BESU is ready to be utilized for support mode. If the target kW rating can not be matched due to fault in one of the bays (strings), error report is sent to the PFTM layer.

Table 4.11. Input and output parameters for BESU discharging in control layer (bay)

Input	Receive	DT	Output	Send	DT
Process start/end	DL-CTL-ACDC	B	Process status	DL-CTL-ACDC	B
Battery voltage	DL-BESU	F	BESU mode (discharge)	CPL-BESU	DO
DOD level	DL-PFTM	I	kWh measurement	DL-BESU	F
Initial SOC level	DL-BESU	F	kWh price	DL-BESU	F
Imax discharge BESU	DL-BESU	I	kWh cost	DL-BESU	F
Stop request	DL-STATION	B	Current measurement	DL-BESU	F
AC-DC output parameters	DL-ACDC	D	DC-DC input parameters	CPL-DCDC	D
DC-DC output parameters	CPL-DCDC	D	Closing of bay switches	CPL-SWP/ CPL-SWS	DO
Current measurement	CPL-DCDC	F	Error reports	DL	D
Imax bay	DL-MPL	I	Store data	DSTORAGE	D
kWh price (discharge)	DL-PFTM	F			
kWh measurement	CPL-SM	F			
Protection status	DL-MPL	B			
Emergency stop	CPL-STATION	DI			

Table 4.12. Input and output parameters for BESU discharging in control layer (AC-DC converter)

Input	Receive	DT	Output	Send	DT
Process start/end	DL-PFTM	B	Process status	DL-PFTM	B
Process status	DL-CTL-BAY(s)	B	Process start/end	DL-CTL-BAY(s)	B
Imax of all bays (discharge)	DL-MPL	I	BESU mode (sleep)	CPL-BESU	DO
Current of bays	DL-BESU	F	AC-DC input parameters	CPL-ACDC	D
Bays to be connected	DL-CML	B	AC-DC output parameters	DL-ACDC	D
ACDC input parameters (kW)	DL-PFTM	D	Closing of station switch	CPL-AC BUS	DO
LV side consumption (EVs or consumers)	DL-STATION	F	Error reports	DL	D
ACDC block mode (on/off)	DL_MPL	B	Recalculation	DL-CML	D
AC-DC output parameters	CPL-ACDC	D	Store data	DSTORAGE	D
Protection status	DL-MPL	B	Resynchronization completed	ENERGY ROUTING	B
Emergency stop	CPL-STATION	DI			
Operation mode and direction	DL-PFTM/ ENERGY ROUTING	B			
Load status	DL-AC BUS	F			

When EV support is required by PFTM EV support sequence is initiated. kW rating for the BESU is either pre-set or adjusted with active monitoring for peak shaving of utility network loads. BESU is set into inverter mode with phase lock loop (PLL) monitoring. Input parameters for the AC-DC converter are forwarded. When the operation of the sequence is ended, kW rating of the inversion is ramped down and operation of the AC-DC converter is blocked. BESU stays in support mode.

When consumer side consumption exceeds pre-set threshold monitoring sequence for the AC level consumption is initiated. kW rating for the BESU is adjusted with active monitoring for peak shaving of consumer loads.
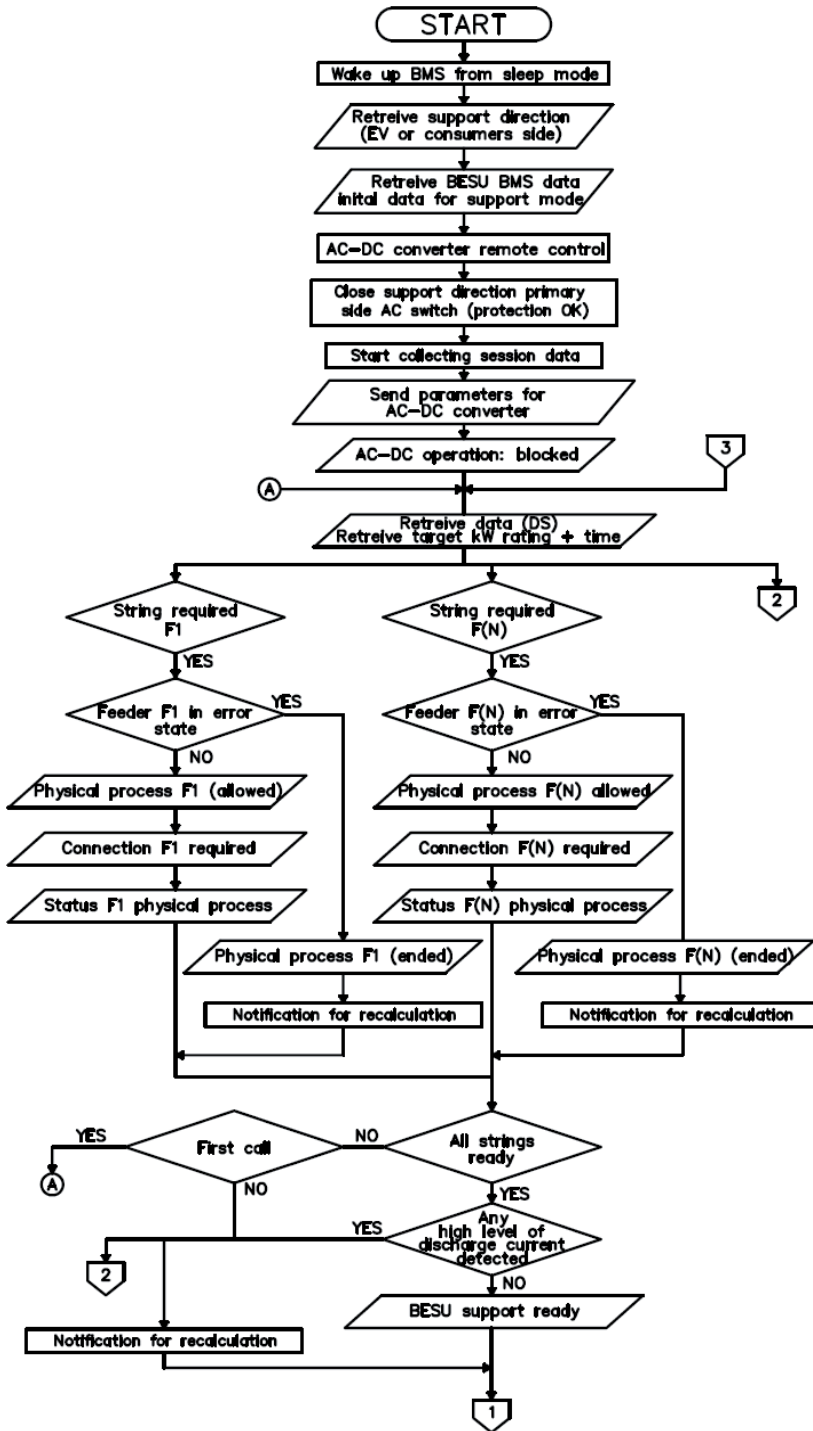
Fig. 4.26 Flowchart of BESU discharging in control layer (AC-DC) – Part 1/3
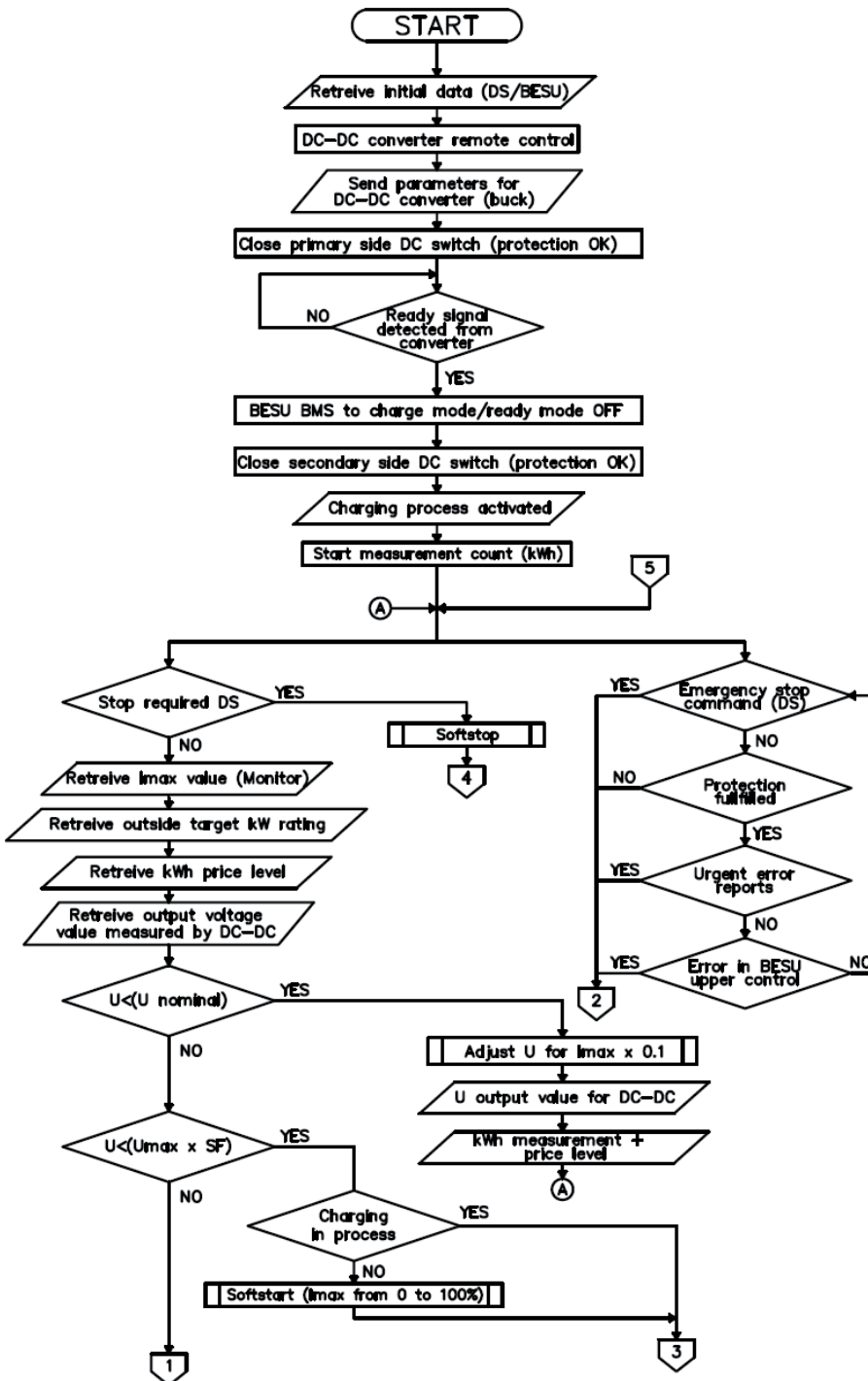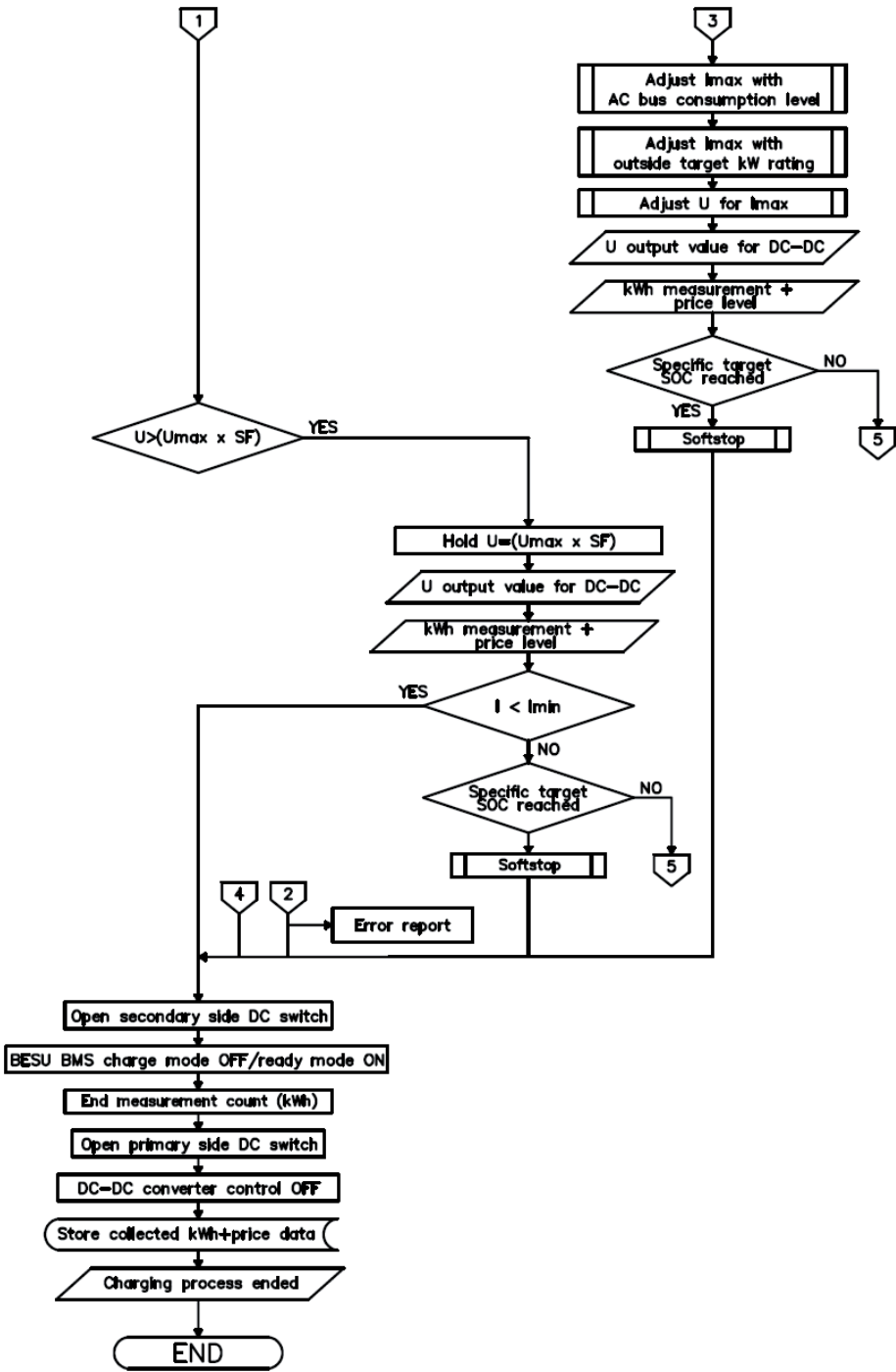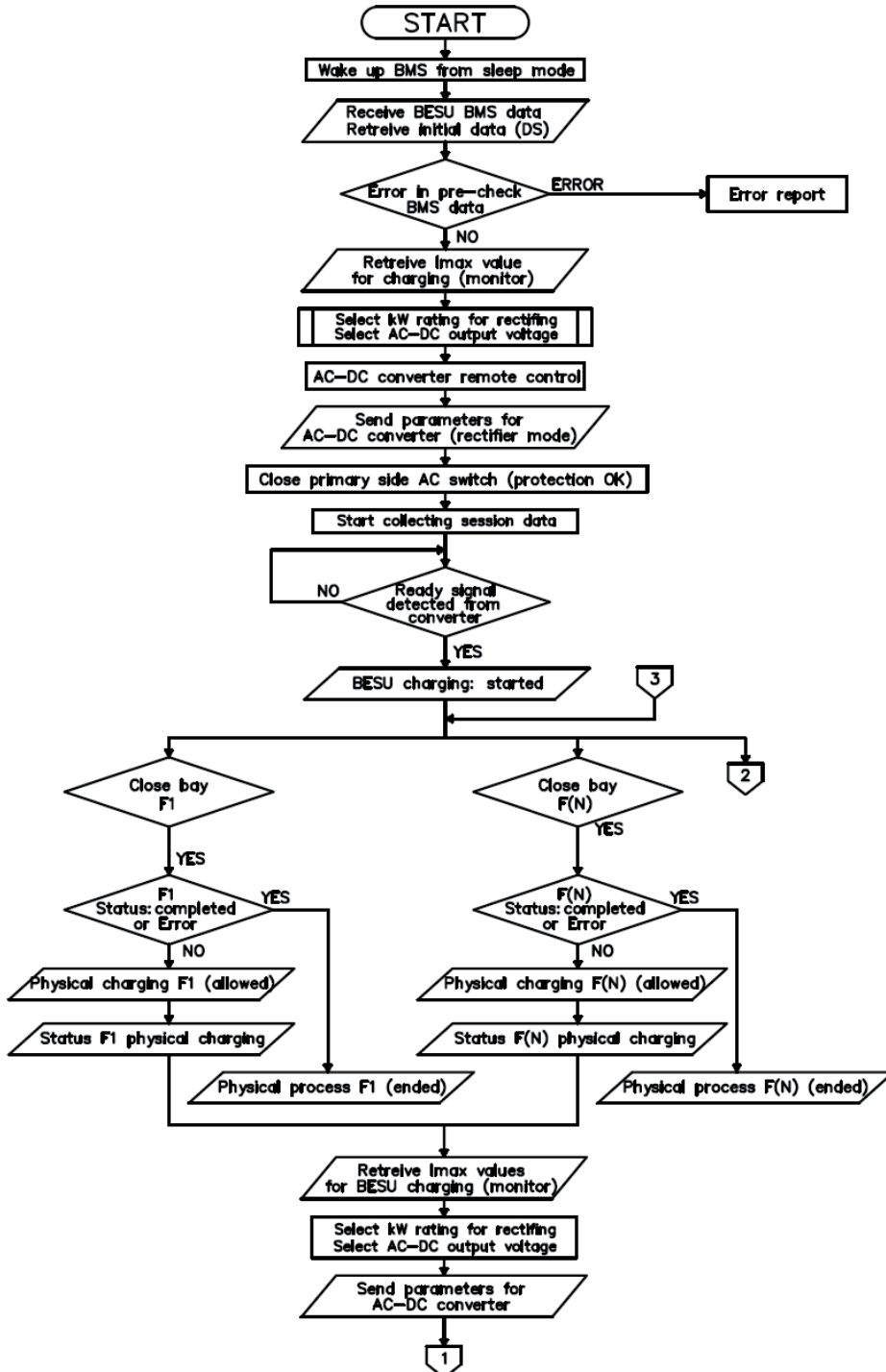
176
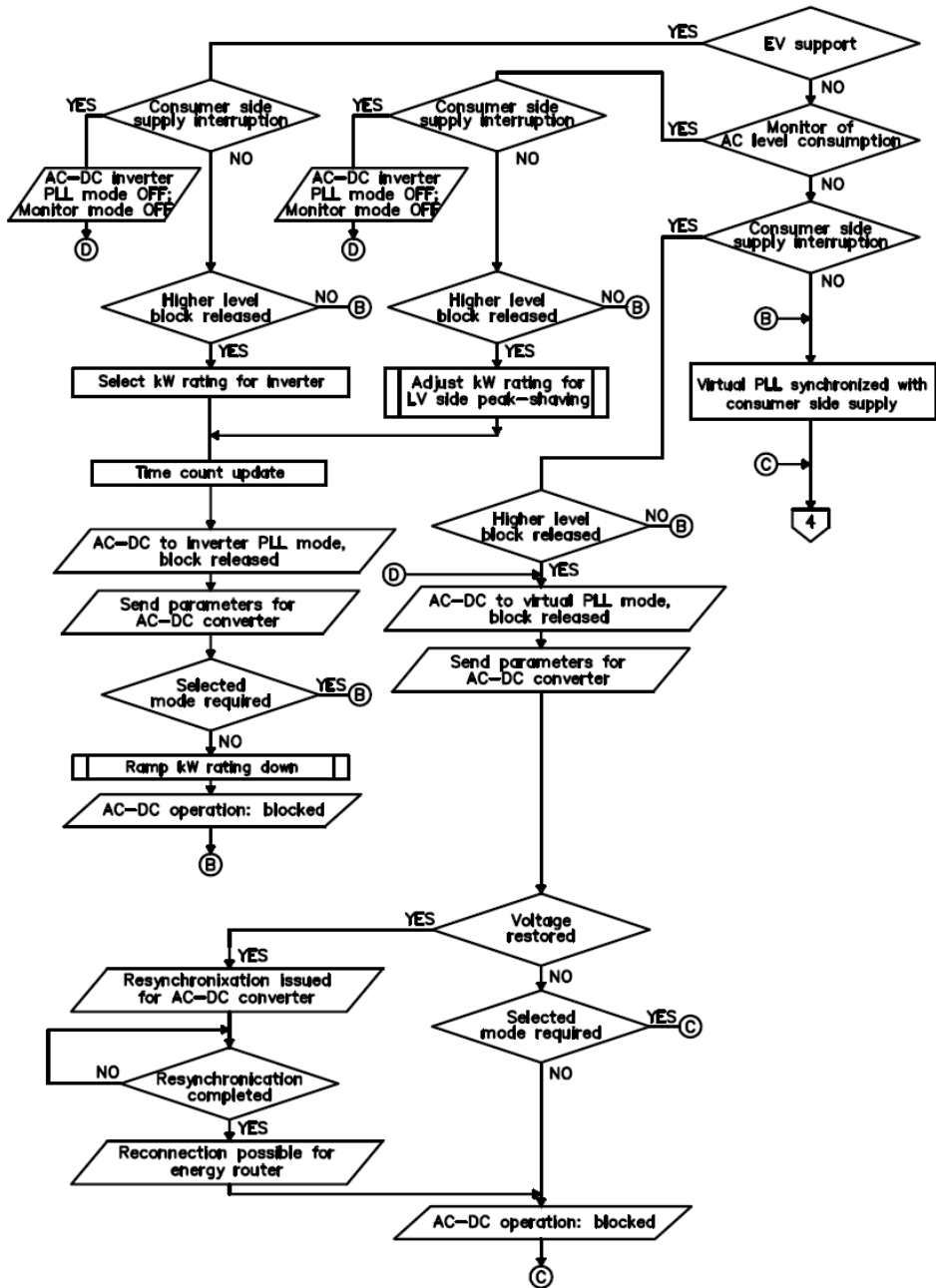
Fig. 4.26 Flowchart of BESU discharging in control layer (AC-DC) – Part 2/3

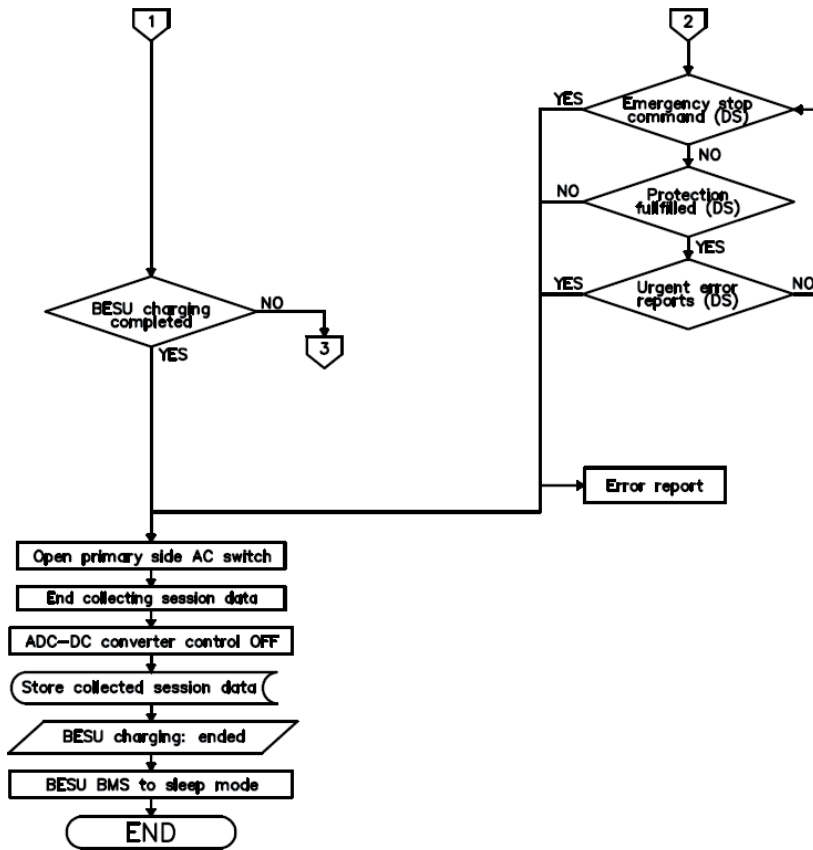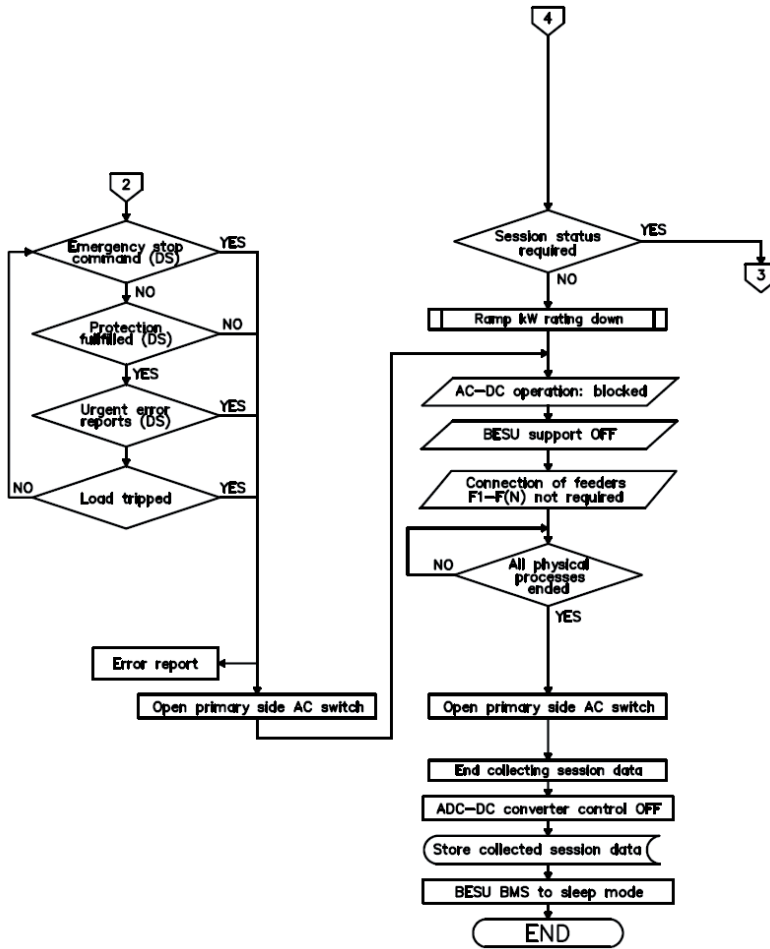*Fig. 4.26 Flowchart of BESU discharging in control layer (AC-DC) – Part 3/3*

When power outage is detected on the consumers side by energy routing layer the AC-DC converter is set into virtual PLL mode. Virtual PLL is always synchronized with the consumers side voltage. When the BESU is either in the EV support or in AC side consumption monitoring during power outage detection, exit gates are placed into the flowchart sequences to go to the virtual PLL mode. When the voltage is restored resynchronization is issued for the AC-DC converter. When phase shift of the converter operation is completed, energy routing can reconnect main supply for the consumers and disconnect the BESU from virtual PLL mode. BESU stays in support mode.

When BESU support session has expired, operation of the AC-DC converter is stopped, primary side AC switch is opened and session data (e.g. events, charging currents, kWh consumption with prices, efficiency of discharging) is stored to the data storage. For safety reasons, all capacitors in the AC-DC converter and DC-DC converters are discharged with the end of the discharging session.

Discharging of BESUs to the LV side for peak shaving of the utility network load during fast charging of EVs was simulated with MATLAB Simulink (Fig. 4.3) [141]. The second utility network supply was considered as unavailable and all the loads had fallen for the first utility network supply. Circuit breakers LVA, LVC and bus coupling breaker BC_LV were closed. Circuit breakers LVB and LVD were open. Examined substation was loaded with 100 kW of consumers (total of 500 kW for the utility network). All three EV charging stations were loaded simultaneously at 0.22 s (fast charging with 100 A and 36 kW). Energy stored in both BESUs were discharged to the common AC bus simultaneously at 0.1 s (target value of 50 kW for each BESU). The results from the simulated model are presented in Fig. 4.27 – 4.31. Fig. 4.27 illustrates the rms active power (e.g. 50.21 kW at 0.5 s) produced and rms reactive power (e.g. 2.4 kvar at 0.5 s) consumed by ACDC2 (cosφ≈0.99). Fig 4.28 illustrates voltage and current (e.g. peak current 137.5 A at 0.493 s) of ACDC2 at AC side. Fig. 4.29 illustrates voltage (e.g. 793.6 V DC at 0.5 s) and current (e.g. 63.75 A DC at 0.5 s) of ACDC2 at DC side. Fig. 4.30 illustrates state of charge (SOC), current (120 A at 0.5 s) and voltage (439 V at 0.5 s) of the BESU1. Fig. 4.31 illustrates rms active power (e.g. 514.6 kW at 0.5 s) and rms reactive power (5.62 kvar at 0.5 s) of the utility load at MV side 1. The maximum load for the utility was not exceeded. The discharging of BESUs in parallel with fast charging of EVs reduces load for the utility network. $THD_{I\_UT1}<0.1$ % and $THD_{I\_SMA2}<0.3$ % at continuous operation of ACDCS1.
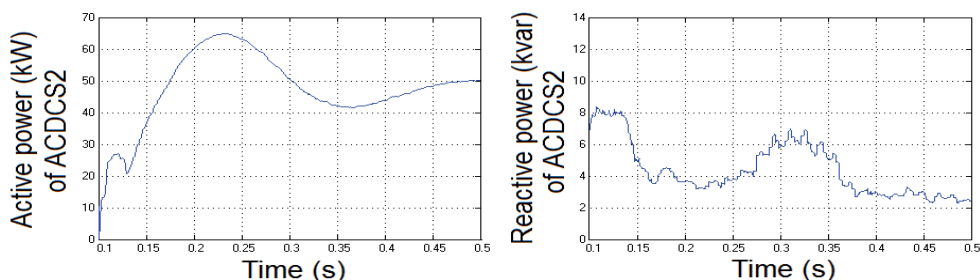
Fig. 4.27 Active and reactive power consumed by ACDCS2 in the MATLAB Simulink model during discharging of BESUs to LV side for support of EV fast charging
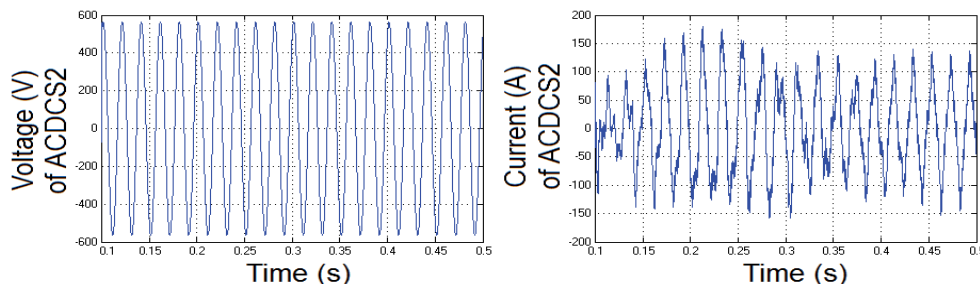
Fig. 4.28 Voltage and current of ACDCS2 at LV AC side in the MATLAB Simulink model during discharging of BESUs to LV side for support of EV fast charging
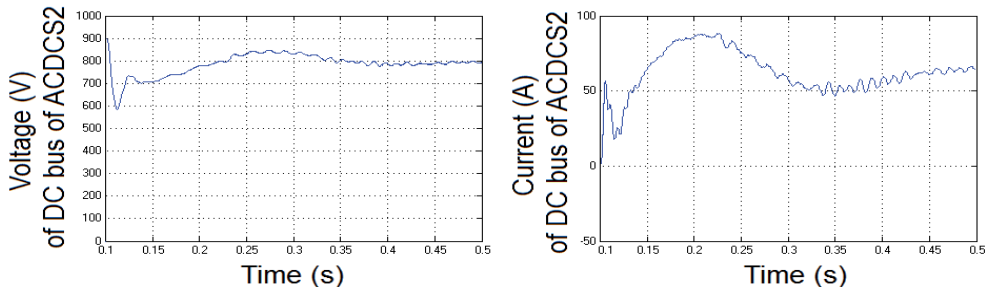
Fig. 4.29 Voltage and current of ACDCS2 at DC side in the MATLAB Simulink model during discharging of BESUs to LV side for support of EV fast charging
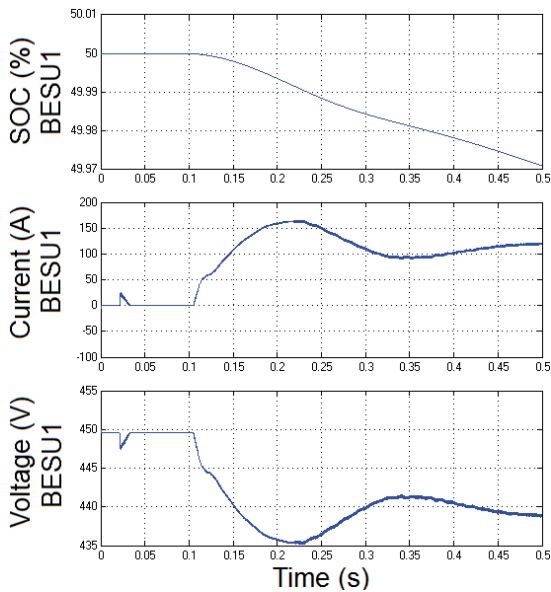
Fig. 4.30 SOC, current and voltage of the BESU1 in the MATLAB Simulink model during discharging of BESUs to LV side for support of EV fast charging
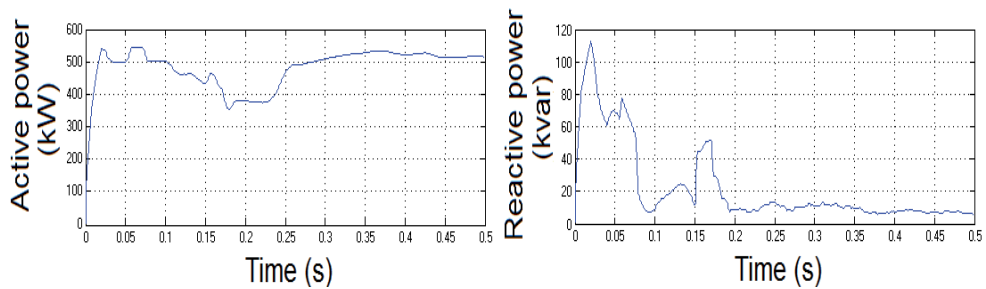
Fig. 4.31 Active and reactive power of the utility load at MV side 1 in the MATLAB Simulink model during discharging of BESUs to LV side for support of EV fast charging

4.3.6 Voltage mitigation and reactive power compensation

Control layer executes the utilization of the common DC bus for voltage mitigation and reactive power compensation for the support of the AC side consumers. The program for the AC-DC converter receives input data from the PFTM layer and the data layer. The program controls the operation of the bays and the AC-DC converter. Only capacitors of the primary side of the DC-DC converter are utilized. The operation does not influence the electric vehicles as the secondary side switches of the DC-DC converters are opened. In Table 4.13 are presented the input and output parameters for the control program of the AC-DC converter. Figure 4.32 shows the flowcharts regarding the operation of the AC-DC converter for voltage mitigation and reactive power compensation. When the AC-DC is operational, AC-DC converter monitors AC bus and initiates mode selection according to detected measurements.

Voltage mitigation was simulated with MATLAB Simulink (Fig. 4.3). AC consumers are supplied through second utility network supply. Circuit breakers LVB and bus coupling breaker BC_LV were closed. Circuit breakers LVA, LVC and LVD were open. Examined substation was loaded with 100 kW of consumers (total of 500 kW for the utility network). AC-DC converter was set to voltage mitigation mode with the start of the simulation. Voltage level at the DC side was increased to 900 V. The results from the simulated model are presented in Fig. 4.33 – 4.36. Fig. 4.33 illustrates the voltage levels of the utility in the MV side and consumers in the LV side. Voltages are presented per unit (divided by nominal values). Voltage at MV side is 1.005 PU at the beginning and at the end of the simulation. At time 0.17 s voltage level in the MV side rises to 1.096 PU and at time 0.23 s drops to 0.977 PU. AC-DC converter improves the voltage level close to nominal value. Transmission changes the voltage levels at LV side to 1.02 PU and 0.973 PU respectively for short term. Fig 4.34 illustrates instantaneous active and reactive power measurements during voltage mitigation. When the voltage level is higher reactive power is consumed by the ACDC1 to improve the voltage level at the LV consumers side (153 kvar at 0.2 s). When the voltage level is lower reactive power is produced (-73.5 kvar at 0.25 s) by ACDC1 to improve the voltage level at the consumers side. Fig. 4.35 illustrates voltage and current (e.g. peak current 365.3 A at 0.197 s, 108 A at 0.28 s, 23.3 A at 0.4996 s) of ACDC1 at AC side. Fig. 4.36 illustrates voltage (e.g. 943 V DC at 0.197 s, 866 V at 0.28 s) and current (e.g. between -4 A to +6 A at 0.495 s to 0.5 s, between -60 A and 60 A at 0.198 s to 0.202 s) of ACDC1 at DC side. The voltage mitigation mode keeps the consumer side voltage close to nominal voltage.

Reactive power compensation was simulated with MATLAB Simulink. The simulation is based on the same principle as voltage mitigation simulation, with the difference that AC-DC converter is set to the reactive power compensation mode. The results from the simulated model are presented in Fig. 4.37 – 4.40. Consumers side includes 25 kvar load at 0.15 s. With the compensation mode the reactive power consumption is suppressed close to zero.
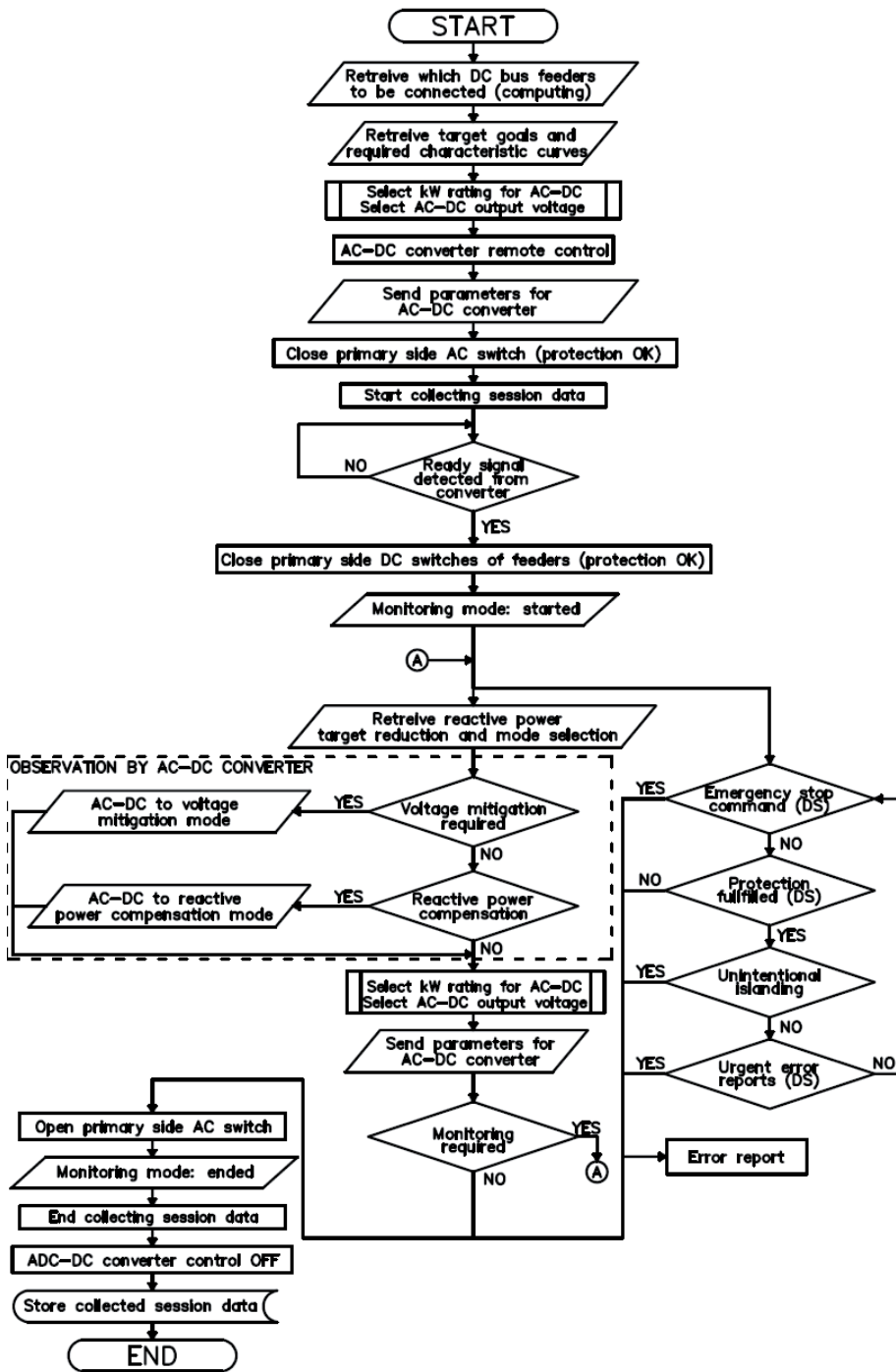
Fig. 4.32 Flowchart of voltage mitigation and reactive power compensation in control layer (AC-DC)
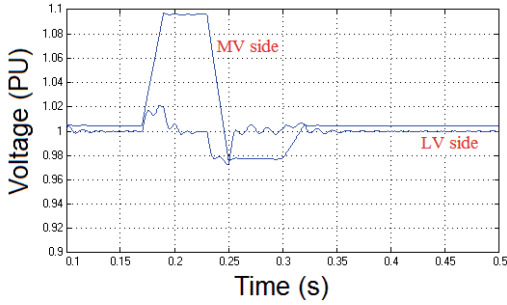
Fig. 4.33 Voltage levels (per unit) at MV side and LV side in the MATLAB Simulink model during voltage mitigation
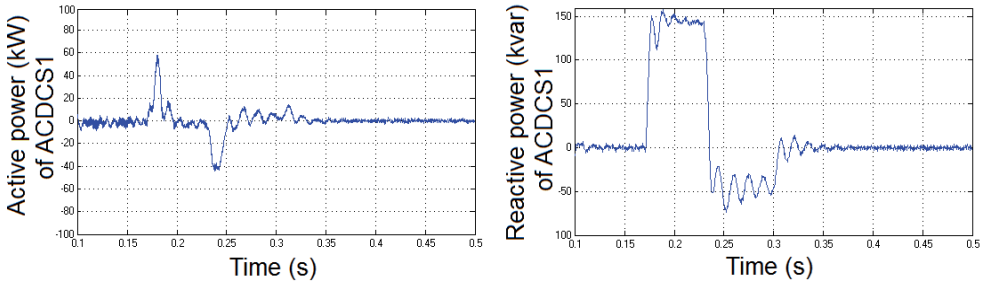
Fig. 4.34 Instantaneous active and reactive power measurements by ACDCS1 in the MATLAB Simulink model during voltage mitigation
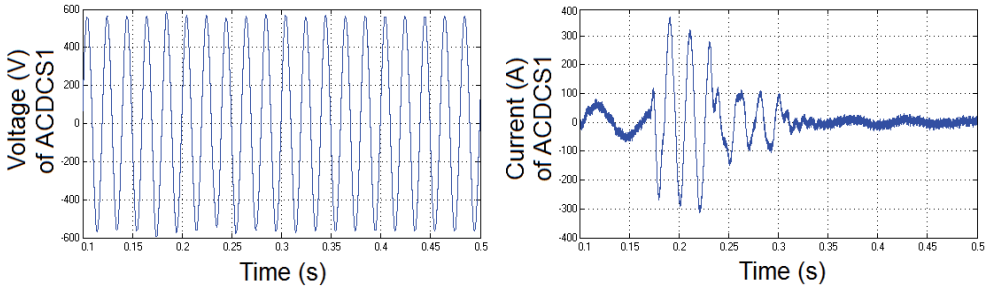
Fig. 4.35 Voltage and current of ACDCS1 at AC side in the MATLAB Simulink model during voltage mitigation
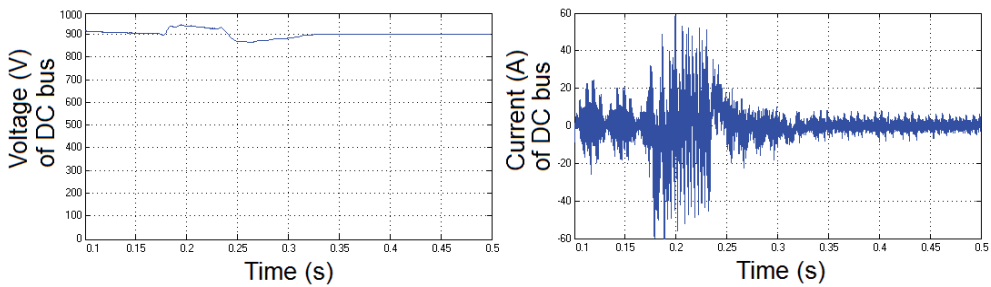
Fig. 4.36 Voltage and current of ACDCS1 at DC side in the MATLAB Simulink model during voltage mitigation
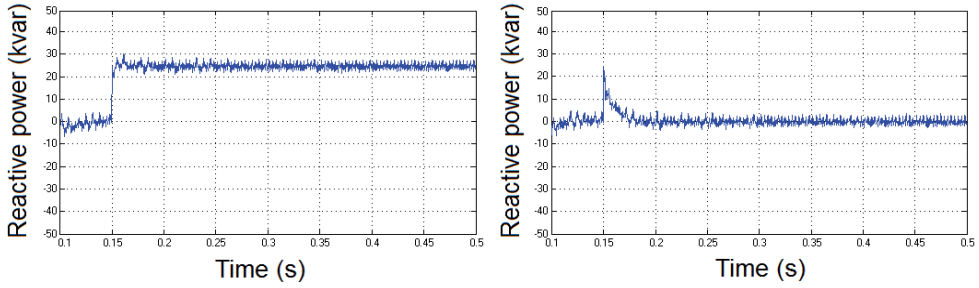
Fig. 4.37 Instantaneous reactive power measurements by smart meter SMB2 in the MATLAB Simulink model: without reactive power compensation (left) and with reactive power compensation (right)
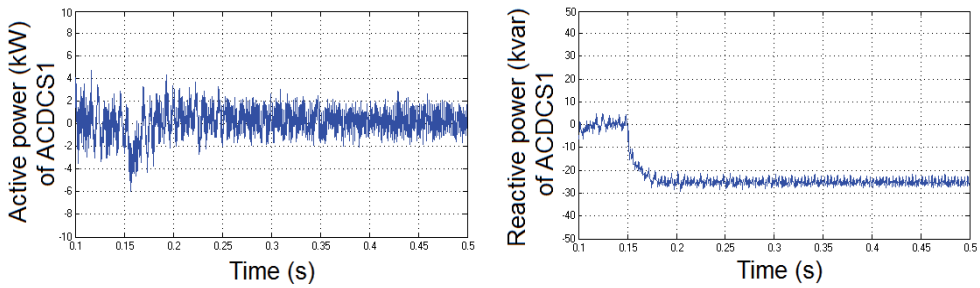
Fig. 4.38 Instantaneous active and reactive power measurements by ACDC1 in the MATLAB Simulink model during reactive power compensation

Fig. 4.39 Voltage and current of ACDCS1 at AC side in the MATLAB Simulink model during reactive power compensation
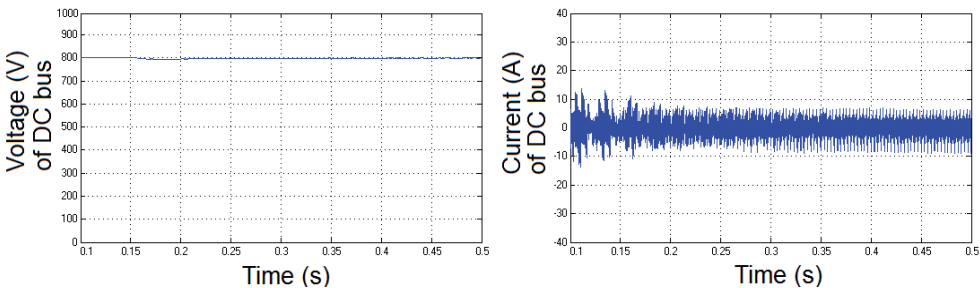
Fig. 4.40 Voltage and current of ACDCS1 at DC side in the MATLAB Simulink model during reactive power compensation

Table 4.13. Input and output parameters for reactive power compensation in control layer (bay)

Input	Receive	DT	Output	Send	DT
Process start/end	DL-PFTM	B	Process status	DL-PFTM	B
Reactive power consumption at consumers side	DL-STATION	F	BESU mode (discharge)	CPL-BESU	DO
Bays to be connected	DL-CML	B	kvar measurement	DL-STATION	F
AC-DC output parameters	DL-ACDC	D	kvar price	DL-STATION	F
Imax bay	DL-MPL	I	kvar cost	DL-STATION	F
kvar price (discharge)	DL-PFTM	F	AC-DC input parameters	CPL-ACDC	D
kvar measurement	CPL-SM	F	Closing of bay switches	CPL-SWP	DO
Target goals and characteristics	DL-PFTM	D	Error reports	DL	D
Threshold values	DL-PFTM	D	Store data	DSTORAGE	D
Protection status	DL-MPL	B			
Emergency stop	CPL-STATION	DI			

4.4 Layers of protection algorithm

4.4.1 Monitor and protection layer for EV bay and AC-DC converter

General protection functions and target control values are realized through MPL layer. Monitor and protection layer (MPL) of the EV bay monitors the status of the bay and forwards the target values for the control layer of the bay. In Table 4.14 are presented the input and output parameters for the MPL layer of bay. The main inputs for the MPL are the parameters from EVSE, station parameters (positions of circuit breakers and contactors, security breach), target parameters from PFTM and bidirectional DC-DC output parameters.

Fig. 4.41 shows the flowchart regarding the operation of the MPL layer of bay. MPL layer of bay is activated with the request by EVSE. MPL layer of bay detects the position of the isolation monitor and writes response to the data layer for forwarding to EVSE, whether EVSE is connected with distribution substation.

MPL layer compares constantly BMS transmitted temperature and voltage with minimum and maximum values. BMS error codes are analysed for stopping the operation of the bay. Fig. 4.42 shows the flowchart regarding the calculation of the maximum charging current for the bay. Maximum current of the bay is determined

constantly by the maximum current of the installation (cables, protection and control devices), maximum charging current determined by the BMS, current ordered by EV, reduction request by the utility network, temperature measured by the BMS and the bidirectional DC-DC converter. Input of maximum current is given by computing layer or if not calculated by the bay itself. Energy routing layer may also reduce the bay current in the case of power outage detection. If one of those parameters are exceeded the MPL layer of the bay reduces the maximum current for the control layer of bay. If error is detected, MPL layer of bay forces the stop of the control layer of the bay. Error report is sent to the computing layer and to the operator of the distribution substation (if required). Fig. 4.43 shows the flowchart regarding the calculation of the maximum discharging current for the bay. As an option, the adjustment of maximum charging current can be used for frequency regulation in the utility network.

MPL layer of bay determines from station inputs constantly, whether the protection criteria for the bay are matched regarding the station level.

Table 4.14. Input and output parameters for EV bay in MPL layer

Input	Receive	DT	Output	Send	DT
Process start/end	DL-EVSE	B	Protection status	DL-MPL	B
Operation of bay	DL-CTL	B	Imax bay	DL-MPL	I
Bay current direction	DL-PFTM	I	Connected	DL-EVSE	B
EVSE connection required	DL-CML	B			
Target input data	DL-PFTM	D			
EVSE data	DL-EVSE	D			
DC-DC converter data	DL-DCDC	D			
Station level protection	DL-MPL/ DL-STATION	D			
Emergency stop	CPL-STATION	DI			

Fig. 4.44 shows the flowchart of MPL layer for the protection and control of the AC-DC converter during EV charging/discharging. Program is started by PFTM layer. Program monitors station parameters (e.g. protection status of smart meters in AC bus) and input data from the PFTM layer. In addition, the program controls the discharging of BESUs (ready in support mode) when AC-DC converter can not achieve target goals in the inversion mode. When utility requests utilization of renewable energy generation the MPL reduces the kW rating for the AC-DC converter in the inverter mode. In case of power outage the MPL layer is responsible for safe release and blocking the operation of the AC-DC converter.

Charging current reduction by the MPL layer was simulated with MATLAB Simulink (Fig. 4.3). The set-up of the simulation was the same as for the EV

charging without any peak shaving by BESUs. Request by the utility network to reduce consumption by 30 % was ordered at 0.35 s and released at 0.45 s. The results from the simulated model are presented in Fig. 4.45 – 4.46. Fig. 4.45 illustrates the current and voltage of EV1. The reduction was completed in 0.04 s and restored in 0.06 s. Fig. 4.46 illustrates the active and reactive power consumed by ACDC1.
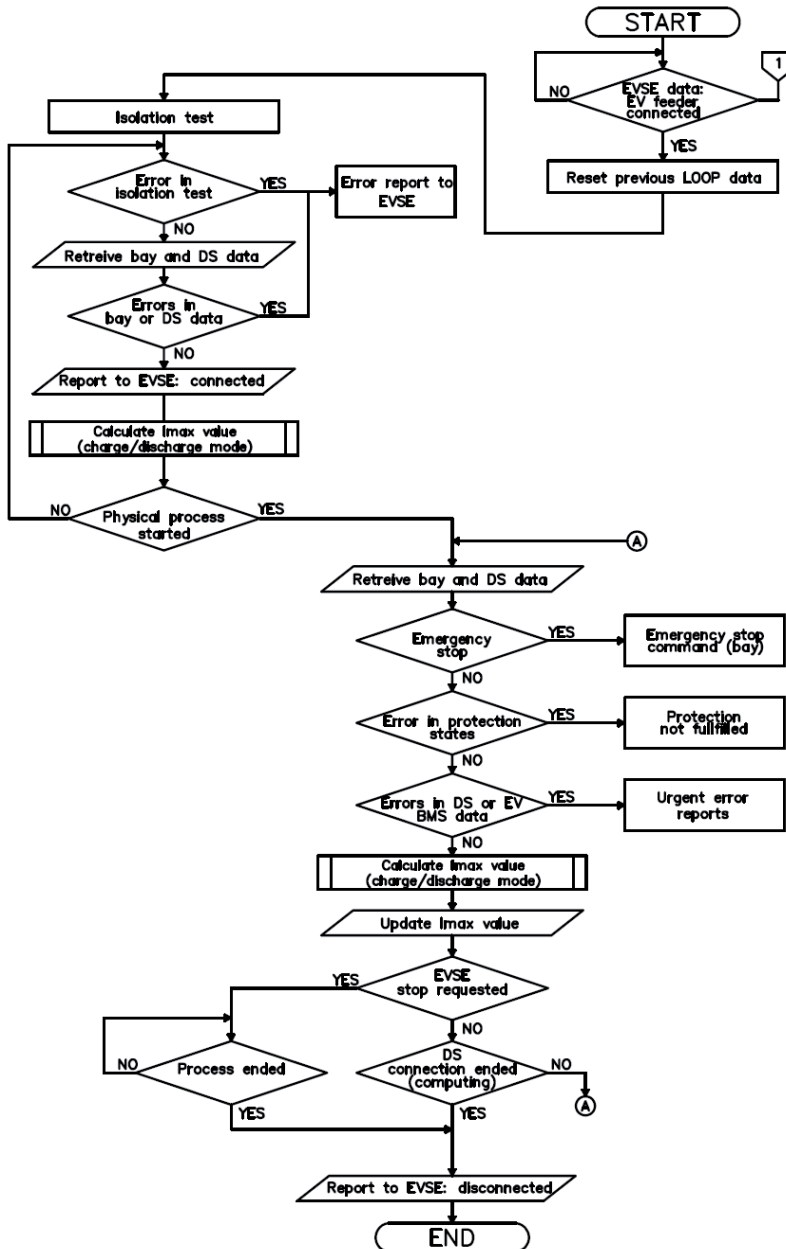
Fig. 4.41 Flowchart of monitor and protection layer for EV bay

START

A

Physical process started — YES

NO

CALCULATED INPUT

Imax = installation Imax

Imax = BMS Imax ← BIGGER — Imax compared to BMS data

SMALLER

Imax = Calculated ← Calculated Smaller than previous — Imax compared to calculation

Not calculated

$Imax_{INIT} = Imax$

Retreive EV BMS Imax ordered

$Imax = Imax_{EV}$ ← BIGGER — $Imax_{INIT}$ compared to EV order

SMALLER

$Imax = Imax_{INIT}$

$Imax_{DSO} = Imax_{TEMP} = Imax_{DS} = Imax$

$Imax_{DSO} = Imax_{DSO} - \Delta_{DSO}$ ← BIGGER — DSO restrictions compared — SMALLER → $Imax_{DSO} = Imax_{DSO} + \Delta_{DSO}$ $max(Imax_{DSO}) = Imax$

MATCH

$Imax_{TEMP} = Imax_{TEMP} - \Delta_{TEMP}$ ← BIGGER — BMS temp. restrictions compared — SMALLER → $Imax_{TEMP} = Imax_{TEMP} + \Delta_{TEMP}$ $max(Imax_{TEMP}) = Imax$

MATCH

$Imax_{DS} = Imax_{DS} - \Delta_{DS}$ ← BIGGER — DS level or devices restrictions compared — SMALLER → $Imax_{DS} = Imax_{DS} + \Delta_{DS}$ $max(Imax_{DS}) = Imax$

MATCH

$Imax = min(Imax_{DSO} = Imax_{TEMP} = Imax_{DS})$
$max(Imax) = Imax_{INIT}$

Imax monitoring required — YES → A

NO

END

Fig. 4.42 Flowchart of maximum charging current calculation for EV bay

START

A

Physical process started — YES

NO

Imax = installation Imax

Imax = BMS Imax — BIGGER — Imax compared to BMS data

SMALLER

$Imax_{INIT}$ = Imax

Retreive EV V2G support data

Imax = $Imax_{EV}$ — BIGGER — $Imax_{INIT}$ compared to EV max

SMALLER

Imax=$Imax_{INIT}$

$Imax_{TEMP}$=$Imax_{DS}$=Imax

$Imax_{TEMP}$= $Imax_{TEMP}$ −Δ_{TEMP} — BIGGER — BMS temp. restrictions compared — SMALLER — $Imax_{TEMP}$= $Imax_{TEMP}$ +Δ_{TEMP} max($Imax_{TEMP}$)= Imax

MATCH

$Imax_{DS}$ = $Imax_{DS}$ −Δ_{DS} — BIGGER — DS devices restrictions compared — SMALLER — $Imax_{DS}$ = $Imax_{DS}$ +Δ_{DS} max($Imax_{DS}$)= Imax

MATCH

Imax=min($Imax_{TEMP}$ =$Imax_{DS}$) max(Imax)= $Imax_{INIT}$

Imax monitoring required — YES — A

NO

END

Fig. 4.43 Flowchart of maximum discharging current calculation for EV bay

189
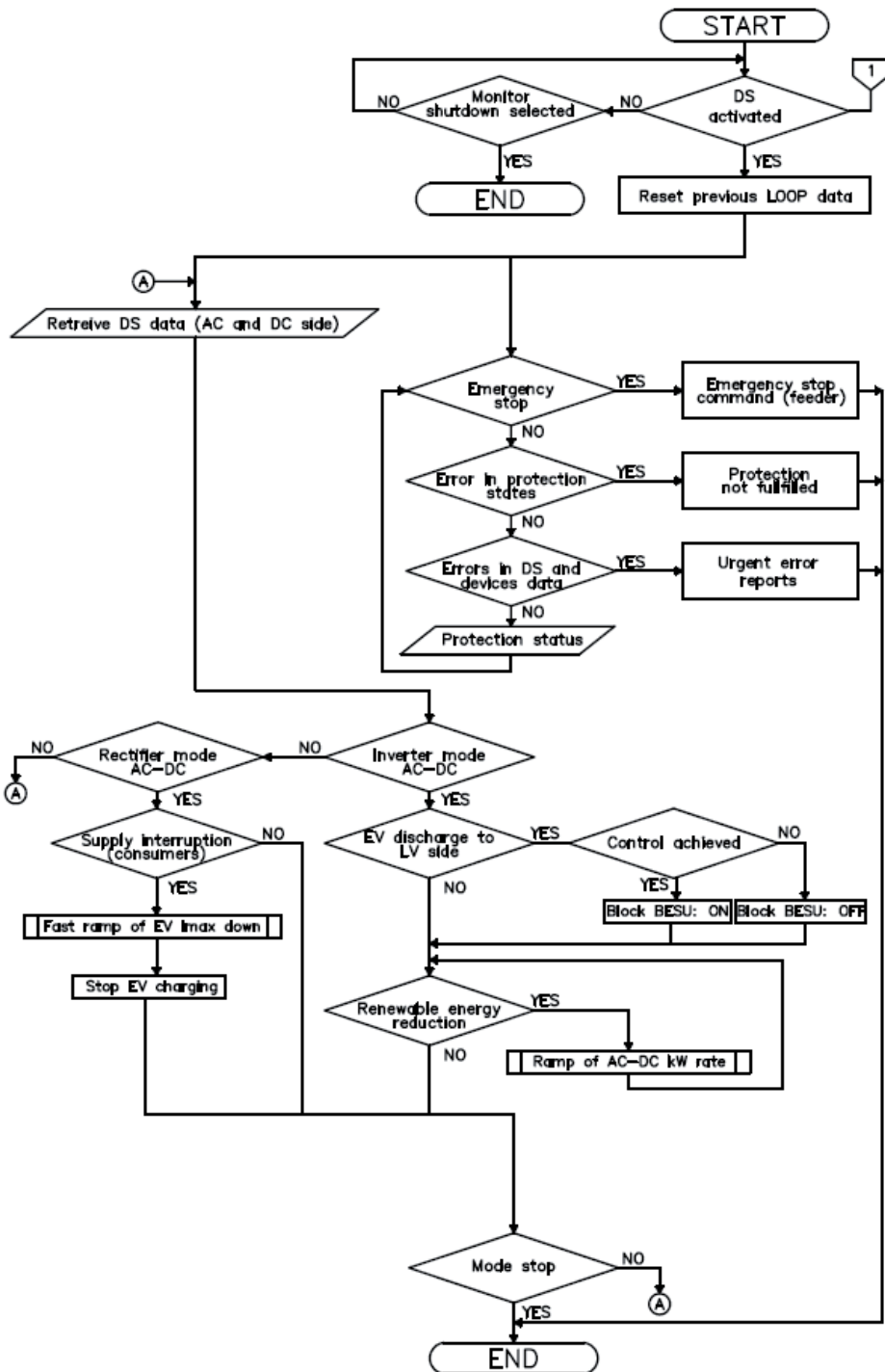
Fig. 4.44 Flowchart of monitor and protection layer for EV charging/discharging (AC-DC)
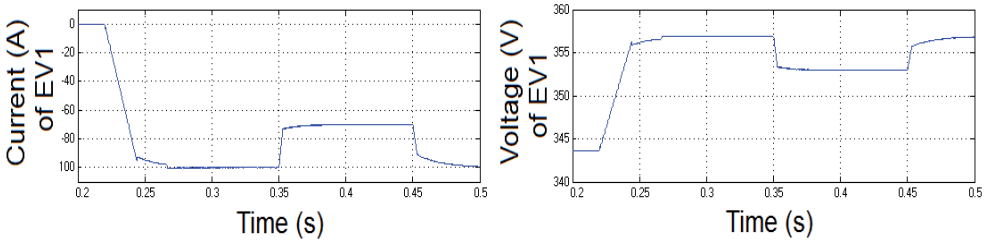
Fig. 4.45 Current and voltage of EV in the MATLAB Simulink model with charging current reduction by MPL layer
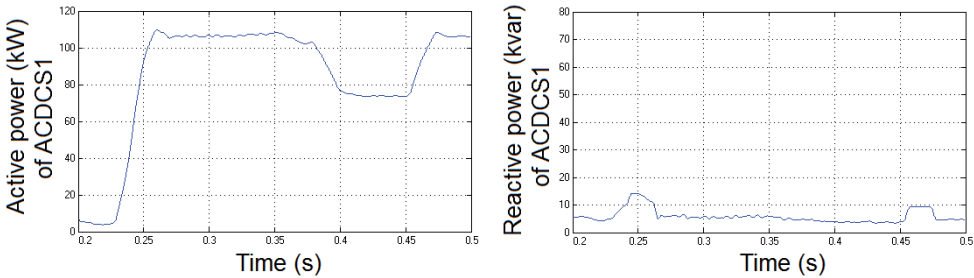
Fig. 4.46 Active and reactive power measurements by ACDC1 in the MATLAB Simulink model with charging current reduction by MPL layer

4.4.2 Monitor and protection layer for BESU bay and AC-DC converter

Monitor and protection layer (MPL) of the BESU bay monitors the status of the bay (string). Monitor and protection layer (MPL) of the BESU AC-DC converter monitors the status of the AC-DC converter during BESU charging/discharging. The operation of the MPL of BESU bay is similar to the MPL of EV bay. The main differences include changing of EV data with BMS data, operation of EVSE is not required. Fig. 4.47 shows the flowchart of MPL layer for the protection and control of the AC-DC converter during BESU charging/discharging. The control of AC-DC converter includes monitoring of consumers consumption to release the block signal in the inversion mode of the AC-DC converter. Additional block is set to BESU if EVs are used for peak shaving of consumer side loads.

Maintaining BESUs in LV side consumption monitoring, requires keeping the BESU operational also when the LV side consumption is lower from threshold value. Operating BESU in standby derates BESU batteries for some extent. The operation of DC-DC converters is to consume energy to maintain the target output voltage on its output terminals for common DC bus (maintaining voltage level at output capacitor). When the DC-DC power converter operates in standby the IGBT switches are turned off if voltage level has been exceeded. In the model it was calculated that the operation of BESU in standby discharges 40 Ah batteries of DOD=1.1 % in 1 hour.
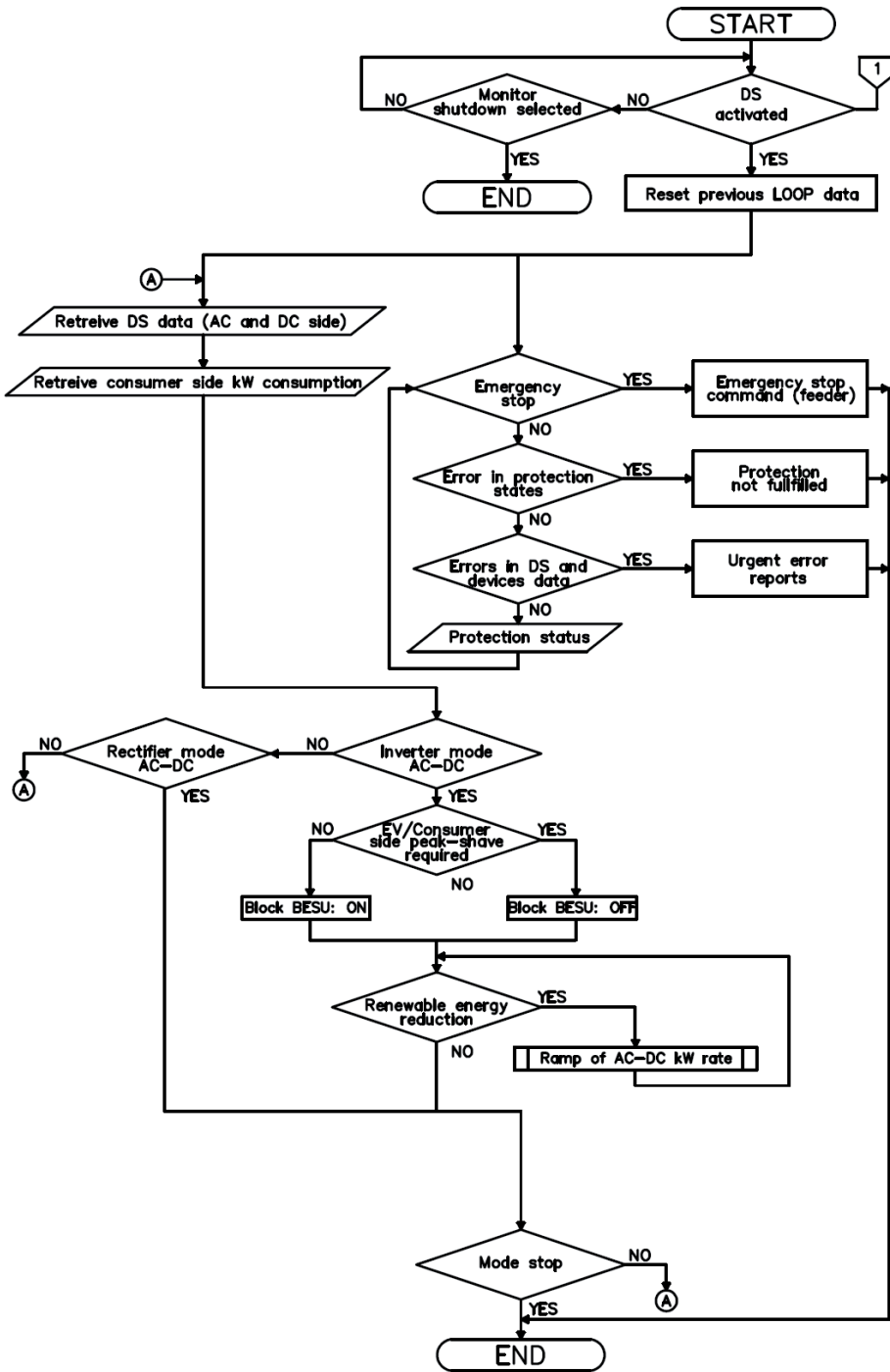
Fig. 4.47 Flowchart of monitor and protection layer for BESU charging/discharging (AC-DC)

4.5 Computing layer and data storage

Function of the computing layer (CML) is to retrieve the data, process the data and based on process results send and distribute data to other layers at the right time. In Table 4.15 are presented the input and output parameters for the computing layer apart from the PFTM layer. In Table 4.16 are presented the input and output parameters for the computing layer regarding PFTM layer. Fig. 4.48 shows the flowchart of computing layer.

Table 4.15. Input and output parameters for computing layer apart from PFTM layer

Input	Receive	DT	Output	Send	DT
Connected bays	DL-MPL	D	Bays to be connected	DL-CTL	D
EV and EV owner data	DL-EVSE	D	Scheduled times	DL-EVSE	D
EV in slow charge mode	DL-EVSE	D	Release EV connection	DL-MPL	D
Errors	DL-EVSE/ DL-BESU/ DL-STATION	D	Error reports to EVSE	DL-EVSE	D
Notification for rescheduling	DL-CTL	D	Imax bays	DL-MPL	D
BESU data	DL-BESU	D	BESU data retrieval (sleep mode)	DL-BESU	B
Power outage	ENERGY ROUTING	B	Target BESU SOC/DOD	DL-BESU	D
BESU utilized	ENERGY ROUTING	B			
Maintenance modes for parts of station	DL-STATION	D	BESU direction for charging	ENERGY ROUTING	I
History for forecast and congestion management	DSTORAGE	D			
Modifications by EV owners	DL-EVSE	D	Responses for modifications	DL-EVSE	D
Owner layer			**Owner layer**		
Timezone settings	DL-OWL	D	Profit data	DSTORAGE	D
Owner preferred settings	DL-OWL	D			

Table 4.16. Input and output parameters for computing layer regarding PFTM layer

Input	Receive	DT	Output	Send	DT
EV mode selection (reschedule)	DL-PFTM	D	Required: EV charging kW, kWh at time X for period X	DL-PFTM	D
BESU mode selection (reschedule)	DL-PFTM	D	Required: BESU charging kW, kWh at time X for period X	DL-PFTM	D
kW, kWh contracts made	DL-PFTM	D	Support: EV (kW,kWh) in timeframe X	DL-PFTM	D
High power consumption order/prediction	DL-PFTM	D	Support: BESU (kW,kWh) in timeframe X	DL-PFTM	D
Match charging with renewable gen. at time X	DL-PFTM	D	Order: EV charge at time X	DL-PFTM	D
			Order: EV discharge with BESU at time X	DL-PFTM	D
			Order: BESU discharge with EVs at time X	DL-PFTM	D
			Order: BESU charge at time X	DL-PFTM	D
			Forecast	DL-PFTM	D

Functions regarding EVs are the following. EV charging times have to be scheduled according to EVSE data and selected timezones (based on open circuit voltage, SOC is for indication). Scheduling equals in some cases with demand response. Average charging current for bays have to be calculated to get higher efficiency from AC-DC converter. Bays have to be selected for particular charging or discharging session of EVs. Discharging selection is influenced by EV departure time. EVs that are recharged and have no other purpose for utilization are disconnected with the substation. Required capacities for charging and support capacity of EVs for V2G applications have to be calculated and forwarded to PFTM layer. The discharging through common DC bus makes discharging current equal between all the bays. The maximum support is therefore either equal with the "weakest bay" (low SOC, low open circuit voltage), which are allowed for V2G applications, or combined with the "strongest bays" ("weakest bays" are disconnected in V2G mode). Additional safety factor is implemented in the calculations for V2G support capability. During V2G mode charging capacities for bays have to be recalculated for the next charging session. If charging of one bay has stopped due to error, new charging time is scheduled for that bay when error has been cleared or EV owner is notified, if the contract can not be fulfilled.
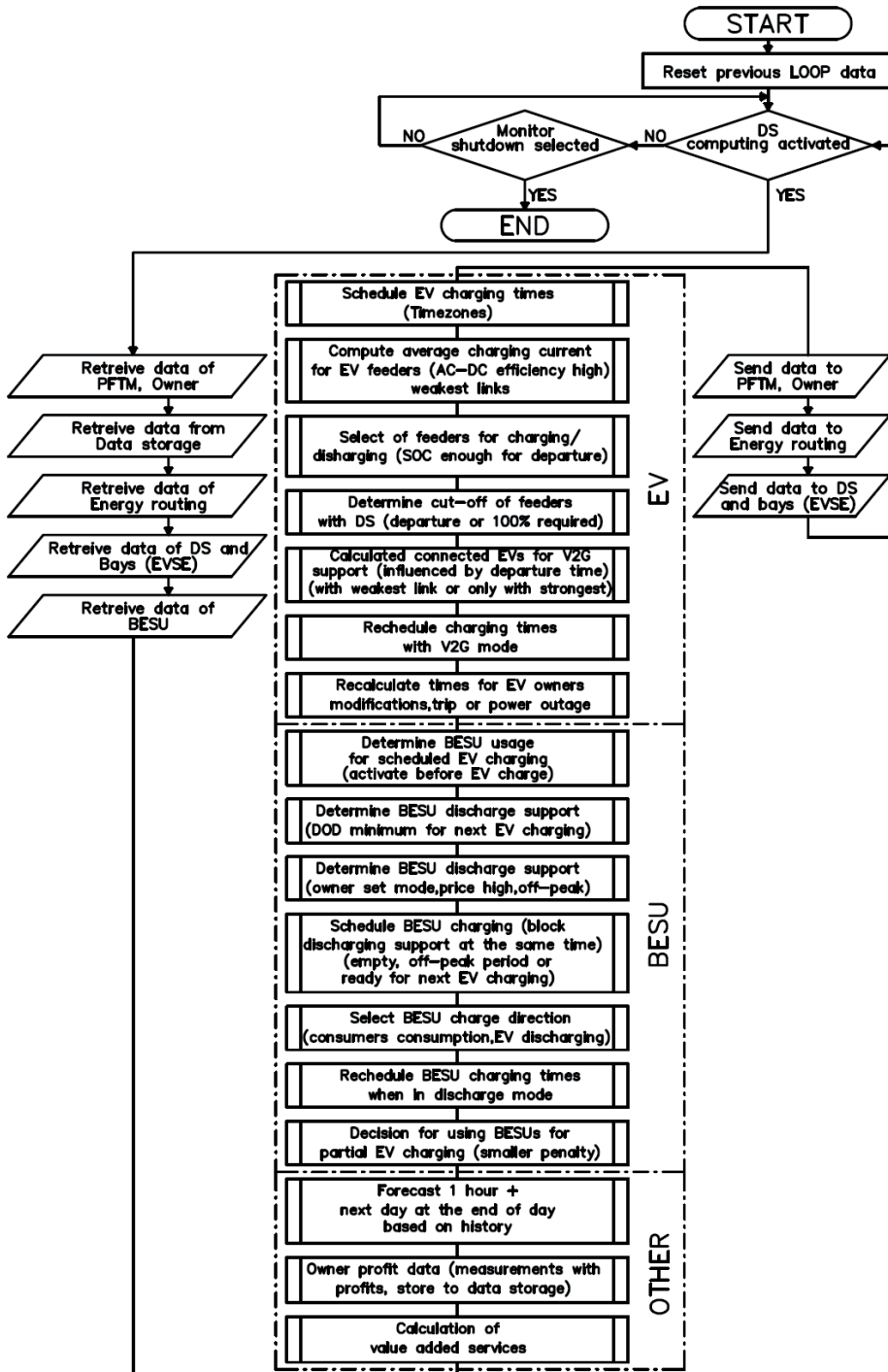
Fig. 4.48 Flowchart of computing layer

Modifications made by EV owners through EVSE have to be analysed and response have to be sent to EVSE for notifying EV owner.

The main functions regarding BESUs are the following. BESU usage and capacity for the next EV charging session has to be determined and calculated. BESU charging has to be scheduled (when the SOC level drops below the lowest set threshold value). If BESU is unavailable, EVs might have to be charged with lower currents.

Other functionalities for the computing layer include forecasting [135] (influenced by whether, price, load, production, historic statistics) for the upcoming period and for the next day. Calculations for the owner (e.g. profit data) and for other value added services.

The function of the data storage layer is to collect general substation measurements (e.g. consumed/produced kW and kvar in month); collect charging/discharging session events and measurements (e.g. store BESU lifetime cycle data for comparing with manufacturers specifications); generate statistical reports. Data could be stored and accessed through cloud storage application.

The seventh layer is the computing layer of parallel distribution substations or extension substations (CMLDS) to divide PFTM layer tasks between different substations and compute data for aggregated number of substations. Extension substations may provide opportunity for different charging timezones.

4.6 Priority filter and task manager

Function of the priority filter and task manager layer (PFTM) is to receive/send the data with DSO, Retailer, LV consumers side and between 11L layers; generate task list queue with time stamp and execute tasks at given time. Requests from DSO, Retailer, LV consumers are given priorities through owner's set priority filter. Priority filter can be built with time based trigger or price based trigger. Request with higher priority is added to the task list and time period for execution is reserved. As the distribution substation is oriented for EV charging, EV charging has the highest priority of all tasks. Other requests for reserved timeframes are neglected if the later requests do not have common connection point (e.g. charging of BESU can be executed in parallel with storage of renewable energy generation). Figures 4.49 – 4.50 show the flowchart of priority filter and task manager layer. In Table 4.17 are presented the input and output parameters for DSO in PFTM layer. Input data from DSO may include reducing of charging power for EV charging, active power supply for peak shaving of utility network loads in MV level, storage of renewable energy generation, reactive power level reduction. In Table 4.18 are presented the input and output parameters for Consumers in the PFTM layer. In Table 4.19 are presented the input and output parameters for Retailer in PFTM layer. In Table 4.20 are presented the input and output parameters for substation in the PFTM layer.

Table 4.17. Input and output parameters for DSO in PFTM layer

Input	Send	DT	Output	Receive	DT
Power level for EV charge (100% or not)	DL-PFTM	D	Required: kW, kWh at time X for period X	DL-CML	D
Active power supply (V2G) (kW,kWh,Time)	DL-PFTM	D	Support: kW,kWh, in timeframe X	DL-CML	D
Renewable energy storage (kW,kWh,Time)	DL-PFTM	D	Prices for charging support/ discharging	DL-OWN	D
Reactive power level reduction (kvar,kvarh,Time)	DL-PFTM	D	Alarm: contract terminated in X minutes or DS in alarm mode	DL-PFTM	D
			Data storage and forecast reports	DL-CML/ DSTORAGE	D
			Requests confirmed/ denied	DL-PFTM	D

Table 4.18. Input and output parameters for Consumers in PFTM layer

Input	Send	DT	Output	Receive	DT
Active power supply (V2G) (kW,kWh,Time)	DL-PFTM	D	Alarm: contract terminated in X minutes or DS in alarm mode	DL-PFTM	D
Reactive power support/ voltage mitigation (kvar,Time)	DL-PFTM	D	Requests confirmed/ denied	DL-PFTM	D
Harmonic compensation list	DL-PFTM	D			
Reverse energy flow (kW,kWh,Time)	DL-PFTM	D			
Energy consumption prediction (requirements, limits)	DL-PFTM	D			

Table 4.19. Input and output parameters for Retailer in PFTM layer

Input	Send	DT	Output	Receive	DT
Prices for charging/ discharging/ penalty (kWh, kvarh) for live and whole day	DL-PFTM	D	Required: kW, kWh at time X for period X	DL-CML	D
Order: active power supply (V2G) (kW,kWh,Time)	DL-PFTM	D	Support: kW,kWh, in timeframe X	DL-CML	D
			Prices for charging support/ discharging	DL-OWN	D
			Alarm: contract terminated in X minutes or DS in alarm mode	DL-PFTM	D
			Data storage and forecast reports	DL-CML/ DSTORAGE	D
			Requests confirmed/ denied	DL-PFTM	D

Table 4.20. Input and output parameters for Substation in PFTM layer

Input	Send	DT	Output	Receive	DT
EV charging (mode, kW)	DL-CML	D	Process start/end (EV, BESU)	DL-CTL	B
EV discharging (mode, kW)	DL-CML/ DL-CTL	D	Inversion kW rating and direction (EV, BESU)	DL-CTL	D
BESU charging (mode, kW)	DL-CML	D	Rectifying kW rating	DL-CTL	F
BESU discharging (mode, kW)	DL-CML/ DL-CTL/ ENERGY ROUTING	D	Target goals, threshold values and characteristic curves for reactive/harmonic compensation	DL-CTL	F
BESU set for support mode	DL-CML	D			
Errors/Alarms	DL-MPL	D			
Process status	DL-CTL	B			
Maintenance modes	DL-STATION	D			

START

Reset previous LOOP data

Monitor shutdown selected — NO — DS computing activated — NO

YES → END

YES

Retrieve data of DSO

Retreive data of Retailer

Retreive data of Energy routing

Retreive data of DS

Retreive data of Consumers

Send data to DSO

Send data to Retailer

Send data to DS

Send data to DS Consumers

Retreive request signals and data (charging, discharging) forecast at beginning of day, during day

Rewrite RTU settings according to outside signals

Auction prices and tasks with Retailer (charging, discharging)

Send/Retreive status with Retailer (e.g. kWh consumption)

Send/Retreive status with DSO (e.g. RTU signals, live measurements, support possibility, forecast)

Priority Filter (requests for open times) (option: adjust requests according to profit)

Task list generation (Queue prioritized) immediate orders are managed first

Execute tasks

First charging algorith for BESU

Error reports for outside participants

Unused BESU always set to Monitor mode

Fig. 4.49 Flowchart of priority filter and task manager

1. EV CHARGING

1.1. DS owner	Set: Profit margins for selling to EV owners (active time changes)	Block: price high, no contracts get violated
1.2. EV owners	Requests represented by DS computing	–
1.3. Process	Control: Utilize reverse energy flow for EV charging	Block: energy required for process itself (active/reactive)
1.4. Utility	Control: Utilize renewable energy for EV charging	Block: energy required for utility itself (active/reactive)

2. EV DISCHARGING

2.1. DS owner	Set: Profit margins for Retailer, compensation price for EV owners	Block: certain periods of day (e.g. not profitable at nights)
2.2. EV owners	–	–
2.3. Process	Control: Power required at LV side	Block: requires reactive support, reverse energy flow, BESU backup
2.4. Utility	Control: Power required at MV side	Block: requires reactive support, renewable energy storing

3. BESU CHARGING

3.1. DS owner	Set: if designed, select margins for BESU charging	Block: price high, no contracts get violated
3.2. EV owners	–	–
3.3. Process	Control: Utilize reverse energy flow for BESU charging	Block: requires BESU support itself
3.4. Utility	Control: Utilize renewable energy for BESU charging	Block: energy required for utility itself (active/reactive)

4. BESU DISCHARGING

4.1. DS owner	Set: if designed, select margins for BESU discharging	Block: certain periods of day (e.g. not profitable at nights)
4.2. EV owners	–	–
4.3. Process	Control: Power required at LV side	Block: requires reactive support, reverse energy flow
4.4. Utility	–	Block: requires reactive support, renewable energy storing

Fig. 4.50 Flowchart of priority filter execution (Part 1/2)

5. REACTIVE POWER COMPENSATION		
5.1. DS owner	Set: if designed, select margins for reactive power compensation	Block: certain periods of day (e.g. not profitable at nights)
5.2. EV owners	–	–
5.3. Process	Control: mode (voltage mitigation, VAR support, harmonic compensation)	Block: requires reverse energy flow, BESU support
5.4. Utility	Control: Lower system reactive power consumption (system overload)	Block: requires active power support, renewable energy storing

IMMEDIATE CONTROL	
BLOCK EV CHARGING (system overloaded, power outage)	
ACTIVATE BESU DISCHARGING (EV charging support)	ACTIVATE BESU DISCHARGING (power outage, consumer side overload)
ACTIVATE BESU DISCHARGING (forecast scenario)	ACTIVATE BESU DISCHARGING (together with EVs)

Fig. 4.50 Flowchart of priority filter execution (Part 2/2)

4.7 Energy routing

One of the main functions of the energy routing is to monitor the network status continuously and provide continuous supply for the consumer side (ATS). In addition, energy routing must provide physical switching of main circuit breakers in accordance with charging/discharging of EVs and BESUs (tasks from PFTM layer). The inputs for the energy routing layer are the input supply voltages (voltage level and frequency measured by supply side smart meters), PFTM layer tasks including energy transfer direction, substation maintenance mode. The outputs from the energy routing layer are the physical control of ATS, switching of main circuit breakers, provide status of main breakers states for data layer and forward tasks to MPL layer with performing ATS. It is the task for energy routing to prepare transformer reversing for discharging EVs to MV side and restore initial transformer state after the session.

In Table 4.21 are presented the actions from Energy Routing layer during power outage in the secondary supply side. If BESU is utilized and voltage restores when ATS have not been yet performed, BESU is resynchronised with secondary side supply, secondary side supply circuit breaker is closed and operation of BESU is turned off. If ATS have been performed and secondary supply side restores, ATS is performed for going back to secondary side supply. If option selected, less important pre-defined bays may be turned off during power outage (e.g. slow charge supply for EVSEs). If power outage is in the first supply side EV charging is stopped. It is the task for computing layer to decide whether to continue charging

in the secondary supply side (depending on power available) with lower charging currents or not. Different operations include station start-up, normal station state, ATS (power outage and restore), maintenance state, fault state in the station.

Table 4.21. Actions from Energy Routing layer during power outage in the secondary supply side

EV side state	BESU side state	Action in power outage of secondary supply
OFF	BESU OFF	Select of first supply (ATS)
OFF	BESU charging	Select of first supply, BESU charging ramp down
OFF	BESU in consumer side peak shave	BESU to virtual PLL, BESU synchronization with first supply, select of first supply and BESU to consumer side peak shave
EV charging	BESU unutilized (blocked) in support mode (SM)	Select of first supply, EV charging ramp down
EV charging	BESU in EV peak shave	Select of first supply, EV charge and BESU discharge ramp down
EV discharging MV	BESU unutilized in support mode (SM)	BESU to virtual PLL, end EV discharging, transformer reversing, BESU synchronization with first supply, select of first supply and BESU to SM
EV discharging LV	BESU unutilized in support mode	BESU to virtual PLL, end EV discharging, BESU synchronization with first supply, select of first supply and BESU to SM
EV in X mode	BESU in consumer side peak shave	BESU to virtual PLL, timeout (supply restore or not), EV mode OFF, BESU synchronization with first supply, select of first supply and BESU to consumer side peak shave

4.8 Owner layer and Market layer

The decisions required from the distribution substation owner are: BESU discharge mode type (when to discharge at for what purposes), BESU charge prices (when charging is allowed), EV discharge times, Profit margins for EV charging, EV discharging prices (for selling to Retailer or DSO, compensation prices for EV owners), how often or when to ask energy prices from the DSO or Retailer, when reactive power compensation or voltage mitigation is required. The input and output parameters of OWL layer are presented in Table 4.22. Market layer inputs may change owner decisions.

Table 4.22. Input and output parameters for Owner in OWL layer

Input	Send	DT	Output	Receive	DT
Profit calculations	DL-CML	D	General settings	DL-PFTM, DL-STATION	D
Errors/Alarms/ Faults (future improvements)	DSTORAGE	D	Profit margins	DL-PFTM	D
			Compensation prices (EV discharge)	DL-PFTM	D
			Times when to ask prices from Retailer (auction)	DL-PFTM	D
			Price limits to execute EV/ BESU commands	DL-PFTM	D
			EV/BESU operation strategy (charge/ discharge occasions, times)	DL-PFTM	D
			Timezone settings for EV charging	DL-PFTM	D
			Which immediate operations are allowed without queue	DL-PFTM	D

4.9 Further implementation

The 11L design is not independent solution but has connection points with other Smart Grid architectures. The 11L describes the design architecture primarily for electrical engineers how to build up V2G capable distribution substations. Exchange of information with DSO or Retailer has to be carried out with communication protocols developed by Smart Grid committees.

According to SGAM Framework [67] the information and function communication protocols can be exchanged through the PFTM layer (Fig. 4.51). Business functions can be exchanged though the Market layer. Also data composed in CML and measurement values sent to PFTM layer can be composed for Secondary Substation Node (Fig. 4.51) and transmitted to Middleware [68].
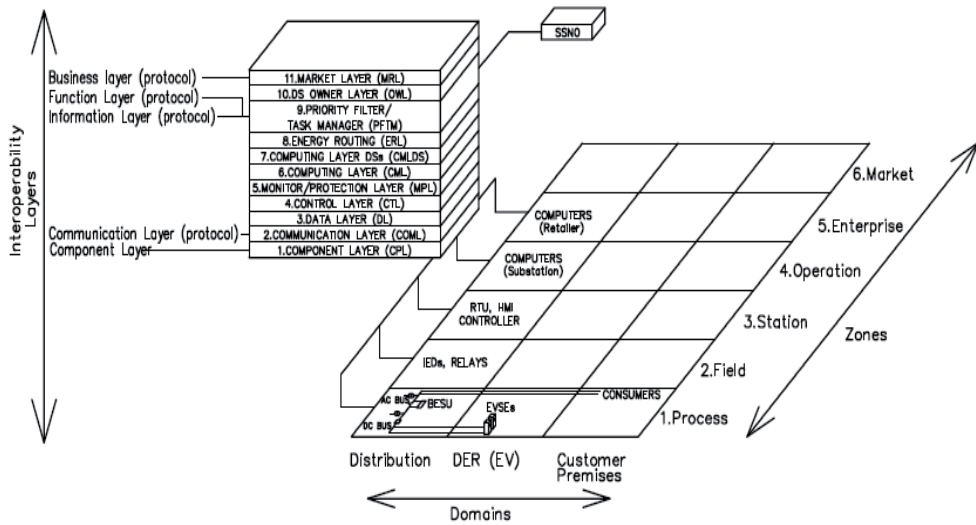
Fig. 4.51 Connections of 11L architecture with SGAM framework and SSN

Distributed energy resources (DER) can be connected to the common DC bus, common AC bus or with MV switchgear depending on how DERs will be utilized. Control of DERs can be implemented in CTL layer. The microgrid can go to islanding mode if the generation of DERs can be matched with consumption combined with the utilization of BESU. The core program of PFTM (representation of prosumer) is required to present consumption and available generation data to DSO or Retailer (Fig. 4.52).

Consumption	497.2 kW	
Consumption	37.1 kvar	
Generation:		
Available power	117 kW	-
Available time	-	
Ordered	yes	
Time expires in	5 min	

Consumption	317.3 kW	
Consumption	10.1 kvar	
Generation:		
Available power	152 kW	5 min
Available time	27 min	
Ordered	no	
Time expires in	-	
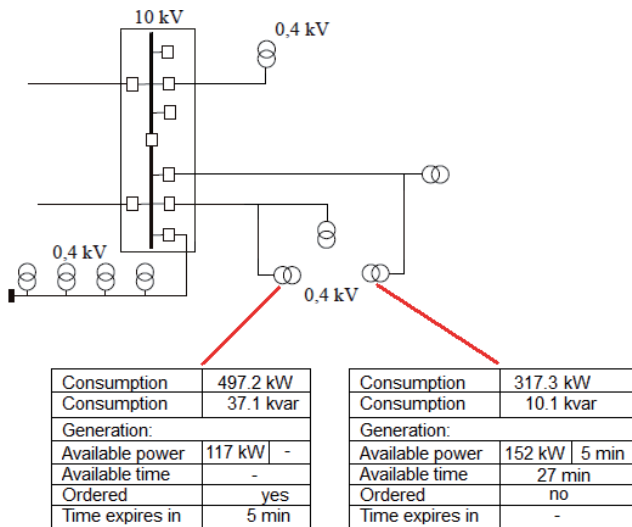
Fig. 4.52 Illustration of overview of consumption and available generation from the V2G capable distribution substations

4.10 Generalizations

The chapter has presented the architecture of eleven layers (11L). The 11L concept can be implemented in the programming of SAS. The architecture allows implementation of control and protection functions for bidirectional energy flow between EVs and the utility network.

Different control algorithms were simulated with MATLAB Simulink. With simplifications in the modelling the efficiencies of energy conversions were higher than presented in literatures (Chapter 3). The simulations due not include losses in the transformers and conductions and switching losses in IGBTs. The actual efficiency of energy conversions is expected to be equal with values presented in literatures. The efficiencies of energy conversions for designing of distribution substations are presented in Chapter 6. From different operations of the AC-DC power converter, rectifying mode for charging of EVs has to be preferred to have the highest efficiency of several energy conversions. Due to simplifications in the modelling the real THD values of the system compared to simulations are expected to be in the range of 3-5 % according to EN 50160. The simulation models can be used for testing of different control algorithms, which has been the main target in the modelling. Control algorithms tested in the simulations can be implemented in the programming of RTU of the laboratory test bench presented in Chapter 5. The substation for microgrid applications should be ready to simultaneously serve AC and DC buses. This means that the core control program in its main controller should integrate control and protection functions for AC bus, common DC bus and the link from AC bus to the utility grid.

The 11L architecture assumes that EV car manufacturers are willing to give the control of charging and discharging over to a higher control system of SAS. EV BMS has still control over the EV side contactor, which can be opened if batteries of EVs are subjected to excess stress. The SAS can only transfer charging currents equal or less compared to ordered values of EV BMS. Safety of the system must always be ensured in the designing of SAS.

5. PRACTICAL DESIGN ISSUES AND EXPERIMENTAL RESULTS

5.1 Overview of laboratory test bench

In order to test the microgrid functionality in distribution substations an experimental microgrid development project was initiated in Tallinn University of Technology (TUT) at the beginning of the year 2011. The aim of the project was to develop and implement new control architectures in the microgrids. The TUT microgrid was constructed by TUT microgrid research team consisting of three doctoral students (described in Chapter 1 including the author of this thesis). The purpose of this doctoral thesis in the laboratory test bench were:

- Development of control strategies for bidirectional energy flow between electric vehicles (as prosumer) and the microgrid smart substation (as prosumer);
- Development and design for the construction of an new experimental sub-station prototype based on the results of research in the experimental microgrid;
- Control functions, protection functions and simulation results presented in Chapter 4 were planned to be tested in practice.

The architecture of the laboratory test bench is illustrated in Fig. 5.1. The laboratory test bench is implemented with the integrated AC and DC bus topology, including 5 bays in the AC bus and 3 bays in the DC bus. The experimental microgrid is located near the substation of the laboratory and is connected to one of the low voltage bay's of the substation. The substation is connected with the local utility network. The nominal apparent power of the laboratory test bench is 170 kVA. The component layer is illustrated in Fig. 5.2.

The core program of the 11L architecture is implemented in the IEC61850 compliant RTU32 (Fig. 5.3 and Fig. 5.4) from Brodersen Systems A/S. The RTU operates the bidirectional AC-DC converter in the CTL layer. The RTU controls the physical switching of all DC side apparatuses. RTU gathers current measurements from the common DC bus (DC current sensors in the supply side and in the individual bays) and status of devices in the bays (auxiliary contacts of circuit breakers and contactors) to the data layer (DL), which are utilized in the MPL layer. MPL layer monitors that all circuits are properly connected, no errors or faults are presented, all voltages and currents are in the pre-defined limits. Isolation monitors are included in every bay of the DC switchgear.

The laboratory test bench consists of IEC61850 compliant and programmable smart meters (Satec SA330 and Satec EM720T power meters) in the AC side. The smarts meters (Fig. 5.3) measure amongst several parameters voltages and currents of phases and neutral, active and reactive power measurements, phase angels, harmonic content (up to the 63th harmonic). Measurement results are utilized in the

monitor and protection layer (MPL). Smart meters are programmed to forward safety signals to RTU, when the voltages, currents and frequency of the system are in the pre-defined limits. The main smart meter (SA330) controls the physical switching of the main supply contactor, but waits for the initiating signal from the RTU. Smart meters monitor the status of bays (auxiliary contacts of devices in bay). Measurement data are archived.

The laboratory test bench includes BESU (Fig. 5.4), which consists of 144 pcs of 3.2 V 40 Ah Li-ion batteries. The nominal voltage of the BESU is 460 V DC and capacity is 18.4 kWh. The BMS of the BESU is manufactured by Orion. Control of the BMS is through CANbus.
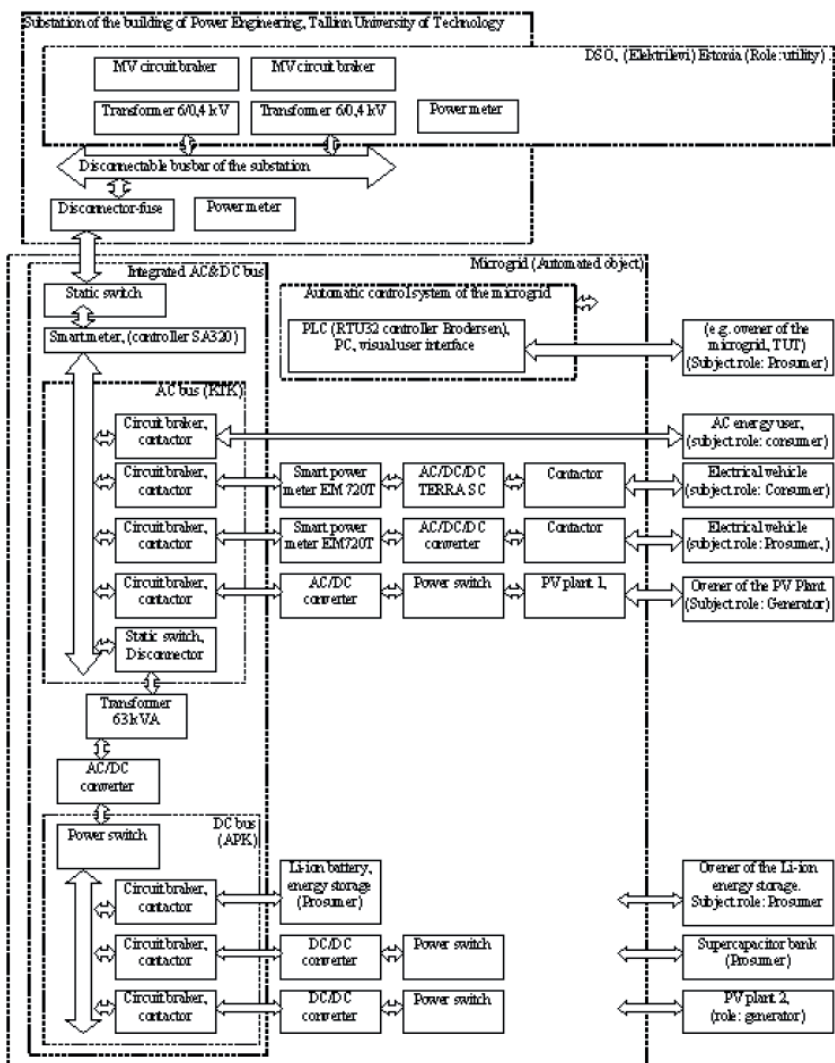
Fig. 5.1 Architecture of laboratory test bench in TUT

Fig. 5.2 Laboratory test bench in TUT (component layer)
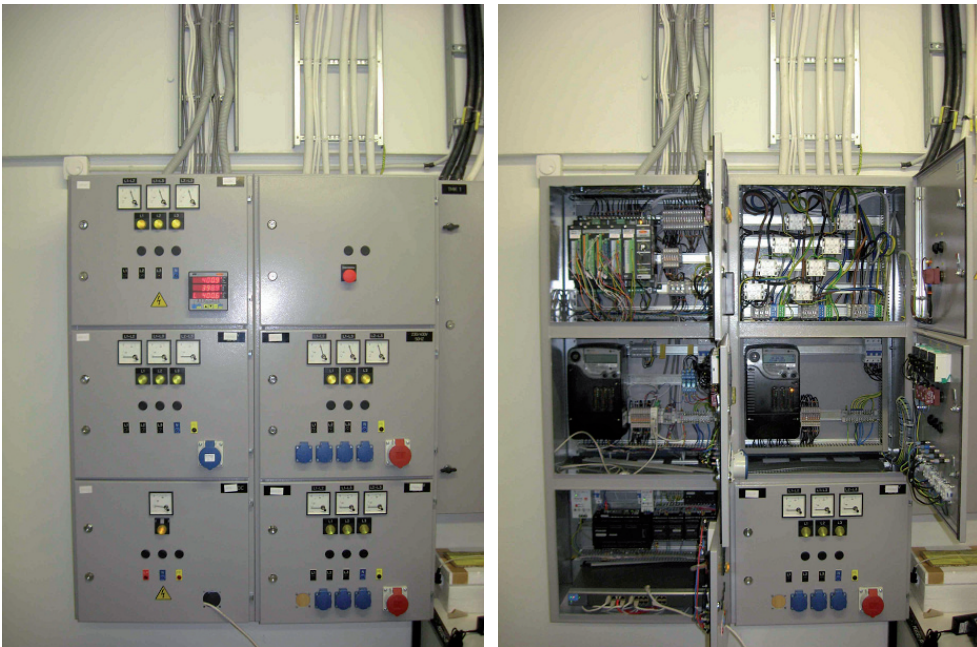
Fig. 5.3 Laboratory test bench in TUT – AC switchgear with smart meters, controller and switch (component layer)

Fig. 5.4 Laboratory test bench in TUT – controller and switch (left), BESU (right) (component layer)

Laboratory test results can be compared to state of art ABB 20 kW fast charger TERRA SC Duo (Fig. 5.5).

Fig. 5.5 Fast charger TERRA SC Duo (charging of serial electric vehicle in TUT Department of Electrical Engineering)

The experimental bidirectional AC-DC power converter is manufactured by ABB. The power converter coverts AC voltage to DC voltage (for common DC bus) and vice versa. The AC-DC power converter can be utilized for active filtering and reactive power compensation. Control of the AC-DC power converter is through CANbus.

Additional gateway (CANbus/Modbus) is required to communicate with the RTU. A dedicated and manageable Ethernet switch of Moxa PT-7324 series is utilized for IP-based communications between the RTU and the devices of the laboratory test bench.

The 11L layer architecture implemented in the RTU is illustrated in Fig. 5.6. Programming of smart meters is illustrated in Fig. 5.7. Measurement graphs of energy meter SA330 (Fig. 5.8 and Fig. 5.9) of voltages and currents during the activation of the AC-DC power converter are illustrated through the programming and monitoring software of Satec energy meters (PAS). The accuracy of voltages, currents, active power and energy measurements are 0.2 %. Accuracy of THD measurements are 1.5 %.

Fig. 5.10 illustrates communication layer in the RTU (IEC61850 and Modbus). Fig. 5.11 illustrates data layer in the RTU. Fig. 5.12 illustrates the control layer of BESU charging in the RTU.

Fig. 5.13 illustrates BESU parameters through the programming and monitoring software of Orion BMS. The accuracy of cell voltage measurements is 0.25 %.
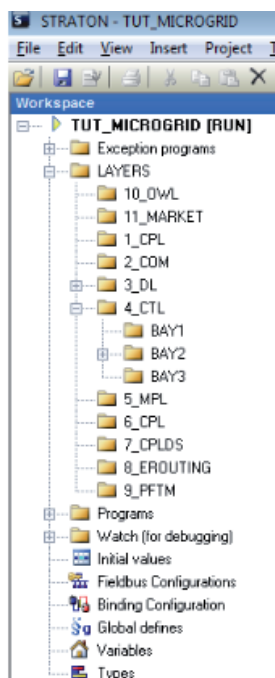
Fig. 5.6 Controller set-up with layers in the laboratory test bench of TUT
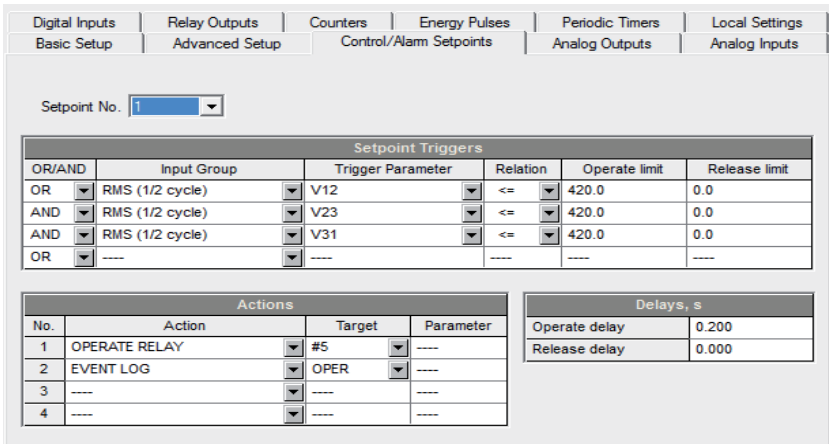
Fig. 5.7 Programming of smart meters in the laboratory test bench of TUT
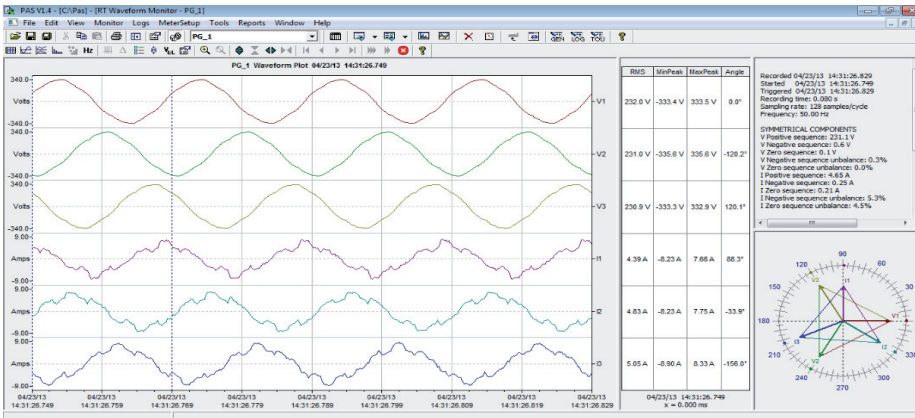
Fig. 5.8 Example of voltages and currents measured by smart meters in the activation of AC-DC power converter in the laboratory test bench of TUT
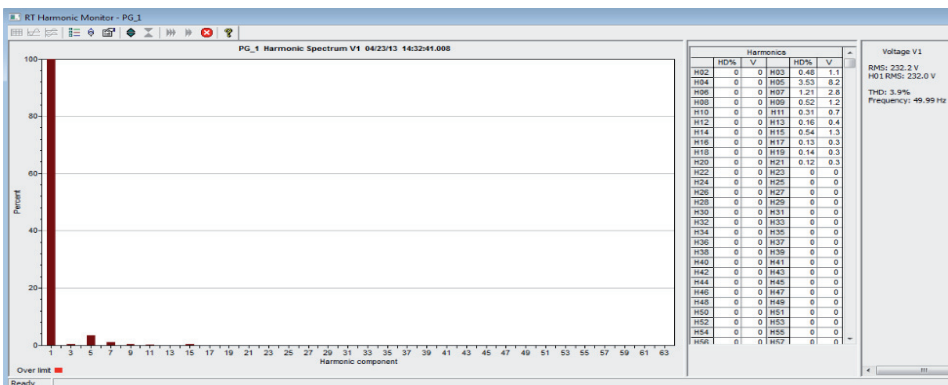
Fig. 5.9 Harmonic content measured by smart meters in the activation of AC-DC power converter in the laboratory test bench of TUT
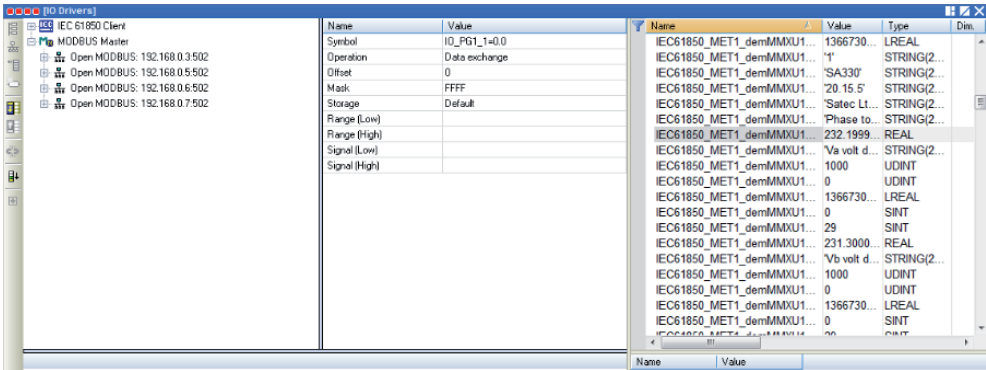
Fig. 5.10 Communication layer in the laboratory test bench of TUT
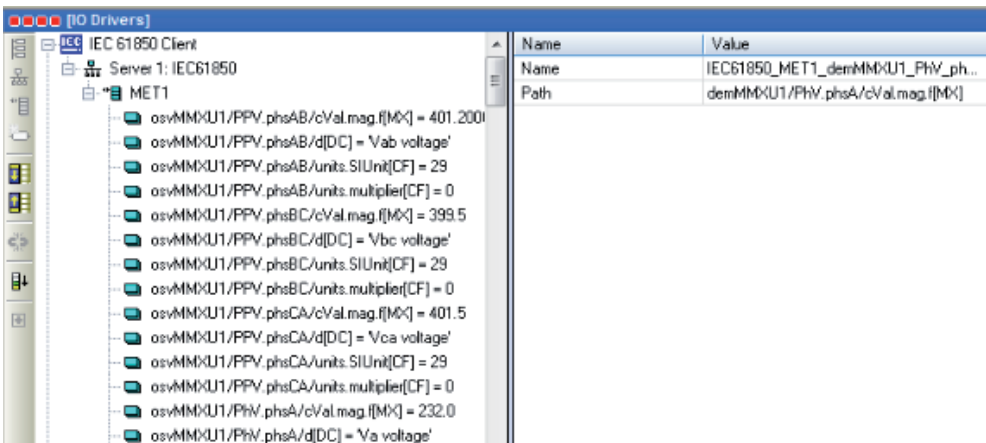
Fig. 5.11 Implementation of IEC 61850 in the data layer of the laboratory test bench of TUT
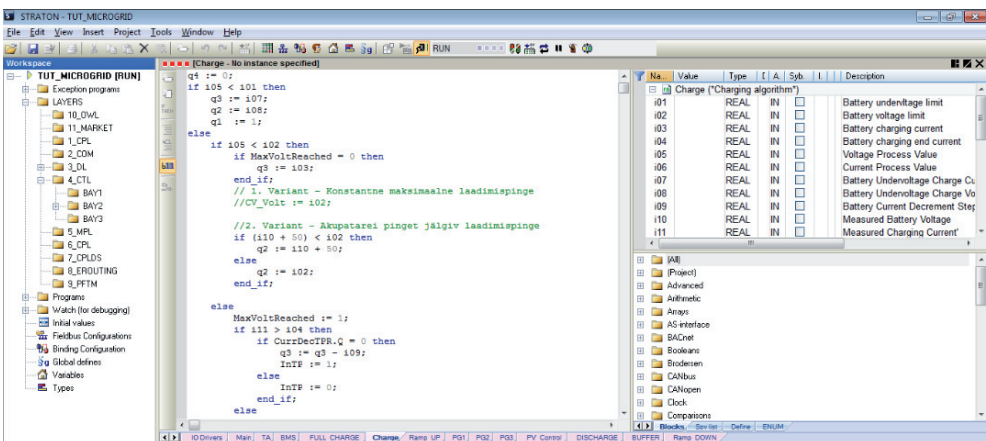
Fig. 5.12 Control layer of BESU charging in the laboratory test bench of TUT
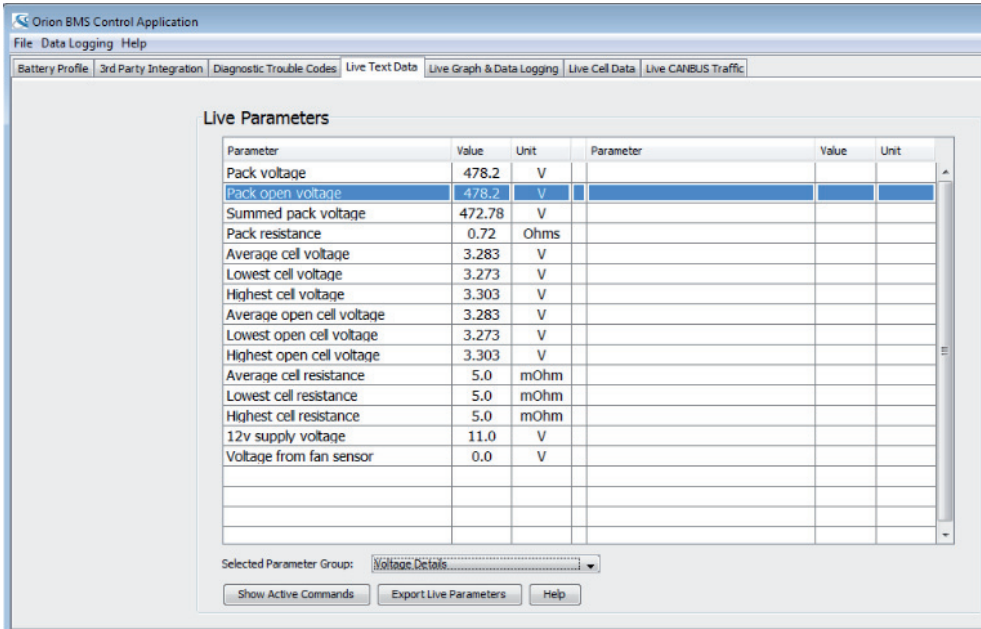
Fig. 5.13 Set-up of BMS of BESU in the laboratory test bench of TUT

5.2 Experimental results

5.2.1 Control of AC-DC conveter in parallel with electric motor

Electric motors running in the no-load state consume reactive power more than active power and decrese the power factor of the electric system. A laboratory test set-up was assembled (Fig. 5.14) with an electric motor. 3-phase 400 V 3.0/0.4 kW electric motor (HXA 112 M 4/8 B3 from ABB) was used in the test set-up. Initiating signal was sent from the RTU to activate the bidirectional AC-DC converter in parallel with the electric motor.

Measurement results are shown in Table 5.1 and in figures Fig. 5.15 and Fig. 5.16. Electric motor operating alone in the electric system consumed 0.5 kW of active power and 2.79 kvar of reactive power. The appearent power was 2.84 kVA. The power factor of the electric system was 0.17. When the bidirectional AC-DC converter was turned on, the reactive power consumption was surpressed and excess reactive power was transmitted into the network -0.451 kvar. Appearant power in the test was 0.77 kVA and power factor was -0.81. The bidirectional AC-DC converter reduced the reactive power consumption in the electric system.

Fig. 5.14 Test set-up with electric motor in the no-load state with bidirectional AC-DC converter operating in parallel

Table 5.1. Measurement results of test set-up with electric motor in the no-load state with bidirectional AC-DC converter operating in parallel

Parameter	Electric motor alone	Electric motor with AC-DC converter in parallel (standby mode)
Average phase current	4.111 ± 0.008 A	1.350 ± 0.003 A
Active power	0.504 ± 0.001 kW	0.626 ± 0.001 kW
Reactive power	2.795 ± 0.008 kvar	-0.451 ± 0.001 kvar
Appearent power	2.840 ± 0.006 kVA	0.772 ± 0.001 kVA
Power factor	0.177 ± 0.0006	-0.812 ± 0.003
Average V THD	4.1 ± 0.06 %	4.1 ± 0.06%
Average I THD	10.56 ± 0.16 %	0 %
Phase angle I1	66.6 ± 1 degree	-16.5 ± 1 degree
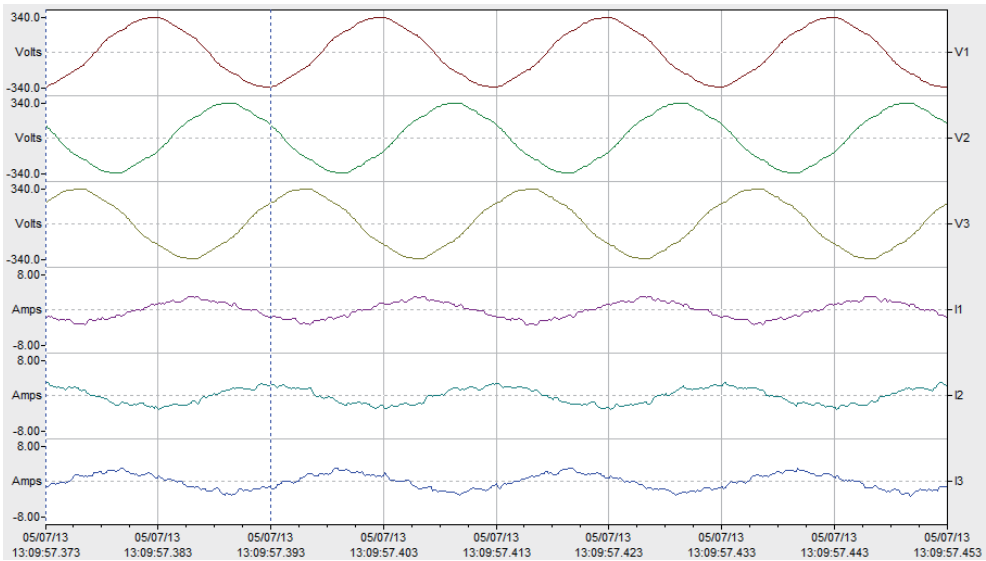
Fig. 5.15 Waveform plot of voltages and currents from smart meter Satec SA330 in the laboratory test bench during the no-load state of the electric motor alone
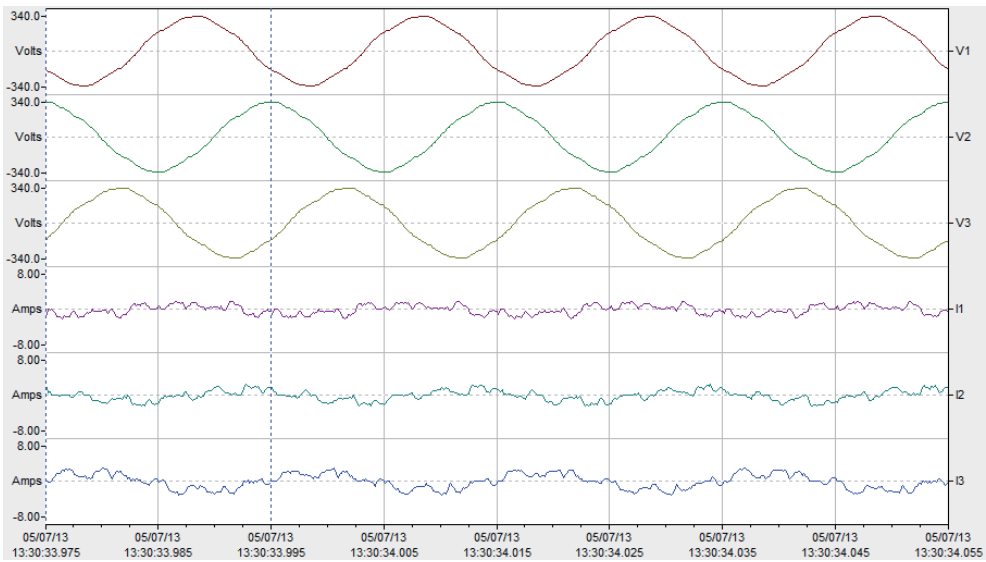
Fig. 5.16 Waveform plot of voltages and currents from smart meter Satec SA330 in the laboratory test bench during the no-load state of the electric motor with bidirectional AC-DC converter operating in parallel

5.2.2 Control of bidirectional AC-DC conveter in parallel with EVSE

A measurement test (Fig. 5.17) was made with EVSE (ABB Terra SC Duo) with bidirectional AC-DC converter operating in parallel. The EVSE was supplied through the AC switchgear (Fig. 5.3). Initiating signal was sent from the RTU to activate the bidirectional AC-DC converter in parallel with the EVSE. Measurement results are shown in Table 5.2 and in figures Fig. 5.18 and Fig. 5.19. As the EVSE is capable of compensating reactive power itself sucessfully, additional compensation from the AC-DC converter is not required.

Fig. 5.17 Test set-up with EVSE with bidirectional AC-DC converter operating in parallel

Table 5.2.Measurement results of test set-up with TERRA SC Duo fast charger and with bidirectional AC-DC converter operating in parallel

Parameter	EVSE alone	EVSE with with AC-DC converter in parallel (standby mode)
Max average phase current	29.79 ± 0.06 A	30.39 ± 0.06 A
Max active power	20.45 ± 0.04 kW	20.50 ± 0.04 kW
Max reactive power	-2.23 ± 0.007 kvar	-5.53 ± 0.02 kvar
Max appearent power	20.57 ± 0.04 kVA	21.24 ± 0.04 kVA
Average power factor	-0.994 ± 0.003	-0.965 ± 0.003
Average V THD	4.3 ± 0.06 %	4.5 ± 0.06 %
Average I THD	7.5 ± 0.11 %	10.2 ± 0.15 %
Phase angle I1	-7.9 ± 1 degree	-15.5 ± 1 degree
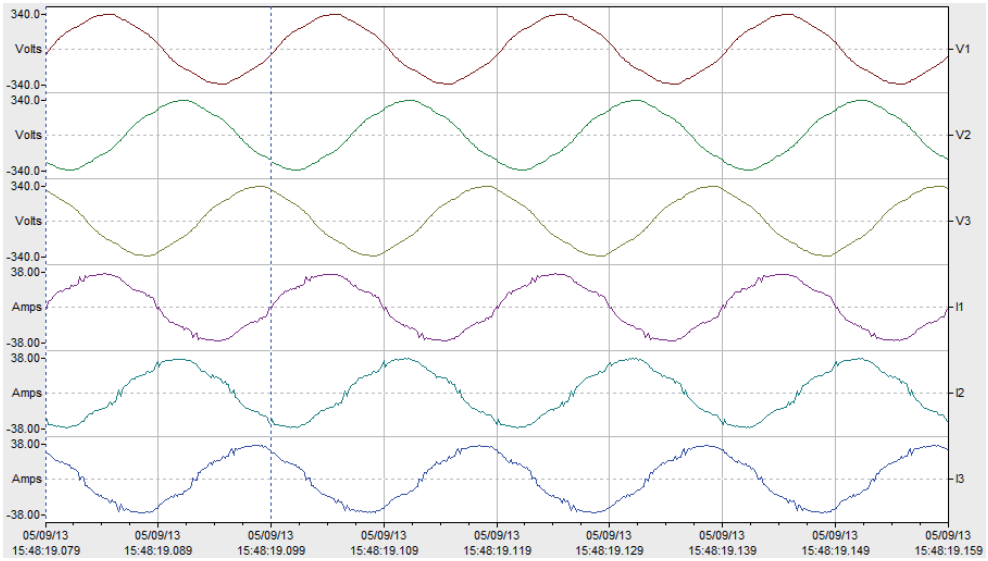
Fig. 5.18 Waveform plot of voltages and currents from smart meter Satec SA330 in the laboratory test bench during charging of EV with TERRA SC Duofast charger
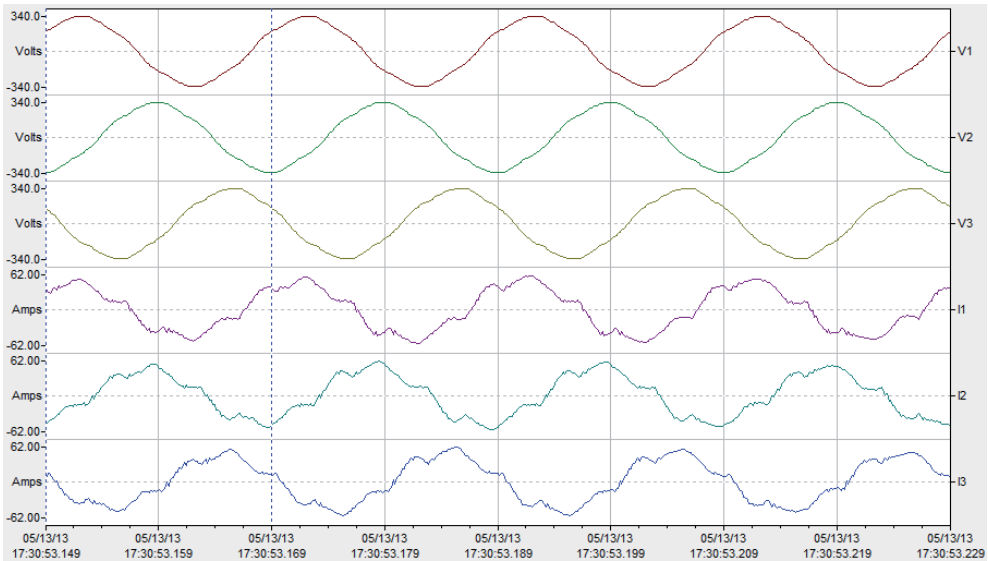
Fig. 5.19 Waveform plot of voltages and currents from smart meter Satec SA330 in the laboratory test bench during charging of EV with TERRA SC Duofast charger with bidirectional AC-DC converter operating in parallel

217

5.3 Status of laboratory test bench testing

Due to setbacks in the development of the laboratory test bench the practical testing of charging and discharging of EV and BESU in the microgrid is scheduled after this doctoral thesis. The new scheduled time is at the end of the year 2013 and in the year 2014. Test results will be published in international journals and conferences. During the construction of the microgrid and initial programming of the RTU there have been indications of limitations in the concept of the 11L architecture (besides physical CPU memory of 128 MB in the RTU eventually). In such case the RTU will act as a central (master) controller in the test bench and each prosumer will include its own control unit handled as a slave device that serves the purpose of controlling prosumer related lower level tasks. The purpose of the RTU is to read operational parameters of microgrid prosumers, to send control values and configuration information to the slave devices. All data needs to be collected and logged by the RTU in order to generate reports and report errors.

The simulations in the MATLAB Simulink have verified the main control principles in the control of the bidirectional energy flow. Practical programming will indicate where the flowcharts and input/output tables in the Chapter 4 have to specified, though the main concept will remain unchanged.

6. DESIGNING

This chapter describes designing of a BESU for a distribution substation and general input data, which is required for manufacturing a distribution substation with V2G capability. The designing must consider general utility network requirements (e.g. nominal voltage, nominal frequency and wiring configuration). As these requirements are influenced by a particular location, where the substation will be installed, this chapter is focused more on designing of active power management inside the microgrid. The chapter considers the same type of distribution substation topology with IT earthing system, which was described in chapter 4.

Main optimization principles in the designing of distribution substation:
- Application requirements (duration of backup support, size);
- Price optimization;
- Market advantage;
- Efficiency.

6.1 Selection of power converters and BESU for distribution substation

The designing of power converters and BESU is divided into sixteen steps (STEP1-STEP16). Examples are presented for each step. The designing procedure is presented in a generalized way that it could be effectively utilized by electrical engineers. The designing of BESU is influenced by the number of EVs that are charged through the distribution substation, by the constraints of the utility network or microgrid and by the backup power capability for consumers during power outage.

STEP1 requires defining the number of EVSEs that will be connected with the distribution substation. Example: 3 pcs of EVSEs with fast charging capability.

STEP2 requires the calculation of nominal active power for distribution substation bays P_{bay}. The active power can be calculated by defining the following parameters:
- the maximum battery pack capacity of EVs that can be connected with EVSEs;
- the minimum initial and the maximum final SOC value of EV battery pack that is charged with fast charging;
- duration of fast charging session;
- combined efficiency of the AC-DC power converter, the DC-DC power converter and the efficiency of the EV battery pack to accept fast charging currents.

Example: maximum battery pack capacity of EV is Q_{EV}=25 kWh [43] (e.g. Mitsubishi i-MiEV has 16 kWh), fast charging between SOC_i=10 % and SOC_f=90 %, duration of charging session 30 minutes (0.5 hours), efficiency of the

AC-DC power converter 96 % [81], efficiency of the DC-DC power converter 95 % [125], efficiency of the EV battery pack during charging 93 % [136]. The efficiency of the EV battery pack charging is influenced by weather conditions, but for simplification this is neglected in this chapter. Total combined efficiency η_{comb} for fast charging is 85 % (0.96 x 0.95 x 0.93 ≈ 0.85). Nominal active power for distribution substation bay can be calculated as:

$$P_{bay} = \frac{Q_{EV} \cdot (SOC_f - SOC_i)}{h \cdot (\eta_{comb})} = \frac{25 \cdot (0.9 - 0.1)}{0{,}5 \cdot 0{,}85} = 47 (kW). \qquad (70)$$

The power converters should be selected for 50 kW, but for the further utility load calculations 47 kW can be considered. Three bays occupied at the same time require 141 kW of active power.

STEP3 requires the calculation of active power support from BESU $P_{BESU,LV}$ to the common AC bus based on the required maximum average load P_{AV} for the utility network during fast charging of bays. P_{AV} is influenced by the active power let through of the utility network or by limitations set by the microgrid (e.g. apparatuses and cables of existing electric power system). Without BESU support the P_{AV} may influence the number of EVs that can be charged simultaneously.

Example: maximum average load for the utility network should not exceed 100 kVA. As the AC-DC converter operates nearly with unity power factor P_{AV} can be considered 100 kW. $P_{BESU,LV}$ can be determined as:

$$P_{BESU,LV} = \sum_{i=1}^{n} P_{bay,i} - P_{AV}, \qquad (71)$$

which for the given example is 41 kW (141 kW – 100 kW) during fast charging of all bays (30 minutes). This therefore requires 20.5 kWh of BESU support.

In the case of where e.g. only Mitsubishi i-MiEVs occupy all three bays, the load for the utility network is nearly 3x30 kW≈90 kW according to equation (70) and (71). The control strategy for the computing layer must be selected accordingly to still utilize BESUs in such cases.

STEP4 requires defining the charging control strategy for BESUs. Dimensioning of timezones for charging EVs should consider that there would be enough time to recharge BESUs for the next EV charging session without overloading the utility network. There are two possible strategies for sizing BESUs for V2G capable distribution substations. First of which is to charge BESUs to full capacity only during nights and then utilized the energy stored during day time (requires a large size of BESU and bigger DOD, which reduces cycling of batteries and is more expensive). Second of which is to allow active charging of BESUs during day time (optimized size of BESU). For semi-public charging this requires separate timezone. For public charging this requires either limiting the operation of bays in charging session or increasing the maximum average load (e.g. transformer

size) for the utility network. The unused power which is achieved by disconnecting of some of the bays can be used for charging BESUs.

Example: distribution substation with V2G capability for a nearby factory has three 1 h pre-defined charging sessions distributed along the work day. In the first half of the 1 h charging sessions all bays are charged simultaneously with BESU support (141 kW – 41 kW = 100 kW). In the second half of the 1 h charging session BESU is charged. For the final pre-determined session BESU charging is postponed for the night. During weekends or after the work day, when there are not specific timezones, two EVSEs stay operational and one EVSE is disconnected (2 x 47 kW = 94 kW < 100 kW).

STEP5 requires defining the capacity of BESU for peak shaving of AC consumer loads in the LV side and for backup capability during power outage for AC consumers. This requires defining the following parameters:
- Minimum power support and service time for BESU;
- Power factor of the AC consumer loads;
- Bays which may be disconnected during power outage;
- Charging of EVs during power outage.

Example: for electric system designed for 200 kVA for AC consumers 100 kVA of support is required for critical bays, other bays may be disconnected, power factor 0.8 (80 kW of active power support) for 15 minutes (20 kWh), charging of EVs during power outage not allowed. Peak shaving of AC consumer loads is not considered for regular basis (only for extreme situations).

STEP6 requires defining the storage capacity and session time for storing renewable energy sources.

Example: no particular capacity selected. Provide service for storage based on the state of BESU.

STEP7 is the final selection of BESU capacity for the common AC bus based on previous steps. Example: support of fast charging of EVs (41 kW, 30 minutes, 20.5 kWh), backup capability for AC consumers during power outage (80 kW, 15 minutes, 20 kWh) and no particular level for renewable energy storing. The selection is based on the power peak of backup support for AC consumers and capacity required for supporting EV fast charging (80 kW/100 kVA and 20.5 kWh).

STEP8 requires the selection of power transformers for the microgrid. Example: 100 kVA for EV charging with BESU support and 200 kVA for AC consumers. Sum of apparent powers results in 300 kVA and the next standardized size of transformer is 315 kVA. 315 kVA transformer can supply consumers and allows charging of EVs if one of the MV supplies should be unavailable. For noting, without the BESU support 400 kVA transformers would have been required (200 kVA + 141 kVA).

STEP9 is the correction of BESU size in the correspondence of efficiencies of power converters and discharging current efficiency that is required to support common AC bus. Example: AC-DC power converter 96 % [81], efficiency of the

DC-DC power converter 95 % [125], efficiency of the BESU Li-ion battery pack with the maximum allowed discharging rate of 1 C is 99 % [137]. The combined BESU discharge efficiency is 90.3 %. The corrected parameters for BESU are 88.6 kW and 22.7 kWh.

STEP10 is the correction of BESU size due to ambient temperature. Li-ion batteries are efficient around room temperatures ($25\,^{\circ}C - 45\,^{\circ}C$). At lower temperatures the BESU capacity during discharging is lower. At winter times the temperature kept inside distribution substations is around $5\,^{\circ}C - 15\,^{\circ}C$ depending of equipment that are installed inside the substation. According to Table 6.1 [137] additional factor of 1.19 has to be considered in designing of BESUs.

Table 6.1. Li-ion charging and discharging efficiencies depending on ambient temperature at 0.5C rate [137]

Temp. °C	Factor of Discharge	Factor of Charge
60	1.01	0.996
45	0.997	0.994
25	1.00	1.00
0	1.19	1.01
-10	1.11	1.04
-20	1.23	1.13
-30	1.5	1.59

Example: considering factor of 1.19 for discharging the corrected parameters for STEP9 BESU are 105.4 kW and 27.0 kWh.

STEP11 is the correction of BESU size with reserves, if required, for reducing stress to the batteries. Example: for cost effective solution, reserves at this step is not considered. Parameters for STEP11 are equal with STEP10.

STEP12 is the correction of BESU size in regards to predicted discharge cycles. As mentioned in chapter 1, regardless of battery type and cost, the longest service life will be achieved by discharging batteries as little as possible. The lowest DOD rate prolongs the batteries the longest, but increases the size and cost of BESUs. Lower DOD value allows utilizing BESU in consecutive hours, if charging in the current time period would be unavailable.

Example: the BESU is utilized 3 times during workdays for EV charging support. This corresponds to discharge cycles of 15 times per week and 780 times per year. For application of 5 years this generates 3900 discharge cycles. According to Table 1.1 the number of acquired discharge cycles is only possible with DOD of 10 %. The corrected size for BESU is therefore 105.4 kW with capacity of 270 kWh.

STEP13 is the selection of battery pack voltage and the number of strings required. This requires calculation of battery string voltages based on the active power required and discharge currents of standard size batteries. This is presented in Table 6.2 and highlighted for the given example (e.g. 105.4 kW divided by 200 A results in 527.1 V). The battery string voltage should be selected according

to the nominal voltage of the BESU internal common DC bus and selection of DC-DC power converters (e.g. for the given example <600 V for DC-DC converters with 800V/600V high frequency transformers). From the selected voltage can be determined the required capacity of batteries. This is presented in Table 6.2 (e.g. 270 kWh divided by 527.1 V results in 512.2 Ah of 1 string or 256.1 Ah of 2 strings, which is the choice in the given example).

Table 6.2. Selection of Li-ion battery pack voltage and capacity

				1 string	1 string	2 parallel	2 parallel
P, kW	I, A DC	U, V DC	E, kWh	Bat, Ah	Bat, pcs	Bat, Ah	Bat, pcs
105,4	100	1054,3	270,0	256,10	351,4	128,1	702,8
105,4	160	658,9	270	409,76	219,6	204,9	439,3
105,4	200	527,1	270	512,21	175,7	256,1	351,4
105,4	300	351,4	270	768,31	117,1	384,2	234,3
105,4	400	263,6	270	1024,41	87,9	512,2	175,7
105,4	700	150,6	270	1792,72	50,2	896,4	100,4
105,4	1000	105,4	270	2561,03	35,1	1280,5	70,3

STEP14 is the correction of STEP13 in correspondence with standard battery sizes. Example: capacity required for two strings is 256.1 Ah. The next size standardized battery is 300 Ah. For two strings the combined capacity is 600 Ah. The required voltage for parameters 270 kWh and 600 Ah is 450.0 V. With Li-ion batteries of nominal voltage of 3.0 V this requires 150 pcs of Li-ion batteries (total battery pack voltage is therefore 450 V). The selected BMS of choice must be able to manage the number of Li-ion batteries in series. The actual battery pack capacity is 270 kWh. The discharge current of one string for 105.4 kW is 117 A, which corresponds to discharge rate of 0.39 C. The final choice of BESU is 150 pcs of 3.0 V 300 Ah Li-ion batteries in series for one string and total of two strings are required.

STEP15 is the checking of the selected choice to make any corrections in the previous steps. In the example the BESU capacity is 270 kWh. Taking into consideration of total discharge efficiency to the common AC bus (90.3 %) during winter times (1.19 factor) the BESU can support common AC bus with 204.9 kWh. The support of EVs (20.5 kWh) is DOD of 10.01 % and for consumers during power outage (20 kWh) is DOD 9.76 %. The BESU for the given DOD rates is capable of operating for 5 years and even longer if the batteries are not subjected to extreme stress.

If the operation of the DOD rate is designed in the middle of the SOC rate (45 %-55 %) the BESU is capable of providing capacity of 92.2 kWh-112.7 kWh to the common AC bus. This makes possible to utilize BESUs for EV fast charging support consecutively for 2 h and provide backup power capability for AC consumers consecutively for 1 h. Storing of renewable energy generation is

possible of 92.2 kWh-112.7 kWh. Although appealing, the consecutive charging or discharging over DOD 10 % rate shortens the number of battery pack discharge cycles.

STEP16 is to select appropriate ratings for the bidirectional power converters. As three EV bays require total of 141 kW of active power, AC-DC power converter operates with power factor close to unity the appropriate size for AC-DC power converter is 150 kVA. This meets the requirements for rectifying and as presented in the next chapter also for inversion.

According to STEP9 and STEP10 the total combined efficiency of discharging is 75.9 % - 90.3 % depending of the ambient temperature. Charging according to Table 6.1 is not affected from ambient temperature as much as discharging. The turnaround efficiency of charging and discharging is 68.5 % - 81.5 %. According to the BESU charging strategy, BESU should be ready to provide 41 kW of active power to the common AC bus for the next charging timezone in 30 minutes. Calculating according to coldest ambient temperatures the charging power required for BESU for supporting fast charging of EVs is 59.85 kW for 30 minutes (29.9 kWh). The maximum power required by the BESU AC-DC power converter is during the support of backup power capability. Therefore 100 kVA or higher bidirectional AC-DC power converter should be selected. According to STEP10 the maximum actual active powered required from the battery side during power outage was 105.4 kW. Therefore 2 pcs of 55 kW bidirectional DC-DC power converters are required for battery strings.

For given example E_{BESU}=20.5 kWh. The necessary storage media required is 150 pcs x 2 x 10.5 kg = 3150 kg [GWL/Power group]. It can be concluded that values presented in literatures [55] can be misleading. The reported energy densities Wh/kg are for suitable for mainly laboratory environments and limited number of discharge cycles. In practice, reserve considerations, number of discharge cycles for expected service life, discharge currents and temperature influences have to be considered. The benefit for Li-ion batteries is that Li-ion batteries are maintenance free and can last up to 5 years (even up to 10 years according to utilization) if selected accordingly. Ultracapacitors and flywheels do not enable long term backup support. Utilization of ultracapacitors and flywheels for similar applications have to be recalculated for particular applications and economical aspects considered before deciding on the optimum storage medium.

The methodology of sixteen steps gives the initial selection of the BESU size. The final BESU size should adjusted through economical and business side optimisations. The main economical benefits from utilizing V2G or BESU support comes from utilizing battery storage in a bigger electric system – reducing the cost of spinning reserves (start-up and shut-down), storing renewable energies [76], [77], [138]. Calculation of costs for running electric systems is out of the scope of this doctoral thesis.

6.2 Selection of BESU for extension distribution substation

In Fig. 2.8 the BESU for extension distribution substations is installed in the common DC bus side. The maximum active power available on common DC bus $P_{com}(t_{ch})$ (W) in Fig. 2.8 is:

$$P_{com}(t_{ch}) = P_{grid}(t_{ch}) \cdot \eta_{acdc} + P_{BESU}(t_{ch}) \cdot \eta_{dcdc} \cdot \eta_{BESU}(t_{ch}), \tag{72}$$

where $P_{grid}(t_{ch})$ is the maximum available grid active power (W), η_{acdc} is the efficiency of the AC-DC converter, $P_{BESU}(t_{ch})$ is the maximum power that can be drawn from BESU (W), η_{dcdc} is the efficiency of the DC-DC converter, $\eta_{BESU}(t_{ch})$ is the charging/discharging efficiency of the BESU batteries (including temperature influences and reserve considerations), and t_{ch} is the charging time (h). $P_{grid}(t_{ch})$ value can be lower than the total required charging power for the common DC bus to charge EVs. If one EV should require charging power $P_{EV,1}(t_{ch})$ (W) that is equal to the active power available on common DC bus, $P_{EV,1}(t_{ch})$ can be derived as:

$$P_{EV,1}(t_{ch}) = P_{com}(t_{ch}) \cdot \eta_{dcdc} \cdot \eta_{EV}(t_{ch}), \tag{73}$$

where $\eta_{EV}(t_{ch})$ is the charging efficiency of the EV battery to store electric energy. $P_{com}(t_{ch})$ can be derived for single EV as follows:

$$P_{com}(t_{ch}) = \frac{P_{EV,1}(t_{ch})}{\eta_{dcdc} \cdot \eta_{EV}(t_{ch})} = \sum_{j=1}^{n=1} \frac{P_{EV,j}(t_{ch})}{\eta_{dcdc,j} \cdot \eta_{EV,j}(t_{ch})}, \tag{74}$$

where n is the number of connected EV output feeders with the common DC bus (for simplification different EVs are assumed to have the same charging characteristics). If all active power is consumed that is available on the common DC bus, the necessary $P_{BESU}(t_{ch})$ can be derived from the following equations:

$$\sum_{j=1}^{n} \frac{P_{EV,j}(t_{ch})}{\eta_{dcdc,j} \cdot \eta_{EV,j}(t_{ch})} = P_{grid}(t_{ch}) \cdot \eta_{acdc} + P_{BESU}(t_{ch}) \cdot \eta_{dcdc} \cdot \eta_{BESU}(t_{ch}), \tag{75}$$

$$P_{BESU}(t_{ch}) \cdot \eta_{dcdc} \cdot \eta_{BESU}(t_{ch}) = \sum_{j=1}^{n} \frac{P_{EV,j}(t_{ch})}{\eta_{dcdc,j} \cdot \eta_{EV,j}(t_{ch})} - P_{grid}(t_{ch}) \cdot \eta_{acdc}, \tag{76}$$

The power required to charge EV battery depends on the EV battery capacity and the charging cycle from initial SOC to final SOC. Using equation (74) the necessary power for one substation feeder can be deducted as:

$$P_{ch}(t_{ch}) = \frac{E_{EV,1\_r}}{t_{ch}} \cdot \frac{SOC_f - SOC_i}{\eta_{dcdc} \cdot \eta_{EV}(t_{ch})} = \sum_{j=1}^{n=1} \frac{E_{EV,j\_r}}{t_{ch}} \cdot \frac{SOC_{f,j} - SOC_{i,j}}{\eta_{dcdc,j} \cdot \eta_{EV,j}(t_{ch})}, \qquad (77)$$

where $P_{ch}(t_{ch})$ is the power required to charge EV battery (W), $E_{EV,1\_r}$ is the rated full energy capacitance (kWh) of a EV battery pack, SOC_f is the final battery SOC value (%) at the end of the charging, and SOC_i is initial battery SOC value (%) at the beginning of the charging. The faster the EV battery is required to be charged (e.g. in 30 minutes) the more charging power is required. BESU can provide the necessary additional energy boost for charging to avoid loading the grid. The required support from BESU can be deducted from equations (76), (77):

$$P_{BESU}(t_{ch}) = \sum_{j=1}^{n} \frac{E_{EV,j\_r}}{t_{ch}} \cdot \frac{SOC_{f,j} - SOC_{i,j}}{\eta_{TEV,j}(t_{ch}) \cdot \eta_{TBESU}(t_{ch})} - P_{grid}(t_{ch}) \cdot \frac{\eta_{acdc}}{\eta_{TBESU}(t_{ch})}, \qquad (78)$$

where $\eta_{TBESU}(t_{ch})$ is total efficiency of the BESU circuit ($\eta_{TBESU}(t_{ch}) = \eta_{dcdc} * \eta_{ESU}(t_{ch})$) and $\eta_{TEV}(t_{ch})$ is total efficiency of the EV circuit ($\eta_{TEV,j}(t_{ch}) = \eta_{dcdc,j} * \eta_{EV,j}(t_{ch})$). The necessary amount of stored energy required from an BESU ($E_{ESU}(t_{ch})$) to support common DC bus output feeders in fast charging can be deduced as follows:

$$E_{ESU}(t_{ch}) = \sum_{j=1}^{n} \frac{E_{EV,j\_r} \cdot (SOC_{f,j} - SOC_{i,j})}{\eta_{TEV,j}(t_{ch}) \cdot \eta_{TESU}(t_{ch})} - P_{grid}(t_{ch}) \cdot \frac{\eta_{acdc}}{\eta_{TESU}(t_{ch})} \cdot t_{ch}. \qquad (79)$$

In addition DOD ratings for prolonging batteries have to be considered. For a distribution substation, which has to supply several EVs at the same time, the average power (burden to the grid) in the observed time scale (T) can be expressed as an arithmetic mean value:

$$P_{av} = \frac{n_{EV}}{T} \cdot \int_0^T P_{gr}(t_{ch}) dt, \qquad (80)$$

where P_{av} is the average power drawn from the grid (W), $P_{gr}(t_{ch})$ is the charging power required to charge one EV (W), T is the observed time scale (h), and n_{EV} is the number of EVs connected to the grid. The expression can be simplified for a pre-determined charging time:

$$P_{av}(t_{ch}) = \frac{\sum_{j=1}^{n} E_{EV,j\_r} \cdot (SOC_{f,j} - SOC_{i,j})}{T \cdot \eta_{conv} \cdot \eta_{EV}(t_{ch})}, \qquad (81)$$

where η_{conv} is the efficiency of the converter (e.g. DC-DC converter).

6.3 Capacities of EVs for peak shaving of utility network loads

Battery electric vehicles are becoming more and more attractive with the advancement of Li-ion battery technology. Many car manufacturers have developed their own versions of EVs. E.g. Mitsubishi i-MiEV [39] and Citroën C-Zero have a 16 kWh 50 Ah Li-ion battery pack with nominal voltage of 330 V. If these EVs are discharged at 2 C rate (100 A), the output power from the EV battery is 33 kW. Considering efficiencies of power converters 95 % for the bidirectional DC-DC power converter [125], 96 % for the bidirectional AC-DC power converter [81] and discharge efficiency of EV Li-ion battery pack (93 % [136]), maximum of 28 kW of active power can be extracted from one EV to the common AC bus of LV side (total combined efficiency of 85 %). Electric vehicle owners prefer that their EV batteries are discharged as little as possible as every discharge cycle degrades the batteries. Considering depth of discharge (DOD) of 20 % (3.2 kWh from EV side), 28 kW of active power to the LV side can be extracted from one EV for ≈6 minutes (3.2 kWh with 33 kW from EV side). The more EVs are connected to the common DC bus the more active power can be extracted.

For example three bays can provide 84 kW of active power for 6 minutes during summer times in Northern Europe (25 $^{\circ}$C). Considering factor of 1.5 (-30 $^{\circ}$C) in the Table of 6.1, three bays can provide 56 kW of active power for 6 minutes during winter times. Considering power factor of 0.8, the maximum inverter size required would be 105 kVA which demand is met by the 150 kVA bidirectional AC-DC power converter. The extraction of active power from EVs is illustrated in Fig 6.1 (DOD=10%) and in Fig. 6.2 (DOD=20%). The more EVs are connected the more active power can be extracted. Differences between DOD rates are in the duration of active power extraction.
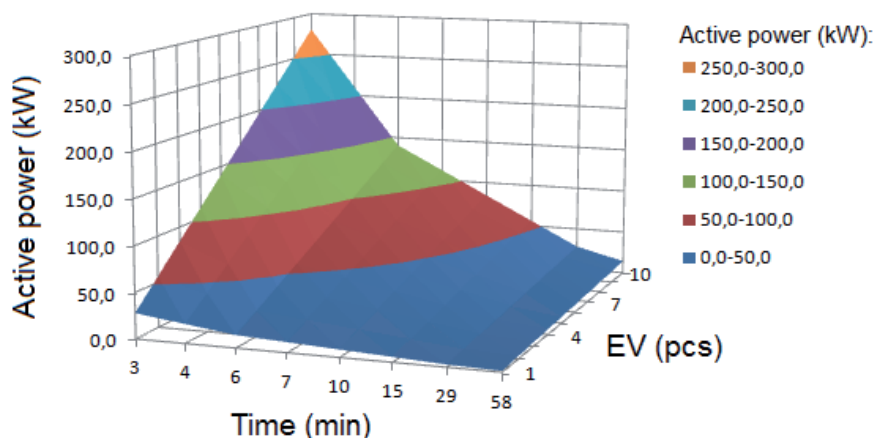
Fig. 6.1 Extraction of active power from EVs for V2G session (DOD=10 %)
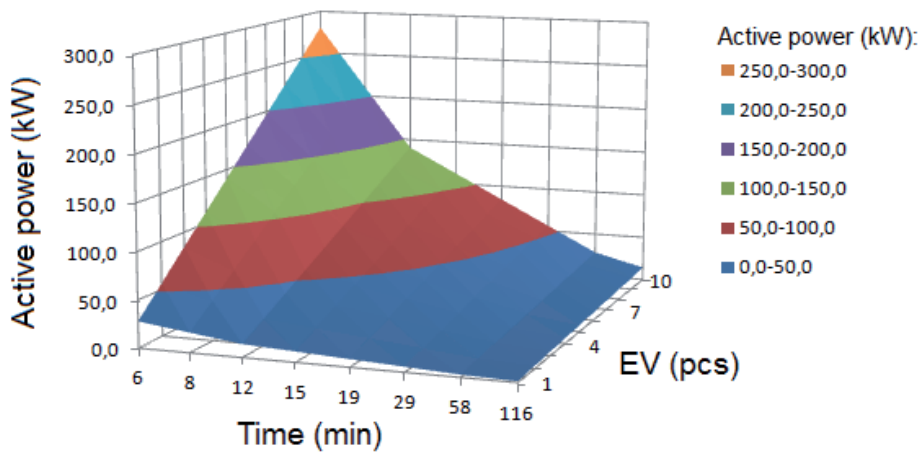
Fig. 6.2 Extraction of active power from EVs for V2G session (DOD=20 %)

Considering total combined efficiency of 85 % for both charging and discharging of EVs, the turnaround efficiency of storing energy into EVs and extraction of energy for V2G applications is 72.2 %.

6.4 Designing of distribution substation with V2G capability

The construction of distribution substations depend on several parameters which have to be clarified with the future owner of the distribution substation (influences the cost of the substation). The general design parameters are presented in Table 6.3 with some practical examples. The main design issues are the requirements for the housing of the distribution substation depending on where it is installed; requirements for the MV switchgears, LV switchgears and auxiliary switchgears inside the distribution substation; requirements for bidirectional power converters and supply of EVSEs; requirements for remote terminal unit how the distribution substation is controlled remotely and which data can be accessed remotely.

Tables 6.4 describes the selection of AC-DC converters, transformers and BESUs for common AC bus for charging aggregated number of EVs. The selection of AC-DC power converters are taken e.g. from ABB series ESI-M and ESI-I, which enable to connect 32 inverters in parallel [4]. Transformer ratings are e.g. reduced to one size lower rating. Depth of discharge for BESUs is 10 % for prolonging up to 5 years (10 years).

Table 6.5 describes the selection of AC-DC converters and BESUs for backup support during power outage. Depth of discharge for BESUs is not limited as power outages are seldom. Discharge rate for BESUs is limited e.g. up to 2C.

The selection of BESU should be selected from previous sixteen steps or from selecting the according maximum ratings between Tables 6.4 and 6.5.

Table 6.3. Technical specification for distribution substations with V2G capability

SUBSTATION DATA	
Serviced from inside or outside	Inside service
Foundation	Concrete foundation
Heat insulation requirements	Uninsulated concrete
Wall material and colour	Concrete 100mm, RR21 light grey
Roof material, insulation and colour	Weather-proof profiled sheet, insulated, RR21 light grey
Door material and colour	Fire resistant door, RR21 light grey
Ventilation for transformers (natural, forced)	Forced ventilation
Ventilation power for transformers	according to requirements
Ventilation for switchgears (natural, forced)	Forced ventilation for bidirectional power converters
Ventilation power for switchgears	according to requirements of power converter manufacturers
Filters	Dust filters
IP degree of ventilation	IP43D
IP degree of substation	IP43D
Heating	1x1000W radiators on the wall
Heating required for switchgear and devices	yes
Class of fire safety for substation enclosure	EI60
Class of fire safety for ventilation	not required
Construction requirements (substation and devices)	technical description
Main earthing bar	40x10 Cu
Security boom for door	yes
Direction of output cabling	bottom
Cable cellar underneath	yes
Oil collectors for transformers	included
Fire alarm systems	technical description
Security and maintenance systems	technical description
List of corresponding standards	technical description

ELECTRIC SYSTEM ARCHITECTURE FOR ELECTRIC VEHICLES	
Number of EVSE bays	according to el.drawing
Timezones and active power management	technical description
BESU requirements	technical description
Computing requirements for SAS	technical description
Data storage and access (e.g. cloud application)	technical description

Table 6.3. Technical specification for distribution substations with V2G capability (continued)

MEDIUM VOLTAGE SWITCHGEAR	
Type of MV switchgear (SF6, vacuum, air insulated)	SF6
Electric circuit diagram of MV switchgear	according to el.drawing
Construction requirements (switchgear and devices)requirements for SAS	technical description
IP degree of MV switchgear	IP3X
Rated voltage, current, short-time and peak withstand current	according to el.drawing
Rated insulation level	according to el.drawing
Control of devices	motorized circuit-breakers
Control voltage of devices	110 V DC
Auxiliary contacts and mechanical interlocking	technical description
Heating	50W heaters
Voltage transformers or sensors	technical description
Transformer for substation own consumption	technical description
Commercial measurements	technical description
Relay protection and remote reading	technical description
Parametrising and testing of relay protections	included
List of signals for outgoing terminals	technical description
Local control requirements	technical description
Auxiliary system	technical description
Automatic reserve switching (ARS)	technical description
Earth fault compensation system, Current limitation, Capacitor bank	technical description
Incoming/outgoing connection types, sizes and direction	technical description
List of corresponding standards	technical description

POWER TRANSFORMERS	
Size (kVA, dimensions) and number of transformers	according to el.drawing
Temperature protection for transformers	according to el.drawing
Data for reversing power transformers	technical description
Scope of supply	Utility network on site

Table 6.3. Technical specification for distribution substations with V2G capability (continued)

LOW VOLTAGE SWITCHGEAR	
Electric circuit diagram of LV switchgear	according to el.drawing
Construction requirements (switchgear, devices, earthing)	technical description
Technical parameters (Rated voltage, current, IP degree etc)	according to el.drawing
Technical requirements for devices (e.g. bidirectional power converters)	technical description
Technical requirements for isolation monitoring and islanding operations	technical description
Communication protocol between devices (e.g. IEC61850)	technical description
Incoming/outgoing connection types, sizes and direction	technical description
Heating	not required
Commercial measurements	technical description
Automatic reserve switching (ATS)	technical description
Reserve space	10%
List of corresponding standards	technical description

OWN CONSUMPTION OF SUBSTATION	
Electric circuit diagram of LV switchgear (sockets, lighting etc)	according to el.drawing
Construction requirements (switchgear and devices)	technical description
Technical parameters (Rated voltage, current, IP degree etc)	according to el.drawing
Heating	not required
Commercial measurements	not required
List of corresponding standards	technical description

Table 6.3. Technical specification for distribution substations with V2G capability (continued)

CABLING DATA	
Cabling list	according to specifications
Cable installations	technical description
Internal MV power cabling	technical description
Internal LV power cabling	technical description
Internal auxiliary distribution cabling	technical description
Internal auxiliary measurement cabling	technical description
Internal telecommunication and data cabling	technical description
Internal optical cabling	technical description
Cable marking and labelling	technical description

REMOTE TERMINAL UNIT (RTU)	
Telemechanics	
Construction and technical requirements (switchgear and devices)	technical description
Heating	75W heater
Single line diagram (or list) of RTU devices and terminals	according to el.drawing
Channel and protocol for SCADA connection	IEC 60870-5-101
Protocol for data transmission	IEC 60870-5-103
Time synchronization	technical description
List of corresponding standards	list
Parametrising and testing of RTU	included
Telecommunication signals (State signals)	
Positions/States of MV equipment	list
Positions/States of LV equipment	list
Relay protection data	list
RTU data	list
Substation data (e.g. position of door, burglar alarm)	list
Alarm and indication signals	
Device fault or trip signals (MV and LV switchgears)	list
Device fault or trip signals (DC auxiliary power switchgear)	list
Monitoring signals (no voltage present, over/under temperature)	list
Protection signals	list
Alarm signals (e.g. fire alarm)	list

Table 6.3. Technical specification for distribution substations with V2G capability (continued)

REMOTE TERMINAL UNIT (RTU)	
Telecommunication control (Control signals)	
Remote control of MV switchgear devices (e.g. motors in/out)	list
Remote control of LV switchgear devices (e.g. motors in/out)	list
Return signals for alarm states	list
Relay protection signals	list
RTU control	list
Telecommunication measurements (Remote reading)	
MV switchgear values (e.g. voltages, currents, kW, kvar)	list
LV switchgear values (e.g. voltages, currents, kW, kvar)	list
Relay protection data	list

DC AUXILIARY POWER SWITCHGEAR	
Construction and technical requirements (switchgear and devices)	technical description
Technical parameters (Rated voltage, current, IP degree etc)	according to el.drawing
Electric circuit diagram of DC switchgear	according to el.drawing
Heating	100W heating mat around batteries
List of corresponding standards	technical description
Battery data	
Battery data (type, voltage, Ah, lifetime)	technical description
Requirements for batteries	technical description
Battery charger data	technical description
Control and state signals	technical description
Measurement signals	technical description
Alarm and indication signals	technical description
List of corresponding standards	technical description

DESIGNING	
Design and layout of distribution substation	manufacturer
Design and layout of MV switchgear	manufacturer
Design and layout of LV switchgear	manufacturer
Design and layout of DC switchgear	manufacturer
Design and layout of RTU switchgear	manufacturer
Design and layout of BESU switchgear	manufacturer

Table 6.3. Technical specification for distribution substations with V2G capability (continued)

TRAINING	
Operation of MV, LV, DC and BESU switchgear	according to agreement
Operation of relay protection	according to agreement
Operation of RTU	according to agreement
Exploitation and maintenance	according to agreement
ADDITIONAL	
Testing requirements	according to agreement
Transportation requirements	according to agreement
Documentation requirements	according to agreement
Spare parts and accessories	according to agreement

Table 6.4. Selection of AC-DC converters and BESUs for charging EVs (transformer rating lowered by one size, DOD of BESU is 10%)

EVSE, pcs	Max load, kVA	Limited load, kVA	BESU Support, kVA/kWh	AC-DC converters for EV side	BESU size required	BESU strings
3	141	100	41/20.5	3x51kW (3x70A)	54 kW 270 kWh	2x 300Ah 450 V DC (150x3V) 0.2C
4	188	160	28/14	3x72kW (3x100A)	36.9 kW 184 kWh	2x 300 Ah 309 V DC (103x3V) 0.2C
5	235	200	35/17.5	3x94kW (3x130A)	46.1 kW 231 kWh	2x 300Ah 387 V DC (129x3V) 0.2C
6	282	250	32/16	3x94kW (3x130A)	42.2 kW 211 kWh	2x 300Ah 354 V DC (118x3V) 0.2C
7	329	315	14/7	4x94kW (4x130A)	18.4 kW 92 kWh	1x 200 Ah 462 V DC (154x3V) 0.2C
8	376	315	61/30.5	4x94kW (4x130A)	80,4 kW 402 kWh	2x 400Ah 504 V DC (168x3V) 0.2C
9	423	400	23/11.5	4x108kW (4x150A)	30,3 kW 152 kWh	2x 200 Ah 381 V DC (127x3V) 0.2C
10	470	400	70/35	5x94kW (5x130A)	92,2 kW 461 kWh	3x 300Ah 513 V DC (171x3V) 0.2C

Table 6.5. Selection of AC-DC converters and BESUs for backup support during power outage (DOD of BESU is 100%, maximum discharge rate 2C)

BESU load, kVA	BESU load, kW	Duration, min	Support, kW/kWh	AC-DC converters for BESU side	BESU size required	BESU strings
100	80	15	80/20	1x108kW (1x150A)	105.4 kW 26 kWh	1x 100Ah 540 V DC (180x3V) 1.95C
100	80	30	80/40	1x108kW (1x150A)	105.4 kW 53 kWh	1x 100Ah 540 V DC (180x3V) 1.95C
100	80	60	80/80	1x108kW (1x150A)	105.4 kW 105 kWh	2x 100Ah 540 V DC (180x3V) 0.98C
200	160	15	160/40	1x216kW (1x300A)	210.9 kW 53 kWh	1x 200Ah 540 V DC (180x3V) 1.95C
200	160	30	160/80	1x216kW (1x300A)	210.9 kW 105 kWh	1x 200Ah 540 V DC (180x3V) 1.95C
200	160	60	160/160	1x216kW (1x300A)	210.9 kW 211 kWh	2x 200Ah 540 V DC (180x3V) 0.98C
300	240	15	240/60	1x324kW (1x450A)	316.3 kW 79 kWh	1x 300Ah 540 V DC (180x3V) 1.95C
300	240	30	240/120	1x324kW (1x450A)	316.3 kW 158 kWh	1x300Ah 540 V DC (180x3V) 1.95C
300	240	60	240/240	1x324kW (1x450A)	316.3 kW 316 kWh	2x300Ah 540 V DC (180x3V) 0.98C

6.5 Generalizations

The parameters calculated in this chapter are summarized in the single line diagram (Fig. 6.3). Protection devices for power converters should be selected according to manufacturer's specifications. Selection of power transformers must consider higher voltages in the secondary winding during reverse feeding sequence. Energy density of Li-ion batteries in distribution substations for 5-10 year service time is around 6.5 Wh/kg (for Northern Europe).

The turnaround efficiency of charging and discharging in the extension substation (BESU in the DC side) is 71.3 % - 84.9 % for peak shaving of EV side charging loads, which is 2.8 % - 3.4 % better than in the main distribution substation, but does not have the variety of utilization options for the LV AC side applications.
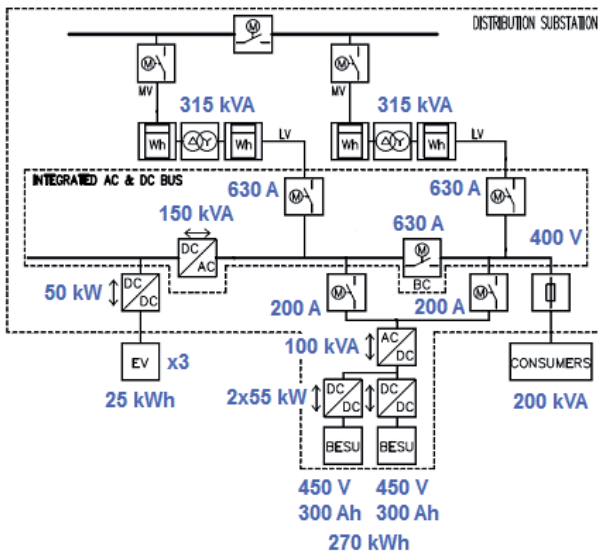

Fig. 6.3 Selection of parameters for an example distribution substation with V2G capability (IT earthing system)

7. FUTURE RESEARCH AND DEVELOPMENT

The current doctoral thesis was concentrated on the control system development for distribution substations with V2G capability. The next challenge for the author is to use the acquired knowledge and experience in the experimental laboratory test bench to finish research of energy flows and data communication during EV charging and discharging. The basic functions and operation modes (including protection algorithms), such as energy transmission from the power grid to the energy storing system, EV battery charging and discharging, balancing power loads and other functions have to be tested and analyzed. Management and control algorithms for the microgrid controller have to be fine-tuned. During experimentation, data values will be collected for further analysis. Primary goals in the construction of the microgrid are to analyze the quality of energy flow, efficiency and harmonic levels during EV charging and discharging through the microgrid and electromagnetic compatibility related issues. The analysis will indicate needs for modifications to be made in the microgrid structure to optimize and improve the overall efficiency and power factor levels in the system to ensure the quality of electricity in accordance with international standards. The efficiency and overall performance depend directly on the chosen control algorithm. Practical applications will show possible drawback areas in the communication between the devices, which will then have to be solved with different control algorithms. Future studies will focus more on microgrid solutions with distributed energy resources. Further studies will address possibilities to transfer energy to the common AC bus or to the power grid for peak shaving of loads with synchronization related issues. Results from microgrid experiments will be reported in the scientific papers and future doctoral theses of the Department of Electrical Engineering of Tallinn University of Technology.

Currently the main efforts are focused on:
- Experiments with the microgrid will give vital data about the charging and discharging algorithms for EVs and communication between the devices. From these studies it will be possible to construct a larger real life substation capable of supplying power to several EV charging stations and that will be part of a microgrid or even a viable module of Smart Grid solutions;
- New type of MMI-type bidirectional AC-DC power converters and bidirectional DC-DC converters have to be developed and tested on the laboratory test bench;
- Specific control algorithms for reverse feeding of transformers have to be developed and tested. Another technical solution proposed in TUT is the usage of electronic transformers [139]. The economical selection, benefits and limits between those two solutions has to be analyzed in more detail;
- Further development of distribution substations with V2G capability have to consider the usage of TN-C and TN-S earthing systems;

- Communication with DSO and Retailer through Smart Grid communication protocols have to analyzed and tested.

A pilot V2G project on a real test site with a real distribution substation is under development with cooperation of AS Harju Elekter Elektrotehnika. The behaviour of the complete system of the pilot project has be studied and analyzed before mass production of distribution substations with V2G capability. Thus, these are the perspective topics for the postdoctoral studies of the author.

The author considers that three main EV charging types will be utilized in the future. In the public charging current state of art unidirectional fast charging stations or ultra-fast charging stations will be used. For new semi-public charging next generation distribution substations with V2G capability will be used. In home charging V2H charging stations will be used. The rise of V2G demand will make commercial bidirectional power converters more available than in the current market situation. The control of aggregated number of EVs will depend on the control and protection system architectures implemented in distribution substations. The main limitation in the implementation of new technologies, as it is for Smart Grid solutions in general, is the overall higher cost of the system, which requires a long term commitment for return of investments.

CONCLUSIONS

In the current doctoral thesis topologies and control systems for distribution substations with V2G capability were studied and analyzed. That knowledge was used to design and assemble of laboratory test bench for microgrid applications. As the developed control system has been built and optimised according to the most recent development trends and design requirements of Smart Grids together with novel design proposals from the author, the doctoral thesis has a great practical value for the industry.

In general, the doctoral thesis has the following results:

1. distribution substation topology with integrated AC and DC bus was developed to solve the problem of integrating aggregated number of EVs for both to the low voltage and the medium voltage side of the utility network;
2. based on the valuable information that was gathered from the analysis of recent technologies and development trends, the author has developed a novel control system architecture with eleven layers;
3. from the analysis of recent technologies in the bidirectional power converter topologies the selection of power converter topologies for distribution substations with integrated AC and DC bus was proposed with additional improvements to the power converter topologies from the author;
4. during the analytical part of the doctoral thesis computer models for distributions substations with V2G capability were developed. The models create an excellent basis for further development and research. The models have demonstrated the feasibility of distribution substations with V2G capability to provide ancillary services to the utility network and to low voltage side consumers;
5. development and construction of a laboratory test bench allows to study real energy flows in distribution substations for microgrid applications. The results can be implemented in further development of the substation automation system;
6. development of prototype of modular 460 V DC Li-ion battery pack energy storage device in cooperation with Estonian company AS Harju Elekter Elektrotehnika;
7. general design guidelines and recommendations for constructing distribution substations with V2G capability for the EV infrastructure were elaborated.

In general, the doctoral thesis has the following results regarding to current problems in Smart Grid applications (summarized in the proposal of international collaborative project FP7-ICT-2013-11 under the 7th framework programme [30]):

-   distribution substation topology was developed for active distribution grids/networks;
-   control schemes for the microgrid central controller at the MV/LV substation automation system was studied and developed;
-   the performance of developed schemes was evaluated through computer simulations. It has been proven through simulations that an integrated AC and DC bus is the main topology solution for integrating fast charging stations for EVs to power grids. Simulation results have verified that bidirectional energy exchange between the utility network and EVs can be used for peak shaving of utility networks loads.

The current doctoral thesis involved both theoretical and practical investigations. The control architecture was developed in accordance with requirements from AS Harju Elekter Elektrotehnika and corresponding norms. Recent technologies and components were combined with several improvements proposed by the author. As a result a new type of distribution substations with V2G capability was designed.

The general thesis objectives were fulfilled. The doctoral thesis includes scientific and practical novelties. Research findings have been published in international scientific publications. Tallinn University of Technology sold a manufacturing licence with appropriate technical documentation to AS Harju Elekter Elektrotehnika.

REFERENCES

[1]   Smart grids: infrastructure, technology and solutions. / ed. S. Borlase. CRC Press, 2013.

[2]   ELMO – Estonian Electromobility Programme, http://www.elmo.ee/en/, 22. May 2013.

[3]   AS Harju Elekter Elektrotehnika, http://www.harjuelekter.com/et/as-harju-elekter-elektrotehnika, 22. May 2013.

[4]   ABB Energy Storage Modules (ESM), http://www.abb.com, 22. May 2013.

[5]   Dehaghani, E.S.; Williamson, S.S., "On the Inefficiency of Vehicle-to-Grid (V2G) Power Flow: Potential Barriers and Possible Research Directions," Transportation Electrification Conference and Expo, ITEC 2012. IEEE, pp. 1-5, 2012.

[6]   Zhang, Y.; Chen, L., "Model and Harmonic Control Strategy of Electric Vehicle Chargers Connected with the Power System," Power Engineering and Automation Conference, PEAM 2011. IEEE, pp. 524-528, 2011.

[7]   Gao, S.; Chau, K.T.; Chan, C.C.; Wu, D., "Loss Analysis of Vehicle-to-Grid Operation," Vehicle Power and Propulsion Conference, VPPC 2010. IEEE, pp. 1-6, 2010.

[8]   Ota, Y.; Taniguchi, H.; Nakajima, T.; Liyanage, K.M.; Baba, J.; Yokoyama, A., "Autonomous Distributed V2G (Vehicle-to-Grid) Satisfying Scheduled Charging," Innovative Smart Grid Technologies Conference Europe, ISGT 2010. IEEE, pp. 1-6, 2010.

[9]   Lassila, J.; Haakana, J.; Tikka, V.; Partanen, J., "Methodology to Analyze the Economic Effects of Electric Cars as Energy Storages," Smart Grid, IEEE Transactions on. IEEE, pp. 506-516, 2011.

[10]   He, Y.; Venkatesh, B.; Guan, L., "Optimal Scheduling for Charging and Discharging of Electric Vehicles," Smart Grid, IEEE Transactions on. IEEE, pp. 1095-1105, 2012.

[11]   Wang, S.; Zhang, N.; Li, Z.; Shahidehpour, M., "Modelling and Impact Analysis of Large Scale V2G Electric Vehicles on the Power Grid," Innovative Smart Grid Technologies, ISGT Asia 2012. IEEE, pp. 1-6, 2012.

[12]   Soares, J.; Morais, H.; Sousa, T.; Vale, Z.; Faria, P., "Day-Ahead Resource Scheduling Including Demand Response for Electric Vehicles," Smart Grid, IEEE Transactions on. IEEE, pp. 595-605, 2013.

[13]   Liu, H.; Ning, H.; Zhang, Y.; Guizani, M., "Battery Status-aware Authentication Scheme for V2G Networks in Smart Grid," Smart Grid, IEEE Transactions on. IEEE, pp. 99-110, 2013.

[14]   Han, S.; Han, S., "Economics of V2G Frequency Regulation in Consideration of the Battery Wear," Innovative Smart Grid Technologies, 2012 3rd IEEE PES International Conference and Exhibition on, ISGT 2012. IEEE, pp. 1-8, 2012.

[15]   Marra, F.; Sacchetti, D.; Tr holt, C.; Larsen, E., "Electric Vehicle Requirements for Operation in Smart Grids," Innovative Smart Grid Technologies, 2011 2nd IEEE PES International Conference and Exhibition on, ISGT 2011. IEEE, pp. 1-7, 2011.

[16]   Arancibia, A.; Strunz, K., "Autonomous Control of Electric Vehicles in Grid-connected and Islanded Modes," Innovative Smart Grid Technologies, 2012 3rd IEEE PES International Conference and Exhibition on, ISGT 2012. IEEE, pp. 1-7, 2012.

[17]   Venayagamoorthy, G.K.; Mitra, P.; Corzine, K.; Huston, C., "Real-Time Modelling of Distributed Plug-in Vehicles for V2G Transactions," Energy Conversion Congress and Exposition, ECCE 2009. IEEE, pp. 3937-3941, 2009.

[18]   Singh, M.; Kumar, P.; Kar, I., "Coordination of Multi Charging Station for Electric Vehicles and its Utilization for Vehicle to Grid Scenario," Transportation Electrification Conference and Expo, ITEC 2012. IEEE, pp. 1-7, 2012.

[19]   Esmaeilian, H.R.; Bioki, M.M.H.; Rashidinejad, M.; Abdollahi, A., "Economic-Driven Measure in Constructing a V2G Parking Lot from DisCo. Perspective," International Journal of Economics and Management Engineering (IJEME), pp. 117-124, 2012.

[20]   Shumei, C.; Xiaofei, L.; Dewen, T.; Qianfan, Z.; Liwei, S., "The Construction and Simulation of V2G System in Micro-grid," Electrical Machines and Systems, ICEMS 2011. IEEE, pp. 1-4, 2011.

[21]   Wu, D.; Liu, C.; Gao, S., "Coordinated Control on a Vehicle-to-Grid System," Electrical Machines and Systems, ICEMS 2011. IEEE, pp. 1-6, 2011.

[22]   Tian, W.; He, J.; Niu, L.; Zhang, W.; Wang, X.; Bo, Z., "Simulation of Vehicle-to-Grid (V2G) on Power System Frequency Control," Innovative Smart Grid Technologies, ISGT Asia 2012. IEEE, pp. 1-3, 2012.

[23]   Bao, K.; Zheng, H., "Battery Charge and Discharge Control for Energy Management in EV and Utility Integrations," Power and Energy Society General Meeting, 2012 IEEE. IEEE, pp. 1-8, 2012.

[24]   Kim, K.; Yoon, T.; Byeon, G.; Jung, H.; Kim, H.; Jang, G., "Power Demand and Power Quality Analysis of EV Charging Station using BESS in Microgrid," Vehicle Power and Propulsion Conference, VPPC 2012. IEEE, pp. 996-1001, 2012.

[25]   Kempton, W.; Udo, V.; Huber, K.; Komara, K.; Letendre, S.; Baker, S.; Brunner, D.; Pearre, N., "A Test of Vehicle-to-Grid (V2G) for Energy Storage and Frequency Regulation in the PJM System," University of Delaware Report, pp. 1-32, 2008.

[26]   INL Idaho National Laboratory, "Vehicle-to-grid (V2G) Power Flow Regulations and Building Codes Review by the AVTA", Sep. 2012.

[27]   Andersen, P.B.; Garcia-Valle, R.; Kempton, W., "A Comparison of Electric Vehicle Integration Projects," Innovative Smart Grid

Technologies, 2012 3rd IEEE PES International Conference and Exhibition on, ISGT 2012. IEEE, pp. 1-7, 2012.

[28]	Projects of European Geen Cars Initiative,
http://www.green-cars-initiative.eu/projects, 22. May 2013.

[29]	NIST Special Publication 1108R2, "NIST Framework and Roadmap for Smart Grid Interoperability Standards, Release 2.0", Feb. 2012.

[30]	Proposal of collaborative project (STREP) FP7-ICT-2013-11 under 7th framework programme, "Smart, Scalable On-Line Optimization Platform for prosumers", April 2013.

[31]	Electropaedia, Rechargeable Lithium Batteries,
http://www.mpoweruk.com/lithiumS.htm, 22. May 2013.

[32]	Panasonic, Lithium Ion Batteries Technical Handbook,
http://industrial.panasonic.com/www-data/pdf/ACI4000/ACI4000PE5.pdf, 22. May 2013.

[33]	Lithium-ion battery, https://en.wikipedia.org/wiki/Lithium-ion_battery, 22. May 2013.

[34]	Is Lithium-ion the Ideal Battery?,
http://batteryuniversity.com/learn/article/is_lithium_ion_the_ideal_battery, 22. May 2013.

[35]	Continental, Electric Battery Actual and future Battery Technology Trends, http://www.futureage.eu/files/dd33e86df1_prezentace_Birke.pdf, 22. May 2013.

[36]	http://en.wikipedia.org/wiki/Mitsubishi_i-MiEV, 22. May 2013.

[37]	Mitsubishi Motors Corporation, Features of the "i MiEV",
http://www.mitsubishi-motors.com/special/ev/whatis/index.html, 22. May 2013.

[38]	Green Car Congress, The Battery Pack for Mitsubishi's i MiEV,
http://www.greencarcongress.com/2008/05/the-battery-pac.html, 22. May 2013.

[39]	Kamachi, M.; Miyamoto, H.; Sano, Y., "Development of Power Management System for Electric Vehicle "i-MiEV"," Power Electronics Conference (IPEC) 2010. IEEE, pp. 2949-2955, June. 2010.

[40]	Andersson, D.; Carlsson, D., "Measurements of ABB's Prototype Fast Charging Station for Electric Vehicles. A contribution towards standardized models for voltage and transient stability analysis," Master of science thesis, Chalmers University of Technology, Göteborg, Sweden, 2012.

[41]	http://en.wikipedia.org/wiki/Nissan_Leaf, 22. May 2013.

[42]	Automotive Energy Supply Corporation,
http://www.eco-aesc-lb.com/en/product/liion_ev/, 22. May 2013.

[43]	Foosn s, A.H., "Report: WP1.1 Electric Vehicle Technology," EDISON Deliverable 1.1, pp. 44, Nov. 2010, http://www.edison-net.dk, 22. May. 2013.

[44] NetCarShow.com, Mitsubishi i-MiEV,
http://www.netcarshow.com/mitsubishi/2011-i-miev/, 22. May 2013.

[45] Dearborn, S., "Charging Li-ion Batteries for Maximum Run Times," Power Electronics Technology, vol. 31, issue 4, pp. 9, April 2005.

[46] Fleischer, C., "State of the Art of Batteries and Charging Concepts," ECPE Workshop on Power Electronics for Charging Electric Vehicles, 26 p., March 2011.

[47] Schwartz, R., "Battery Charging Strategies. Control & Battery Monitoring System," ECPE Workshop on Power Electronics for Charging Electric Vehicles, 30 p., March 2011.

[48] Nørgaard, P.; Camacho, O.M.F., "D4.2/D4.3/D4.6 Fast Charging of EV Batteries – Tests at Syslab," EDISON   D4.2/D4.3/D4.6, pp. 49, April 2012, http://www.edison-net.dk, 22. May 2013.

[49] Orion BMS manuals, http://www.orionbms.com/resources/, 22. May 2013.

[50] Hu, Y.; Liu, H.; Liu, P., "Criterion of Constant Current Charging End for Lithium Iron Phosphate Batteries," Journal of Convergence Information Technology (JCIT), Volume 7, Number 6, pp. 24-32, April 2012.

[51] GWL/Power group, Long time balancing – a slow way to damage the lithium cells, http://gwl-power.tumblr.com/tagged/TechReport, 22. May 2013.

[52] Battery University, How to Prolong Lithium-based Batteries,
http://batteryuniversity.com/learn/article/how_to_prolong_lithium_based_batteries, 22. May 2013.

[53] Buchmann, I., "High-power lithium-ion, a new area in portable power," http://www.buchmann.ca/Article27-Page1.asp, 22. May 2013.

[54] Lukic, S.M.; Cao, J., "Energy Storage Systems for Automotive Applications," IEEE Transactions on Industrial Electronics, Volume 55, Number 6, pp. 2258-2267, June 2008.

[55] Policy Department Economic and Scientific Policy, Outlook of Energy StorageTechnologies, http://www.storiesproject.eu/docs/study_energy_storage_final.pdf, 22. May 2013.

[56] Muñoa, J.A., "Infrastructure for Domestic, Workshop abd Shopping AC Charging," ECPE Workshop on Power Electronics for Charging Electric Vehicles, 50 p., March 2011.

[57] http://www.chademo.com/, 22. May 2013.

[58] Magraner, J.M., "Ultra-Fast DC Charging Stations," ECPE Workshop on Power Electronics for Electric Vehicles, pp. 23, March 2011.

[59] Anegawa, T., "Safety Design of CHAdeMO Quick Charging System," World Electric Vehicle Journal, vol. 4, pp. 855-859, Nov. 2010.

[60] Terra 51, http://www.abb.com, 22. May 2013.

[61] Hõimoja, H.; Rufer, A., "Infrastructure Issues Regarding the Ultrafast Charging of Electric Vehicles," International Advanced Mobility Forum IAMF 2012, Geneva, Switzerland, pp. 8, March 2012.

[62] Altairnano, http://www.b2i.cc/Document/546/50Ah_Datasheet-012209.pdf, 22. May 2013.

[63] Power Quality Application Guide, http://www.copperinfo.co.uk/power-quality/downloads/pqug/542-standard-en-50160-voltage-characteristics-in.pdf, 22. May 2013.

[64] EN 50160, "Voltage characteristics of electricity supplied by public electricity networks," 2010.

[65] Vinnal, T., "Study of Electric Power Consumption in Estonian Companies and Recommendations for Optimization of Consumption," Ph.D. Thesis, Tallinn University of Technology, Tallinn, Estonia, 2011.

[66] Eesti elektrisüsteemi varustuskindluse aruanne 2011, http://elering.ee/public/Infokeskus/Aruanded/Elering_Varustuskindluse_aruanne_2011.pdf, 22. May 2013.

[67] CEN-CENELEC-ETSI Smart Grid Coordination Group, "CEN-CENELEC-ETSI Smart Grid Coordination Group, First Set of Standards", Nov. 2012.

[68] Alberto, M.; Soriano, R.; Götz, J.; Mosshammer, R.; Espejo, N.; Leménager, F.; Bachiller, R., "OpenNode: A Smart Secondary Substation Node and its Integration in a Distribution Grid of the Future," Computer Science and Information Systems (FedCSIS), 2012 Federated Conference on. IEEE, pp. 1277-1284, 2012.

[69] Brand, K.P.; Ostertag, M.; Wimmer, W., "Safety related, distributed functions in substations and the standard IEC 61850," Power Tech Conference proceedings, 2003 IEEE Bologna. IEEE, vol. 2, pp. 5, June 2003.

[70] Liang, Y.; Campbell, R.H., "Understanding and simulating the IEC 61850 standard," Computer Science Research and Tech Reports, UIUCDCS-R-2008-2967, University at Illinois at Urbana-Champaign, May 2008.

[71] Jalali, M., "Substation and IEC 61850," IEEE Toronto section, seminar, http://toronto.ieee.ca/chapters/ias/IEEE_IEC61850_Seminar_MJ_Nov14.pdf, 22. May 2013.

[72] Brand, K.P..; Janssen, M., "The Specification of IEC 61850 Based Substation Automation Systems," DistribuTECH 2005, Jan. 2005.

[73] Prefabricated substations HEKA, http://www.harjuelekter.ee/elektrotehnika, 22. May 2013.

[74] Makansi, J.; Abboud, J., "Energy Storage: The Missing Link in the Electricity Value Chain – An ESC White Paper," Energy Storage Council, May 2002.

[75] Shah, S.; Shuflat, S., "Energy Storage Technologies in Utility Markets Worldwide," USA: SBI Energy, pp. 183, 2010.

[76] Teodorescu, R.; Sauer, D.; Rodriguez, P.; Swierczynski, M., Industrial/ PhD Course "Storage Systems Based on Li-Ion Batteries for Stationary Applications," Aalborg University, Denmark, 01-03 May 2012.

[77] Oudalov, A.; Cherkaoui, R.; Beguin, A., "Sizing and Optimal Operation of Battery Energy Storage System for Peak Shaving Application," Power Tech 2007 IEEE Lausanne. IEEE, pp. 621-625, 2007.

[78] Report sponsored by IEEE Smart grid with analyzis by Zpryme, "Power Systems of the Future: The Case for Energy Storage, Distributed Generation, And Microgrids," pp. 37, Nov. 2012.

[79] Technology performance report, Smart Grid Demonstration Project, Public Service Company of New Mexico, "PV Plus Battery for Simultaneous Voltage Smoothung and Peak Shifting," 2012.

[80] Gantenbein, D.; Jansen, B.; Dykeman, D.; Andersen, P.B.; Hauksson, E.B.; Marra, F.; Pedersen, A.B.; Andersen, C.A.; Dall, J., "WP3 – Distributed Integration Technology Development," EDISON Deliverable D3.1, pp. 59, April 2011, http://www.edison-net.dk, 22. May 2013.

[81] Makkonen, H.; Partanen, J.; Silventoinen, P., "Concept of Battery Charging and Discharging in Automotive Applications," Power Electronics Electrical Drives Automation and Motion (SPEEDAM), 2010 International Symposium. IEEE, pp. 1664-1669, June 2010.

[82] Man, E.A., "Control of Grid Connected PV Systems with Grid Support Functions," Master of science thesis, Aalborg University, Aalborg, Denmark, 2012.

[83] VDE-AR-N 4105, "Generators connected to the low-voltage distribution network – Technical requirements for the connection to and parallel operation with low-voltage distribution networks," August 2011.

[84] Tsili, M.; Patsiouras, C.; Papathanassiou, S., "Grid Code Requirements for Large Wind Farms," Renewable Power Generation, IET. IEEE, Vol. 3, issue 3, pp. 308-332, Sept. 2009.

[85] Brabandere, K.D., "Voltage and Frequency Droop Control in Low Voltage Grids by Distributed Generators with Inverter Front-End," Ph.D. Thesis, Katholieke Universiteit Leuven, Leuven, Belgium, 2006.

[86] Engler, A., "Control of Parallel Operating Battery Inverters," PV Hybrid Power Systems Conference, pp. 4, 2000.

[87] Kotsopoulos, A.; Duarte, J.L.; Hendrix, A.M., Heskes, P.J.M., "Islanding Behaviour of Grid-Connected PV Inverters Operating Under Different Control Schemes," Power Electronics Specialists Conference, 2002 PESC02. 2002 IEEE 33rd Annual. IEEE, Vol. 3, pp. 1506-1511, 2002.

[88] Timbus, A., "Grid Monitoring and Advanced Control of Distributed Power Generation Systems," Ph.D. Thesis, Aalborg University, Aalborg, Denmark, 2007.

[89] IEEE 1547-2003, "Interconnecting Distributed Resources with Electric Power System," 2003.

[90] Wittmann, T., "The General Scenario of Electric Vehicles and its Charging Infrastructure," ECPE Workshop on Power Electronics for Electric Vehicles, pp. 24, March 2011.

[91] Public E-Procurement of Estonia,
https://riigihanked.riik.ee/register/hange/127167, 22. May 2013.

[92] ABB Review Special report IEC 61850, http://www.abb.com, 22. May 2012.

[93] IEC 61850-5 Ed.2, "Communication networks and systems for power utility automation – Part 5: Communication requirements for functions and device models," July 2003.

[94] Tremblay, O.; Dessaint, L-A.; Dekkiche, A-I., "A Generic Battery Model for the Dynamic Simulation of Hybrid Electric Vehicles," Vehicle Power and Propulsion Conference VPPC 2007. IEEE, pp. 284-289, Sept. 2007.

[95] Mathworks, Implemented generic battery model,
http://www.mathworks.se/help/toolbox/physmod/powersys/ref/battery.html 22. May 2013.

[96] Le, D.; Tang, X., "Lithium-ion Battery State of Health Estimation Using Ah-V Characterization," Annual Conference of the Prognostics and Health Management Society PHM 2011, pp. 361-367, Sept. 2011.

[97] GWL/Power group, Product Information and Technical Support Blog,
http://gwl-power.tumblr.com, 22. May 2013.

[98] GWL/Power group, Discharge of 90AH and 100AH batteries,
http://gwl-power.tumblr.com/tagged/Testdata, 22. May 2013.

[99] Hartmann, M.; Friedli, T.; Kolar, J.W., "Three-Phase Unity Power Factor Mains Interfaces of High Power EV Battery Charging Systems," ECPE Workshop on Power Electronics for Charging Electric Vehicles, 67 p., March 2011.

[100] Power semiconductor device,
http://en.wikipedia.org/wiki/Power_semiconductor_device, 22. May 2013.

[101] Blake, C.; Bull, C., "IGBT or MOSFET: Choose Wisely,"
http://www.irf.com, 22. May 2013.

[102] Malinowski, M., "Sensorless Control Strategies for Three-Phase PWM Rectifiers," Ph.D. Thesis, Warsaw University of Technology, Warsaw, Poland, 2001.

[103] Cichowlas, M., "PWM Rectifier with Active Filtering," Ph.D. Thesis, Warsaw University of Technology, Warsaw, Poland, 2004.

[104] Kisacikoglu, M-C.; Ozpineci, B.; Tolbert, L-M., "Examination of a PHEV Bidirectional Charger System for V2G Reactive Power Compensation," Applied Power Electronics Conference and Exposition (APEC) 2010. IEEE, pp. 458-465, Feb. 2010.

[105] Fazel, S-S., "Investigation and Comparison of Multi-level Converters for Medium Voltage Applications," Ph.D. Thesis, Technische Universität Berlin, Berlin, Germany, 2007.

[106] Rockhill, A.A.; Liserre, M.; Teodorescu, R., Rodriguez, P., "Grid Filter Design for a Multi-Megawatt Medium-Voltage Voltage Source Inverter," Industrial Electronics, IEEE Transactions. IEEE, Vol. 58, issue 4, pp. 1205-1217, April 2011.

[107] Swisselectric Research, "Ultra-Fast Charging of Electric Vehicles: Annual Report 2011," Sept. 2011.

[108] Raducu, G-A., "Control of Grid Side Inverter in a B2B Configuration for WT Applications," Master of science thesis, Aalborg   University, Aalborg, Denmark, 2008.

[109] Mohamed, K.; Ahmed, Z.S.;   Samir, H.; Karim, F.M.; Rabie, A., "Performance Analysis of a Voltage Source Converter (VSC) based HVDC Transmission System under Faulted Conditions," Leonardo Journal of Sciences ISSN 1583-0233, Issue 15 (July-December), pp. 33-46, 2009.

[110] Mathworks, VSC-Based HVDC Link, http://www.mathworks.se/help/physmod/powersys/ug/vsc-based-hvdc-link.html, 22. May 2013.

[111] Liserre, M.; Blaabjerg, F.; Hansen, S., "Design and Control of an LCL-Filter-Based Three-Phase Active Rectifier," Industry Applications Conference 2001. IEEE, pp. 299-307, 2001.

[112] Peltioniemi, P.; Pöllänen, R.; Niemelä, M., Pyrhönen, J., "Comparison of the Effect of Output Filters on the Total Harmonic Distortion of Line Current in Voltage Source Line Converter – Simulation Study," International Conferance on Renewable Energies and Power Quality 2006 (ICREPQ 06), pp. 5, April 2006.

[113] Sun, W.; Chen, Z.; Wu, X., "Intelligent Optimize Design of LCL Filter for Three-Phase Voltage-Source PWM Rectifier," Power   Electronics   and Motion Control Conference, 2009 (IPEMC 09). IEEE, pp. 970-974, May 2009.

[114] Çetin, A., "Design and Implementation of a Voltage Source Converter Based STATCOM for Reactive Power Compensation and Harmonic Filtering," Ph.D. Thesis, Middle East Technical University, Ankara, Turkey, 2007.

[115] Sundeep, S.; MadhusudhanaRao, G., "Modelling and Analysis of Custom Power Devices for Improve Power Quality," International Journal of Electrical and Computer Engineering (IJECE), pp. 43-48, 2011.

[116] Balanuta, C.; Gurguiatu, G.; Munteanu, T.; Fetecau, G., "Three-phase Active Power Filter Control Using Synchronous Reference System, Indirect and Maximum Method," Scientific Bulletin of Electrical Engineering Faculty, Valahia University of Târgovişte, 2011 no.3, pp. 6, 2011.

[117] Mariun, N.; Masdi, H.; Bashi, S.M., Mohamed, A., Yusuf, S., "Design of a Prototype D-STATCOM Using DSP Controller for Voltage Sag Mitigation," Power India Conference, 2006 IEEE. IEEE, pp. 6, 2006.

[118] Hannan, M.A., "Effect of DC Capacitor Size on D-STATCOM Voltage Regulation Performance Evaluation," Przeglad Elektrotechniczny, 88(12A), pp. 243-246, 2012.

[119] Power factor correction and harmonic filtering, http://www.schneider-electric.com.au/documents/electrical-distribution/

en/local/electrical-installation-guide/EIG-L-power-factor-harmonic.pdf, 22. May 2013.

[120] DSTATCOM, http://www.donsion.org/calidad/cc8/c8-12.pdf, 22. May 2013.

[121] Araújo, S.V.; Engler, A.; Sahan, B.; Antunes, F.L.M., "LCL Filter Design for Grid-Connected NPC inverters in Offshore Wind Turbines," The 7th International Conference on Power Electronics (ICPE 07). IEEE, pp. 1133-1138, 2007.

[122] ABB Power Quality Filters (PQF), http://www.abb.com, 22. May 2013.

[123] Mathworks, Detailed model of D-STATCOM, http://www.mathworks.se/help/physmod/powersys/examples/d-statcom-average-model.html, 22. May 2013.

[124] Mathworks, Three-Phase AC-DC-AC PWM Converter, http://www.mathworks.com/matlabcentral/fileexchange/34272-three-phase-ac-dc-ac-pwm-converter/content/ThreePhase_ACDCAC_PMWconverter/Three_Phase_ACDCAC_PWMconverter.mdl, 22. May 2013.

[125] Erfani, M., "Design of a Bidirectional On-board Battery Charger in Hybrid Electric Vehicle Applications," Master of science thesis, Chalmers University of Technology, Göteborg, Sweden, 2011.

[126] Zhao, L.; Qian, J., "DC-DC Power Conversions and System Design Considerations for Battery Operated System," Texas Instruments, 2006 Portable Power Design Seminar.

[127] IEC 60364-7-722, "Low Voltage Electrical Installations Part 7-722: Requirements for Special Installations or Locations - Supply of Electric Vehicle," 2012.

[128] Zhao, J.F.; Jiang, J.G.; Yang, X.W., "AC-DC-DC isolated converter with bidirectional power flow capability," Power Electronics, IET. IEEE, Vol. 3, issue 4, pp. 472-479, July 2010.

[129] Apecor "EV bi-directional DC-DC" 200 kW, http://apecor.com/highpower.php, 24. April 2013.

[130] MGM transformer company general purpose dry-type distribution transformers, http://www.mgmtransformer.com/wp-content/uploads/2012/03/100-10A-02-2012.pdf, 22. May 2013.

[131] Siemens Dry Type Transformers, http://w3.usa.siemens.com/us/internet-dms/Internet/ConsultingEngineersComm/General/Docs/drytrans.pdf, 22. May 2013.

[132] GE Reverse Feeding Dry-Type Transformers, http://www.geindustrial.com/publibrary/checkout/Transformer2?TNR=White%20Papers|Transformer2|generic, 22. May 2013

[133] Priority queue, http://en.wikipedia.org/wiki/Priority_queue, 22. May 2013.

[134] The IT earthing system: a solution to improve electrical network availability, http://www.global-download.schneider-electric.com/85257849002EB8CB/all/A1790063E9BFEB8D85257856005C1CB9/$File/plsed110006en%20(web).pdf, 22. May 2013.

[135] Ahlert, K-H., "Economics of Distributed Storage Systems. An Economic Analysis of Arbritage-Maximizing Storage Systems at the End of Consumer Level," Ph.D. Thesis, Fakultät für Wirtschaftswissenschaften am Karlsruher Institut für Technologie, Karlsruher, Germany, 2010.

[136] Eberhard, M.; Tarpenning, M., "The 21st Century Electric Car," Tesla Motors Inc., pp. 10, July 2006.

[137] GWL/Power group, CALB SE70AHA Test Report, http://gwl-power.tumblr.com/tagged/Testdata, 22. May 2013.

[138] Nguyen, M.Y.; Yoon, Y.T.; Choi, N.H., "Dynamic Programming Formulation of Microgrid Operation with Heat and Electricity Constraints," in Transmission & Distribution Conference & Exposition: Asia and Pacific. IEEE, pp. 4, 2009.

[139] Roasto, I.; Romero-Cadaval, E.; Martins, J.; Smolenski, R., "State of the Art of Active Power Electronic Transformers for Smart Grids," IECON 2012 38th Annual Conference on IEEE Industrial Electronics Society. IEEE, pp. 5241-5246, 2012.

[140] Mägi, M.; Peterson, K.; Pettai, E., "Analysis of Protection and Control Functions of Low Voltage Part of Substation for Smart Grid Applications," In: Proceedings of 8th International Conference 2012 Electric Power Quality and Supply Reliability: 2012 Electric Power Quality and Supply Reliability. IEEE, pp. 297-304, 2012.

[141] Mägi, M., "Utilization of Electric Vehicles Connected to Distribution Substations for Peak Shaving of Utility Networks Loads," The Scientific Journal of Riga Technical University - Electrical, Control and Communication Engineering, Volume 2, Issue 1, pp. 47-54, 2013.

ABSTRACT

Use of modern electric vehicles and their effective integration into power grids depends on the technologies applied around distribution substations. Distribution substations equipped with energy storing and V2G capability enable peak load shaving and demand response, which will reduce the need to make new investments into building new power sources or power grids to meet peak demand.

This thesis is devoted to design and development of a novel control system for distribution substations to include V2G capability. The new distribution substation topology is implemented with integrated AC and DC bus, which supplies AC low voltage consumers and allows charging and discharging of electric vehicles. In addition, the topology includes Li-ion energy storing units, which can support either the low voltage side of AC consumers or the fast charging of electric vehicles. The distribution substation with V2G capability can be part of a microgrid or even a viable module for Smart Grid solutions.

In order to define exact tasks for the control system, current technologies and trends in the development of Li-ion batteries and charging methods for electric vehicles, Smart Grid solutions and distribution substations were specified. Recent trends and technologies in the control of aggregated number of electric vehicles for V2G applications were studied in detail.

In the analytical part of the thesis general requirements, topology and control architecture for the distribution substation with V2G capability were specified. First, recent technologies and development trends used in bidirectional power converters and their control systems were analyzed and simulated. It is shown, which power converter topologies are suitable for the integrated AC and DC bus topology. Based on the opportunities of low level control of power electronic converters the control architecture for the substation's main controller in the higher level was developed. Also, several new algorithms have been developed by the author of the thesis to solve some typical control and protection functions in the management of low voltage bays of the distribution substation. The complete system of the distribution substation was simulated with computer models.

That knowledge that was gathered from the analytical part was used in the design, development and assembly of the laboratory test bench for microgrid applications. In addition, a prototype of modular 460 V DC Li-ion battery pack based energy storage device was developed in cooperation with Estonian company AS Harju Elekter Elektrotehnika As the developed control system has been built and optimised according to the most recent development trends and design requirements of Smart Grids together with novel design proposals from the author, the doctoral thesis has a great practical value for the industry. Practical recommendations and general guidelines to design distribution substations with V2G capability were given.

In the seventh part of the thesis, postdoctoral research topics of the author are covered. Further experiments with the microgrid test bench will give vital data about the behaviour of the substation automation system.

Novelty and profitability of the work have been confirmed with the selling of a manufacturing licence with the appropriate technical documentations to AS Harju Elekter Elektrotehnika from Tallinn University of Technology.

KOKKUVÕTE

Nüüdisaegsete elektriautode integreerimine tarkvõrkude koosseisu (V2G) sõltub jaotusalajaamades rakendatavatest tehnoloogiatest. Jaotusalajaamad, mis sisaldavad kahesuunalist energiavahetust elektriautode ja energiasalvestite vahel, võimaldavad pakkuda kasutajatele elektrivõrgust võetava tipuvõimsuse silumist ja süsteemi koormuste tasakaalustamist, mis omakorda vähendab vajadust või võimaldab edasi lükata uute investeeringute tegemist uutesse toiteallikatesse või elektrivõrkudesse tipuvõimsuste edastamiseks.

Doktoritöö eesmärgiks oli uurida ning välja töötada uus arukas juhtimissüsteem V2G tehnoloogiaga varustatud jaotusalajaamadele. Väljapakutud jaotusalajaamade topoloogias on rakendatud integreeritud AC ja DC jõusiini, mille kaudu saab tagada madalpinge tarbijatele kvaliteetset elektrienergia kättesaadavust ja samal ajal teostada elektriautode kiirlaadimist või tühjendamist. Jaotusalajaamade koosseisu on lülitatud nüüdisaegsed kahesuunalised energiasalvestid (Li-ioon akupatareid), mis võimaldavad pakkuda kasutajatele erinevaid tugiteenuseid ja siluda elektriautode kiirlaadimistest tulenevaid tipuvõimsusi. V2G tehnoloogiaga varustatud jaotusalajaamu saab rakendada mikrovõrkude või tarkvõrkude koosseisus.

Ülesande lahendamiseks uuriti ja süstematiseeriti antud valdkonna teaduse ja tehnoloogia viimase aja trendid Li-ioon akude, elektriautode laadimismeetodite, tarkvõrkude ja jaotusalajaamade vallas.

Töö analüütilises osas kirjeldatakse jaotusalajaamadele esitatavaid nõudeid, topoloogiat ja uue juhtimissüsteemi ülesehitust. Esmalt uuritakse integreeritud AC ja DC jõusiinile sobivaid kaasaegseid kahesuunalisi jõumuundureid. Analüüsi ja simulatsioonide tulemuste põhjal leitakse optimaalsed jõumuundurite topoloogiad jaotusalajaamadele. Lähtudes jõumuundurite madalama astme juhtimis-võimalustest, esitatakse uus kõrgema astme jaotusalajaama juhtimissüsteem. Autor esitab enda loodud täiesti uusi algoritme, mis lahendavad mitmeid jaotusalajaamade madalpingefiidrite juhtimis- ja kaitsealaseid tüüpfunktsioone. Erinevaid juhtimisalgoritme ja jaotusalajaama kui tervik süsteemi simuleeritakse arvutimudelitega.

Doktoritöö praktilise tulemusena töötati välja ja ehitati mikrovõrgu laboratoorne katseseade, mis vastab kaasaegsetele nõuetele ja normidele. Lisaks arendati koostöös Eesti ettevõtte AS Harju Elekter Elektrotehnikaga välja 460 V DC Li-ioon akupatarei prototüüp. Doktoritöös esitatud praktilised nõuanded ja soovitused V2G tehnoloogiga varustatud jaotusalajaamade ehitamiseks lisavad tööle praktilist väärtust.

Tallinna Tehnikaülikool müüs valmistuslitsentsi õigused koos vajalike projekteerimisdokumentidega AS Harju Elekter Elektrotehnikale, mis tõestab tehtud töö uudsust ja vajalikkust. Autori edasine uurimistöö jätkub mikrovõrkude uurimise valdkonnas.

AUTHOR'S MAIN PUBLICATIONS

1. Mägi, M. (2013). Utilization of Electric Vehicles Connected to Distribution Substations for Peak Shaving of Utility Networks Loads. The Scientific Journal of Riga Technical University - Electrical, Control and Communication Engineering, Volume 2, Issue 1, pp. 47 – 54.
2. Korõtko, T.; Mägi, M.; Peterson, K.; Teemets, R.; Pettai, E. (2013). Analysis and Development of Protection and Control Functions for Li-Ion Based Prosumers Provided by Low Voltage Part of Distribution Substation. 8th International Conference-Workshop Compatibility and Power Electronics, CPE 2013. IEEE, pp. 1 – 6. [*forthcoming, June 2013*]
3. Mägi, M; Peterson, K; Pettai, E. (2012). Analysis of Protection and Control Functions of Low Voltage Part of Substation for Smart Grid Applications. In: Proceedings of 8th International Conference 2012 Electric Power Quality and Supply Reliability: 2012 Electric Power Quality and Supply Reliability, Tartu, June 11 - 13, 2012. IEEE, pp. 297 – 304.
4. Mägi, M. (2013). Analysis of Peak Shaving of Utility Networks Loads with Electric Vehicles Connected to Distribution Substations. 13th International Symposium "Topical problems in the field of electric and power engineering". Doctoral school of energy and geotechnology II: Pärnu, Estonia, January 14-19, 2013, pp. 184 – 191.
5. Mägi, M. (2012). Overview of Development in the Field of Energy Exchange between Electric Vehicles and Utility Network. 12th International Symposium "Topical Problems in the Field of Electrical and Power Engineering". Doctoral School of Energy and Geotechnology II: Kuressaare, Estonia, June 11-16, 2012, pp. 123 – 124.
6. Mägi, M. (2012). Analysis of Distribution Substation Topologies for Energy Exchanging between EV and Utility Networks. 11th International Symposium "Topical problems in the field of electrical and power engineering". Doctoral school of energy and geotechnology II : Pärnu, Estonia, January 16-21, 2012, pp. 158 – 167.
7. Mägi, M. (2007). Analysis of Modelling Electric Transportation Networks. 4th International Symposium "Topical problems of education in the field of electrical and power engineering". Doctoral school of energy and geotechnology: Kuressaare, Estonia, January 15-20, 2007, pp. 73 – 77.
8. Mägi, M. (2006). Topical problems of teaching of electrical apparatus. 3rd International Symposium "Topical Problems of Education in the Field of Electrical and Power Engineering". Doctoral School of Energy and Geotechnology: Kuressaare, Estonia, January 16, 21, 2006, pp. 145 – 147.
9. Mägi, M. (2004). Hoonesisend, Jaotuskilbid. Elamute elektripaigaldised, Tallinn: EETEL-Ekspert OÜ, pp. 122 – 130.

Elulookirjeldus

1. Isikuandmed

Ees- ja perekonnanimi	Marek Mägi
Sünniaeg ja -koht	25. veebruar 1982, Tallinn, Eesti
Kodakondsus	eesti
E-posti aadress	marek.magi@he.ee

2. Hariduskäik

Õppeasutus (nimetus lõpetamise ajal)	Lõpetamise aeg	Haridus (eriala/kraad)
Tallinna Tehnikaülikool	2005	tehnikateaduste magister
Tallinna Tehnikaülikool	2004	tehnikateaduste bakalaureus
J. Westholmi Gümnaasium	2000	keskharidus

3. Keelteoskus (alg-, kesk- või kõrgtase)

Keel	Tase
eesti	emakeel
inglise	kesktase
soome	kesktase

4. Teenistuskäik

Töötamise aeg	Tööandja nimetus	Ametikoht
2005 -	AS Harju Elekter Elektrotehnika	Tootearendusosakonna elektriinsener
2005-2005	AS Harju Elekter	Tootearendusosakonna elektriinsener
2004-2005	AS Harju Elekter	Müügiosakonna müügiinsener
2003-2003	AS Harju Elekter; Elektriseadmete tehas	tehnik

5. Teadustegevus

2006-2007	631F Energiasalvestid ja nende kasutusvõimaluste uurimine Eestis

6. Kaitstud lõputööd

Marek Mägi, magistrikraad, 2005, (juh) Tõnu Lehtla, TTÜ elektriaparaatide ja andurite laboratooriumi lühisrootoriga asünkroonmootori käivitusstendi koostamine koos metoodiliste juhenditega, Tallinna Tehnikaülikool, Energeetikateaduskond, Elektriajamite ja jõuelektroonika instituut, Elektriajamite ja elektrivarustuse õppetool.

Marek Mägi, bakalaureusekraad, 2004, (juh) Raik Jansikene, Mecha-Flex kooste tüüpsõlmede projekteerimine, Tallinna Tehnikaülikool, Energeetika-teaduskond, Elektriajamite ja jõuelektroonika instituut, Elektriajamite ja elektrivarustuse õppetool.

7. Teadustöö põhisuunad
   - Energeetikaalased uuringud

Curriculum vitae

1. Personal data

Name	Marek Mägi
Date and place of birth	25. February 1982, Tallinn, Estonia
Citizenship	Estonian
E-mail address	marek.magi@he.ee

2. Education

Educational institution	Graduation year	Education (field of study/degree)
Tallinn University of Technology	2005	Master of science degree
Tallinn University of Technology	2004	Bachelor degree
J. Westholm Gymnasium	2000	Secondary education

3. Language competence/skills (fluent, average, basic skills)

Language	Level
Estonian	native
English	average
Finnish	average

4. Professional employment

Period	Organisation	Position
2005 -	AS Harju Elekter Elektrotehnika	R&D department electrical engineer
2005-2005	AS Harju Elekter	R&D department electrical engineer
2004-2005	AS Harju Elekter	Sales department sales engineer
2003-2003	AS Harju Elekter; Elektriseadmete tehas	technician

5. Scientific work

2006-2007	631F Research of energy storages and their possible application fields in Estonia

6. Defended theses

Marek Mägi, Master's Degree, 2005, (sup) Tõnu Lehtla, TTÜ elektriaparaatide ja andurite laboratooriumi lühisrootoriga asünkroon-mootori käivitusstendi koostamine koos metoodiliste juhenditega (The design of the squirrel cage asynchronous motor's operating stand for the Laboratory of Electrical Apparatus and Sensors with operating manuals), Tallinn University of Technology , Faculty of Power Engineering, Department of Electrical Engineering, Chair of Electrical Drivers and Electrical Supply.

Marek Mägi, Bachelor's Degree, 2004, (sup) Raik Jansikene, Mecha-Flex kooste tüüpsõlmede projekteerimine (The design of Mecha-Flex assembly type-tested units), Tallinn University of Technology , Faculty of Power Engineering, Department of Electrical Engineering, Chair of Electrical Drivers and Electrical Supply.

7. Main areas of scientific work / Current research topics
    - Energetic Research

DISSERTATIONS DEFENDED AT
TALLINN UNIVERSITY OF TECHNOLOGY ON
POWER ENGINEERING, ELECTRICAL ENGINEERING, MINING ENGINEERING

1. **Jaan Tehver**. Boiling on Porous Surface. 1992.

2. Salastatud.

3. **Endel Risthein.** Electricity Supply of Industrial Plants. 1993.

4. **Tõnu Trump**. Some New Aspects of Digital Filtering. 1993.

5. **Vello Sarv.** Synthesis and Design of Power Converters with Reduced Distortions Using Optimal Energy Exchange Control. 1994.

6. **Ivan Klevtsov**. Strained Condition Diagnosis and Fatigue Life Prediction for Metals under Cyclic Temperature Oscillations. 1994.

7. **Ants Meister**. Some Phase-Sensitive and Spectral Methods in Biomedical Engineering. 1994.

8. **Mati Meldorf**. Steady-State Monitoring of Power System. 1995.

9. **Jüri-Rivaldo Pastarus**. Large Cavern Stability in the Maardu Granite Deposit. 1996.

10. **Enn Velmre**. Modeling and Simulation of Bipolar Semiconductor Devices. 1996.

11. **Kalju Meigas**. Coherent Photodetection with a Laser. 1997.

12. **Andres Udal**. Development of Numerical Semiconductor Device Models and Their Application in Device Theory and Design. 1998.

13. **Kuno Janson**. Parallel- ja järjestikresonantsi parameetrilise vaheldumisega võrgusageduslik resonantsmuundur ja tema rakendamine. 2001.

14. **Jüri Joller**. Research and Development of Energy Saving Traction Drives for Trams. 2001.

15. **Ingo Valgma**. Geographical Information System for Oil Shale Mining – MGIS. 2002.

16. **Raik Jansikene**. Research, Design and Application of Magnetohydrodynamical (MHD) Devices for Automation of Casting Industry. 2003.

17. **Oleg Nikitin**. Optimization of the Room-and-Pillar Mining Technology for Oil-Shale Mines. 2003.

18. **Viktor Bolgov**. Load Current Stabilization and Suppression of Flicker in AC Arc Furnace Power Supply by Series-Connected Saturable Reactor. 2004.

19. **Raine Pajo**. Power System Stability Monitoring – an Approach of Electrical Load Modelling. 2004.

20. **Jelena Shuvalova**. Optimal Approximation of Input-Output Characteristics of Power Units and Plants. 2004.

21. **Nikolai Dorovatovski**. Thermographic Diagnostics of Electrical Equipment of Eesti Energia Ltd. 2004.

22. **Katrin Erg**. Groundwater Sulphate Content Changes in Estonian Underground Oil Shale Mines. 2005.

23. **Argo Rosin**. Control, Supervision and Operation Diagnostics of Light Rail Electric Transport. 2005.

24. **Dmitri Vinnikov**. Research, Design and Implementation of Auxiliary Power Supplies for the Light Rail Vehicles. 2005.

25. **Madis Lehtla**. Microprocessor Control Systems of Light Rail Vehicle Traction Drives. 2006.

26. **Jevgeni Šklovski**. LC Circuit with Parallel and Series Resonance Alternation in Switch-Mode Converters. 2007.

27. **Sten Suuroja**. Comparative Morphological Analysis of the Early Paleozoic Marine Impact Structures Kärdla and Neugrund, Estonia. 2007.

28. **Sergei Sabanov**. Risk Assessment Methods in Estonian Oil Shale Mining Industry. 2008.

29. **Vitali Boiko**. Development and Research of the Traction Asynchronous Multimotor Drive. 2008.

30. **Tauno Tammeoja**. Economic Model of Oil Shale Flows and Cost. 2008.

31. **Jelena Armas**. Quality Criterion of road Lighting Measurement and Exploring. 2008.

32. **Olavi Tammemäe**. Basics for Geotechnical Engineering Explorations Considering Needed Legal Changes. 2008.

33. **Mart Landsberg**. Long-Term Capacity Planning and Feasibility of Nuclear Power in Estonia under Certain Conditions. 2008.

34. **Hardi Torn**. Engineering-Geological Modelling of the Sillamäe Radioactive Tailings Pond Area. 2008.

35. **Aleksander Kilk**. Paljupooluseline püsimagnetitega sünkroongeneraator tuuleagregaatidele. 2008.

36. **Olga Ruban**. Analysis and Development of the PLC Control System with the Distributed I/Os. 2008.

37. **Jako Kilter**. Monitoring of Electrical Distribution Network Operation. 2009.

38. **Ivo Palu**. Impact of Wind Parks on Power System Containing Thermal Power Plants. 2009.

39. **Hannes Agabus**. Large-Scale Integration of Wind Energy into the Power System Considering the Uncertainty Information. 2009.

40. **Kalle Kilk**. Variations of Power Demand and Wind Power Generation and Their Influence to the Operation of Power Systems. 2009.

41. **Indrek Roasto**. Research and Development of Digital Control Systems and Algorithms for High Power, High Voltage Isolated DC/DC Converters. 2009.

42. **Hardi Hõimoja**. Energiatõhususe hindamise ja energiasalvestite arvutuse metoodika linna elektertranspordile. 2009.

43. **Tanel Jalakas**. Research and Development of High-Power High-Voltage DC/DC Converters. 2010.

44. **Helena Lind**. Groundwater Flow Model of the Western Part of the Estonian Oil Shale Deposit. 2010.

45. **Arvi Hamburg**. Analysis of Energy Development Perspectives. 2010.

46. **Mall Orru**. Dependence of Estonian Peat Deposit Properties on Landscape Types and Feeding Conditions. 2010.

47. **Erik Väli**. Best Available Technology for the Environmentally Friendly Mining with Surface Miner. 2011.

48. **Tarmo Tohver**. Utilization of Waste Rock from Oil Shale Mining. 2011.

49. **Mikhail Egorov**. Research and Development of Control Methods for Low-Loss IGBT Inverter-Fed Induction Motor Drives. 2011.

50. **Toomas Vinnal**. Eesti ettevõtete elektritarbimise uurimine ja soovituste väljatöötamine tarbimise optimeerimiseks. 2011.

51. **Veiko Karu**. Potential Usage of Underground Mined Areas in Estonian Oil Shale Deposit. 2012.

52. **Zoja Raud**. Research and Development of an Active Learning Technology for University-Level Education in the Field of Electronics and Power Electronics. 2012.

53. **Andrei Blinov**. Research of Switching Properties and Performance Improvement Methods of High-Voltage IGBT based DC/DC Converters. 2012.

54. **Paul Taklaja**. 110 kV õhuliinide isolatsiooni töökindluse analüüs ja töökindluse tõstmise meetodid. 2012.

55. **Lauri Kütt**. Analysis and Development of Inductive Current Sensor for Power Line On-Line Measurements of Fast Transients. 2012.

56. **Heigo Mõlder**. Vedelmetalli juhitava segamisvõimaluse uurimine alalisvoolu kaarleekahjus. 2012.

57. **Reeli Kuhi-Thalfeldt**. Distributed Electricity Generation and its Possibilities for Meeting the Targets of Energy and Climate Policies. 2012.

58. **Irena Milaševski**. Research and Development of Electronic Ballasts for Smart Lighting Systems with Light Emitting Diodes. 2012.

59. **Anna Andrijanovitš**. New Converter Topologies for Integration of Hydrogen Based Long-Term Energy Storages to Renewable Energy Systems. 2013.